

SEDIMENTOLOGY, STRATIGRAPHY, GEOCHEMISTRY AND DIAGENESIS OF GIANT LACUSTRINE
CARBONATE SEEP MOUNDS (IKPIARJUK FORMATION), MESOPROTEROZOIC BORDEN BASIN, NUNAVUT,
ARCTIC CANADA

by

Katherine Elizabeth Hahn

A thesis submitted in partial fulfillment
of the requirements for the degree of
Doctor of Philosophy (PhD) in Mineral Deposits and Precambrian Geology

The Faculty of Graduate Studies
Laurentian University
Sudbury, Ontario, Canada

© Katherine Elizabeth Hahn, 2016

THESIS DEFENCE COMMITTEE/COMITÉ DE SOUTENANCE DE THÈSE
Laurentian Université/Université Laurentienne
Faculty of Graduate Studies/Faculté des études supérieures

Title of Thesis Titre de la thèse	SEDIMENTOLOGY, STRATIGRAPHY, GEOCHEMISTRY AND DIAGENESIS OF GIANT LACUSTRINE CARBONATE SEEP MOUNDS (IKPIARJUK FORMATION), MESOPROTEROZOIC BORDEN BASIN, NUNAVUT, ARCTIC CANADA	
Name of Candidate Nom du candidat	Hahn, Katherine	
Degree Diplôme	Doctor of Philosophy	
Department/Program Département/Programme	Mineral Deposits and Precambrian Geology	Date of Defence Date de la soutenance March 23, 2016

APPROVED/APPROUVÉ

Thesis Examiners/Examineurs de thèse:

Dr. Elizabeth Turner
(Supervisor/Directeur(trice) de thèse)

Dr. Alessandro Ielpi
(Committee member/Membre du comité)

Dr. Mairi Best
(Committee member/Membre du comité)

Dr. Denis Lavoie
(External Examiner/Examineur externe)

Approved for the Faculty of Graduate Studies
Approuvé pour la Faculté des études supérieures
Dr. David Lesbarrères
Dean, Faculty of Graduate Studies
Doyen, Faculté des études supérieures

Dr. Mazen Saleh
(Internal Examiner/Examineur interne)

ACCESSIBILITY CLAUSE AND PERMISSION TO USE

I, **Katherine Hahn**, hereby grant to Laurentian University and/or its agents the non-exclusive license to archive and make accessible my thesis, dissertation, or project report in whole or in part in all forms of media, now or for the duration of my copyright ownership. I retain all other ownership rights to the copyright of the thesis, dissertation or project report. I also reserve the right to use in future works (such as articles or books) all or part of this thesis, dissertation, or project report. I further agree that permission for copying of this thesis in any manner, in whole or in part, for scholarly purposes may be granted by the professor or professors who supervised my thesis work or, in their absence, by the Head of the Department in which my thesis work was done. It is understood that any copying or publication or use of this thesis or parts thereof for financial gain shall not be allowed without my written permission. It is also understood that this copy is being made available in this form by the authority of the copyright owner solely for the purpose of private study and research and may not be copied or reproduced except as permitted by the copyright laws without written authority from the copyright owner.

Abstract

The Ikpiarjuk Formation consists of a group of very large (kms long and hundreds of metres thick), isolated, deep-water, vent-related dolostone mounds that are unlike any documented example of vent-related carbonate rocks in the geological record. The mounds lack ‘normal’ features of Proterozoic carbonates: the mounds contain thrombolites (microbially clotted carbonate), formed below the photic zone, and lack the stromatolitic fabric characteristic of most Proterozoic reef structures. The sedimentology, stratigraphy, geochemistry, and diagenetic history of the mounds were investigated through field work, standard petrographic methods, and various geochemical and other analytical techniques.

Shale-normalised rare earth element patterns of various depositional components of the mounds depicts binary mixing between basin-water-derived precipitates and seep-fluid-derived carbonate. Basin fluid has characteristics that are consistent with deposition in an alkaline lake, and seep fluid features are consistent with circum-neutral groundwater that had interacted extensively with basement blocks before seeping into the lake bottom through faults.

The sedimentology and mineralogy of the mounds indicates that they were formed by thrombolites that were made up of a microbiota that was not photosynthetic or aerobic. The Ikpiarjuk Formation thrombolite microbiota was probably dominated by an anaerobic chemoautotrophic or chemoheterotrophic metabolism, and records visible preservation of a community that has never before been described from the Mesoproterozoic.

The diagenetic history of the Ikpiarjuk Formation is complicated. Dolomitisation occurred early during diagenesis, and subsequently, five different fluids flowed through primary pore space in

the mounds and precipitated successive generations of cement. One of the cements contains sulphides inclusions and may correlate with base-metal bodies elsewhere in the basin.

Keywords: Mesoproterozoic; carbonate sedimentology; alkaline lake; lacustrine carbonate; thrombolite; seep mound; diagenesis; fluid inclusion

Co-authorship statement

Several collaborators, listed as co-authors, contributed to the work presented herein. The co-authors provided scientific guidance, supervision, and help with laboratory analyses. The project was conceived by Dr. Turner.

Chapter 2 is co-authored with Drs. Turner, Babechuk, and Kamber. Field work was completed by the candidate and sample selection was completed by the candidate under the supervision of Dr. Turner. Sample preparation was completed by the candidate under supervision by Drs. Babechuk and Kamber. Analyses were run by Dr. Babechuk. Dr. Babechuk wrote a subsection of “methods” because the analytical protocol was custom run by Dr. Babechuk for the study. The first draft and initial interpretations were completed by the candidate. The co-authors edited subsequent drafts of the manuscript and provided scientific input for the candidate to investigate and follow up on.

Chapter 3 is co-authored with Dr. Turner. Chapter 3 is based on fieldwork and samples collected by the candidate as well as archived sample material and unpublished field results collected by Dr. Turner between 2003 and 2009. The first draft of Chapter 3 was prepared by the candidate. Dr. Turner wrote a subsection of the results on the field work completed by Dr. Turner between 2003 and 2008. All macro-scale and micro-scale descriptions and interpretations were written by the candidate with subsequent drafts edited by Dr. Turner.

Chapter 4 is co-authored with Drs. Turner and Kontak. Chapter 4 is based on fieldwork completed by and samples collected by the candidate with supplemental material provided by Dr. Turner. The candidate selected the samples and completed the analytical work. The fluid inclusion microthermometry work was completed by the candidate under the instruction of Dr. Kontak. The candidate wrote the first draft of Chapter 4 and subsequent drafts were edited by Drs. Turner and Kontak.

Acknowledgements

Dr. Turner is gratefully acknowledged for the providing the opportunity for me to complete this project. Dr. Turner provided expertise, guidance, and patient instruction through this entire project. Field work was financially supported by Canada-Nunavut Geoscience Office, a Natural Sciences and Engineering Research Council Discovery Grant to ECT, and a Northern Scientific Training Program Grant awarded to KH. Field work was assisted by T. Chevrier and J. Mathieu. LA-ICP-MS work was completed with the help of J. Petrus. Logistical support was provided by Polar Continental Shelf Project (Natural Resources Canada). Analytical work at Trinity College Dublin was supported by EC-FP7-MC grant “Chemical fingerprinting”. The Nunavut Research Institute is gratefully acknowledged for assistance with permitting. G. Baldwin is gratefully acknowledged for many helpful discussions. Sample prep and SIMS analysis for oxygen isotopes were completed by R. Sharpe at University of Manitoba facilities that are supported by funding to M. Fayek. Drs. Lavoie, Saleh, Ielpi, and Best all helped improve the quality of this thesis through critical reviews of the entire thesis.

Table of Contents

Abstract	iii
Co-authorship statement	v
Acknowledgements	vi
List of Figures	xi
List of Tables	xiv
Chapter 1	1
1. Introduction to thesis	1
1.1 Statement of problem	1
1.2 Research questions.....	2
1.3 Regional geology.....	4
1.4 Methods.....	7
1.5 Structure of thesis	8
1.6 Statement of responsibilities.....	9
1.7 Statement of original contributions	10
1.8 References	11
Chapter 2	15
2. Deep-water seep-related carbonate mounds in a Mesoproterozoic alkaline lake, Borden Basin (Nunavut, Canada)	15
2.1 Abstract.....	15
2.2 Introduction.....	16
2.3 Geologic Setting.....	18
2.3.1 Regional setting and stratigraphy of the Milne Inlet Graben.....	18
2.3.2 Ikpiarjuk Formation	20
2.4 Methods.....	23
2.4.1 Samples	23
2.4.2 LA-ICP-MS analytical details	25
2.4.3 Solution ICP-MS analytical details	26
2.4.4 Stable C and O isotope analysis.....	29
2.5 Results.....	29
2.5.1 REE+Y Systematics	29
2.5.2 Detrital content	30

2.5.3	Redox-sensitive metal systematics (V, Mo and U)	30
2.5.4	Stable Isotopes	33
2.6	Interpretation	34
2.6.1	Origin of variation in REE +Y patterns	34
2.6.2	Interpretation of basin water REE+Y pattern	39
2.6.3	Supporting evidence for alkalinity.....	43
2.6.4	Trace metal systematics and mound chemostratigraphy	46
2.7	Discussion	50
2.7.1	Geology, sedimentology, and geochemistry of the Milne Inlet Graben	50
2.7.2	Nature of the seep fluid	52
2.7.3	Precambrian lacustrine carbonates.....	54
2.7.4	Problems with using carbonate systems as proxies for global geochemistry.....	57
2.8	Summary.....	58
2.9	Acknowledgements	59
2.10	References	60
2.11	Figures	72
Chapter 3	107
3. Composition and history of giant lacustrine carbonate seep mounds, Mesoproterozoic Borden Basin, Arctic Canada	107
3.1	Abstract.....	107
3.2	Introduction.....	108
3.3	Geological Background	110
3.4	Methods.....	112
3.5	Results.....	113
3.5.1	Mound Geometry and Paleoenvironments.....	113
3.5.2	In situ lithofacies.....	117
3.5.3	Dolomudstone	124
3.5.4	Stable isotope results	124
3.6	Interpretation of in situ lithofacies.....	124
3.6.1	Benthic precipitates.....	127

3.6.2	Pelagic carbonate mud	133
3.7	Discussion	134
3.7.1	Mound and basin evolution	134
3.7.2	Depositional environment.....	140
3.7.3	Comparison with modern carbonate seep mounds in lakes.....	143
3.7.4	Paleobiology of the mounds.....	148
3.8	Summary.....	154
3.9	Acknowledgements	155
3.10	References	156
3.11	Figures	168
Chapter 4	204
4. Diagenetic history of deep-water carbonate mounds in the Mesoproterozoic Nanisivik zinc district, Nunavut	204
4.1	Abstract.....	204
4.2	Introduction.....	206
4.3	Geologic Setting.....	208
4.4	Methods.....	211
4.4.1	Samples	211
4.4.2	Scanning electron microscopy (SEM) and energy dispersive spectroscopy (EDS)	211
4.4.3	Laser ablation inductively coupled plasma mass spectrometry (LA ICP-MS).....	212
4.4.4	Fluid inclusion microthermometry.....	212
4.4.5	Evaporate mound analysis	213
4.4.6	Secondary ion mass spectrometry (SIMS).....	214
4.5	Results.....	215
4.5.1	Petrography/Paragenesis	215
4.5.2	Fluid inclusion petrography.....	218
4.5.3	Microthermometry and salinity	219
4.5.4	Evaporate mounds	221
4.5.5	Major, Trace, and REEs.....	222

4.5.6	Stable O isotopes.....	225
4.6	Discussion	226
4.6.1	Sources and interaction of fluids.....	226
4.6.2	Temperature of fluid entrapment and pressure correction of fluid inclusions	226
4.6.3	Evolution of fluid salinity	229
4.6.4	Evaporate mound geochemistry	229
4.6.5	REE+Y composition of cements.....	230
4.6.6	O isotope composition of cements	234
4.6.7	Fluids.....	237
4.6.8	Comparison with base metal showings in the Borden Basin	240
4.6.9	Timing of fluid-flow events.....	244
4.7	Summary.....	248
4.8	Acknowledgements	249
4.9	References	249
4.10	Figures 261	
Chapter 5	298
5. Concluding Statements	298
5.1	Conclusions.....	298
5.2	Future work	300
5.3	References	301

List of Figures

Figure 2-1 - Geological map.....	72
Figure 2-2 - Tectonic history	73
Figure 2-3 - Schematic cross-section through the Milne Inlet Graben.....	74
Figure 2-4 - Field exposures of the Ikpiarjuk Formation.....	75
Figure 2-5 - Schematic configurations of four mounds.....	77
Figure 2-6 - Thin section photomicrograph.....	78
Figure 2-7 - Comparison of REE+Y data with different normalisation	79
Figure 2-8 - Shale-normalised REE+Y patterns	81
Figure 2-9 - Stratigraphic plots of geochemistry	82
Figure 2-10 - Covariance diagrams of the Eu anomaly and trace elements	84
Figure 2-11 - Covariance diagrams of the enrichment factor of Mo and Fe (wt. %)	85
Figure 2-12 - Covariance diagram of stable isotopes	86
Figure 2-13 - Normalised plots of Pr/Yb vs Pr/Dy.....	87
Figure 2-14 - Analysis of REE+Y systematics.....	89
Figure 2-15 - Comparison of interpreted data with modern lakes	91
Figure 2-16 - A-CN-K diagram of shale.....	92
Figure 2-17 - Histograms of enrichment factors of Mo and V	94
Figure 2-18 - Schematic cross-section showing mound growth.....	95
Figure 3-1 Geological map of the Milne Inlet Graben	168
Figure 3-2 - Stratigraphy of the Bylot Supergroup.....	169
Figure 3-3 - Map of known mound exposures.....	170
Figure 3-4 - Schematic diagrams of six mounds	171

Figure 3-5 Mound histories.....	173
Figure 3-6 Mound exposure field photos.....	175
Figure 3-7 Mound exposure field photos.....	177
Figure 3-8 Outcrop photos of solution breccia	179
Figure 3-9 Schematic diagram of in situ mound.....	180
Figure 3-10 Porous thrombolite lithofacies	181
Figure 3-11 Layered thrombolite lithofacies	183
Figure 3-12 Densely packed thrombolite.....	185
Figure 3-13 Photomicrographs of blunt-tipped crystals and length-fast dolomite	187
Figure 3-14 Photomicrographs of length-slow dolomite	189
Figure 3-15 Photomicrographs of hematitic cement.....	191
Figure 3-16 Photomicrographs of euhedral dolomite cement.....	193
Figure 3-17 Chemostratigraphic sections	195
Figure 3-18 Interpretative diagram	196
Figure 3-19 Paragenetic chart	197
Figure 4-1 - Geological map.....	261
Figure 4-2 - Tectonic history	262
Figure 4-3 -Basin cross section.....	263
Figure 4-4 - Paragenetic chart.....	265
Figure 4-5 - Photomicrographs of paragenetic history	266
Figure 4-6 - Photomicrographs of paragenetic history (2).....	268
Figure 4-7 - Photomicrographs of fluid inclusions	269
Figure 4-8 - H ₂ O-NaCl-CaCl ₂ ternary diagram.....	271

Figure 4-9 - Results of SEM-EDS analysis of evaporate mounds.....	272
Figure 4-10 - Results of SEM-EDS analysis of evaporate mounds (2).....	274
Figure 4-11- Summary of LA-ICP-MS results.....	276
Figure 4-12 - PAAS-normalised REE plots.....	278
Figure 4-13 - La and Ce anomaly discrimination diagram.....	280
Figure 4-14 - Oxygen isotope data.....	281
Figure 4-15 - Pressure-temperature diagrams.....	283
Figure 4-16 - Backscattered electron image.....	285
Figure 4-17 - Summary diagram of paragenetic stages.....	289

List of Tables

Table 1 - Major element (wt. %) and trace element (ppb) laboratory data.....	97
Table 3-1 - Summary of mound exposures.....	198
Table 3-2 - Mound section locations.....	194
Table 3-3- Original mineralogy of primary phases.....	195
Table 3-4 - Stable Isotope Results.....	196
Table 4-1 - Microthermometry results.....	290
Table 4-2 – LA-ICP-MS elemental concentrations (ppm)	291
Table 4-3 - Summary of SIMS results	297

Chapter 1

1. Introduction to thesis

1.1 Statement of problem

This thesis documents the stratigraphy, sedimentology, geochemistry, and diagenesis of unusual carbonate mounds of the Ikpiarjuk Formation (Baffin Island, Nunavut). The Ikpiarjuk Formation consists of a group of very large (kms long and hundreds of metres thick), isolated carbonate mounds that developed in deep water along intragaben fault zones, presumably related to fluid venting along faults, in the Mesoproterozoic Milne Inlet Graben (MIG) of the Borden basin (Baffin Island, Nunavut). Previous studies on contemporaneous black shale in the MIG show geochemical evidence of an anoxic deep-water environment (Turner and Kamber, 2012). The purpose of this project is to test the hypothesis that the mounds formed due to fluid venting along fault zones and to investigate how the various components of these unusual dolostone mounds formed.

The Borden Basin Project is a multi-year academic study supported by the Canada-Nunavut Geoscience Office and based at Laurentian University (Sudbury, Ontario). The project was developed to evaluate the geological history and economic potential of Mesoproterozoic basins in eastern Nunavut (Turner et al., 2012). This PhD research project is one of five sub-projects of the Borden Basin Project. The Borden Basin is a Mesoproterozoic sedimentary basin that is located on northwestern Baffin Island in the Canadian Arctic Archipelago. The basin contains up to 6 km of supracrustal rocks (Bylot Supergroup) that unconformably overlie crystalline basement of the Rae Province. Part of the basin is a known Zn district, including the Nanisivik mine (in operation from 1976-2002) as well as numerous other unstudied Zn showings. The basin is relatively

underexplored for both Zn and other metals. The basin was initially mapped and its stratigraphic units established as the product of a Geological Survey of Canada mapping project in the 1970s (Jackson and Iannelli, 1981; Scott and deKemp, 1998). More focused stratigraphic work in the early 2000s identified inconsistencies in the description of a thick and widespread carbonate unit in the lower Bylot Supergroup (formerly the Society Cliffs Formation) and resulted in its subdivision into four new formations (Turner, 2009). The Ikpiarjuk Formation is one of these new formations, and consist of a group of isolated very large (>200 m thick, >5 km long) dolostone bodies that are not comparable with any descriptions of conventional Precambrian carbonate lithofacies.

The Ikpiarjuk Formation mounds lack “normal” Mesoproterozoic reefal facies (stromatolites) and their association with enclosing deep-water strata is unique among Mesoproterozoic carbonate rocks. Lithofacies of associated level-bottom environments indicate that the mounds grew below the photic zone and below storm wave-base (Turner, 2009). Subtly clotted textures, comparable to thrombolites, are present in outcrop, which suggests that mound formation may have in part been influenced by microbial activity. Mounds are elongate parallel to syndepositional faults and may have grown along sea-floor fissures that vented fluids. The mounds represent relict seep deposits that accumulated where seeping fluid mixed with basin water and precipitated carbonate. Specific research questions, aimed at fully deciphering the depositional history of the mounds, are outlined below.

1.2 **Research questions**

- *Were there vents, and if so what was their composition?*

The chemistry of the vent fluid has major implications for evaluating the economic potential of the basin, and understanding the types of microbes that may have been exploiting vent fluid. Turner (2004a; Turner, 2009) originally suggested that a major component of the vent fluid was methane, given the similarities in textures of the mounds with modern methane seep deposits. Carbonate minerals incorporate the rare earth elements (REE) into their crystal structure in a predictable manner, usually without fractionating the REEs from the water from which the carbonate precipitates (e.g., Webb and Kamber, 2000). The presence of vent fluid and its chemistry was evaluated through investigating the REE composition of mound-derived carbonate as well as stable C and O isotopes.

- *What was the chemistry of the basin water?*

A major topic of study in Proterozoic sedimentary basins is the redox state of basin water and how that links to the evolution of the ocean-atmosphere system through time. The Ikpiarjuk Formation mounds provide a unique opportunity to model the chemistry of deep water in a restricted sedimentary environment from the perspective of carbonate rocks, rather than the more usual method of iron formations (Paleoproterozoic, Neoproterozoic) or shale (e.g., Planavsky et al., 2010). The REEs, were investigated in the Ikpiarjuk Formation mounds in order to test whether a redox-stratified water column was present in the MIG.

- *What types of microbes lived in the vicinity of vents?*

Chemotrophic organisms have long been implicated in the early evolution of life, but very little fossil evidence has been documented (e.g., Westall, 2015). Rare microfossils have been preserved in black smoker environments, and in one occurrence in phosphate

nodules, but there are no macroscopic buildups of carbonate related to chemotrophic organisms in the Precambrian (Lepland et al., 2013). The clotted texture in the Ikpiarjuk Formation was investigated in order to determine whether a microbial component was present, and if it was in fact chemotrophic.

- *What are the economic implications of these repeatedly reactivated fault-zones?*

The fault zones that the mounds nucleated over of are hypothesised to represent long-lived structures, which intermittently through the basin history could have been porous zones of fluid flow. The Nanisivik Zn-Pb deposit, along with numerous other base metal showings through the Borden basin, is known to be contemporaneous with deposition of the upper Bylot Supergroup (Turner, 2011). The fluid-flow history through the Ikpiarjuk Formation was explored through various microanalytical techniques.

1.3 Regional geology

The Borden Basin is one of the Bylot basins, a group of four basins exposed in northeastern Nunavut and northwestern Greenland. The basins were at one time interpreted to have formed during rifting related to the Mackenzie igneous event (ca. 1270 Ma; LeCheminant and Heaman, 1989), based on geochemical similarities between basalt of the Mackenzie igneous event and basalt preserved at the base of the basin-filling succession in the Bylot basins (Nauyat Formation; Jackson and Iannelli, 1981; Dostal et al., 1989). The depositional age of black shale near the base of the basin is now known to be ca. 1.1 Ga, and rifting during deposition of the black shale has been linked to tectonic stress associated with the amalgamation of Rodinia (Long and Turner, 2012; Turner and Kamber, 2012), so most, if not all, of the succession is ≤ 1.1 Ga. The entire basin is cross-

cut by dykes of the Franklin large igneous province (ca. 720 Ma; Heaman et al., 1992; Pehrsson and Buchan, 1999; Denyszyn et al., 2009).

The Borden Basin contains three fault-bounded troughs, the largest of which is the Milne Inlet graben (MIG), which contains the Nanisivik Zn-Pb deposit, all of the known base-metal showings, and the unusual dolostone mounds of the Ikpiarjuk Formation. The MIG is bounded by northwest-trending synsedimentary faults and is filled with the ~6-km-thick Bylot Supergroup (Jackson and Iannelli, 1981).

The tectonic history of the basin is complex and has been recently revised (Turner, 2009, 2011; Long and Turner, 2012; Turner and Kamber, 2012). The current model proposes that the Borden basin initially formed during mild extension accompanying the Mackenzie igneous event. Tholeiitic basalt erupted subaqueously during this phase and was then overlain by marine sand represented by the Adams Sound Formation, deposited during a phase of thermal relaxation (Long and Turner, 2012).

Significant extension began during deposition of the Arctic Bay Formation (Turner and Kamber, 2012), with the first appearance of graben-like geomorphic features. During this stage, the basin deepened to the northwest and deepened upward. This stage of basin development was characterised by synsedimentary slope failures adjacent to deep-water fault zones, which resulted in pronounced lateral thickness and lithofacies changes (Turner and Kamber, 2012). Wedges of detrital material (Fabricius Fiord Formation; Jackson and Iannelli, 1981; Scott and deKemp, 1998) were deposited at the margins of the MIG, marking the initiation of localised sedimentation into newly formed grabens, and also in the vicinity of subaqueous fault scarps (Turner, 2004b). During a phase of

extension that coincided with deposition of black shale of the upper Arctic Bay Formation, fluid venting through active faults resulted in the voluminous accumulation of deep-water dolostone, the highly distinctive carbonate mounds of the Ikpiarjuk Formation (Turner, 2004a, 2009).

The dolostone mounds (Ikpiarjuk Formation) are underlain and surrounded by black shale of the Arctic Bay Formation, and are interpreted to have formed beneath wave-base and below the photic zone (Turner 2004a, 2009; Hahn and Turner, 2013). The mounds are linear in plan view and are parallel to mapped or inferred faults that were known to be active during their formation. The mounds are characterised by two dominant lithofacies: clotted carbonate that formed as a benthic precipitate and characterises large zones in the mound centres, and featureless carbonate, which formed as a mud-grade water-column precipitate and represents the bulk of the mounds, including void-fills among benthic clots. Field relationships show that the mounds formed during subaqueous fluid venting along fault zones during accumulation of black shale. Several of the mounds are associated with smaller ‘moundlets’ (tens of metres in scale) that are stratigraphically lower than the main mound and are dominated by the clotted (benthic) lithofacies.

Fluid expulsion ended at the same time as an abrupt shift from deposition of black shale to accumulation of deep-water, laminated carbonate strata in the northwestern part of the MIG (Nanisivik Formation; Turner 2009, 2011).

Following deposition of the Nanisivik and laterally equivalent (southeast) Angmaat formations, the basin was uplifted and tilted to the northeast, and underwent significant subaerial erosion (Turner, 2011). The basin was then resubmerged, as revealed by

overlying shale and limestone of the Victor Bay Formation that were deposited throughout the basin as a northwest-deepening ramp during an interval of tectonic quiescence (Sherman et al., 2000, 2001, 2002; Turner, 2011). The Victor Bay Formation was then tilted to the northeast such that northwestern strata were subaerially eroded, but southeastern locations were drowned (Athole Point Formation; Sherman et al., 2002). The tectonic history of the upper part of the succession (Nunatsiaq Group) records a major influx of terrigenous clastic material in a shallowing-upward succession (Knight and Jackson, 1994).

1.4 **Methods**

The Ikpiarjuk Formation is exposed as massive, resistant-weathering cliffs along valleys through the Milne Inlet Graben. Access through cliffs is limited owing to the very steep and treacherous exposures. Stratigraphic sections were measured at breaks in the cliffs where access permitted, and were sampled at approximately 5 m vertical spacing.

Because there is no bedding in the mounds, and the enclosing strata are relatively flat-lying, sample spacing was measured using a vertical range pole set to 1.5 m. Where it was not possible to measure vertical sections, the relationship of mounds with enclosing strata was documented by mapping lateral facies changes along mound-tops.

All samples (~300) were cut into slabs and documented under a low-powered binocular microscope. Samples collected by E. Turner between 2003 and 2008 were also examined under binocular microscope during this study (~450 samples). Unpolished thin sections (150 samples), polished thin sections (50 samples), and polished thick sections (10 samples) were prepared from samples collected by the candidate and analysed using

standard petrographic methods. Cathodoluminescence petrographic analyses were completed on polished thin sections, and standard fluid inclusion microthermometry was completed on polished thick sections. Major, minor, and trace elements were analysed using both in situ laser-ablation ICP-MS on unpolished thin sections, and using solution ICP-MS on samples that had been microdrilled from cut slabs. Stable isotope analyses undertaken both on powder that had been microdrilled from slabs, and using in situ techniques on thin sections. Details of each analytical method are outlined in chapters 2 through 4.

1.5 Structure of thesis

This dissertation is presented in five chapters. Chapters 2-4 are written as manuscripts for publication in refereed scientific journals. Each of these manuscripts will be published as independent articles, so there is repetition in the introduction and geological setting of each chapter.

Chapter 2 is a manuscript published paper entitled “**Deep-water seep-related carbonate mounds in a Mesoproterozoic alkaline lake, Borden Basin (Nunavut, Canada)**” (published 2015, *Precambrian Research*, vol. 271, p. 173-197). This paper presents a trace element study, with emphasis on the REEs, on least-altered samples from four mounds of the Ikpiarjuk Formation (Uluksan, Red Rock, Bellevue, and K-Mesa mounds). The paper proposes that the Borden basin was filled with an alkaline lake during deposition of the Ikpiarjuk Formation, and that the fluids that caused mound precipitation were derived from modified basin-water brines that vented along fissures in the basin floor.

Chapter 3 is written as a manuscript entitled “**Composition and history of giant lacustrine carbonate seep mounds, Mesoproterozoic Borden Basin, Arctic Canada**”.

Part of Chapter 3 was published as a technical report entitled “**Deep-water carbonate mound lithofacies, Borden Basin, Nunavut**” (*published 2013, Geological Survey of Canada, Current Research, 2013-11, 14 p.*). Chapter 3 is formatted to be submitted to the journal Precambrian Research. Chapter 3 includes detailed field descriptions of the mounds, as well as detailed results of petrographic analyses. Chapter 3 classifies the Ikpiarjuk Formation as microbial buildups that were formed by chemotrophic microbes together with abiogenic precipitation of pelagic carbonate mud.

Chapter 4 is written as a manuscript entitled “**Diagenetic history of deep-water carbonate mounds in the Mesoproterozoic Nanisivik zinc district, Nunavut**” (to be submitted). Chapter 4 is a diagenetic study that documents the fluid-flow history through the Ikpiarjuk Formation mounds from Mesoproterozoic to Cenozoic, and compares cement phases to those in the Nanisivik Zn-Pb deposit.

1.6 **Statement of responsibilities**

Field work and sample collection was completed by the candidate with the assistance of T. Chevrier (2011) and J. Mathieu (2012). Field work was completed over two summer field seasons (2011 and 2012) and five field exposures of mounds were visited. The results in Chapter 3 include information from samples and field data collected by E. Turner during summer field work between 2001 and 2009. It was not possible for the candidate to visit all field sites due to logistical constraints.

All samples were cut by the candidate and thin sections were prepared by Willard Desjardins at Laurentian University. Sample selection and preparation for stable C and O isotopes and solution ICP-MS was completed by the candidate. Petrography, microthermometry, and SEM-EDS analysis were completed by the candidate at Laurentian University. In situ LA-ICP-MS was completed by Dr. Joe Petrus with assistance by the candidate in the Geochemical Fingerprinting Laboratory at Laurentian University. Raw data reduction of LA-ICP-MS data was completed by the candidate with the assistance of J. Petrus. Solution ICP-MS was completed by Dr. Michael Babechuk with assistance by the candidate at Trinity College, Dublin. The raw data reduction was completed by M. Babechuk. Samples were analysed for stable C and O isotopes at the G.G. Hatch isotope lab at University of Ottawa. Samples for SIMS oxygen isotope analysis were prepared and analysed by Ryan Sharpe at the University of Manitoba.

1.7 **Statement of original contributions**

The following points outline the original contributions made by this study:

- Documents the sedimentology of the Ikpiarjuk Formation. No detailed sedimentologic study has been published thus far.
- Documents the stratigraphy of the Ikpiarjuk Formation through the entire Borden basin (a combination of field work completed by the candidate and unpublished data from E. Turner). No previous publications have provided a detailed field description of the Ikpiarjuk Formation.
- Provides the first geochemical data set (major, minor, and trace elements) for the Ikpiarjuk Formation.

- Provides a new interpretation that the Borden basin was filled with an alkaline lake during deposition of the Ikpiarjuk Formation.
- Provides the first macroscopic evidence of chemotrophic microbes in the Precambrian.
- Provides the first diagenetic study of fluid flow through the Ikpiarkjuk Formation

1.8 References

Denyszyn, S.W., Halls, H.C., Davis, D.W. and Evans, A.D. 2009: Paleomagnetism and U-Pb geochronology of Franklin Dykes in High Arctic Canada and Greenland: a revised age and paleomagnetic pole constraining block rotations in the Nares Strait region; *Canadian Journal of Earth Sciences*, v. 46, no. 9, p. 689–705.

Dostal, J., Jackson, G.D. and Galley, A. 1989: Geochemistry of Neohelikian Nauyat plateau basalts, Borden rift basin, northwestern Baffin Island, Canada; *Canadian Journal of Earth Sciences*, v. 26, no. 11, p. 2214–2223.

Hahn, K.E. and Turner, E.C. 2013: Deep-water carbonate mound lithofacies, Borden Basin, Nunavut; *Geological Survey of Canada, Current Research 2013-11*, 14 p.

Heaman, L.M., LeCheminant, A.N. and Rainbird, R.H. 1992: Nature and timing of Franklin igneous events, Canada: implications for a late Proterozoic mantle plume and the break-up of Laurentia; *Earth and Planetary Science Letters*, v. 109, no 1–2, p. 117–131.

- Jackson, G.D. and Iannelli, T.R. 1981: Rift-related cyclic sedimentation in the Neohelikian Borden Basin, northern Baffin Island; *in* Proterozoic Basins of Canada, Geological Survey of Canada, Paper 81-10, p. 269–302.
- Knight, R.D. and Jackson, G.D. 1994: Sedimentology and stratigraphy of the Mesoproterozoic Elwin Subgroup (Aqigilik and Sinasiuvik formations), uppermost Bylot Supergroup, Borden rift basin, northern Baffin Island; Geological Survey of Canada, Bulletin 455, p. 48.
- LeCheminant, A.N. and Heaman L.M. 1989: Mackenzie igneous events, Canada: Middle Proterozoic hotspot magmatism associated with ocean opening; *Earth and Planetary Science Letters*, v. 96, no. 1–2, p. 38–48.
- Lepland, A., Joosu, L., Kirsimäe, K., Prave, A.R., Romashkin, A.E., Crne, A.E., Martin, A.P., Fallick, A.E., Somelar, P., Upraus, K., Mänd, K., Roberts, N.M.W., Van Zuillen, M.A., Wirth, R., Schreiber, A., 2014, Potential influence of sulphur bacteria on Palaeoproterozoic phosphogenesis: *Nature Geoscience*, v. 7, p. 20-24
- Long, D.G.F. and Turner, E.C. 2012: Tectonic, sedimentary and metallogenic re-evaluation of basal strata in the Mesoproterozoic Bylot basins, Nunavut, Canada: are unconformity-type uranium concentrations a realistic expectation?; *Precambrian Research*, v. 214–215, p. 192–209.
- Pehrsson, S.J. and Buchan, K.L. 1999: Borden dykes of Baffin Island, Northwest Territories: a Franklin U-Pb baddeleyite age and a paleomagnetic reinterpretation; *Canadian Journal of Earth Sciences*, v. 36, no. 1, p. 65–73.

Planavsky, N., Bekker, A., Rouxel, O.J., Kamber, B.S., Hofmann, A., Knudsen, A. and Lyons, T.W., 2010. Rare earth element and yttrium compositions of Archean and Paleoproterozoic Fe formations revisited: new perspectives on the significance and mechanisms of deposition. *Geochimica et Cosmochimica Acta* 74, 6387–6405.

Scott, D.J. and de Kemp, E.A. 1998: Bedrock geology compilation, northern Baffin Island and northern Melville Peninsula, Northwest Territories; Geological Survey of Canada, Open File 3633.

Sherman, A.G., James, N.P. and Narbonne, G.M. 2000: Sedimentology of a late Mesoproterozoic muddy carbonate ramp, northern Baffin Island, Arctic Canada; *in* Carbonate Sedimentation and Diagenesis in the Evolving Precambrian World, J.P. Grotzinger and N.P. James (ed.); Society for Sedimentary Geology (SEPM), Special Publication 67, p. 275–294.

Sherman, A.G., James, N.P. and Narbonne, G.M. 2001: Anatomy of a cyclically packaged Mesoproterozoic ramp in northern Canada; *Sedimentary Geology*, v. 139, p. 171–203.

Sherman, A.G., James, N.P. and Narbonne, G.M. 2002: Evidence for reversal of basin polarity during carbonate ramp development in the Mesoproterozoic Borden Basin, Baffin Island; *Canadian Journal of Earth Sciences*, v. 39, p. 519–538.

Turner, E.C. 2004a: Kilometre-scale carbonate mounds in basinal strata: implications for base-metal mineralization in the Mesoproterozoic Arctic Bay and Society Cliffs formations, Borden Basin, Nunavut, Geological Survey of Canada, Current Research 2004-B4, 12 p.

- Turner, E.C. 2004b: Origin of basinal carbonate laminites of the Mesoproterozoic Society Cliffs Formation (Borden Basin, Nunavut), and implications for base-metal mineralization; Geological Survey of Canada, Current Research 2004-B2
- Turner, E.C. 2009: Mesoproterozoic carbonate systems in the Borden Basin, Nunavut; Canadian Journal of Earth Sciences, v. 46, no. 12, p. 915–938.
- Turner, E.C. 2011: Structural and stratigraphic controls on carbonate-hosted base metal mineralization in the Mesoproterozoic Borden Basin (Nanisivik District), Nunavut; Economic Geology, v. 106, no. 7, p. 1197–1223.
- Turner, E.C. and Kamber, B.S. 2012: Arctic Bay Formation, Borden Basin, Nunavut (Canada): basin evolution, black shale, and dissolved metal systematics in the Mesoproterozoic ocean; Precambrian Research, v. 208–211, p. 1–18.
- Turner, E.C., Kamber, B.S., Kontak, D.J., Long, D.G.F, Hnatyshin, D., Creaser, R., Morden, R. and Hahn, K. 2012: Economic potential of the Mesoproterozoic Borden Basin zinc district, northern Baffin Island, Nunavut: update 2011–2012; *in* Summary of Activities 2012, Canada-Nunavut Geoscience Office, p. 1–12.
- Webb, G. E., and Kamber, B.S., 2000. Rare earth elements in Holocene reefal microbialites; a new shallow seawater proxy. *Geochimica et Cosmochimica Acta* 64, 1557-1565.
- Westall, F., Campbell, K.A., Bréhéret, J.G., Foucher, F., Gautret, P., Hubert, A., Sorieul, S., Grassineau, N., Guido, D.M., 2015, Archean (3.33 Ga) microbe-sediment systems were diverse and flourished in a hydrothermal context: *Geology*, v. 43, no. 7, p. 615-618

Chapter 2

2. Deep-water seep-related carbonate mounds in a Mesoproterozoic alkaline lake, Borden Basin (Nunavut, Canada)

Katherine E. Hahn¹, Elizabeth C. Turner¹, Michael G. Babechuk² and Balz S. Kamber²

¹Department of Earth Sciences, Laurentian University, 935 Ramsey Lake Road, Sudbury, ON, Canada, P3E 1R9

²Department of Geology, Museum Building, Trinity College Dublin, Dublin 2, Ireland

2.1 Abstract

The Mesoproterozoic (1.1 Ga) Borden Basin contains extremely large, deep-water dolostone seep mounds (Ikpiarjuk Formation) whose distribution is controlled by faults. Four mounds were investigated along measured stratigraphic sections. Petrographic study revealed several depositional components, and a mixture of at least two distinct carbonate sources. Stable isotope data showed no significant methane contribution to the carbonate phases. Detritus-corrected REE+Y patterns, obtained using solution ICP-MS, depict binary mixtures between basin-water-derived precipitates and seep-fluid-derived carbonate. The purest pelagic REE+Y signal is from mound tops, suggesting that mound accumulation ceased when the seep fluid waned. The REE+Y pattern of the pelagic precipitates resembles that of modern alkaline lake water. The shale-normalised pattern of the basin water is LREE-depleted, has a positive Ce anomaly and pronounced Y-

excess, but lacks the La and Gd anomalies typical of seawater. The seep-fluid-related dolomite has flat shale-normalised REE+Y patterns, no Ce anomaly, and a negative Eu anomaly. This combination of characteristics points to circum-neutral (Ca and Mg-bearing?) fluids that interacted with the underlying basement before seeping into the lake bottom through faults. The chemostratigraphic patterns of the mounds result from the relative contribution of elements from the basin water vs. seep fluids. When combined with published geochemical data for coeval black shale surrounding the mounds, the new data suggest a lacustrine setting, surrounded by catchments with a preponderance of moderately to strongly weathered alkali basalt whose runoff drove the lake to alkalinity. Seep fluid was probably evaporatively concentrated basin water that acquired new geochemical characteristics both during evaporation and through water-rock interaction in the subsurface. The new understanding of this depositional stage of the Borden Basin highlights the importance of lacustrine deposits in the Mesoproterozoic, and presents an obvious impediment to using carbonate stable isotope or trace element geochemistry to reconstruct global atmosphere-hydrosphere conditions for this time for any units that cannot be demonstrated conclusively to be of marine origin.

2.2 Introduction

The behaviour of the rare earth elements (REE+Y) in modern seawater is well understood and provides reliable information about water-column redox conditions (e.g., Elderfield and Greaves, 1982; Elderfield, 1988; Bau et al., 1997). In both the modern environment and the rock record, shallow-water carbonate microbialites have been established as good proxies for the REE+Y composition of seawater (e.g., Webb and Kamber, 2000;

Nothdurft et al., 2004; Allwood et al., 2010) and lake water (e.g., Bolhar and van Kranendonk, 2007; Awramik and Buchheim, 2009).

The Mesoproterozoic Milne Inlet graben (Borden Basin; ~1.1 Ga; Fig. 1) contains large, isolated, mound-shaped accumulations of dolostone related to fluid seepage along synsedimentary faults (Turner 2004a, 2009; Hahn and Turner, 2013). The mounds (Ikpiarjuk Formation; Turner, 2009) are enclosed by black shale and were deposited in deep water, below wave-base and below the photic zone (Turner, 2004a, 2009; Hahn and Turner, 2013). The mounds contain both featureless dolomudstone, inferred, based on sedimentary context and petrography, to have precipitated in the water column and then settled to the sea-floor (pelagic dolostone), and a clotted texture that was probably produced by benthic carbonate precipitation in the presence of microbes. Precipitation of these carbonate materials is inferred to have been driven by fluid seepage at the basin floor and mixing of this fluid with basin water, based on the geographic limitation of mounds to the immediate vicinity of regional fault systems. Although the mounds come from a comparatively deep-water setting, the seep-related carbonate mound lithofacies of the Ikpiarjuk Formation satisfy the main criterion that has established shallow-water microbialites as reliable proxies for ambient water REE composition (Webb and Kamber, 2000): they are composed predominantly of precipitated carbonate, and thus provide a petrographically “instantaneous” record of the fluid(s) from which they precipitated. Different types of fluid-seep-related accumulations of carbonate material are known in the rock record. Recent studies on modern seep deposits show that REE patterns of seawater may be preserved in the carbonate precipitates resulting from the interaction of seep fluids with seawater (e.g., Himmler et al., 2010).

The Ikpiarjuk Formation mounds consist of deep-water hydrogenous carbonate rocks that provide an alternative, and possibly unique, avenue for making observations about the depositional environment of Mesoproterozoic carbonates. This study presents data collected through a combination of in situ LA-ICP-MS and high-sensitivity solution ICP-MS, in an attempt to (a) chemically distinguish pelagic and benthic carbonate facies, (b) reconstruct the geochemistry of basin water and vent fluids, and (c) constrain the redox chemistry of the Mesoproterozoic Borden Basin.

2.3 **Geologic Setting**

2.3.1 *Regional setting and stratigraphy of the Milne Inlet Graben*

The Borden Basin is one of a several late Mesoproterozoic intracratonic basins in Canada's Arctic archipelago. The depositional age of most of the basin-filling strata is now known to be approximately 1.1 Ga or younger (Turner and Kamber, 2012), and the basin's origin is probably related to tectonic stress associated with the assembly of Rodinia (Long and Turner, 2012). Strata of the Borden Basin lie unconformably on undifferentiated Paleoproterozoic and Archean crystalline rocks of the Rae Province. The Borden Basin consists of three "troughs" (Jackson and Iannelli, 1981), the largest of which is the Milne Inlet graben (MIG; Fig. 1). The MIG is bounded by northwest-trending faults and is filled by the ~6 km-thick Bylot Supergroup (Jackson and Iannelli, 1981; Scott and deKemp, 1998; Fig. 2). These strata are cross-cut by northwest-trending Franklin-aged dykes (~723 Ma; Heaman et al., 1992; Pehrsson and Buchan, 1999; Denyszyn et al., 2009).

The basin initially formed during mild extension, when tholeiitic basalt of the Nauyat Formation (Jackson and Iannelli, 1981; Dostal et al., 1989) erupted subaqueously (Long

and Turner, 2012). Marine sandstone of the Adams Sound Formation was deposited regionally above the basalt during sag-phase sedimentation (Long and Turner, 2012). Pronounced extension began only during deposition of the westward-deepening and deepening-upward siliciclastic succession of the Arctic Bay Formation, of which the upper part, in the northwestern MIG, is a thick black shale (Turner and Kamber, 2012). This black-shale phase of the northwestern MIG is characterised by pronounced lateral lithofacies and thickness changes, and synsedimentary slope failure in deep water near fault zones (Turner and Kamber, 2012). Pronounced faulting during deposition of the Arctic Bay Formation also initiated the development of a graben system, with associated deposition of graben-margin detrital wedges (Fabricius Fiord Formation; Jackson and Iannelli, 1981). During deposition of upper Arctic Bay Formation black shale, unusual carbonate mounds of the Ikpiarjuk Formation formed locally in the shale basin, probably as a result of fluid expulsion through active faults (Turner, 2004a; Turner, 2009; Hahn and Turner, 2013). A coeval, NW-deepening carbonate ramp, the Iqqittuq Formation, developed in the shallower, southeastern part of the basin (Turner, 2009). Fluid expulsion along the faults ended at approximately the same time as a major shift in sedimentation (Fig. 2); the carbonate ramp of the Iqqittuq Formation is overlain by a rimmed platform (Angmaat Formation) in the southeastern MIG, and black shale of the Arctic Bay Formation is overlain by deep-water laminated carbonate strata in the northwestern MIG (Nanisivik Formation; Turner, 2009, 2011). During at least the initial phase of Nanisivik and Angmaat formation deposition, the MIG was tectonically active (Turner, 2009). Local, subaqueous debris flows were shed off fault scarps in the basin (Turner, 2004b; 2009), and wedges of terrigenous clastic material were deposited along graben-bounding

faults (continued deposition of Fabricius Fiord Formation; Jackson and Iannelli, 1981; Scott and deKemp, 1998).

Following deposition of the Nanisivik and Angmaat formations, the MIG was twice uplifted and tilted to the northeast, and underwent significant erosion (Sherman et al., 2002; Turner, 2011). The tectonic history of the Nunatsiaq Group (upper part of the Bylot Supergroup) is less well understood, but probably reflects yet another type of basin regime that included a large influx of shallowing-upward terrigenous material (Knight and Jackson, 1994; Sherman et al., 2002).

2.3.2 *Ikpiarjuk Formation*

The Ikpiarjuk Formation (Turner, 2009) consists of regionally mappable but spatially delimited dolostone mounds. Evidence of six mounds is known from present-day exposure (Fig. 1). The elongate mounds, interpreted as fossilised cold-seep carbonate precipitates, are present only in the immediate vicinity of major intra-graben faults, and are kilometres long and hundreds of metres thick (Turner 2004a, 2009). Mounds are composed primarily of massive dolostone that is interpreted to have formed by deposition of particulate carbonate mud that precipitated in the water column. Large zones of the mounds, however, are characterised by millimetre- to centimetre-scale fine-grained crystalline carbonate clots surrounded by multiple generations of isopachous, fibrous, inclusion-rich carbonate cement. The clots and cement are interpreted as benthic precipitates that were produced by the interaction of vent fluid and basin water, and clot formation may have been mediated by a microbial community (Turner 2004a, 2009; Hahn and Turner, 2013). The Ikpiarjuk Formation mounds are unusual in that they accumulated as isolated build-ups, below the photic zone, each apparently representing

its own distinct carbonate factory. The mounds are coeval with black shale of the upper Arctic Bay Formation, and mound bases are interstratified with the black shale, supporting the concept that they formed in a comparatively deep-water setting. This suite of characteristics makes the mounds strikingly dissimilar to Proterozoic photic-zone stromatolite reefs.

The large-scale lithofacies distribution, shared by all mounds, is dominated by massive dolostone and areas of microbial clotted fabric. All mounds are flanked by mound-derived debrites, which indicates that there was significant topographic relief above the seafloor. Many of the mounds have sub-vertical centimetre- to decimetre-scale paleofractures near their tops, which are filled with mound-derived carbonate clasts and hematite-rich red cement (Fig. 5), and may relate to post-mound karsting.

The MIG is underlain by basement blocks (Iannelli, 1992; Turner, 2011) that are separated by the same intra-graben faults that are implicated in synsedimentary basin compartmentalisation during Arctic Bay Formation deposition (Turner and Kamber, 2012), subaqueous debris-flow generation during upper Ikpiarjuk Formation and lowermost Nanisivik Formation deposition (Turner, 2004b, 2009), and mound development (Fig. 3). The intra-graben and graben-margin faults were reactivated repeatedly from the Mesoproterozoic to the present (Jackson and Cumming, 1981; Turner, 2004b; 2009, 2011; Turner and Kamber, 2012), and therefore present-day displacements cannot be assumed to have a relation to offsets that prevailed at any time during the graben's depositional history. It is not possible to discern what the exact configuration of the basin-floor was during deposition of the Ikpiarjuk mounds, but the fact that most mounds are free from significant non-mound sediment suggests that basin-

floor topography was not generally pronounced enough in most locations to expose older rocks that could shed terrigenous clastic material. The fact that mounds probably had syndepositional relief on the scale of ≥ 100 m, based on flank geometry, also means that *in situ* mound-related carbonate surfaces would have been elevated above the level-bottom sea-floor, and thus spared from most turbiditic influxes of fine clastic material of the Arctic Bay Formation.

The present-day exposure of Ikpiarjuk Formation carbonate mounds is a function of Pleistocene glacial erosion, which produced broad valleys (typically >2 km wide) that follow the traces of the intra-graben faults across the Borden Peninsula. This means that the remaining mound exposures do not include the rocks that formed closest to the inferred linear sea-floor vents, and consist of material that was deposited slightly away from the centres of the vent systems; the nature of mound cores cannot be determined based on the outcrop exposures used in this study... Buried mound facies are known from drill-core from the Nanisivik mine property (Turner, 2004a, 2009), and preserved mound cores may be present elsewhere in the subsurface in the vicinity of faults, where the stratigraphic level of present-day exposure permits.

Ikpiarjuk Formation rock is almost completely massive; the lack of layering means that these rocks are among the most resistant-weathering and cliff-forming of all of the carbonate types present in the MIG. The contrast of weathering and erosional properties between the Ikpiarjuk Formation and the overlying Nanisivik, Angmaat, and (in at least one case) Victor Bay formations means that the upper contacts of mounds are generally poorly exposed (because the overlying units were eroded away), and that the upper limit of some mounds' exposures approximates the top of the Ikpiarjuk Formation.

2.4 Methods

This geochemical study is based on extensive, detailed field work in which vertical sections through mounds were measured and described. Samples were taken from outcrop at 5 m intervals through vertical sections of Red Rock mound, Bellevue mound, K-Mesa mound, and Uluksan mound (Fig. 1). All samples were cut into slabs from which regular, uncovered thin sections were produced for examination in plane- and cross-polarised light. Samples with no cross-cutting veins or coarse-grained replacement dolomite were selected for *in situ* laser ablation (LA)-ICP-MS. All material is dolomite, but the presence of primary sedimentary features (i.e., microbial clots and synsedimentary cement) suggests that dolomitisation occurred early during diagenesis, and was not fabric-destructive. It has been shown that REE+Y composition and stable C isotopic values are robust through diagenetic alteration to dolomite (e.g., Banner and Hanson, 1989). Petrographic and LA-ICP-MS results guided the selection of carbonate phases, which were then sampled for high-precision ultra-trace solution ICP-MS. Iron, Mn, and Sr are considered highly mobile during diagenesis and were also used to screen for “least altered” samples. The phases analysed included clots, early isopachous fibrous cement, dolomudstone, medium-grained featureless dolomudstone (inter-clot and as large masses), and coarsely crystalline burial dolospar.

2.4.1 Samples

2.4.1.1 Northwestern Milne Inlet Graben, Milne Block

Two very large mounds were sampled in the northwestern MIG. Red Rock Mound (Milne Block) is exposed for ~12 km along both sides of northwest-trending Red Rock Valley, along a splay of the TFZ (Figs. 1, 3, and 4a). A smaller “moundlet” is exposed

approximately 100 m stratigraphically below the main mound, surrounded by black shale of the upper Arctic Bay Formation. The main mound is ~150 m thick, underlain by black shale, and laterally flanked by black shale passing upward to Nanisivik Formation dolostone (Fig. 5a). The mound is dominated by clotted texture and has unstructured intraclast wackestone-floatstone debrite tongues that are interstratified with the Nanisivik Formation along its upper flanks (Fig. 4b and c; Turner, 2004a, 2009; Hahn and Turner, 2013). In one location, the top of the mound is in unconformable contact with the Victor Bay Formation.

Uluksan Mound (Milne Block/Tremblay Block) is exposed in 250 m-high, ~8 km-long cliffs west of the hamlet of Arctic Bay (Figs. 1 and 4d; type section of the Ikpiarjuk Formation; Turner, 2009) and is thinly overlain by the Nanisivik Formation (Fig. 5b). This mound's core is dominated by massive, seemingly featureless dolomudstone, from which a small suite of samples was analysed.

2.4.1.2 *Central MIG, Tremblay Block and Magda Block*

Two mounds were studied in the central MIG (Figs. 1 and 3). Bellevue Mound (Tremblay Block / Milne Block; Fig. 3) is exposed as resistant cliffs ~5 km long; 250 m thick) along the Alpha River valley in the Tikirarjuaq Fault Zone (TFZ). Two moundlets enclosed by outer-ramp strata of the Iqqittuq Formation are dominated by clotted texture and are stratigraphically lower than the main mound (Fig. 4e). Bellevue Mound is underlain by black shale of the upper Arctic Bay Formation. The southeastern lower margin of the mound is interstratified with outer-ramp strata of the Iqqittuq Formation, and the southeastern upper margin is overlain by shallow-water dolostone lithofacies of the Angmaat Formation. Bellevue Mound's northwestern lower margin is interstratified with

black shale of the upper Arctic Bay Formation, and its upper margin is interstratified with deep-water carbonate strata of the Nanisivik Formation (Fig. 5c). The central part of the exposure is erosionally truncated, and it is therefore unknown what may have overlain the mound, but ooid-filled Neptunian dykes cross-cut upper parts of the mound, suggesting that the mound was overlain by shallow-water ooid shoals, a common lithofacies of the Angmaat Formation in the area (Fig. 5c).

A vertical section measured through the main part of the mound is dominated by massive, featureless dolostone, with minor zones of a subtly clotted texture. The top of the mound contains vertical paleofractures filled with mound clasts and purple hematitic dolomite cement. Ooid shoals of the Angmaat Formation onlap and overlie the easternmost part of Bellevue Mound.

K-Mesa Mound (Magda Block; Fig. 3) is an isolated mesa near the Magda Fault Zone (MFZ; Fig. 1), ~50 km south of Bellevue Mound in a separate sub-graben (Fig. 3; Iannelli, 1992; Turner, 2009, 2011). The mound is approximately 7 km long and ~150 m thick. Smaller moundlets stratigraphically below the main mound and enclosed by Arctic Bay Formation shale (Fig. 4f), are characterised by clotted texture. The main mound is characterised by a complicated lithofacies association of clots, benthic precipitates and breccias. The mound passes up-section into ooid dolograinstone, which is in turn overlain by laminated dolostone of the Nanisivik Formation (Fig. 5d).

2.4.2 LA-ICP-MS analytical details

In situ LA-ICP-MS analyses were performed on unpolished and uncovered thin sections using a RESolution M-50 laser attached to an X-Series II quadrupole mass spectrometer at Laurentian University (Sudbury, Canada). Samples were analysed with a 103 µm spot

size at 5 Hz with a fluence of ca. 6 J cm^{-2} . The aerosol was carried to the ICP-MS in ultra-pure He and ionisation was enhanced with a 5 ml min^{-2} addition of ultra-pure N_2 to the auxiliary Ar stream. A combination of line scans and spot analyses was performed on discrete components of the dolostone in order to explore the chemical characteristics of the petrographically defined carbonate components. Both late-stage, burial-related, coarsely crystalline dolomite and dolomitised primary fabrics were analysed, in order to test for the effect of late diagenetic alteration on trace element systematics (Fig. 6). The REE concentration in the samples analysed, especially the HREEs, was close to the detection limit of the instrument, and therefore the data are not as precise as the solution ICP-MS data. The LA-ICP-MS data were used as a pre-screening method to select samples and are not reported in this study.

2.4.3 *Solution ICP-MS analytical details*

The LA-ICP-MS data were used to guide the preparation of material for solution ICP-MS analysis (Baldwin et al., 2011). Very small aliquots of carbonate powder (0.1 to 1 mg) were drilled from thin section offcuts using a 1 mm diameter steel drill bit under a binocular microscope in order to extract specific carbonate phases with minimal contamination from surrounding material. Late-stage veins and evidence of terrigenous material (e.g., stylolites) were avoided. Some samples proved to be contaminated in Mo, W, and V from the steel bit. These samples are identified in the data table and their Mo, W, and V were not used for plots and in the discussion. Other elements remained unaffected.

Digestion, dilution, and trace element analysis were performed at Trinity College Dublin, under clean-room conditions. Carbonate powders were transferred to pre-cleaned 2 mL micro-centrifuge tubes. The powder was transferred without weighing, because the amount of powder was too small to be recorded accurately (<1 mg). Samples were digested by adding 1.5 mL of ultra-clean 5% HNO₃ to the micro-centrifuge tubes and left to react overnight. From this stock solution, a diluted sample totalling 2 g was prepared gravimetrically to 2% HNO₃ with internal standards ⁶Li, Re, Rh, Bi, and ²³⁵U added. The diluted samples were vortexed and centrifuged prior to analysis. Trace element analysis was performed using a Thermo iCAPQs coupled to an ESI SC-2 DX autosampler equipped with a microFAST sample introduction system. Silicate standards were digested using in-house triply distilled HF and HNO₃ following the method for terrestrial samples outlined in Babechuk et al. (2010), and were diluted in 2% HNO₃ and spiked with the same internal standards as the sample unknowns. Oxide production rates, which are important for precise and accurate REE analysis, were determined by analysing pure element solutions prior to the experiments (Ulrich et al., 2010). Trace element analyses were performed in two experimental runs, which also included procedural blanks, USGS silicate rock standards (W-2, JA-3, BCR-2), the carbonate standard BR-1, and drift monitors (dilute standard solutions), following the methods of Eggins et al. (1997), with modifications explained in Kamber (2009). Samples were loaded into a 1.5 mL teflon tube loop, from which they were injected (with the aid of a micro-peristaltic pump) over a 7-minute period through a teflon nebuliser into a Peltier-cooled double-pass spray chamber at a rate of 220 µl min⁻¹.

Trace element and major element (Ca, Mg, Al, Mn, Fe) data were analysed for each sample and the instrument response was processed offline with a sequence of steps: internal and external drift correction, oxide interference correction, blank subtraction, and calibration. The corrected instrument intensities were calibrated with the average of several analyses of the standard W-2 from the same experiment using the preferred values reported in Kamber (2009) for the trace elements and the accepted W-2 USGS values for the major elements. Due to the unmeasurable mass of powder, the element concentrations measured in solution were scaled to a total CaO+MgO sum of wt. % of 52 to approximate the concentration per mass of dissolved carbonate (dolomite). The absolute trace element concentrations are of secondary importance to the interpretation of the data in the present study, which relies primarily on the shape and features of the normalised REE+Y patterns and trace element ratios.

Full procedural blanks from the method applied to carbonate samples, using the same triply distilled HNO₃, contained average REE and Y concentrations in units of 10⁻¹⁵ (ppq) as follows: La (152), Ce (197), Pr (29), Nd (89), Sm (21), Eu (4), Gd (32), Tb (5), Dy (24), Ho (5), Er (12), Tm (2), Yb (16), Lu (1), and Y (188). Procedural blank values of the REE+Y never exceeded the analytical response for sample unknowns on the ICP-MS by more than 10% (for samples with the lowest amount of powder) and were mostly negligible (<1%). Samples with the highest blank to analytical response ratio showed no significant change in the shape of the normalised rare earth element pattern or pertinent trace element ratios (e.g., Y/Ho, Pr/Yb, Pr/Dy) with or without blank correction.

2.4.4 Stable C and O isotope analysis

Samples for stable C and O isotope analysis were taken following the same protocol as for the solution ICP-MS work. Approximately 0.5 mg of sample powder was weighed into glass vials followed by the addition of 0.1 ml of pure phosphoric acid to the side of the container. The containers were then capped and helium-flushed while horizontal to ensure no premature reaction of sample and acid. Samples were reacted at 50°C for 24 h, followed by extraction from sample vials in continuous flow. Measurements were performed at the G.G. Hatch Stable Isotope Lab (University of Ottawa) using a Delta XP mass spectrometer and Gas Bench II, both from Thermo Finnigan.

2.5 Results

2.5.1 REE+Y Systematics

The REE+Y data were initially normalised (Fig. 7a) to the modern upper continental crust proxy MuQ (Kamber et al., 2005). Anomalies were calculated as in Lawrence et al. (2006). In the MuQ normalisation, the patterns of many of the studied samples are relatively flat, depleted in the middle REE, have a negative Eu anomaly, and appear generally somewhat dissimilar to typical Proterozoic seawater patterns (e.g., Planavsky et al., 2010). This outcome could suggest a local REE+Y input (e.g., Kamber et al., 2004). Because the carbonate mounds are in a shale basin, it was possible to test the effect of normalisation using the local shale. For this, the average black shale REE+Y composition of the least carbonate-rich black shale samples (09SVC64, 09SVC66, and 09SVC68) of Turner and Kamber (2012) was used. By comparison with the generic normalisation, the local shale-normalised patterns are more LREE-depleted, have a steeper slope (Fig. 7b), lack the apparent depletion in the MREE, and have a diminished negative Eu anomaly.

This suggests that local shale normalisation may be more appropriate than MuQ in identifying how REEs fractionated in a basin that was isolated from global seawater.

The REE+Y normalised to local shale generally show slight depletion in LREEs, which leads to shallowly positively sloping patterns (Fig. 8). Uluksan (Fig. 8b) is the only mound for which patterns are consistently steep, whereas the samples from other mounds show variable steepness. It is also clear that many samples have variably developed positive Ce anomalies and negative Eu anomalies, and that strong positive Y anomalies are ubiquitous.

2.5.2 Detrital content

Trace amounts of detrital (siliciclastic) material can affect REE+Y patterns in hydrogenous (“chemical”) sediment (Webb and Kamber, 2000; Kamber et al., 2004). Such a detrital component was monitored in this study using Al content (a proxy for clay minerals) and a variety of incompatible elements with low solubility in seawater (e.g., Ti, Sc, Zr, Th, and Nb content). The stratigraphic distribution of Al, Zr, Th, and Nb does not correlate with intervals with unusual REE+Y patterns ($r^2 = 0.03$ at Bellevue Mound). At Red Rock Mound, the component of siliciclastic material was greater in pelagic dolomudstone than it was in benthic dolostone (Fig. 8), particularly in the sample taken closest to the mound top, which contains 0.332 wt% Al_2O_3 .

2.5.3 Redox-sensitive metal systematics (V, Mo and U)

The redox-sensitive metals V, Mo, and U were analysed alongside the REE+Y (Fig. 9). The absolute concentration of redox-sensitive elements is affected by the amount of clastic contamination, but this is readily corrected for by normalisation to Al. In this sample set, Al correlates well with the other tracers for detrital contamination, such as Th

($r^2 = 0.83$), Sc, Zr, and Nb (not shown), and Al-normalisation is therefore considered to be an accurate control for detrital contamination.

Red Rock Mound

The concentration of three redox-sensitive metals normalised to Al is plotted against stratigraphic elevation (Fig. 9a). Vanadium/Al and Mo/Al show similar patterns, whereas U/Al has more scatter, but its stratigraphic distribution is still comparable to V and Mo, with apparent enrichment more prominent at the base of the section. Although based on a very small dataset, weak correlations between lithofacies and metal abundance are present.

Superimposed on the stratigraphic trend is a correlation between metal abundance and lithofacies. Most notably, a higher V/Al and Mo/Al one sample (34 m) corresponds to a benthic fibrous carbonate cement (with slightly higher abundance of detrital material; Fig. 9a). By contrast, the stratigraphically equivalent dolomudstone is not metal-enriched. The benthic fibrous cement also differs in having a positive Eu anomaly. Where stratigraphically equivalent samples are present, in general, the benthic clotted dolostone and benthic cement lithofacies show a higher normalised metal abundance than the pelagic dolomudstone. A moderate negative correlation exists between the enrichment factor of Mo and Fe_2O_3 (Fig.10; $r^2=0.6$), but this relationship does not extend to other redox-sensitive metals ($U_{\text{ef}} r^2=0.01$; $V_{\text{ef}} r^2= 0.12$). No other relationships between redox-sensitive metal enrichment and other elements are noted.

Uluksan Mound

The enrichment factor of the redox-sensitive metals Mo, V, Ni, and Cr display coherent patterns in Uluksan Mound and a strong positive correlation to one another ($r^2=0.88-0.99$) This correlation must be interpreted with caution due to the small size of the sample set ($n=4$). In general, the abundance of most trace elements is low when normalised to Al, with enrichment in most transition metals at 83 m above the base of the mound. The distribution of U is different from that of the other redox-sensitive metals, and when normalised to Al, is most abundant at approximately 40 m from the base of the mound. The sample set for Uluksan mound is very small, and other units that are enriched in transition metals may exist. There is no correlation between transition metal abundance and abundance of detrital material, Fe, or any other elements.

Bellevue Mound

The abundance of the redox-sensitive metals U, V, and Mo is low in most Bellevue Mound samples and does not exhibit much variation stratigraphically, except at the top of the section (Fig. 9b), where there is uniform enrichment in all three metals. The stratigraphic trend of the metals does not correlate to that of elements associated with terrigenous detritus. Only two samples of benthic clotted dolostone were analysed, and one of these samples exhibits a higher enrichment in normalised metal abundance than its stratigraphically equivalent pelagic dolomudstone. The sample set is not large enough to characterise this finding as a trend.

Given that most samples from this mound express a negative Eu anomaly (Fig. 8), redox-sensitive elements were plotted against Eu/Eu^* (Fig. 10). There is a positive correlation between the Eu anomaly and a few of the elements that are typically enriched in seawater

(V $r^2=0.9$, U $r^2=0.6$; Fig. 11). A weaker positive correlation is present between Eu/Eu* and Mo, Sr, Fe, Y/Ho, and Ni. Weak negative correlations are present between Eu/Eu* and the Pr_n/Yb_n ratio, and Mn. There is no correlation between V or U and any of the monitors for detrital contamination (Th, Al, Zr, Sc), and so the abundance of metals measured is considered to be the true composition of the carbonate and not enriched owing to the presence of detrital material. The samples collected did not contain any petrographically visible organic matter, and metal enrichment is not considered to be related to organic-bound metals. Trace amounts of pyrite are present in some samples, but were avoided during microdrilling so metal enrichment is not related to pyrite.

K-Mesa Mound

The abundance of the redox-sensitive metals Cr, U, V, Mo, and Ni is low in most samples from K-Mesa Mound. There is some variability, but the spacing of samples is too coarse to identify any stratigraphic trends. In very broad terms, there is an enrichment of all trace metals in the uppermost sample, and variable concentration through the rest of the mound. The enriched sample from the mound top corresponds to the most significant positive Ce/Ce* anomaly.

2.5.4 Stable Isotopes

The $\delta^{13}\text{C}$ isotope values of the Ikpiarjuk Formation are between 0 and +4‰_{VPDB}, which is typical for carbonate rocks of this age (e.g., Bartley and Kah, 2004). There is no correlation present between $\delta^{13}\text{C}$ or $\delta^{18}\text{O}$ and lithofacies (clot, carbonate mud, cement). Overall, $\delta^{13}\text{C}$ and $\delta^{18}\text{O}$ are slightly lower at Uluksan Mound, but no other relationships

among mounds were documented (Fig. 12). There are no correlations between $\delta^{13}\text{C}$ and $\delta^{18}\text{O}$ and any of the trace elements or REE+Y.

2.6 Interpretation

2.6.1 *Origin of variation in REE +Y patterns*

In situ LA-ICP-MS analyses were used to guide micro-sampling for solution ICP-MS, with the intent of identifying the purest possible end-member carbonate facies (i.e., different REE+Y composition due to relative contribution from seep fluid and basin water). During LA-ICP-MS pre-screening, different depositional facies (clots, isopachous cement, pelagic dolomudstone) were analysed in the same thin section. The only major difference in resulting REE+Y patterns is the relative steepness of the patterns, and this was limited to steeper patterns in the pelagic dolomudstone. No systematic differences were apparent in REE+Y patterns between clots and overlying isopachous cement. Most layers of isopachous cement were too thin to sample with a microdrill, so the solution ICP-MS data set is effectively limited to pelagic dolomudstone and clots.

Samples that were found to contain high amounts of detrital material or were significantly altered due to burial were not sampled for solution ICP-MS. Readers are reminded that Banner and Hanson (1990) demonstrated that the REEs are often immobile through diagenesis, including dolomitisation, and that a very high amount of fluid-rock interaction must occur to alter carbonate REE patterns. Therefore, although the samples in this study are now dolomite, modification of carbonate REE+Y content by burial-related fluids is considered improbable. It is important that results for coarsely crystalline burial-related dolomite do not resemble the REE patterns or the recrystallized primary

fabrics. Although burial-related dolomite is depleted in LREEs, its pattern is different from that of the primary carbonate phases, and has extreme La depletion relative to the other LREEs. In addition to La depletion, burial dolomite differs from least-altered primary material in that it has $Y/Ho < 30$, displays no Eu anomaly, has very high Mn concentration ($>10x$), and has much lower Sr. Burial-related dolomite cement is considered to be completely chemically distinct from dolomitised primary fabrics.

From the exploratory in situ data, it was expected that in each mound, there would be a range in REE+Y compositions in the micro-drilled samples. The most conspicuous variation in mound REE+Y patterns is indeed in the degree of steepness, which is largely controlled by the extent of LREE-depletion. The steepness of the slope is conventionally quantified with the normalised Pr/Yb ratio. Note that Pr is the lightest of the LREE that does not exhibit anomalous behaviour in seawater (Lawrence and Kamber, 2006).

However, some samples of ancient carbonates (e.g. Kamber and Webb, 2001) have a flat to slightly negative slope in the heaviest REE, from Ho to Lu. This is also seen in a few of the samples studied here (Fig. 8). In order to compare the Mesoproterozoic samples with putative analogues, the steepness of the slope was also expressed with the normalised Pr/Dy ratio (Fig. 13), which avoids incorporating possible complexities from depletion in the heaviest HREE. In the normalised Pr/Dy vs. Pr/Yb plot, data from all of the mounds produced the expected strong positive correlations (Fig. 13a ($r^2=0.93$); 13b ($r^2=0.94$); 13c ($r^2=0.89$); 13d ($r^2=0.57$)). Mounds' $\delta^{13}C$ and $\delta^{18}O$ values do not correlate with Pr/Yb and Pr/Dy ratios.

The positions of all individual mound datasets in normalised Pr/Yb vs. Pr/Dy space is similar (Fig. 13), such that all samples could be combined into a single plot ($r^2 =$

0.84 Fig.14a). Combining the mounds' datasets confirms the impression from the individual plots, showing that all measured carbonates fall along a trend between steep normalized patterns and much flatter patterns. The samples from K-Mesa mound plot at slightly lower Pr/Yb, because overall, this dataset shows a depletion of the heaviest HREE. Of all mounds analysed, the detritus-corrected data from Red Rock mound show the largest spread in REE+Y slopes, ranging from the steepest to the flattest pattern. The interpretation of this mound's systematics will therefore be discussed first, and the other mounds will then be compared.

Red Rock Mound

Recalling that at Red Rock mound the siliciclastic content is greatest (though still relatively low; max. $\text{Al}_2\text{O}_3 = 0.33$ wt%), particularly in pelagic dolomudstone, a clastic contamination correction was applied to compare the shale-normalised end member REE patterns. Average Borden Basin black shale was subtracted from the measured element concentration according to the Al_2O_3 content, assuming a pure carbonate contained no Al at all. The steepest Arctic Bay Formation shale-normalised REE+Y patterns for Red Rock mound samples exhibit the following consistent features: overall depletion of the LREE, strong positive Y anomalies, Y/Ho ratios >30 , variably positive Ce anomaly, and lack of La and Gd anomalies (Fig. 14; both corrected and uncorrected for siliciclastic contamination). These patterns are envisaged to record precipitation of carbonate from ambient basin water during times of least intense seep-fluid venting. A diminished carbonate accumulation rate would also explain the generally elevated clastic content of carbonates with the steepest REE patterns.

The flattest of the Red Rock mound REE+Y patterns differ markedly from typical marine REE systematics (Fig.14b). Although the flattest of the Red Rock mound REE+Y patterns are from samples that contain an elevated siliciclastic component, the corrected data show that only the abundance of REEs changes, and not the overall pattern. Their slopes are nearly flat, and they show no La or Ce anomalies, but they have elevated Y/Ho. The flatness of the slopes is not caused by detrital contamination, and neither the Pr/Yb nor the Pr/Dy ratios correlate with Fe content ($r^2 \leq 0.01$), indicating that the patterns were not affected by incorporation of REE+Y scavenged onto Fe-oxhydroxides. It is therefore suggested that these patterns most closely approximate the REE+Y character of the seep fluid. Elevated Y/Ho is a characteristic of both seawater and saline groundwater. Fractionation has been documented in estuaries where freshwater mixes with saline water (Lawrence and Kamber, 2006), as well as in saline groundwater (e.g., Johannesson 2006). The elevated Y/Ho ratio suggests that seep fluid was saline, but the absence of a positive Eu anomaly strongly argues against a high-T, mid-ocean-ridge vent fluid, in which such anomalies are typically observed (e.g., Bau et al., 1997). In other words, in agreement with the geological context, there is no evidence for basin-floor spreading.

Uluksan Mound

The sample set from Uluksan Mound is small and displays the most coherent REE+Y patterns, with generally steep slopes resembling those of the pelagic dolostone from Red Rock mound (Fig. 8b). Uluksan Mound is the mound most distant from the shallow-water part of the MIG (Fig. 1). In this limited dataset, there is little evidence for REE+Y supply

from seep fluid, which is also evident from the narrow range in Pr/Yb vs. Pr/Dy (Fig. 13b).

Bellevue Mound

The REE+Y patterns from Bellevue Mound are similar to those from Red Rock Mound, and also have a large range in Pr/Yb vs. Pr/Dy (Fig. 13c), with a higher proportion of samples plotting near the range of the inferred seep-fluid end-member. The magnitude of the negative Eu anomaly varies through the stratigraphy, and disappears at the top of the mound. The Eu anomaly at Bellevue Mound correlates well with several trace elements and is discussed in a later section.

K-Mesa Mound

The REE+Y patterns from K-Mesa are slightly different from those of the other mounds (Fig. 7d). The samples have the characteristic positive Ce and Y anomalies, as well as high Y/Ho and low Pr_n/Yb_n (Figs. 8d and 13d) and a variably developed negative Eu anomaly. The unusual feature at this location is a bulge in the middle REEs, which leads to lower Pr/Dy values at a given Pr/Yb than the other mound samples (Fig. 14a). The REE+Y patterns do not resemble those of the late burial cement analysed in this study, which is characterised by significant La and Ce depletion. The entire mound is cross-cut by enigmatic breccia, whereas breccia in other mounds is only in mound tops.

Petrographic analysis indicates that lithofacies at K-Mesa mound were more strongly affected by recrystallisation than those of other mounds. The brecciation (unknown timing) is associated with replacive dolomite and calcite with hematite. Primary depositional fabrics at K-Mesa mound contain much more abundant disseminated

hematite (and less pyrite) than other mounds. It is possible that the brecciation may have introduced foreign REEs, because iron oxides derived from basin water (e.g., Haley et al., 2004) or possibly phosphates (e.g., Baldwin et al., 2011) can have MREE bulges.

2.6.2 Interpretation of basin water REE+Y pattern

The micro-sampled carbonate facies data suggest that the REE+Y were sourced from at least two separate fluids. The pelagic dolostone facies that dominates Uluksan mound and was also identified in the stratigraphically higher carbonates of the other mounds is interpreted to have sampled the REE+Y inventory of the basin water more than the benthic dolostone did. As explained earlier, the REE+Y pattern has some similarities with open seawater but differs strongly in not having positive La and Gd anomalies.

A literature search for alternative basin water types identified alkaline lake water as the only currently known fluid that combines all of the REE+Y features of the basin-water-derived end-member preserved in the Borden Basin mounds. Modern alkaline lakes are associated with drainage basins with a significant input from weathering volcanic rocks (e.g., Möller and Bau, 1993; Wen et al., 2013) and are found in semi-arid or arid environments. Water chemistry of five lakes in the western U.S.A. (Mono, Walker, Abert, Summer, and Goose Lakes; Johannesson et al., 1994) show HREE enrichment in shale-normalised patterns, and an absence of La and Gd anomalies. A positive Ce anomaly is present in most of the lakes, and the magnitude of the anomaly is variable. The Y/Ho systematics are unknown because Johannesson et al. (1994) did not report Y data. Similar but complete REE patterns have been reported from alkaline Lake Van (Turkey; Möller and Bau, 1993) and alkaline Lake Abhé (east African rift; Dekov et al., 2014).

An obvious difference between seawater and alkaline lake water REE concerns the behaviour of La and Gd. The development of positive La and Gd anomalies in seawater is related to an unfilled f-orbital in these elements. In modern seawater, carbonate complexes are present as mono- and dicarbonate complexes, but in alkaline lake water, higher-order polycarbonate complexes are the dominant species (e.g., Möller and Bau, 1993). These polycarbonate complexes have different stability constants than the mono and dicarbonate complexes present in seawater, which can account for the slight differences between REE+Y patterns (lack of La and Gd anomalies, possibly even steeper REE pattern; Möller and Bau, 1993).

A further difference exists with respect to the behaviour of Ce. Unlike seawater, where positive Ce anomalies typically develop only below redox-chemoclines (e.g., Bau et al., 1997), alkaline lake water can develop Ce anomalies without the presence of a chemocline. In the lacustrine environment, the Ce anomaly is a complex function of ionic strength, carbonate ion concentration, and pH (e.g., Pourret et al., 2008). Cerium can be oxidised at high pH by carbonate ions and preferentially adsorbed onto organic particles (Pourret et al., 2008). Depending on the abundance of organic particles in alkaline lake water, a negative (removal of Ce adhering to organic particles in organic-rich water) or positive (organic-poor preferential complexation on carbonate ions) Ce anomaly can develop. Furthermore, if alkaline water samples are not ultra-filtered, the colloid-associated Ce excess can contribute to misleadingly large apparent positive Ce anomalies in the dissolved load of the lake. Thus, the behaviour of Ce in alkaline lakes is complex, but positive Ce anomalies are common. The magnitude of the positive Ce anomaly, however, cannot be used to infer directly the extent of alkalinity.

Making interpretations about the chemical composition of ancient alkaline lake water in the rock record is further complicated by the complex factors that can drive a lake to alkalinity. The dominant anions in solution in alkaline lakes are HCO_3^- and CO_3^{2-} , but Cl^- and SO_4^{2-} are both present, and in rare cases can be the dominant species (e.g., Lake Nau Co in China; Zheng et al., 2013). The pH of modern alkaline lakes can be anywhere between 9 and 12. The pH and the composition of dissolved anions in alkaline lake water affect the solubility of different elements and makes lake water composition difficult to interpret based solely on carbonate rock geochemistry. Finally, it is currently not well known whether carbonate chimneys in modern alkaline lakes incorporate REEs from lakewater without fractionation. Dekov et al. (2014) reported that carbonate chimneys in Lake Abhé do not display as much LREE depletion as the lake water.

Notwithstanding these complexities, there are two very clear observations. First, it is obvious that in the shale-normalised Pr/Yb vs. Pr/Dy plot (Fig.13) Lake Abhé carbonate chimneys plot in the same field as the Ikpiarjuk Formation mounds. When samples from the Ikpiarjuk Formation mounds are normalised to a generic upper crustal composite (e.g. MuQ) the resulting patterns are shallower, yielding higher normalised Pr/Yb vs. Pr/Dy ratios. The more prominent LREE depletion that is apparent when samples are normalised to local shale shows that the REE were sourced locally. Secondly, other examples of alkaline lacustrine carbonates from the ancient rock record display very different and much flatter REE patterns than the Ikpiarjuk Formation mounds. These lacustrine carbonates are interpreted to have formed from non-alkaline freshwater (e.g., Bohlar and Van Kranendonk, 2007; Coffey et al., 2013).

In summary, as can be seen from the comparison of modern alkaline lake waters with the interpreted basin water component from the Ikpiarjuk Formation mounds (Fig. 15), it is probable that the MIG was, at the time of mound and black shale accumulation, not marine, but a large alkaline lake. Variations in redox-sensitive trace metals in mound-equivalent black shale indicate independently that the basin was redox-stratified and that the mounds were deposited in an anoxic setting (Turner and Kamber, 2012).

It is well documented that extensive interaction of groundwater with country rock can result in groundwater REE patterns that exhibit features of the aquifer (e.g., Tweed et al., 2006). Comparison of the inferred seep-fluid REE+Y pattern with modern ground-water REE+Y data from felsic volcanic rock aquifers in California and Nevada shows that the flat shale-normalised pattern of the inferred seep fluid is compatible with circum-neutral water, which may have percolated through feldspathic basement rocks that may have preferentially retained Eu (Johannesson et al., 2000) during water-rock interaction. In some modern alkaline lakes, subaqueous carbonate accumulations form at sites of groundwater discharge. Mono Lake (California) is known for the formation of subaqueous carbonate ‘towers’ that form where calcium-rich groundwater delivered at lake-bottom springs reacts with alkaline lake water. In the east African rift, carbonate ‘chimneys’ formed in alkaline Lake Abhé along inferred deep extensional structures as a result of both cold and hot fluid-venting (Fig. 14). Lake Abhé seep fluids are considered to be hydrothermal, but both hot and cold seep-fluids are present, and have slightly different REE+Y compositions. The Ikpiarjuk seep fluid end-member’s REE+Y pattern is very similar to that of the cold vent-fluid in Lake Abhé (Fig. 15).

2.6.3 *Supporting evidence for alkalinity*

Very few ancient lacustrine carbonates have been reported and these all show flat-shale normalised REE+Y patterns typical of precipitation in freshwater comparable to modern circum-neutral lakes (e.g. Bolhar and van Kranendonk, 2007; Awramik and Buchheim, 2009; Alvaro et al., 2010). To the best of our knowledge, the REE+Y data reported here are the first in support of precipitation in a Precambrian giant alkaline lake. Considering the novelty of the claim, it is necessary to evaluate the plausibility of alkalinity.

Unfortunately, this cannot be achieved directly because neither the relevant cations nor anions get incorporated quantitatively into carbonate. Rather, the likelihood of development of basin-water alkalinity and only be assessed via sediment source composition and extent of weathering.

Maintaining basin-water alkalinity requires a continuous flux of solutes into the basin.

The basinal black shale provides some constraints on fluvial sediment and solute delivery, the extent of chemical weathering, and, by inference, climatic conditions at the time of weathering. Trace element characteristics of the Arctic Bay Formation black shale, which surrounds the mounds, differ in several ways from ordinary upper continental crust (Turner and Kamber, 2012). Apart from an upward decrease in high field strength element concentration and subtle change in REE pattern, ratios of these elements are consistent throughout the depositional interval, suggesting a relatively constant sediment source. Of these immobile element characteristics, a very conspicuous feature of the black shale is its high Nb/Ta (14-15) and kinked REE pattern, which are consistent with a continental-rift alkali-basalt as the predominant source of detritus and

solutes. Thus, at least in terms of presence of alkali-basalt in the catchment, an alkaline lake setting appears possible.

Maintaining alkalinity also requires climatic conditions capable of releasing a sufficient supply of Ca, Mg, Na, K, and anions (Cl^- , SO_4^{2-} , HCO_3^- , CO_3^{2-}) during chemical weathering (Garrels and Mackenzie, 1967; Cerling, 1994). To approximate the extent of source weathering, the black shale data of Turner and Kamber (2012) were plotted in the Al_2O_3 - $(\text{CaO}+\text{Na}_2\text{O}) - \text{K}_2\text{O}$ (A-CN-K) diagram (Fig. 15). In the A-CN-K diagram, the Ca-corrected shale data exhibit significantly higher Al values, with CIA ranging from 68-79, compared to the values of 40-50 for unweathered igneous rocks (Fig. 16). Chemical weathering trends in this plot emanate from the position of the source rock or rocks parallel to the A-CN join. Very few studies have reported geochemical data for basement rocks, but Dostal et al. (1989) report a limited data set from the Nauyat basalt. This basalt contains evidence for post-depositional Ca-Na-K redistribution, although Dostal et al. (1989) identified a group of least-altered basalts. These are considered to be the most dominant source rock for the shale and they plot close to an average alkali basalt composition in the A-CN-K diagram (range and average in Figure 16). The Arctic Bay shale samples deviate substantially towards the K apex from the expected weathering trend for the basalt. This pattern could have two explanations. First, if the basalt was the dominant sediment source, the deviation of the shale from the basalt weathering trend would suggest that the material experienced K metasomatism at some unconstrained time following deposition. The CIA range of 68-79 would be a minimum, and correcting the CIA back to their pre-metasomatised values would indicate a greater extent of weathering, with CIA ranging from 78-94 (using the method of Fedo et al., 1995).

Second, the deviation of the shale from the basalt weathering trend could indicate that a more K-rich source rock, producing illite during chemical weathering, was an additional component of the sediment source. This is reasonable based on features of immobile elements in the shale. In the Arctic Bay shale, Cr/Th is lower and Th/Sc is higher than expected for purely mafic source rocks, and Cr/Th is lower than that for the Nauyat basalt reported in Dostal et al. (1989). These features suggest that at least a minor felsic component was present in the Arctic Bay shale, and that the degree of source weathering would be somewhere between the two calculated CIA ranges. Regardless of the source-rock-dependent variation of the CIA range of 68-94, it is clear that the sediment source experienced considerable chemical weathering capable of delivering the necessary Ca, Na, and, by inference, Mg and anions to the basin through riverine delivery.

Another important aspect of the Arctic Bay Formation black shale's chemostratigraphy is the presence of several intervals that are strongly enriched in redox-sensitive metals (V, Mo, and U). Unlike many marine black shales, in which transition metal content is a function of euxinia or total reduced carbon (e.g., Lyons et al., 2009), in the Borden Basin, metal enrichment is positively correlated with trace dolomite content. Turner and Kamber (2012) could not conclusively explain this phenomenon, but narrowed possible explanations to a dolomite (or dolomite precursor) particle shuttle or a dolomite metal trap in the sediment. The dolomite-bearing intervals are in shale that underlies distal mound flanks, and may represent a separate type of seep-related pelagic dolomite that precipitated in the upper water column. Dolomite-bearing intervals in the black shale have a negative Ce anomaly (Turner and Kamber, 2012), whereas mound (seep)-related pelagic dolomite has a positive Ce anomaly. It remains unclear whether redox-sensitive

metals were sorbed onto dolomite particles or whether episodes of vent-related pelagic dolomite formation in the upper water column reflect a chemical state of the lake that also favoured metal trapping into the black shale precursor. Regardless of the reason, the black shale was sourced from extensively weathered volcanic rocks, which is a known environmental condition that can drive lakes to alkalinity, and there is evidence for multiple types of pelagic dolomite formation (both upper water column and lower water column) which could have been related to alkalinity.

2.6.4 *Trace metal systematics and mound chemostratigraphy*

One objective of this study was to search for chemostratigraphic trends in the mounds that might reflect basin-wide redox evolution. Even though there is a wide range in the enrichment of redox-sensitive metals (e.g., Mo, V, and U), there is no stratigraphic trend that is common to all mounds: each mound exhibits a distinct pattern of redox-sensitive metal enrichment (Fig. 9). It could be argued that because each mound is from a geographically distinct location (Fig. 3), the lack of correlatable chemostratigraphy reflects differences in the time of mound formation - mound formation was controlled by seep dynamics and probably differed in each location. In view of the REE+Y data, it is probable that in each mound, the relative contribution of pelagic vs. benthic seep carbonate was the dominant local control on trace metal budgets.

In addition to the inventory of dissolved and particulate metal in the basin water, seep fluids may have carried a separate load of metals into the mounds. There is an absence of pronounced positive Eu anomalies in any of the analysed carbonates, which constitutes strong evidence that the basin water was not influenced by very high-temperature fluids, like those associated with mid-ocean ridges. In this respect, the

samples contrast strongly with Palaeoproterozoic BIFs (e.g., Planavsky et al., 2010) that formed in the marine realm at a time when the deep ocean was still anoxic and received significant input from high-temperature hydrothermal vents. Such fluids can therefore be ruled out as a source of redox-sensitive metals.

In fact, whereas the seep-related pelagic carbonate has a positive Ce anomaly and no Eu anomaly, the benthic carbonate, interpreted to have incorporated more REE+Y from seep fluid, has no Ce anomaly, and a negative, rather than positive Eu anomaly (Fig. 14b). At Red Rock mound, the Ce and Eu anomalies anti-correlate reasonably well with the Pr_n/Yb_n ratio (Fig. 14d), suggesting that the seep water consistently maintained a negative Ce anomaly. There are very few correlations between trace metal data and Pr_n/Yb_n , Pr_n/Dy_n and Eu and Ce anomalies. The trace metal data do not correlate with $\delta^{13}C$ and $\delta^{18}O$ (e.g., $r^2=0.01-0.03$ for $\delta^{13}C$ and Cu). The strongest covariations are with MnO and Cu contents: the inferred seep carbonate apparently had elevated Cu (relative to basin water), whereas the pelagic carbonate had elevated Mn. This leads to a hyperbolic relationship between MnO/Cu vs. Pr_n/Dy_n (Fig. 14c), which could reflect binary mixing.

At Bellevue Mound, the extent of the negative Eu anomaly is correlated with the abundance of several transition metals, as demonstrated by variably well-developed correlations with V and U (Fig. 10). These transition metals are generally present in carbonate rocks in significant abundances due to their high abundance in seawater. The largest negative Eu anomalies are associated with the lowest metal abundances, suggesting that the seep fluid was poor in metals and that the main metal budget in the carbonate was incorporated from lake water. There is no correlation between enrichment factors of Mo, U, and V, and Fe at Bellevue Mound ($r^2=0.003$ to 0.03) (Fig. 11). Uluksan

Mound exhibits a strong correlation between Mo and V enrichment factors and Fe ($r^2=0.99$, $r^2=0.99$, respectively), but this relationship is not present for U. The strong correlations at Uluksan Mound appear to be strongly influenced by one point, although when this outlying point is removed, r^2 values are still greater than 0.9 for the three remaining data points. At Red Rock Mound, only a moderate negative correlation of the enrichment of Mo with Fe is evident. It is concluded that other than Cu, most metals were derived from the basin water. This finding is entirely consistent with enrichment patterns of these very metals in the coeval black shale being associated with elevated pelagic dolomite content derived from the upper water column (Turner and Kamber, 2012).

In order to test whether the metals were carried into the mounds by a pelagic dolomite shuttle, histograms of the enrichment factor of Mo and V were produced according to lithofacies (Fig. 17). These plots show that there is no preferential enrichment in any phase of the carbonate (i.e., neither pelagic nor benthic), indicating that the vent-related particulate dolomite in the water column was unlikely to have acted as a particle shuttle for metals. Nevertheless, the strongest correlations of enrichment factors of Mo and V with Fe are from the samples with the steepest REE + Y patterns. This is best illustrated at Uluksan Mound, where very strong correlations of Mo and V with Fe are present and all samples have steep REE+Y patterns. This could indicate that transition metals were sorbed onto Fe-oxyhydroxides that precipitated when pelagic dolomite formation was also taking place. The black shale stratigraphy clearly shows that the pelagic dolomite production rate fluctuated considerably, probably reflecting the evolving lake water chemistry.

In addition to considering what sort of particle shuttles may have been present in the basin, the influence of diagenesis must also be evaluated. Two types of diagenesis must be considered when scrutinising trace element composition of carbonates: early diagenesis on the basin floor or just below the sediment-water interface, and burial diagenesis. It is well known that Fe, Mn, Sr, Ca, and Mg all substitute readily for one another in carbonate minerals. Iron and Mn are both added to carbonate minerals, especially dolomite, under reducing conditions, and Sr is easily removed during dolomitisation. The abundance of Mn in all samples is high, and it is possible that Mn was added to the carbonates through interaction with a Mn rich diagenetic fluid. Given the high Mn/Cu content and correlation to shale-normalised Pr/Yb, high Mn is probably an original feature of the ambient water from which the carbonates precipitated. Importantly, carbonates that have been pervasively modified by diagenesis generally display a correlation between Mn and Sr (Banner and Hanson, 1990; Brand and Veizer, 1980; Veizer, 1983). There is no correlation between these elements in any sample in this study, indicating that burial diagenesis was not a major factor in trace metal geochemistry.

Diagenesis on the basin floor must also be considered when interpreting trace element composition. The Ikpiarjuk Formation mounds were completely dolomitised, and there is no chemically pristine mound related limestone for geochemical comparison. It is probable that different geochemical conditions existed below the sediment-water interface than on the basin floor (i.e., in pore water vs. unmodified basin water). This subsurface geochemical environment would have been further complicated by the presence of ongoing fluid seepage through the older framework of the mounds. No

systematic differences in REE+Y pattern and abundance, or trace element content, of any phase analysed (clots, isopachous cement, or pelagic dolomudstone) were documented during LA-ICP-MS screening. Given the mobility of many trace elements during the transformation of calcite to dolomite it is possible that the trace element composition was modified from the original values (without modifying the REEs). At Bellevue Mound, the magnitude of the Eu anomaly, a feature that is considered primary, correlates with several trace metals (V, Mo, U), and it is probable that at least at Bellevue Mound the trace metal composition is close to primary.

In summary, the metal chemostratigraphy of the mounds is complex. The mounds formed where alkaline lake waters mixed with seep fluids of a very different composition, both probably carrying different metal loads (Fig. 18). The majority of metals appear to have been derived from the alkaline lake water, but they were not carried into the mounds by a dolomite shuttle alone. Instead, the chemical state of the lake, which favoured pelagic dolomite production, also promoted separate reactions (probably involving Fe) that drove redox metal sequestration into the mounds (Fig. 18).

2.7 Discussion

2.7.1 *Geology, sedimentology, and geochemistry of the Milne Inlet Graben*

The time during which the middle part of the Bylot Supergroup was deposited was characterised by tectonically unsettled, rift-like behaviour recorded in the contemporaneous Iqqittuq, upper Arctic Bay, and Ikpiarjuk formations (Turner, 2009; Turner and Kamber, 2012), and in ensuing carbonate formations (Sherman et al., 2002; Turner, 2009, 2011). Onset of carbonate mound and black shale deposition was gradual,

as shown by gradual disappearance of the sand- and silt-grade component of the Arctic Bay Formation, and gradual expansion of basal mound facies over the shale basin floor. All documented mounds seem to have initiated their growth at approximately the same time (relative to stratigraphy of surrounding strata), and are associated with shale strata that show strong evidence of subaqueous slope instability, interpreted as the result of subaqueous fault activity (Turner and Kamber, 2012). Although the temporal relationship is less clear, the onset of mound deposition may also coincide approximately with initiation of the Iqqittuq Formation carbonate ramp in the southeastern part of the basin. None of these three units (upper Arctic Bay Formation black shale, Iqqittuq Formation, or Ikpiarjuk Formation mounds) exhibits conspicuous cyclicity, in contrast to the overlying Angmaat and Victor Bay formations (Sherman et al., 2001; Turner, 2009). With the new understanding that the Iqqittuq/Ikpiarjuk/upper Arctic Bay time interval in the Borden Basin was probably a time of lacustrine rather than marine sedimentation, the lack of cyclicity in these stratigraphic units now takes on greater significance. Strong, high-amplitude cyclicity in the Victor Bay and Angmaat formations was tentatively suggested as evidence of glacioeustasy in a hitherto unidentified late Mesoproterozoic icehouse world (Sherman et al., 2001; Turner, 2009). The presence of a non-cyclic, lacustrine succession in the Borden Basin suggests that it may have alternated between marine and lacustrine sedimentation – in other words, that its location in the interior of Laurentia was barely above sea-level. The basin water appears to have been saline through the carbonate interval of the Bylot Supergroup, regardless of marine versus lacustrine identity, which concurs with the basin's paleolatitude, evidence of aridity

during the middle part of the basin succession (Jackson and Cumming, 1981; Kah et al., 2001; Turner, 2009), and all details of the succession's geochemistry identified to date.

Termination of mound accumulation and black shale deposition was abrupt. Delivery of terrigenous fines ceased abruptly, and was seemingly instantaneously followed by carbonate production in the water column and its accumulation as terrigenous-free basin-floor carbonate laminite (Nanisivik Formation). The abrupt cessation of terrigenous material delivery suggests that basalt-veneered horsts separating the grabens, as well as bedrock exposures in the vicinity of the basin margins, no longer provided sediment to the basin. At the Iqqittuq-Angmaat formation contact, along the newly developed platform margin (Turner, 2009), deep-water laminite of the Nanisivik Formation forms a tongue between Iqqittuq and Angmaat formations, indicating that the water level rose (or most of the basin subsided) at the time of transition between Arctic Bay Formation and Nanisivik Formation in the northwestern MIG, and between Iqqittuq and Angmaat formations in the centre of the MIG. The abrupt contact between Arctic Bay – Iqqittuq – Ikpiarjuk formations and overlying Angmaat-Nanisivik formations may, therefore, record flooding of the formerly lacustrine basin with marine water, and inception of strongly cyclic carbonate sedimentation in a basin that was newly reconnected with global eustatic behaviour.

2.7.2 *Nature of the seep fluid*

The origin of seep fluid remains enigmatic, but several possible sources can be ruled out. There is no evidence of igneous activity during deposition of the Bylot Supergroup and no positive Eu anomaly in mound carbonate, so a magmatic-derived fluid is improbable. The seep fluid was saline and had geochemical attributes that were markedly different

from marine water (flat REE+Y pattern and absence of La and Gd anomalies; negative Eu anomaly). Evidence for regional aridity during Ikpiarjuk Formation mound accumulation is present in the form of coastal evaporites that accumulated in the coeval, southeastern Iqqittuq Formation (Jackson and Cumming, 1981; Kah et al., 2001). Delivery of sand- and silt-grade material had ceased by the time of mound nucleation, indicating that no significant fluvial systems remained to deliver such material, and that no significant topographic gradient was present in the catchment area of the basin. No evidence of meteoric diagenetic effects is present in carbonates of the Iqqittuq Formation, or in the overlying Angmaat and Nanisivik formations. Humid conditions returned only after deposition of the Victor Bay Formation, as shown by pronounced dissolution of uplifted substrates in the western end of the basin and renewed delivery of terrigenous material in the uppermost Bylot Supergroup. Some precipitation probably occurred in the catchment area of the basin, because the lake did not completely dry up, but the lack of fluvial sediment input to the basin and dearth of meteoric alteration in contemporaneous carbonates elsewhere in the basin suggests that it was unlikely that enough precipitation occurred to provide the large volumes of seep-fluid required to produce the mounds. Meteoric fluid, therefore, is unlikely to be the origin of the groundwater that fed basin-floor seeps and mixed with basin water to form Ikpiarjuk Formation mound precipitates. Methane-related seepage is discounted by the absence of anomalously light $\delta^{13}\text{C}$ signatures in any of the mound-related carbonate facies, although a minor contribution of isotopically light carbon is suggested for Uluksan mound (Fig. 12).

The most plausible fluid source for the seeps is modified basin water. Evaporatively concentrated basin water may have become extra-dense and Mg-(and possibly K)-rich

after precipitation of supratidal gypsum at graben margins or on the surfaces of episodically flooded horsts within or between the grabens of the Borden Basin (Jackson and Cumming, 1981; Kah et al., 2001). The dense fluid, oxidised owing to its recent contact with the atmosphere and upper water column, would have sunk through the subsurface, interacting with underlying volcanic rocks of the Nauyat Formation basalt and crystalline rocks of the Rae Province basement (probably Paleoproterozoic gneiss; Scott and de Kemp, 1998), where it acquired a negative Eu anomaly from feldspars, a slight excess of Cu (probably from buried Nauyat Formation basalt), rebalanced its Mg/Ca ratio, and lost the HREE-enrichment of the original basin water (Fig. 18). Heating of the dense and presumably oxidised brine by exposure to the normal geothermal gradient at depth then may have forced the buoyant fluid up through the deep-seated regional faults to emerge as fairly low-temperature subaqueous seeps with an elevated Mg/Ca ratio and an absence of La and Gd anomalies.

2.7.3 *Precambrian lacustrine carbonates*

Lacustrine carbonates have been identified in Precambrian basins using sedimentary and geochemical features. The most common sedimentary features supporting Precambrian lacustrine carbonates are abrupt lateral facies changes over small distances, evidence of basin restriction, lack of tidal sedimentary structures, and proximity to siliciclastic fluvial depositional environments (e.g., Buick, 1992; Awramik and Bucheim, 2009; Álvaro et al., 2010). In some cases, lacustrine carbonates were identified using geochemistry, including REEs, stable C, O, and N isotopes, and Sr isotopes.

It is noted that claims for Precambrian lacustrine carbonates are rare in the literature and are highly variable in their descriptions. In the Ediacaran Ouarzazate Supergroup,

Morocco, small (<1 km) lakes (proposed to have been alkaline) developed in weathered troughs on top of volcanic successions, and decametre-scale stromatolite buildups formed directly on top of the volcanic rocks (Álvarez et al., 2010). These carbonates were interpreted as lacustrine based primarily on their discontinuous lateral distribution. Stromatolite REE patterns are distinctly non-marine (flat) and reflect the composition of the volcanic rocks that the lakes formed on but show no evidence for alkalinity.

The Archean Tumbiana Formation, Australia, was interpreted as lacustrine based on sedimentology and geochemistry (Buick, 1992; Awramik and Buchheim, 2009; Bohlar and Van Kranendonk, 2007; Coffey et al., 2013; Stüeken et al., 2015). The Tumbiana Formation crops out over more than 680 km laterally, but despite similarity in lithofacies associations, there are no distinct marker beds that can be correlated for distances greater than 15 km. There are abrupt lateral facies changes, and carbonate units are in lateral gradational contact with fluvial sandstone (Awramik and Buchheim, 2009). The PAAS- and MuQ-normalised REE patterns of Tumbiana Formation stromatolites lack positive La and Gd anomalies and LREE-depletion, and were interpreted as distinctly non-marine (Bohlar and Van Kranendonk, 2007; Coffey et al., 2013). The flat REE patterns of the Tumbiana Formation are similar to modern freshwater lake patterns. They are different from patterns found in modern alkaline lakes and Bohlar and Van Kranendonk (2007) therefore did not envisage an alkaline lake chemistry. More recently, Stüeken et al. (2015) found $\delta^{15}\text{N}$ much heavier than that documented in contemporaneous marine units and hypothesised that N fractionated under anoxic, alkaline conditions. This is not supported by the REE+Y data.

In the Paleoproterozoic Kuetsjarvi Formation, Russia, 150 m of fluvial siliciclastics and carbonates are present between rift-related volcanic successions (Melezhik and Fallik, 2007; Melezhik et al., 2007). The carbonates include stromatolites as well as subaerial travertine deposits related to hot springs. There is close lateral association of carbonates with fluvial sedimentary rocks, and differences in $\delta^{13}\text{C}$ and $\delta^{18}\text{O}$ and $^{87}\text{Sr}/^{86}\text{Sr}$ isotopes relative to coeval marine environments led to the interpretation that the carbonates were deposited in a lacustrine setting (Melezhik and Fallik, 2007; Melezhik et al., 2007). No modern REE data have yet been reported for these rocks.

The sedimentologic and geochemical features of the Milne Inlet Graben rocks do not perfectly match any of the examples of Precambrian lakes, but this is not unexpected given the vast differences in size and geochemistry of modern lakes. The closest analogue is probably the Kuetzjarvi Formation. The Kuetzjarvi Formation contains an arid carbonate shoreline with travertine and with no evidence for tides or cyclicity; its setting is somewhat similar to the active extensional tectonic environment of the Milne Inlet Graben. As in the Kuetjarvi Formation, carbonate accumulated in shallow water of the Milne Inlet Graben (Iqqittuq Formation), and fluid venting also contributed carbonate to the basin. Different from the Kuetzjarvi Formation, however, is that carbonate deposition was not limited to the very shallow-water environment, and a carbonate ramp was able to develop. Also different from the Kuetjarvi Formation is that the fluids that led to development of the Ikpiarjuk Formation mounds are not obviously hydrothermal, and the greatest volume of seep-related carbonate accumulated in deep water.

2.7.4 Problems with using carbonate systems as proxies for global geochemistry

Reconstructing a consistent paleoredox history and a meaningful, correlatable carbon isotope curve for the Mesoproterozoic has proven frustrating (e.g., Kah et al., 2012). Given the dearth of passive-margin sedimentation through the Mesoproterozoic (Bradley, 2008), and the prevalence of intracratonic and epicratonic basins, it is possible that some of the Mesoproterozoic carbonate successions that have been used to establish these global parameters were unable to deliver meaningful data because they were not, in fact, marine. The seemingly subdued nature of the Mesoproterozoic carbon isotope record should be reconsidered in light of the possibility that some of the successions used to construct it were not marine.

Although REE patterns have been used to make interpretations about paleoredox history in other types of hydrogenous sedimentary rocks (i.e., iron formations), significant variations in supposed “seawater-derived” REE patterns can develop in carbonate rocks owing to paleoenvironmental variables (e.g., Frimmel, 2009; Himmler et al., 2010; Corkeron et al., 2012). In fact, REEs in carbonate rocks may be far more useful indicators of paleoenvironment than they are for paleoredox reconstruction. Frimmel (2009) documented a range in REEs in Neoproterozoic carbonates over different depositional environments, showing that near-shore carbonates were commonly characterised by flat shale normalised REE patterns, whereas offshore equivalents displayed the more characteristic marine pattern of LREE depletion. These differences were attributed to the incorporation of near-shore colloids due to fluvial input (Frimmel, 2009). It has also been shown that differences in REEs can occur on a smaller scale because of seafloor diagenesis. Himmler et al. (2010) demonstrated in authigenic carbonate at modern methane seeps that

differences in REE abundance and patterns can vary significantly between carbonate minerals precipitated on the seafloor versus just below the sediment-water interface.

Mesoproterozoic marine paleoredox history, a widely studied, is complicated by the abundance of data that come from intracontinental, epicontinental, and restricted sedimentary environments. In the Ikpiarjuk Formation of the Milne Inlet Graben, the presence of a Ce anomaly, a widely used paleoredox proxy, cannot be used to make interpretations about basin-water oxygenation because of the MIG's alkaline chemistry and attendant effects on Ce behaviour. The development of a Ce anomaly in alkaline lakewater may be related to Ce oxidation by carbonate at high pH, and so it is impossible to identify redox stratification based solely on the Ce anomaly (Pourret et al., 2008). The geochemistry of the Arctic Bay Formation independently suggests that the MIG was chemically stratified, with an oxygenated upper water column and euxinic bottom water (Turner and Kamber, 2012). Turner and Kamber (2012) suggested that the MIG was restricted from the open ocean and that it should not be used to make large-scale interpretations about global ocean systems. With the view that large lakes were possibly common in the Mesoproterozoic, it should be noted that redox proxies must be interpreted in the context of local conditions rather than automatically assumed to reflect marine conditions.

2.8 Summary

Large late Mesoproterozoic (~1.1 Ga) subaqueous carbonate seep-mounds of the Ikpiarjuk Formation accumulated where groundwater emerged through basin-floor faults and mixed with basin water of the Milne Inlet graben (Borden Basin). Their deep-water

setting (sub-wave-base; sub-photic-zone) and clotted texture makes them unlike typical Precambrian shallow-marine carbonates, and the scale of the mounds is unlike anything known from Phanerozoic seep-related carbonates.

Seep fluid had relatively flat REE+Y patterns and a negative Eu anomaly; the REE+Y patterns closely resemble those measured in modern groundwater affected by water-rock interaction with volcanic material. The seep fluids were probably derived from basin water that was modified first by evaporation and then through subsurface water-rock interaction with Nauyat Formation basalt and possibly underlying basement.

Basin water REE+Y patterns are similar to those of alkaline lake-water patterns. The lake water was saline, alkaline, and probably redox-stratified. This interpretation is supported by geochemical evidence from contemporaneous black shale, which was derived by weathering of local alkali basalt, which delivered solutes to the basin, driving the basin to alkalinity.

The conclusions of this study suggest the possibility that not all continental Mesoproterozoic basins were marine, and brings into question the validity of chemostratigraphic reconstructions (paleoredox, C isotope stratigraphy) for successions that have not been conclusively demonstrated to be marine.

2.9 Acknowledgements

Field work was financially supported by Canada-Nunavut Geoscience Office, a Natural Sciences and Engineering Research Council Discovery Grant to ECT, and a Northern Scientific Training Program Grant awarded to KH. Field work was assisted by T. Chevrier and J. Mathieu. LA-ICP-MS work was completed with the help of J. Petrus

Logistical support was provided by Polar Continental Shelf Project (Natural Resources Canada). Analytical work at Trinity College Dublin was supported by EC-FP7-MC grant “Chemical fingerprinting”. The Nunavut Research Institute is gratefully acknowledged for assistance with permitting. G. Baldwin is gratefully acknowledged for many helpful discussions.

2.10 References

Allwood, A.C., Kamber, B.S., Walter, N.R., Burch, I.W., and Kanik, I., 2010: Trace elements record depositional history of an Early Archean stromatolitic carbonate platform. *Chemical Geology*, v 270, p. 148-163.

Álvaro, J.J., Ezzouhairi, H., Ayad, N.A., Charif, A., Solá, R., and Ribeiro, M.L. 2010. Alkaline lake systems with stromatolitic shorelines in the Ediacaran volcanosedimentary Ouarzazate Supergroup, Anti-Atlas, Morocco: *Precambrian Research*, v. 179, p. 22-38.

Awramik, S.M., and Buchheim, H.P., 2009. A giant, Late Archean lake system: The Meentheena Member (Tumbiana Formation; Fortescue Group), Western Australia: *Precambrian Research*: v. 174, p. 215-240.

Azmy, K., Kaufman, A.J., Misi, A., and Oliveira, T.F., 2006. Isotope stratigraphy of the Lapa Formation, São Francisco Basin, Brazil: implications for Late Neoproterozoic glacial events in South America: *Precambrian Research*, v. 149, p. 231–248.

Azmy, K., Kendall, B., Creaser, R.A., Heaman, L., and de Oliveira, T.F., 2008. Global correlation of the Vazante Group, São Francisco Basin, Brazil: Re–Os and U–Pb radiometric age constraints: *Precambrian Research*, v. 164, p. 160–172.

Azmy, K., Sylvester, P., and de Oliveira, T.F. 2009. Oceanic redox conditions in the Late Mesoproterozoic recorded in the upper Vazante Group carbonates of Sao Fransisco Basin, Brazil: Evidence from stable isotopes and REEs: *Precambrian Research*, v. 168, p. 259-270.

Babechuk, M. G., Kamber, B.S., Greig, A., Canil, D., and Kodolanyi, J., 2010. The behaviour of tungsten during mantle melting revisited with implications for planetary differentiation time scales: *Geochimica et Cosmochimica Acta*, v. 74, p. 1448-1470.

Baldwin, G.J., Thurston, P.C., and Kamber, B.S. 2011. High-precision rare earth element, nickel, and chromium chemistry of chert microbands pre-screened with in-situ analysis: *Chemical Geology*, v. 285, p. 133-143.

Baldwin, G.J., Turner, E.C., and Kamber, B.S. 2012. A new depositional model for glaciogenic Neoproterozoic iron formations: insights from the chemostratigraphy and basin configuration of the Rapitan iron formation: *Canadian Journal of Earth Science*, v. 49, p. 455-476.

Banner, J.L., and Hanson, G.N.1990. Calculation of simultaneous isotopic and trace element variations during water-rock interaction with applications to carbonate diagenesis: *Geochimica et Cosmochimica Acta*, v. 54, p. 3123-3137

Bartley, J.K., and Kah, L.C. 2004. Marine carbon reservoir, C_{org} - C_{carb} coupling, and the evolution of the Proterozoic carbon cycle: *Geology*, v. 32, p. 129-132.

Bau, M., Möller, P., and Dulski, P., 1997. Yttrium and lanthanides in eastern Mediterranean seawater and their fractionation during redox-cycling: *Marine Chemistry*, v. 56, p. 123-131.

Bolhar, R., and Van Kranendonk, M.J., 2007. A non-marine depositional setting for the northern Fortescue Group, Pilbara Craton, inferred from trace element geochemistry of stromatolitic carbonates: *Precambrian Research*, v. 155, p. 229-250.

Bradley, D.C. 2008. Passive margins through earth history: *Earth-Science Reviews*, v. 91, p. 1-26.

Brand, U., and Veizer, J. 1980. Chemical diagenesis of a multicomponent carbonate system: 1. Trace elements: *Journal of Sedimentary Petrology*, v. 50, p. 1219–1236.

Buick, R., 1992. The antiquity of oxygenic photosynthesis—evidence from stromatolites in sulfate-deficient Archean Lakes: *Science*, v. 255, p. 74–77.

Dekov, V.M., Egueh, N.M., Kamenov, G.D., Bayon, G., Lalonde, S.V., Schmidt, M., Liebetrau, V., Munnik, F., Fouquet, Y., Tanimizu, M., Awaleh, M.O., Guirreh, I., Le and Gall, B., 2014. Hydrothermal carbonate chimneys from a continental rift (Afar Rift): Mineralogy, geochemistry, and mode of formation: *Chemical Geology*, v. 387, p. 87-100.

Coffey, J.M., Flannery, D.T., Walter, M.R., and George, S.C. 2013. Sedimentology, stratigraphy and geochemistry of a stromatolite biofacies in the 2.72 Ga Tumbiana Formation, Fortescue Group, Western Australia: *Precambrian Research*, v. 236, p. 282-296

Corkeron, M., Webb, G.E., Moulds, J. and Grey, K. 2012. Discriminating stromatolite formation modes using rare earth element geochemistry: Trapping and binding versus in situ precipitation of stromatolites from the Neoproterozoic Bitter Springs Formation, Northern Territory, Australia: *Precambrian Research*, v. 212-213, p. 194-206

Denyszyn, S.W., Halls, H.C., Davis, D.W. and Evans, A.D., 2009. Paleomagnetism and U-Pb geochronology of Franklin Dykes in High Arctic Canada and Greenland: a revised age and paleomagnetic pole constraining block rotations in the Nares Strait region: *Canadian Journal of Earth Sciences*, v. 46, p. 689–705.

Dostal, J., Jackson, G.D. and Galley, A., 1989. Geochemistry of Neohelikian Nauyat plateau basalts, Borden rift basin, northwestern Baffin Island, Canada: *Canadian Journal of Earth Sciences*, v. 26, p. 2214–2223.

Fedo, C.M., Nesbitt, H.W., and Young, G.M., 1995. Unraveling the effects of potassium metasomatism in sedimentary rocks and paleosols, with implications for paleoweathering conditions and provenance: *Geology*, v. 23, p. 921-924.

Eggins, S. M., J. D. Woodhead, L. P. J. Kinsley, G. E. Mortimer, P. Sylvester, M. T. McCulloch, J. M. Hergt, and Handler, M.R., 1997. A simple method for the precise determination of 40 trace elements in geological samples by ICPMS using enriched isotope internal standardisation: *Chemical Geology*, v. 134, p. 311-326.

Elderfield, H. and Greaves, M.J. 1982. The rare elements in seawater: *Nature*, v. 296, p. 214-219.

Elderfield, H. 1988. The oceanic chemistry of the rare earth elements. *Philosophical Transactions of the Royal Society of London. Series A, Mathematical and Physical Sciences*, v. 325, p. 105-126.

Frimmel, H.E. 2009. Trace element distribution in Neoproterozoic carbonates as paleoenvironmental indicator: *Chemical Geology*, v. 258, p. 338-353

Goodfellow, W.D., and Lydon, J.W., 2007. Sedimentary exhalative (SEDEX) deposits; in *Mineral Deposits of Canada: A synthesis of Major Deposits Types, District Metallogeny, the Evolution of Geological Provinces, and Exploration Methods: Geological Association of Canada, Mineral Deposits Division, Special Publication No. 5*, p. 163-183

Hahn, K.E., and Turner, E.C., 2013. Deep-water carbonate mound lithofacies, Borden Basin, Nunavut: *Geological Survey of Canada, Current Research 2013-11*, 14 p

Haley, B.A., Klinkhammer, G.P., and McManus, J., 2004. Rare earth elements in pore waters of marine sediments: *Geochimica et Cosmochimica Acta*, v. 68, p. 1265–1279.

Heaman, L.M., LeCheminant, A.N. and Rainbird, R.H., 1992. Nature and timing of Franklin igneous events, Canada: implications for a late Proterozoic mantle plume and the break-up of Laurentia: *Earth and Planetary Science Letters*, v. 109, p. 117–131.

Himmler, T., Bach, W., Bohrmann, G., and Peckmann, J., 2010. Rare earth elements in authigenic methane-seep carbonates as tracers for fluid composition during early diagenesis: *Chemical Geology*, v. 277, p. 126-136.

Iannelli, T. R., 1992. Revised stratigraphy of the late Proterozoic Bylot Supergroup, northern Baffin Island, Arctic Canada; implications for the evolution of Borden Basin: Unpublished Ph.D. thesis, London, Canada, University of Western Ontario, 781 pp

Jackson, G.D. and Cumming, L.M. 1981. Evaporites and folding in the Neohelikian Society Cliffs Formation, northeastern Bylot Island, Arctic Canada: Geological Survey of Canada, Paper 81-1C, 35-44.

Jackson, G.D. and Iannelli, T.R., 1981. Rift-related cyclic sedimentation in the Neohelikian Borden Basin, northern Baffin Island. *in* Proterozoic Basins of Canada: Geological Survey of Canada, Paper 81-10, p. 269–302.

Johannesson, K.H., Zhou, X.P., Guo, C.X., Stetzenbach, K.J., and Hodge, V.F., 2000. Origin of rare earth element signatures in groundwaters of circumneutral pH from southern Nevada and eastern California, USA: *Chemical Geology*, v. 164, p. 239-257.

Johannesson, K.H., Lyons, W.B., Bird, D.A. 1994. Rare earth element concentrations and speciation in alkaline lakes from western U.S.A. *Geophysical Research Letters* 21, 773-776.

Kah, L.C., Lyons, T.W., and Chesley, J.T. 2001. Geochemistry of a 1.2 Ga carbonate-evaporite succession, northern Baffin and Bylot Islands: implications for Mesoproterozoic marine evolution: *Precambrian Research*, v. 111, p. 203-234.

Kah, L.C., Bartley, J.K., and Teal, D.A. 2012. Chemostratigraphy of the Late Mesoproterozoic Atar Group, Taoudeni Basin, Mauritania: Muted isotopic variability, facies correlations, and global trends: *Precambrian Research*, v. 200-203, p. 82-103.

Kamber, B.S., Webb, G.E., and Gallagher, M., 2014. The rare earth element signal in Archaean microbial carbonate: information on ocean redox and biogenicity: *Journal of the Geological Society*, v. 171, p. 745-763.

Kamber, B. S., 2009. Geochemical fingerprinting: 40 years of analytical development and real world applications: *Applied Geochemistry*, v. 24, p. 1074-1086.

Kamber, B.S., Bolhar, R. and Webb, G.E., 2004. Geochemistry of late Archaean stromatolites from Zimbabwe: evidence for microbial life in restricted epicontinental seas: *Precambrian Research*, v. 132, p. 379–399.

Kamber, B.S., Greig, A. and Collerson, K.D., 2005. A new estimate for the composition of weathered young upper continental crust from alluvial sediments, Queensland, Australia: *Geochimica et Cosmochimica Acta*, v. 69, p. 1041–1058.

Kamber, B.S., and Collerson, K.D., 2000. Role of 'hidden' deeply subducted slabs in mantle depletion: *Chemical Geology*, v. 166, p. 241-254.

Knight, R.D. and Jackson, G.D., 1994. Sedimentology and stratigraphy of the Mesoproterozoic Elwin Subgroup (Aqigilik and Sinasiuvik formations), uppermost Bylot Supergroup, Borden rift basin, northern Baffin Island. *Geological Survey of Canada, Bulletin 455*, p. 48.

Lawrence, M.G. and Kamber, B.S., 2006. The behaviour of rare earth elements during estuarine mixing – revisited: *Marine Chemistry*, v. 100, p. 147-161.

LeCheminant, A.N. and Heaman L.M., 1989. Mackenzie igneous events, Canada: Middle Proterozoic hotspot magmatism associated with ocean opening: *Earth and Planetary Science Letters*, v. 96, p. 38–48.

Long, D.G.F., and Turner, E.C., 2012. Tectonic, sedimentary and metallogenic re-evaluation of basal strata in the Mesoproterozoic Bylot basins, Nunavut, Canada: Are unconformity-type uranium concentrations a realistic expectation? *Precambrian Research*, v. 214-15, p. 192-209.

Lyons, T.W., Anbar, A.D., Severmann, S., Scott, C., and Gill, B.C., 2009. Tracking Euxinia in the Ancient Ocean: A Multiproxy Perspective and Proterozoic Case Study: *Annual Review of Earth and Planetary Sciences. Annual Reviews*, Palo Alto, pp. 507-534

Mahon, R.C., Dehler, C.M., Link, P.K., Karlstrom, K.E., and Gehrels, G.E., 2014. Detrital zircon provenance and paleogeography of the Pahrump Group and overlying strata, Death Valley, California: *Precambrian Research*, v. 251, p. 102–117.

Maud, R.L., 1983. Stratigraphy, Petrography and Depositional Environments of the Carbonate-Terrigenous Member of the Crystal Spring Formation, Death Valley, California. Pennsylvania State University.

Melezhik, V.A., and Fallick, A.E. 2007. Paleoproterozoic, rift-related, C-rich, lacustrine carbonates, NW Russia. Part 1: Sedimentology and major element geochemistry: *Transactions of the Royal Society of Edinburgh: Earth Sciences*, v. 95, p. 393-421.

Melezhik, V.A., Fallick, A.E., and Kuznetsov, A.B. 2004. Palaeoproterozoic, rift-related, C-rich, lacustrine carbonates, NW Russia. Part II: Global isotope signal recorded in the lacustrine dolostones. *Transactions of the Royal Society of Edinburgh: Earth Sciences*, v. 95, p. 423-444.

Möller, P. and Bau, M. 1993. Rare-earth patterns with positive cerium anomaly in alkaline waters from Lake Van, Turkey: *Earth and Planetary Science Letters*, v. 117, p. 671-676.

Nothdurft, L.D., Webb, G.E., and Kamber, B.S., 2004. Rare earth element geochemistry of Late Devonian reefal carbonates, Canning Basin, Western Australia: Confirmation of a seawater REE proxy in ancient limestones: *Geochimica et Cosmochimica Acta*, v. 68, p. 263-283.

Pavan, K., and Turner, E.C. 2014. Carbon isotope stratigraphy of the Borden Basin (Nunavut): Implications for depositional age and correlation of carbonate strata in the Nanisivik District. GAC-MAC Fredericton. Poster presentation.

Pehrsson, S.J. and Buchan, K.L., 1999. Borden dykes of Baffin Island, Northwest Territories: a Franklin U-Pb baddeleyite age and a paleomagnetic reinterpretation: *Canadian Journal of Earth Sciences*, v. 36, p. 65-73.

Planavsky, N., Bekker, A., Rouxel, O.J., Kamber, B.S., Hofmann, A., Knudsen, A. and Lyons, T.W., 2010. Rare earth element and yttrium compositions of Archean and Paleoproterozoic Fe formations revisited: new perspectives on the significance and mechanisms of deposition: *Geochimica et Cosmochimica Acta*, v. 74, p. 6387-6405.

- Pourret, O., Davranche, M., Gruau, G., Dia, A., 2008. New insights into cerium anomalies in organic-rich alkaline waters: *Chemical Geology*, v. 251, p. 120-127.
- Scott, D.J. and de Kemp, E.A., 1998. Bedrock geology compilation, northern Baffin Island and northern Melville Peninsula, Northwest Territories. Geological Survey of Canada, Open File 3633.
- Sherman, A.G., James, N.P., and Narbonne, G.M., 2000. Sedimentology of a late Mesoproterozoic muddy carbonate ramp, northern Baffin Island, Arctic Canada. in *Carbonate Sedimentation and Diagenesis in the Evolving Precambrian World*, (ed.) J.P. Grotzinger and N.P. James: *SEPM Special Publication*, v. 67, p. 275-294.
- Sherman, A.G., James, N.P., and Narbonne, G.M., 2001. Anatomy of a cyclically packaged Mesoproterozoic ramp in northern Canada: *Sedimentary Geology*, v. 139, p. 171-203.
- Sherman, A.G., James, N.P., and Narbonne, G.M., 2002. Evidence for reversal of basin polarity during carbonate ramp development in the Mesoproterozoic Borden Basin, Baffin Island: *Canadian Journal of Earth Sciences*, v. 39, p. 519-538.
- Stüeken, E.E., Buick, R., and Schauer, A.J. 2015. Nitrogen isotope evidence for alkaline lakes on late Archean continents: *Earth and Planetary Science Letters*, v. 411, p. 1-10.
- Turner, E.C., 2004a: Kilometre-scale carbonate mounds in basinal strata: implications for base-metal mineralization in the Mesoproterozoic Arctic Bay and Society Cliffs formations, Borden Basin, Nunavut. Geological Survey of Canada, Current Research 2004-B4

- Turner, E.C., 2004b. Origin of basinal carbonate laminites of the Mesoproterozoic Society Cliffs Formation (Borden Basin, Nunavut), and implications for base-metal mineralization. Geological Survey of Canada, Current Research. 2004-B2
- Turner, E.C., 2009. Mesoproterozoic carbonate systems in the Borden Basin, Nunavut: Canadian Journal of Earth Sciences, v. 46, p. 915–938.
- Turner, E.C., 2011. Structural and stratigraphic controls on carbonate-hosted base metal mineralization in the Mesoproterozoic Borden Basin (Nanisivik District), Nunavut: Economic Geology, v. 106, p. 1197–1223.
- Turner, E.C. and Kamber, B.S., 2012. Arctic Bay Formation, Borden Basin, Nunavut (Canada): basin evolution, black shale, and dissolved metal systematics in the Mesoproterozoic ocean: Precambrian Research, v. 208–211, p. 1–18.
- Ulrich, T. Kamber, B.S., Woodhead, J.D. and Spencer, L.A. 2010: Long-term observations of isotope ratio accuracy and reproducibility using quadrupole ICP mass spectrometry: Geostandards and Geoanalytical Research, v. 34, p. 161-174.
- Veizer, J., 1983. Geologic evolution of the Archean-early Proterozoic Earth. In: Schopf, J.W. (Ed.), Earth's Earliest Biosphere; Its Origin and Evolution. Princeton Univ. Press, Princeton, NJ, United States, pp. 240–259.
- Webb, G. E., and Kamber, B.S., 2000. Rare earth elements in Holocene reefal microbialites; a new shallow seawater proxy: Geochimica et Cosmochimica Acta, v. 64, p. 1557-1565.

Wen, H., RongCai, Z., Hairuo, Q., MingTao, F., YanAn, L., and BoShi, G. 2013. Primary dolostone related to the Cretaceous lacustrine hydrothermal sedimentation in Qingxi sag, Jiuquan Basin on the northern Tibetan Plateau: *Science China Earth Sciences*, v. 56, p. 2080-2093

Zheng M, Tang J, Liu J, and Zhang F. 1993. Chinese saline lakes: *Hydrobiologia*, v. 267, p. 23–36

2.11 Figures

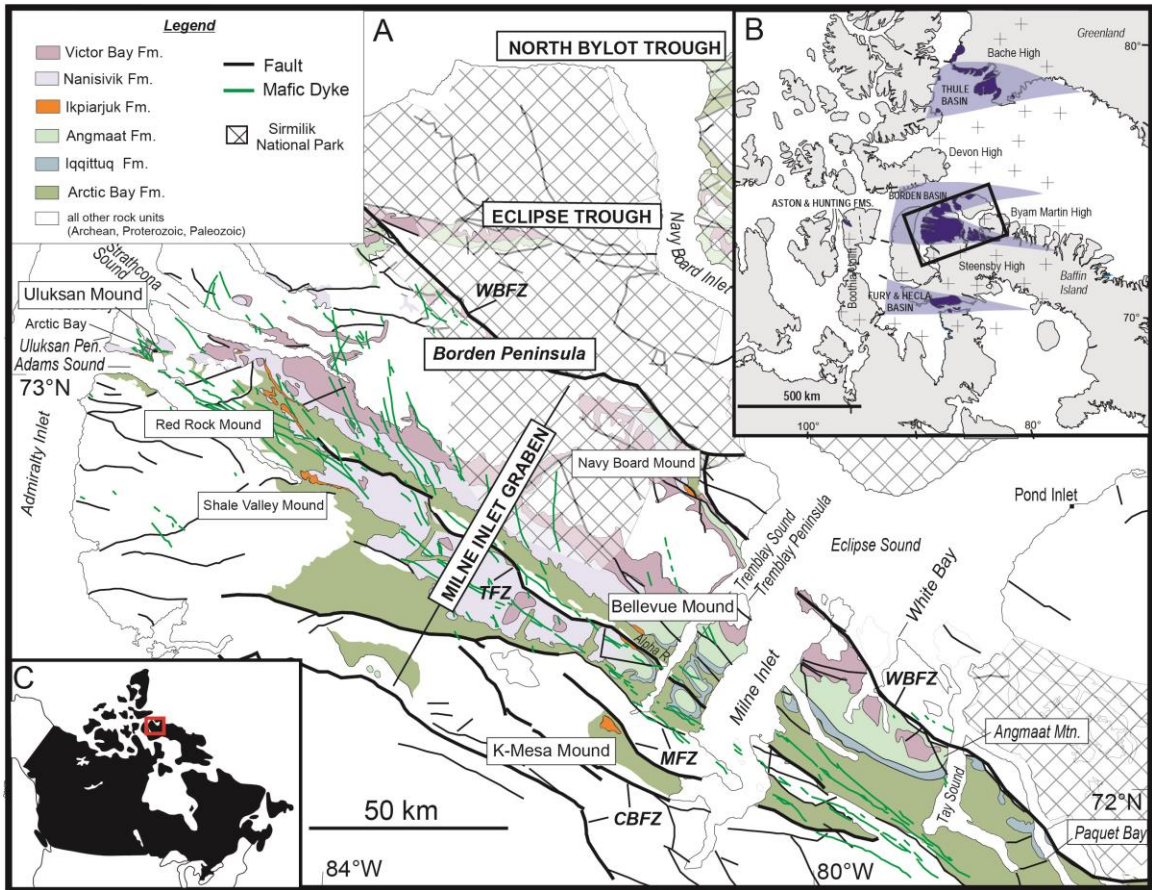


Figure 2-1 - Geological map

Figure 1: (A) Geological map of the Milne Inlet Graben (MIG); only some of the Mesoproterozoic stratigraphic units are shown. Six mound exposures are known (modified from Scott and deKemp, 1998 and Turner, 2009); larger font indicates mounds addressed by this study. CBFZ=Central Baffin fault zone; MFZ=Magda fault zone; TFZ=Tikrarjuaq fault zone; WBFZ=White Bay fault zone. (B) The Bylot Basins of the Canadian Arctic islands; Borden Basin in rectangle. Dark blue areas show the extent of present-day exposure; pale blue indicates inferred extent of the former basins (Jackson and Iannelli, 1981).

	Formation	Tectonic History	Sedimentary Environment	Reference
Bylot Supergroup	Sinasiuvik Fm.	Unknown	Shallowing-upward Complex paleotopography	Knight and Jackson, 1994
	Aqigilik Fm.			
	Strathcona Sound Fm. & Athole Point Fm.			
	Victor Bay Fm.	Uplift/Tilting	Uplift and karsting in W end; Drowning and deepening in E (Athole Point Fm.)	Sherman et al., 2001 Sherman et al., 2002
		Quiescence	Re-submersion, NW-deepening ramp	
		Uplift/Tilting	Dramatic uplift and tilting to the NE	Turner, 2009 Turner, 2011 Turner and Kamber, 2012
		Extension	NW deepening Alluvial fans (Fabricus Fiord Fm.) at graben margins Active faults, local debris flows, soft sed. deformation Prograding carbonate ramp to platform in SE Fault-related carbonate mounds throughout basin	
		Gentle Subsidence	Shallow-marine sandstone	Long and Turner 2012
		Basalt		

Rae Province
Basement

Figure 2-2 - Tectonic history

Figure 2: Stratigraphy of the Bylot Supergroup, with associated tectonic and depositional environments, after Turner (2009, 2011), Turner and Long (2012), and Turner and Kamber (2012).

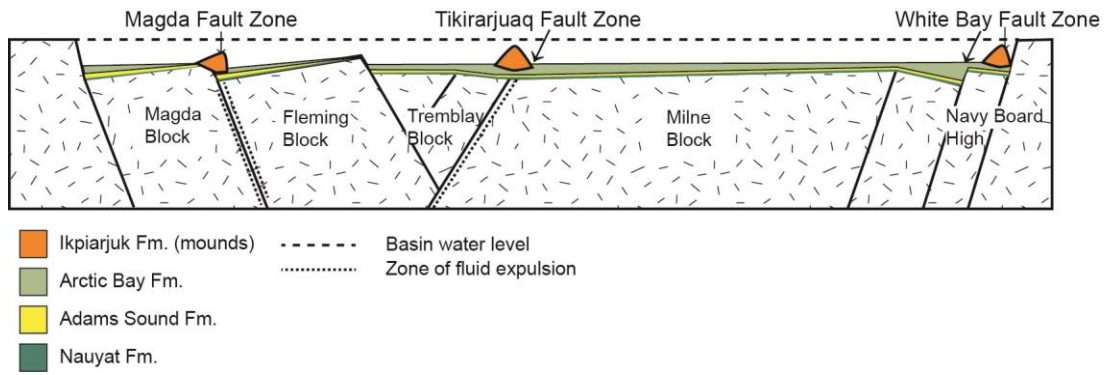


Figure 2-3 - Schematic cross-section through the Milne Inlet Graben

Figure 3: Schematic cross-section through the Milne Inlet Graben (after Iannelli, 1992; Turner, 2012), illustrating basement blocks, sub-basins, and major fault zones at which the Ikpiarjuk Formation mounds nucleated. Mounds formed along major faults in the MIG, where ground water was expelled into the lower water column.

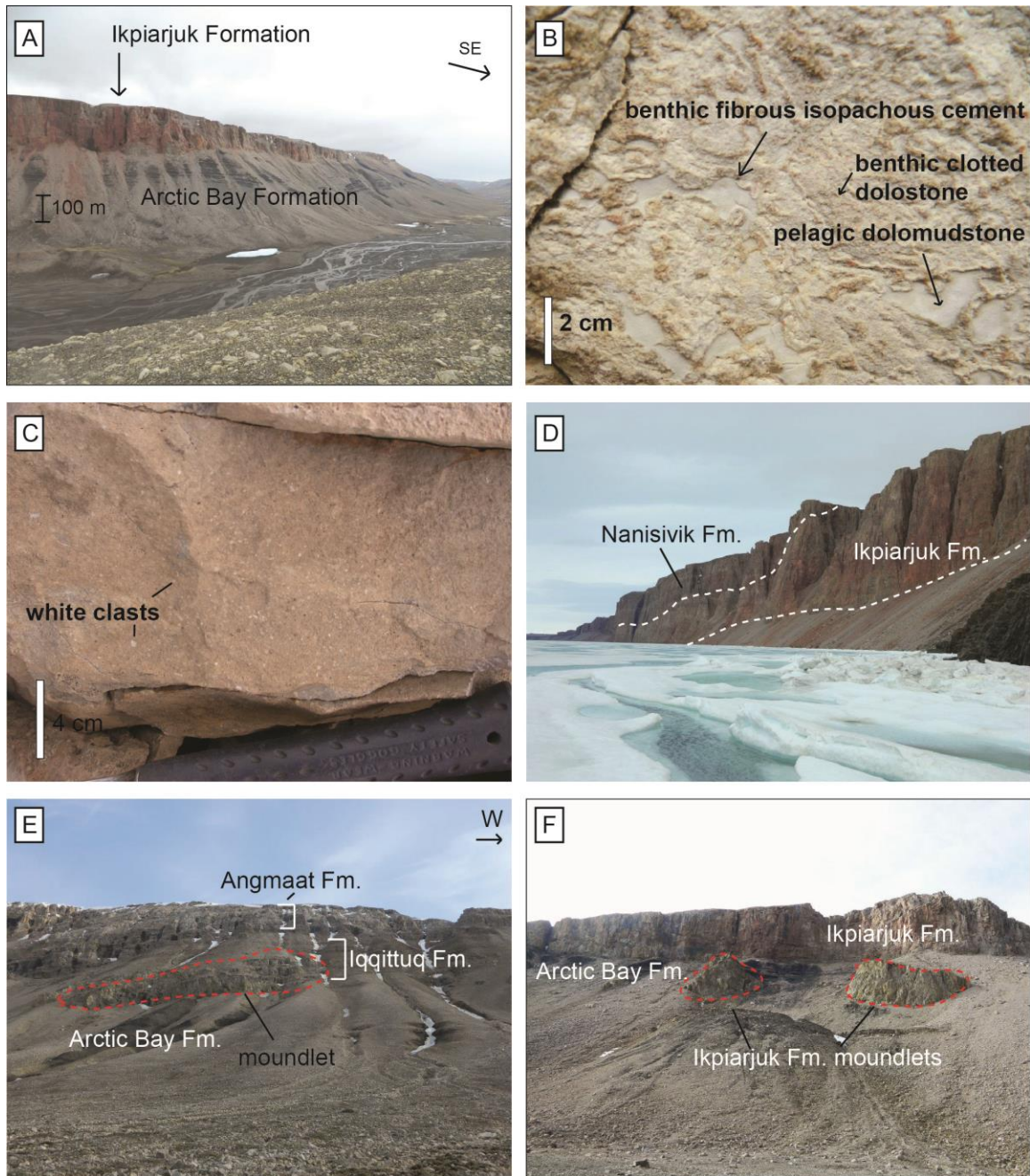


Figure 2-4 - Field exposures of the Ikpiarjuk Formation

Figure 4: Field exposures of the Ikpiarjuk Formation. (A) Field exposure of Red Rock Mound (arrow). The mound pinches out as its base gradually climbs up-section towards the southeast, relative to Arctic Bay Formation black shale. (B) Example of the clotted lithofacies present in most mounds (Red Rock Mound). Resistant-weathering isopachous

fibrous cement rims clots, and carbonate mudstone (pelagic dolomite) fills voids among clots. (C) Example of white-clast debrite facies (Red Rock Mound). (D) Main exposure of Uluksan Mound. Mound facies are distinguished from the overlying Nanisivik Formation by a subtle colour difference and presence of faint layering in the upper parts of the cliffs. The mound exposure is largely inaccessible. (E) A “moundlet” of the Ikpiarjuk Formation enclosed by outer-ramp strata of the Iqqittuq Formation near Bellevue Mound. (F) “Moundlets” of the Ikpiarjuk Formation enclosed by black shale of the Arctic Bay Formation directly beneath the main cliff-forming exposure of K-Mesa mound.

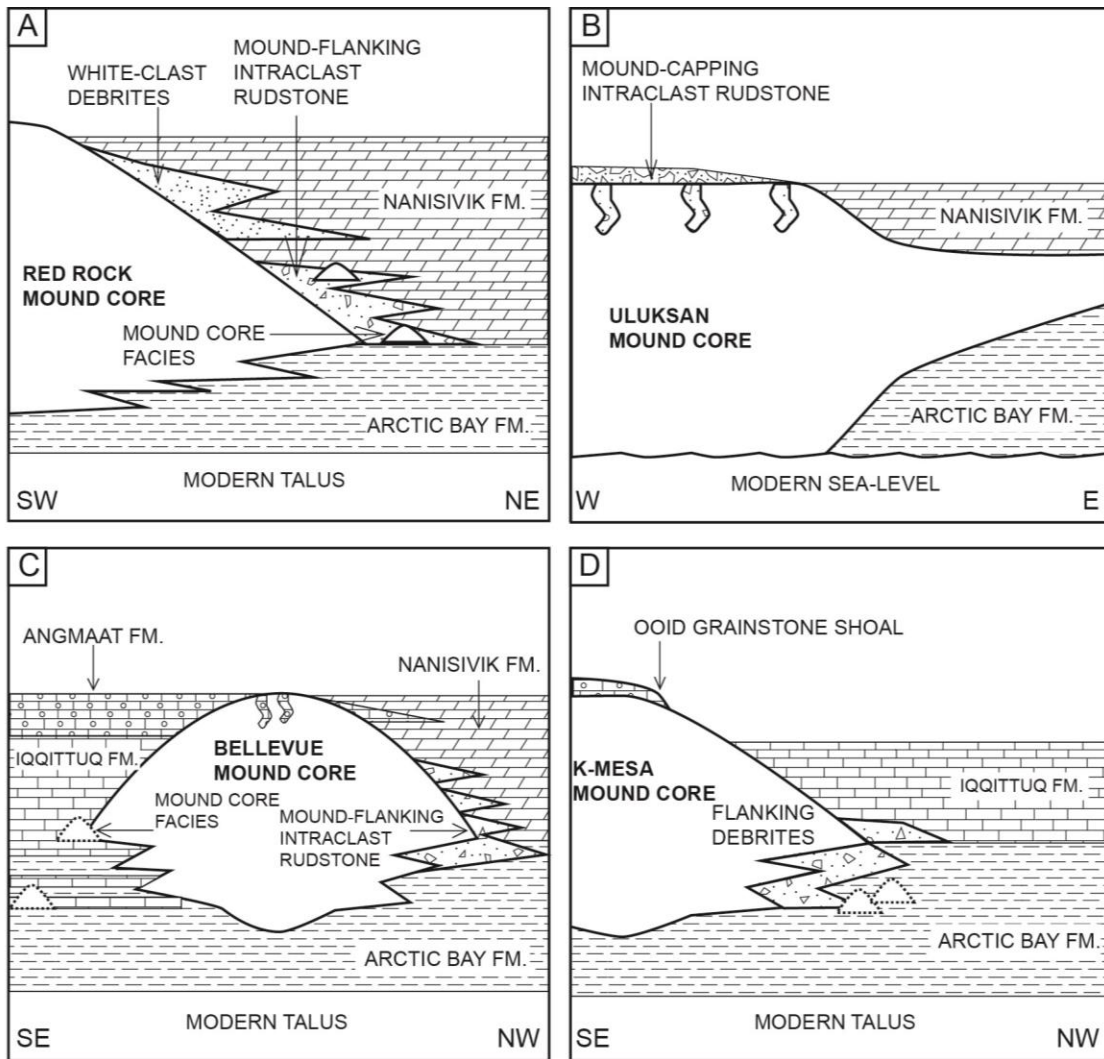


Figure 2-5 - Schematic configurations of four mounds

Figure 5: Schematic configurations of the four mounds examined in this study. (A) Red Rock Mound (B) Uluksan Mound (C) Bellevue Mound (D) K-Mesa mound. Although mounds differ in detail, all are interstratified with black shale at the base, have debrite lithofacies along the flanks, and locally contain clotted texture.

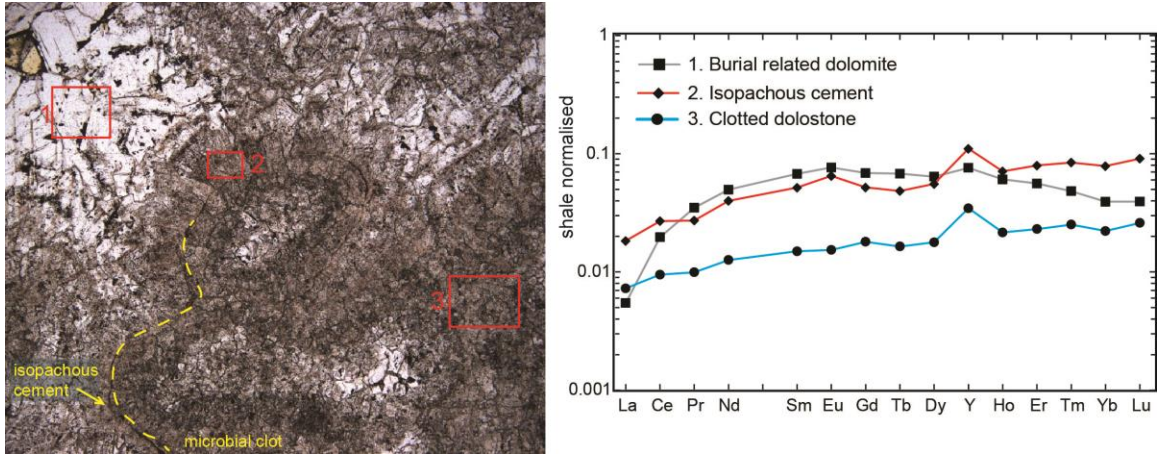


Figure 2-6 - Thin section photomicrograph

Figure 6: Thin section photomicrograph in plane polarized light (FOV: 3 mm) illustrating microbial clots, isopachous cement, and burial related dolomite spar with representative shale normalised REE+Y patterns from LA-ICP-MS. In this example the isopachous cement had a higher shale normalised abundance of REEs, but this was not a consistent observation. No systematic differences were observed between microbial clots and isopachous cement during LA-ICP-MS pre-screening.

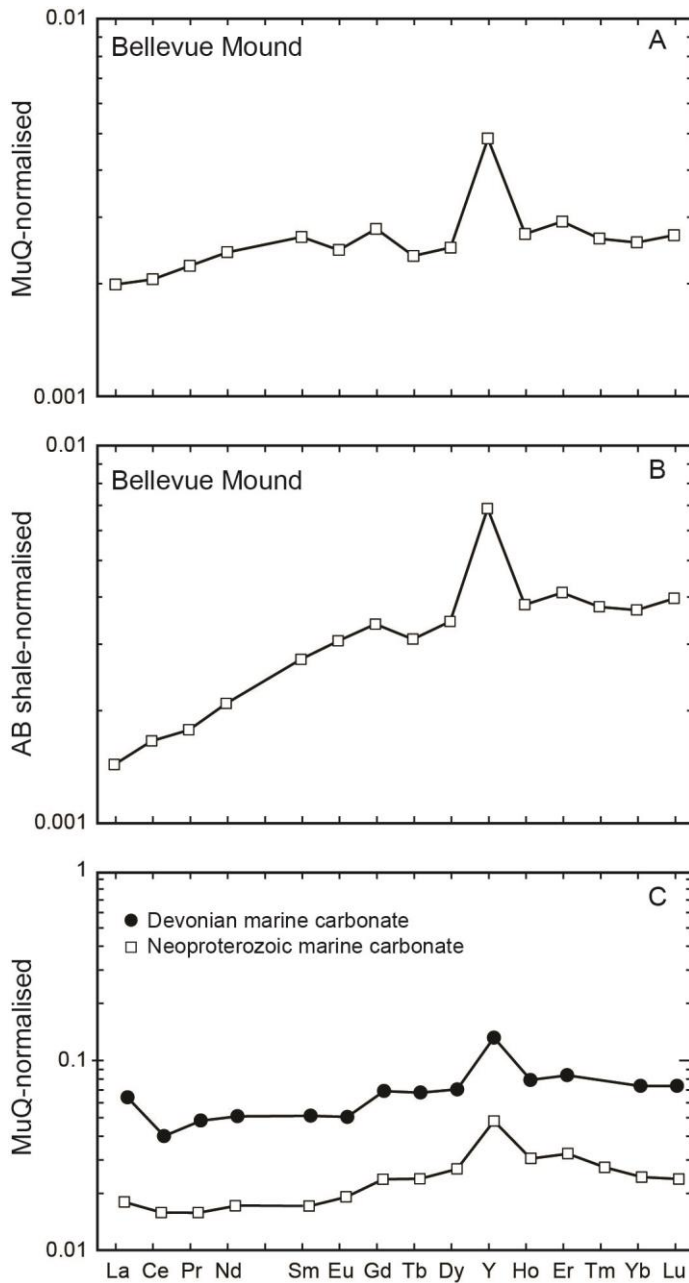


Figure 2-7 - Comparison of REE+Y data with different normalisation

Figure 7: Comparison of REE+Y data for sample KH10 (top of Bellevue Mound; pelagic precipitate) as normalised to MuQ (A) (Kamber, 2009), and as normalised to Arctic Bay Formation shale (B). When normalised to the regional shale, MREE depletion flattens, and magnitude of the negative Eu anomaly decreases. (C) Devonian marine carbonates

(Northdruff et al., 2014) and Neoproterozoic carbonates (Frimmel, 2009), normalised to MUQ, illustrate features typical of marine REE+Y patterns, including enrichment of HREE over LREE, and positive La, Gd, and Y anomalies.

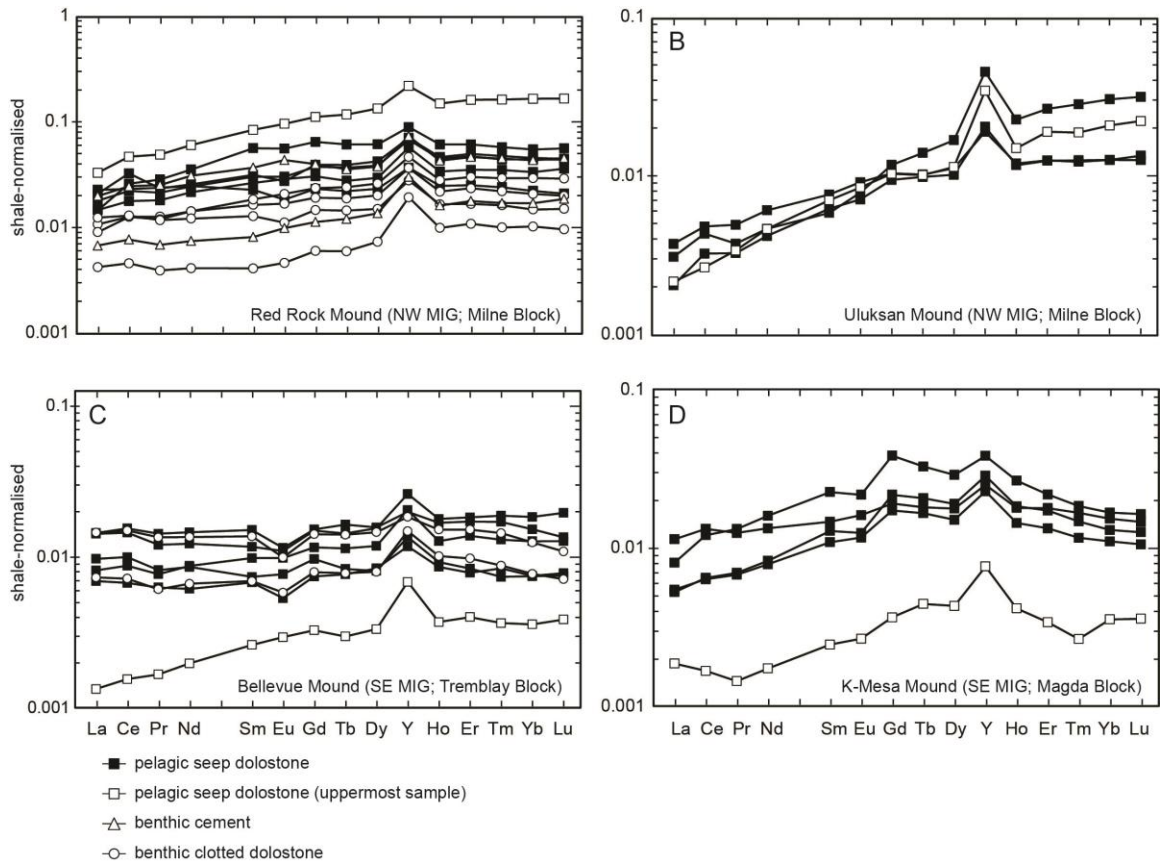


Figure 2-8 - Shale-normalised REE+Y patterns

Figure 8: Shale-normalised (Arctic Bay Formation) REE+Y plots for selected samples from each of four mounds studied. All mounds have shale-normalised REE+Y plots that generally show shallowly positively sloping patterns (A) Red Rock Mound exhibits a negative Eu anomaly in most samples, with the exception of one sample of benthic cement that exhibits a positive Eu anomaly. (B) Uluksan Mound exhibits steep patterns, as compared to those from other sample locations. (C) Bellevue Mound exhibits a significant negative Eu anomaly in all but one sample. The negative Eu anomaly is interpreted as a feature of the seep fluid. (D) K-Mesa Mound patterns are irregular, as compared to other mounds, but still preserve the main aspects of the basin water, such as positive Y and HREE enrichment.

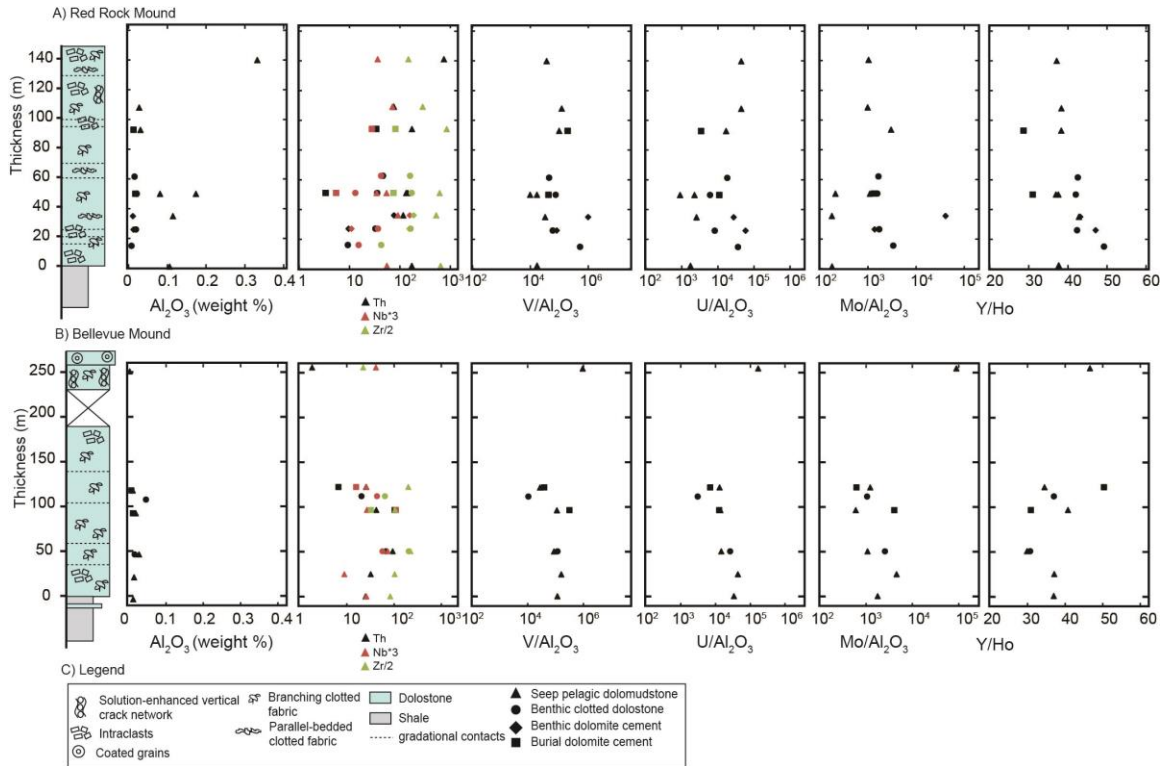


Figure 2-9 - Stratigraphic plots of geochemistry

Figure 9: Stratigraphic plots of (A) Red Rock Mound and (B) Bellevue Mound, illustrating elements that indicate detrital contamination, several redox-sensitive trace elements, and Y/Ho. The stratigraphic column for Bellevue Mound illustrates presence of overlying ooid bed (post-mound). Detrital contamination at Bellevue Mound is low. The contamination from heavy minerals (Th, Zr, Nb) is very low, and the peaks do not correspond with any unusual REE+Y patterns. The clay content (Al₂O₃) is also low and has not influenced the REE+Y patterns. The detrital component in Red Rock Mound is much higher than that of Bellevue Mound, and may have affected the REE+Y patterns slightly, requiring a correction. The Y/Ho is high (>30) in all samples and is considered a primary feature of the basin water. The redox-sensitive trace metals are highly variable through the mounds and no correlatable intervals are present between mounds. The

control on the redox-sensitive metals in the mounds is more likely related to the relative contribution of seep fluid versus basin water.

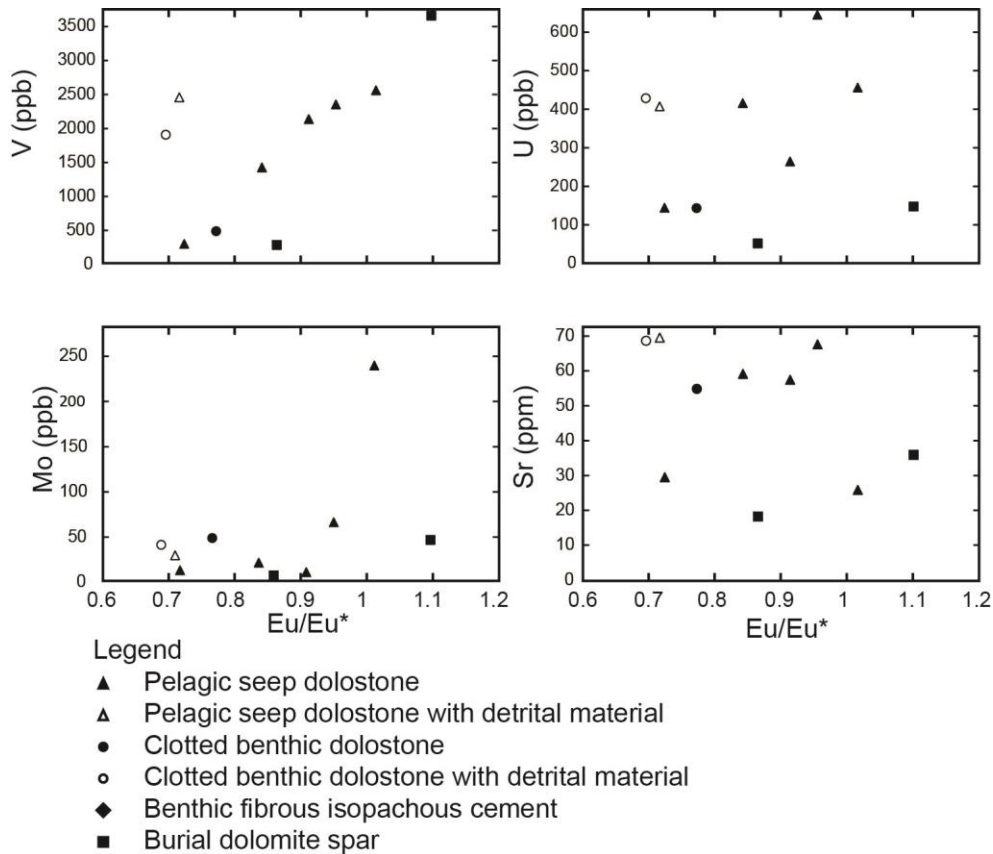


Figure 2-10 - Covariance diagrams of the Eu anomaly and trace elements

Figure 10: Covariance diagrams of the magnitude of the Eu anomaly (Eu/Eu^*) and trace elements (ppb) at Bellevue Mound. Many of the elements generally enriched in basin water (V, U, Mo, and Sr) show good correlation with the magnitude of the Eu anomaly; the more negative the anomaly, the lower the concentration of these elements. The Eu anomaly is interpreted as a characteristic of the vent fluid, which must have had low concentrations of trace elements, including the redox-sensitive trace metals. Samples with a slightly elevated siliciclastic content are plotted as a separate series and were used to calculate r^2 values.

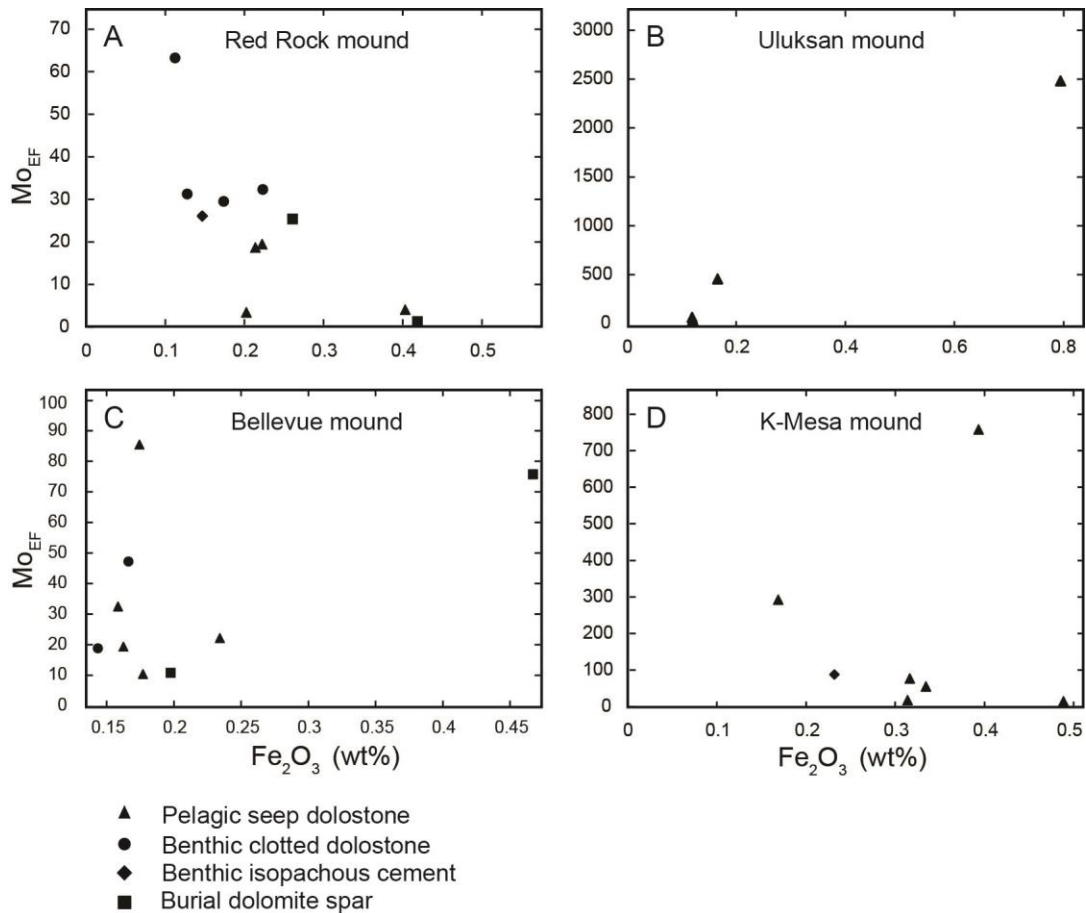


Figure 2-11 - Covariance diagrams of the enrichment factor of Mo and Fe (wt. %)

Figure 11: Covariance diagrams of the enrichment factor of Mo and Fe (wt %). Samples with extremely anomalous Mo_{EF} due to drill bit contamination are not plotted. (A) At Red Rock Mound Mo_{EF} has a weak negative correlation with Fe. (B) At Uluksan Mound Mo_{EF} correlates strongly with Fe. (C) At Bellevue Mound Mo_{EF} does not correlate with Fe. (D) At K-Mesa Mound Mo_{EF} does not correlate with Fe. The strongest correlations of enrichment factors of Mo (and V; not shown) with Fe are from the samples with the steepest REE + Y patterns, and are interpreted as a characteristic of the basin water. The moderate to strong correlation of Mo with Fe (present at Uluksan Mound) could indicate that transition metals were sorbed onto Fe-oxyhydroxides that precipitated when seep-related pelagic dolomite precipitation was also taking place.

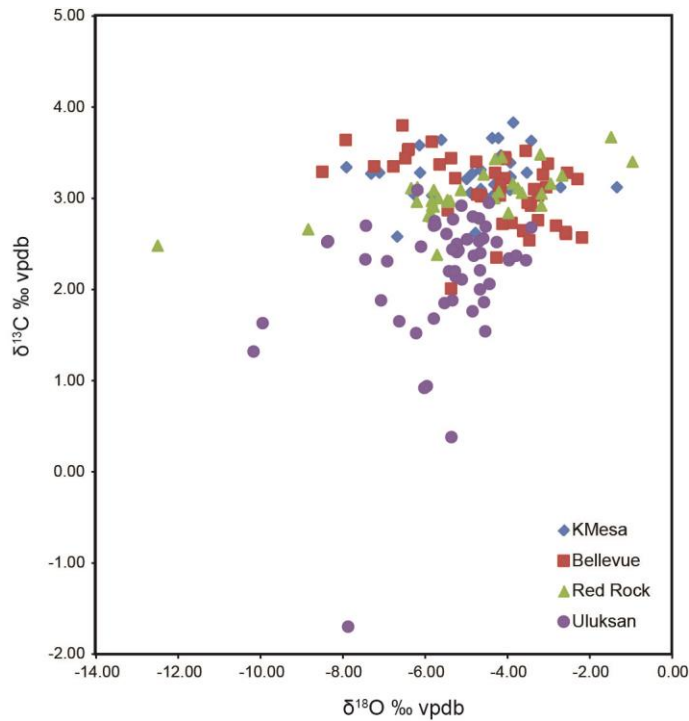


Figure 2-12 - Covariance diagram of stable isotopes

Figure 12: Covariance diagram of $\delta^{18}\text{O}$ and $\delta^{13}\text{C}$. All data are within the range of contemporaneous carbonates from the Milne Inlet Graben and the $\delta^{18}\text{O}$ and $\delta^{13}\text{C}$ of the Ikpiarjuk Formation are interpreted to be derived from the basin water. The carbon isotope signatures are not markedly light, indicating that mound-forming seeps were not methane seeps. The signatures from Uluksan Mound are lighter than those of other mounds, suggesting a minor light carbon component, perhaps from methane generation in underlying black shale.

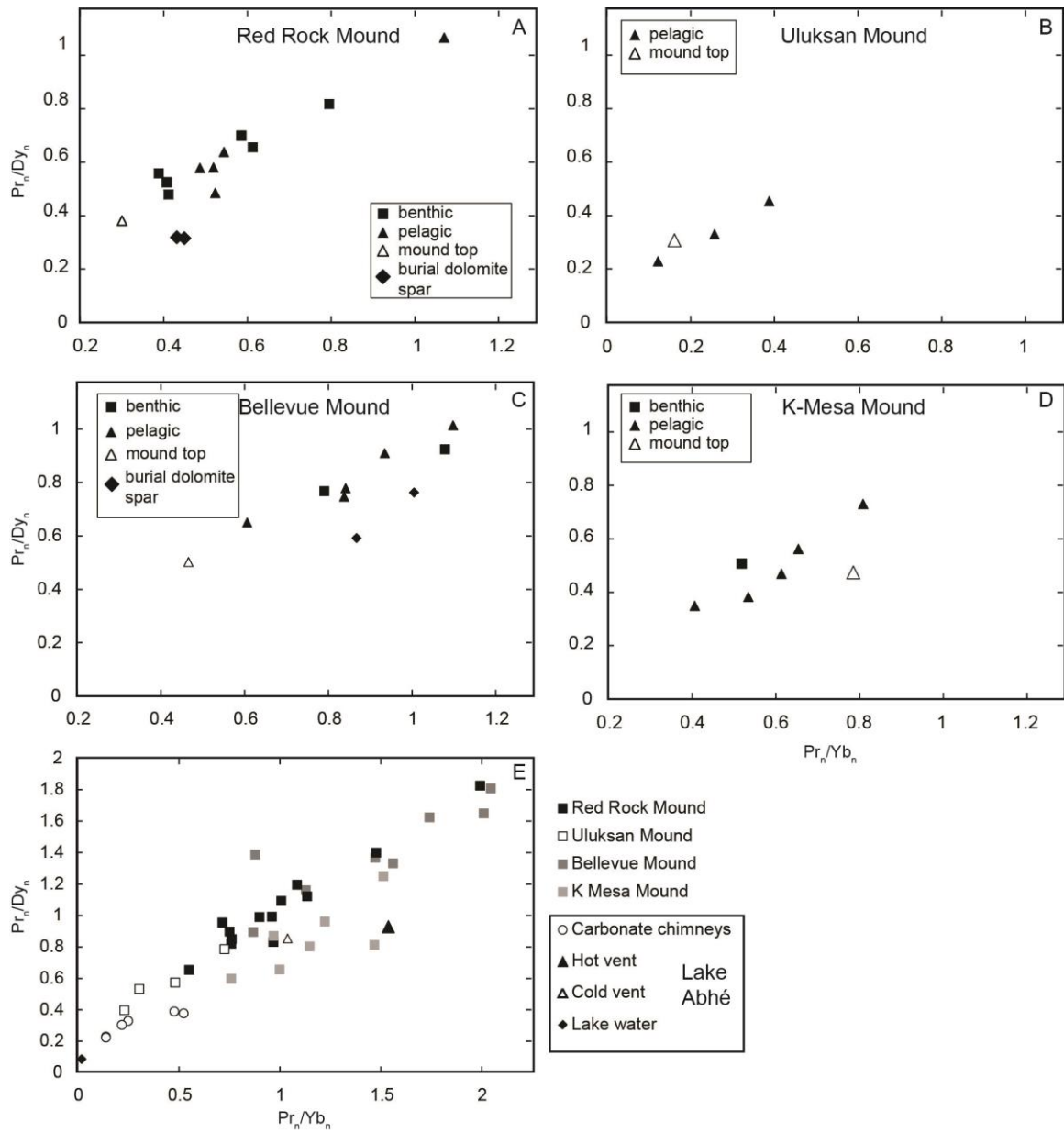


Figure 2-13 - Normalised plots of Pr/Yb vs Pr/Dy

Figure 13: Normalised plots of Pr/Yb vs Pr/Dy for (A) Red Rock Mound, (B) Uluksan Mound, (C) Bellevue Mound, (D) K-Mesa Mound, (E) carbonate chimneys and lake water from Lake Abhé (Dekov et al., 2014), with the results of this study. The lowest values of Pr/Yb and Pr/Dy in this study are interpreted to represent basin water composition, and plot closest to the Pr/Yb and Pr/Dy values for Lake Abhé. The samples

from this study are normalised to local shale in panels A to D. In panel E the results of Dekove et al. (2014), as well as the results of this study, are presented normalised to MuQ.

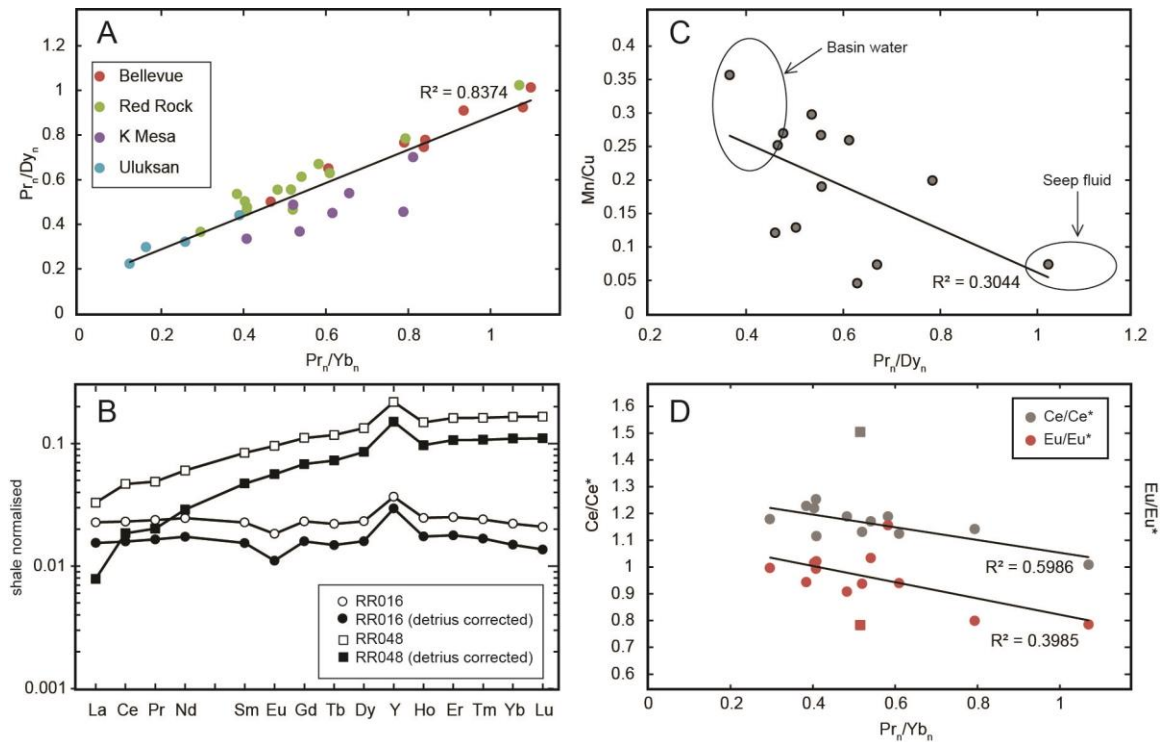


Figure 2-14 - Analysis of REE+Y systematics

Figure 14: Analysis of REE+Y systematics. (A) LREE over very heavy REE depletion (normalised Pr/Yb) versus LREE over medium-heavy (normalised Pr/Dy) REE depletion for samples from all four mounds show strong positive correlation and depict a mixing line (Red Rock mound data are shale-corrected to Al-free). The most seawater-like signatures (lower left end of mixing line) are interpreted as the basin fluid, and the other end of the mixing line as the seep fluid. (B) Contrasting local shale-normalised REE+Y patterns for the two most geochemically extreme samples from Red Rock mound. The most LREE-depleted sample has a positive Ce anomaly, and the sample with the flattest pattern has a negative Eu anomaly. The samples from Red Rock mound have an elevated detrital content and a detrital correction was applied to the two end member fluid compositions for comparison. The shape of the shale normalised patterns did not change with the detrital correction applied. (C) Normalised Pr/Dy ratio vs. Mn/Cu ratio in Red

Rock mound samples. The samples with the strongest LREE depletion (lowest normalised Pr/Dy; interpreted basin fluid) have the highest Mn/Cu, whereas the samples with the flattest patterns (highest normalised Pr/Dy; interpreted seep fluid) have the lowest Mn/Cu. Copper is therefore interpreted as introduced by water-rock interaction of fluid prior to its expulsion into the basin's water column. (D) Normalised Pr/Yb vs. Ce anomaly and Eu anomaly in Red Rock mound samples. The LREE-depleted samples (lowest normalised Pr/Yb; interpreted basin water) have a positive Ce anomaly but no Eu anomaly, whereas the flattest patterns (highest normalised Pr/Yb; interpreted seep fluid) have no Ce anomaly but a negative Eu anomaly. Diagenetic dolomite cements were not plotted, and outlier sample RR037 (square symbol) was not included in linear regressions.

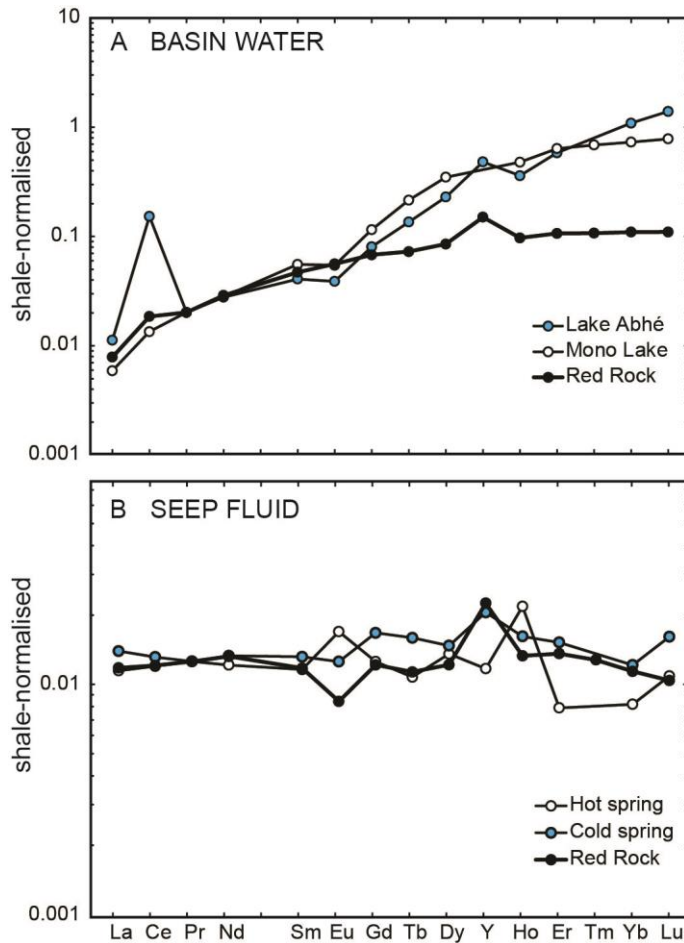


Figure 2-15 - Comparison of interpreted data with modern lakes

Figure 15: Comparison of interpreted basin water and seep fluid composition at Red Rock Mound with modern lake waters and seep fluids (scaled to Pr for ease of comparison and normalised to MuQ). (A) Lake water from Mono Lake (Johannesson et al., 1994) and Lake Abhé (Dekov et al., 2014), carbonate chimneys from Lake Abhé (Dekov et al., 2014), and vent fluids (panel b) from Lake Abhé (Dekov et al., 2014). The REE patterns of modern alkaline lakes are characterised by HREE>LREE, a variable, but usually positive, Ce anomaly, no La anomaly, and in general no Gd anomaly. The cold vent fluids in Lake Abhé closely approximate the inferred seep fluid composition at Red Rock mound (flat REE+Y, negative Eu anomaly, positive Y anomaly).

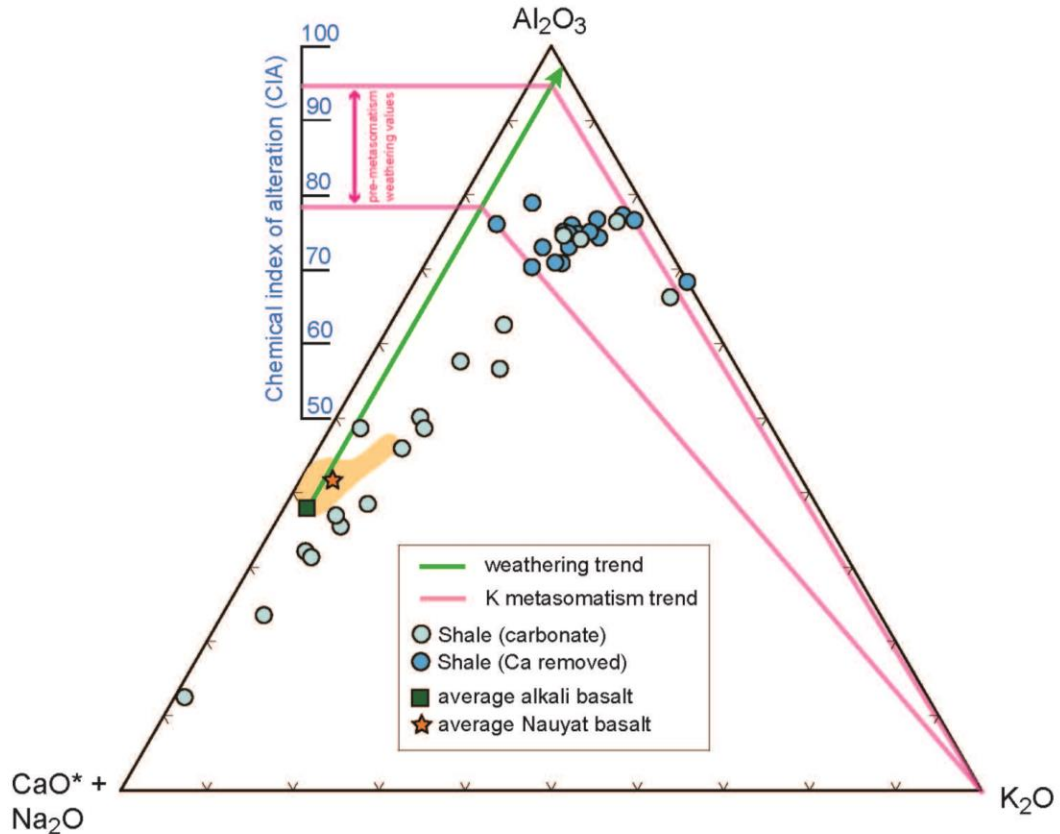


Figure 2-16 - A-CN-K diagram of shale

Figure 16: Al_2O_3 - $\text{CaO}+\text{Na}_2\text{O}$ - K_2O (A-CN-K) diagram with the Borden basin shale (shaded circles; Turner and Kamber, 2012) and the Nauyat Formation alkali plateau basalt (Dostal et al., 1989), which is interpreted to be the primary source of the shale and basalt-derived solute (Na, K, Ca, Mg) flux to the basin. The Nauyat Formation basalt is variably altered and only the range [orange area] and average [orange star] composition of the least-altered (Group I) basalt reported in Dostal et al. (1989) are shown. The average alkali basalt [green square] composition of Nockolds (1954) is plotted for reference and used to show an expected chemical weathering trend of the basalt (green line). The preserved Ca content of the Borden Basin shale is associated with pelagic

dolomite precipitated during shale deposition (Turner and Kamber, 2012), so carbonate-associated Ca was subtracted prior to plotting [pale blue vs. dark blue circles. The position of the Ca-corrected shale is close to but to the right of the expected weathering trend for the alkali basalt; this indicates K addition (metasomatism) to the shale, which can be corrected for by projecting from the K apex through the position of the sample (pink line) to the alkali basalt weathering trend (Fedo et al., 1995) to reveal pre-metasomatism (K-corrected) CIA values. The high pre-metasomatism CIA values (78-94) of the shale indicate substantial loss of Na, Ca, and, by inference, Mg, during chemical weathering of the Nauyat Formation basalt to produce the Arctic Bay Formation shale. Such high degrees of alkali basalt weathering would have exerted a strong control on basin cation chemistry and are inferred to have influenced the alkalinity of the basin.

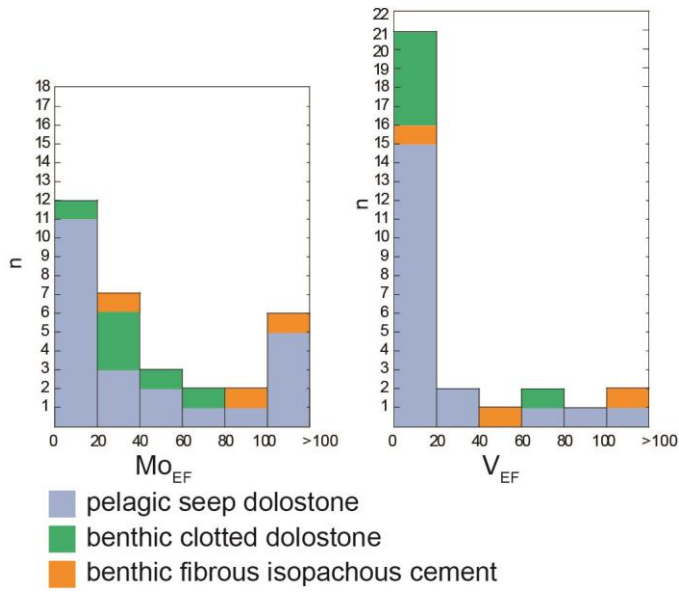


Figure 2-17 - Histograms of enrichment factors of Mo and V

Figure 17: Histograms of the enrichment factors of Mo and V illustrate that no single carbonate phase is preferentially enriched in these redox-sensitive metals.

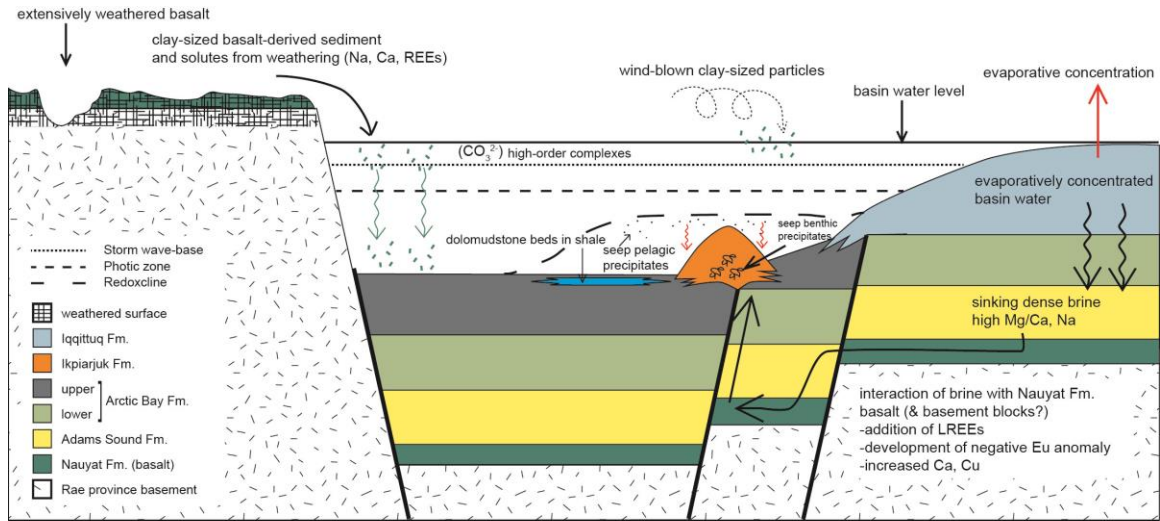


Figure 2-18 - Schematic cross-section showing mound growth

Figure 18: Schematic cross-section showing factors controlling mound growth. Alkaline basin water had high Na, K, and Ca (and Mg?) concentrations produced through weathering of Nauyat Formation basalt (and probably underlying Rae province granitoid basement), which was locally exposed on horst tops. Lake water REE+Y pattern had a positive slope, with HREEs>LREEs, positive Ce anomaly, no La anomaly, and no consistent Gd anomaly. The REEs fractionated due to the high concentration of high-order carbonate complexes (different from seawater, in which low-order carbonate complexes are the species in highest concentration). In the shallow part of the basin, lake water was concentrated through evaporation, and the heavy, Mg-enriched brine produced after gypsum precipitation descended through underlying rocks. Permeable rocks of the Adams Sound and Nauyat formations acted as aquifers; the brine was slightly heated by the normal geothermal gradient. The brine interacted with Nauyat Formation basalt (and possibly underlying Rae basement; probably Paleoproterozoic gneiss) where it acquired a REE+Y pattern resembling that of the basalt (flat REE pattern, negative Eu anomaly) and

where the Mg/Ca ratio was modified by water-rock interaction. The brine (now containing both Mg and Ca) eventually percolated upwards through porous fault zones to emerge at the basin floor, where it reacted with carbonate-rich lake water and caused carbonate minerals to precipitate both benthically and in the water column in the immediate vicinity of the faults.

Height (m)	BM002	BM007	BM013	BM022	BM124	BM212	BM013	BM054
Type	pelagic dolost	benthic clotte						
Ag	17	16	42	38	13	11	24	41
Cd	11	74	9.2	10	12	2.2	6.6	bdl
In	3.8	0.75	bdl	3.1	12	4.6	0.69	7.5
Sn	263	435	158	240	2289	288	256	2117
Sb	9.5	1.9	2.3	11	36	10	10	40
Cs	bdl	1.3	5.9	1.3	3.3	bdl	3.3	bdl
Ba	1094	2325	4173	3608	2341	519	2758	1306
La	697	476	705	399	339	66	710	358
Ce	1378	949	1470	831	641	148	1424	683
Pr	138	94	163	88	72	19	154	70
Nd	500	350	595	356	251	81	553	272
Sm	83	52	107	69	48	19	97	49
Eu	15	10	15	13	7.1	3.9	13	7.7
Gd	82	53	84	63	41	18	78	44
Tb	11	6.7	13	9	6.1	2.4	11	6.2
Dy	69	36	70	53	38	15	65	36
Ho	16	8.3	15	11	7.8	3.3	14	9.1
Er	45	21	43	34	20	10	38	24
Tm	7.0	2.7	6.3	4.8	3.1	1.4	5.3	3.3
Yb	43	18	36	30	18	8.5	29	18
Lu	6.8	2.6	4.7	4.4	2.7	1.3	3.8	2.5
Hf	1.3	2.7	4.3	2.3	4.6	0.71	3.1	0.85
Ta	bdl							
W	670	689	1208	178	113	15040	365	64
Tl	11	22	23	14	bdl	bdl	19	1.7
Pb	584	3384	736	536	459	643	818	481
Th	25	32	94	42	26	1.8	67	20
U	416	645	407	264	144	456	429	143

Height (m)	Type	BM022	BM124	RR016	RR024	RR028	RR028	RR028	RR037	RR040	
		95	120	0	35	50	50	50	93	108	
		diagenetic do pelagic dolost									
Al ₂ O ₃		0.012	0.007	0.106	0.115	0.081	0.174	0.031	0.027		
Fe ₂ O ₃		0.467	0.198	0.203	0.15	0.332	0.403	0.243	0.214		
MnO		0.078	0.093	0.032	0.093	0.067	0.06	0.069	0.058		
MgO		21.8	22.41	21.78	21.95	21.25	21.76	21.85	22.44		
CaO		30.2	29.59	30.22	30.05	30.75	30.24	30.15	29.56		
Na ₂ O	bdl	bdl	bdl	bdl	bdl	bdl	bdl	bdl	bdl		
K ₂ O	bdl	bdl	bdl	bdl	bdl	bdl	bdl	bdl	bdl		
P ₂ O ₅	bdl	bdl	bdl	bdl	bdl	0.022	bdl	bdl	bdl		
Li		433	71	1393	1151	1490	1082	742	594		
Be		58	11	50	57	65	125	51	52		
Sc		38	bdl	294	275	393	499	126	5.4		
Ti		1363	265	4921	3770	2831	7158	1947	1428		
V		3657	283	1813	3730	1376	1707	3074	3354		
Cr		1996	40	1522	1832	3613	2783	3273	2931		
Co		560	210	361	413	498	581	522	388		
Ni		2865	2091	2866	2657	3169	3249	3380	2546		
Cu		1039000	723	3381	2781	1937	1841	2800	1693		
Zn		2702	bdl	4183	5835	13120	4942	2215	bdl		
Ga		70	30	117	148	114	260	54	39		
As		124	33	193	61	71	129	112	115		
Rb		81	bdl	1282	1137	858	1855	206	159		
Sr		35880	18220	45110	37820	49610	36610	44690	35040		
Y		3098	342	836	1301	1160	2023	1596	1535		
Zr		35	bdl	653	543	622	853	286	157		
Nb		37	5.3	18	30	12	18	24	12		
Mo		47	4.5	19	20	90	37	93	27		

Height (m)	BM022	BM124	RR016	RR024	RR028	RR028	RR028	RR037	RR040
	95	120	0	35	50	50	50	93	108
Type	diagenetic do	diagenetic do	pelagic dolost						
Ag	707	13	28	40	19	19	26	14	15
Cd	17	2.3	13	33	4.2	4.2	8.3	17	5.4
In	56	bdl	1.0	bdl	2.2	2.2	12	3.3	8.8
Sn	1211	80	109	107	229	229	74	302	146
Sb	10	bdl	5.8	3.6	7.3	7.3	4.6	3.3	bdl
Cs	2.3	bdl	35	38	25	25	48	5.2	1.3
Ba	2448	3668	2803	5614	3588	3588	5034	2691	2801
La	1624	163	1108	714	549	549	711	1016	875
Ce	6067	524	2188	1680	1308	1308	2449	3070	2097
Pr	831	64	271	206	166	166	324	267	243
Nd	3692	268	1001	877	694	694	1438	1039	992
Sm	925	47	160	186	149	149	396	222	212
Eu	197	8.6	24	38	32	32	74	36	40
Gd	796	64	127	167	150	150	353	214	205
Tb	108	6.5	18	22	22	22	48	31	29
DY	548	33	103	131	136	136	272	188	171
Ho	100	6.8	22	30	31	31	55	42	40
Er	247	19	62	87	90	90	151	123	117
Tm	33	2.4	8.9	13	13	13	21	18	16
Yb	198	13	52	79	84	84	129	107	104
Lu	26.7	2.0	7.2	12.4	12.6	12.6	19.3	15.4	15.1
Hf	1	bdl	15	14	15	15	25	6.2	2.4
Ta	bdl	bdl	bdl	bdl	bdl	bdl	bdl	bdl	bdl
W	105	437	1226	838	5524	5524	1872	4644	148
Tl	43	1.1	11	19	21	21	16	16	9.5
Pb	582	37	1091	698	477	477	2578	705	769
Th	103	6.7	173	117	135	135	144	174	76
U	147	51	185	293	184	184	155	519	1217

Height (m) Type	03SG21	03SG29c	03SG51	03SG66
	1	10	83	150
	pelagic dolost	pelagic dolost	pelagic dolost	pelagic dolostone
Al ₂ O ₃	0.026	0.003	0.006	0.008
Fe ₂ O ₃	0.121	0.167	0.797	0.12
MnO	0.029	0.058	0.041	0.033
MgO	21.85	22.88	21.81	22.26
CaO	30.15	29.12	30.19	29.74
Na ₂ O	bdl	bdl	bdl	bdl
K ₂ O	bdl	bdl	bdl	bdl
P ₂ O ₅	bdl	bdl	bdl	bdl
Li	731	bdl	956	771
Be	21	73	20	27
Sc	10	bdl	bdl	bdl
Ti	1589	619	575	689
V	1955	1002	3987	408
Cr	557	8.2	18380	62
Co	293	199	2251	279
Ni	2205	2314	6579	2305
Cu	1624	4733	8684	3977
Zn	1621	7970	4430	3457
Ga	35	7.3	71	10
As	51	7.9	218	23
Rb	241	bdl	68	74
Sr	34030	30190	35380	31640
Y	430	1025	462	779
Zr	213	bdl	58	86
Nb	2.0	3.6	43	2.9
Mo	14	68	754	3.6

	03SG21	03SG29c	03SG51	03SG66
Height (m)	1	10	83	150
Type	pelagic dolost	pelagic dolost	pelagic dolost	pelagic dolostone
Ag	25	27	129	49
Cd	11	6.7	10	2.3
In	0.75	11	2.2	6.6
Sn	2.4	2296	254	75
Sb	bdl	7.7	33	bdl
Cs	7.1	bdl	4.0	1.6
Ba	2423	905	2728	4693
La	182	150	100	105
Ce	454	409	306	251
Pr	56	43	37	39
Nd	247	189	170	188
Sm	54	41	44	49
Eu	12	10	9.4	11
Gd	57	64	51	56
Tb	8.1	11	7.8	8.0
Dy	50	74	45	50
Ho	11	20	10	13
Er	31	65	31	47
Tm	4.5	10	4.6	6.9
Yb	30	71	30	49
Lu	4.3	10.8	4.6	7.6
Hf	4.2	bdl	0.81	1.6
Ta	bdl	bdl	bdl	bdl
W	309	867	49690	54
Tl	20	1.1	10	1.0
Pb	433	442	1092	212
Th	36	3.4	8.8	5.3
U	786	670	361	190

Chapter 3

3. **Composition and history of giant lacustrine carbonate seep mounds, Mesoproterozoic Borden Basin, Arctic Canada**

Hahn, K.E. and Turner, E.C.

Laurentian University, Sudbury ON

3.1 **Abstract**

Giant, sub-photoc, late Mesoproterozoic carbonate seep mounds (>200 m thick; kms diameter; Ikpiarjuk Fm.) grew on the floor of a lacustrine basin where slightly heated vent fluids issuing from fault-related basin-floor fissures reacted with euxinic, organic-rich alkaline lake water during regional deposition of black shale (Arctic Bay Fm.). The mounds contain vast volumes of benthic thrombolites, which formed a rigid, deep-water biohermal framework containing void space filled with geopetal dolomudstone and lined by fibrous, isopachous cement. Thrombolite mounds are almost exclusive to shallow-marine, photic settings, and are rare in Precambrian rocks.

The mounds formed in several sub-basins and exhibit slightly variable growth histories. Growth of all mounds initiated during an interval of black shale deposition developed >150 m of paleotopographic relief above the basin floor. After cessation of fluid venting, some mound-tops were exposed and karsted owing to differential uplift.

The sedimentology, mineralogy, and geochemistry of the mounds indicates that the thrombolite-forming microbiota was probably not photosynthetic or aerobic, and

consequently is only superficially similar to Phanerozoic thrombolites, whose microbial community was dominated by photosynthesising cyanobacteria. The Ikpiarjuk Formation thrombolite microbiota was probably dominated by an anaerobic chemoautotrophic or chemoheterotrophic metabolism, a community that has never before been described from the Mesoproterozoic.

3.2 Introduction

Precambrian carbonate rocks provide a record of the evolution of ocean and atmosphere chemistry, as well as a record of the early evolution of life. Archean and Paleoproterozoic carbonate rocks are characterised by sea-floor precipitates that reflect the higher saturation state of carbonate in the oceans at that time, whereas Mesoproterozoic and Neoproterozoic carbonate rocks contain abundant lime mud and clastic textures (e.g., Grotzinger and James, 2000). Almost all fossil evidence in the Precambrian carbonate rock record is confined to the photic zone, with stromatolites being the most important reef-builders. In the late Neoproterozoic, the first appearance of thrombolites (clotted structures built by cyanobacteria) as reef builders occurred (e.g., Grotzinger et al., 2000). There is indirect evidence that chemotrophic primary producers were important organisms in the oceans from as early as the Archean (e.g., Westall et al., 2015). Evidence of these early chemotrophs is limited to very rare examples of disputed microfossils and biologically fractionated isotopes (S and C) measured in sedimentary rocks, and one Mesoproterozoic example of deep-water, possibly sub-photoc, stromatolites (Bartley et al., 2015).

The Mesoproterozoic was an interval of time between the break-up and assembly of two supercontinents (Nuna and Rodinia), and its sedimentary rock record is dominated by non-passive-margin sedimentation (Bradley, 2008; Li et al., 2008; Evans and Michell, 2011). In general, it is interpreted that the Mesoproterozoic ocean was chemically stratified, with oxygen-rich conditions in the upper water column and anoxic and sulfidic (euxinic) or iron-rich (ferruginous) in the lower water column (ie., Canfield, 1998; Poulton and Canfield, 2011). Most Mesoproterozoic sedimentary basins are interpreted as epicratonic seas or intracratonic sedimentary basins. The Mesoproterozoic fossil record is dominated by an increasing diversity of muddy stromatolites along with rare fossil eukaryotes. The first known occurrence of eukaryote algae is present in 1.1 Ga marine rocks of the Hunting Formation (Butterfield, 2000), and recent study on lacustrine siltstone and shale of the Mesoproterozoic Torridon Group documented organic-walled mat-forming prokaryotic and eukaryotic (algal; possible fungal) microfossils preserved in phosphate (Strothers et al., 2011; Battison and Brasier, 2012). The Torridon Group fossil assemblage illustrates that diverse benthic communities were capable of thriving in lacustrine settings during the Mesoproterozoic.

The Ikpiarjuk Formation is a group of Mesoproterozoic deep-water, seep-related dolostone mounds that do not resemble lithofacies known from shallow-water Proterozoic carbonate environments. The mounds formed below the photic zone in an alkaline lake (Hahn et al., 2015), and contain a clotted texture that is similar to Neoproterozoic and Paleozoic thrombolites. This study provides a detailed tectonostratigraphic, paleoenvironmental and sedimentologic description of the mounds

in order to understand the depositional history, microbial component and early diagenesis of the Ikpiarjuk Formation.

3.3 Geological Background

The Borden basin is one of a group of Mesoproterozoic sedimentary basins in the Canadian Arctic (Fig. 1). The Borden Basin consists of three grabens (Jackson and Iannelli, 1981), the largest of which is the Milne Inlet graben (MIG). The MIG is bordered and internally subdivided by northwest-trending faults, and is filled with the 6-km-thick Bylot Supergroup (Fig. 2; Jackson and Iannelli, 1981; Scott and deKemp, 1998). These strata are cross-cut by northwest-trending Franklin-aged dykes (~723 Ma; Denyszyn et al., 2009; Heaman et al., 1992; Pehrsson and Buchan, 1999).

Recent revisions to the tectonic history of the MIG have placed the depositional age of the middle and upper parts of the Bylot Supergroup at ~1.1 Ga, about 170 million years later than previously thought; the basin's origin is probably related to complex tectonic stress associated with the assembly of Rodinia (Turner, 2009, 2011; Long and Turner, 2012; Turner and Kamber, 2012; Fig. 2). The basin initially formed during mild extension, when tholeiitic basalt of the Nauyat Formation (Jackson and Iannelli, 1981; Dostal et al., 1989) erupted subaqueously (Long and Turner, 2012). Marine sandstone of the Adams Sound Formation was then deposited regionally during sag-phase sedimentation (Long and Turner, 2012). The Arctic Bay Formation was deposited during pronounced extension, and produced a westward-deepening and deepening-upward siliciclastic succession (Turner and Kamber, 2012). The upper part of the Arctic Bay Formation, in the northwestern MIG, is a thick black shale (Turner and Kamber, 2012)

with pronounced lateral lithofacies and thickness changes, and evidence of synsedimentary slope failure in deep water near subaqueous fault zones (Turner and Kamber, 2012). Pronounced faulting during deposition of the Arctic Bay Formation also initiated the development of the basin's grabens, with associated deposition of graben-margin detrital wedges (Fabricius Fiord Formation; Jackson and Iannelli, 1981). Deposition of the Ikpiarjuk Formation dolostone mounds took place locally in the shale basin as a result of fluid expulsion along active faults (Fig. 3; Turner, 2004a; Turner, 2009; Hahn and Turner, 2013; Hahn et al., 2015); a coeval, NW-deepening carbonate ramp, the Iqqittuq Formation, developed in the shallower, southeastern part of the basin (Turner, 2009). During precipitation of the mounds, black shale, and carbonate ramp, the climate of the Borden Basin was arid as indicated by bedded evaporates in coastal ramp carbonate (Jackson and Cumming, 1981; Kah et al., 2001). The position of the Borden Basin in an arid climate zone indicates that it was located between 15° and 30° from the paleoequator.

Fluid expulsion along the faults ended at approximately the same time as a major shift in sedimentation in the MIG (Fig. 2); the carbonate ramp of the Iqqittuq Formation is overlain by a rimmed platform (Angmaat Formation) in the southeastern MIG, and black shale of the Arctic Bay Formation is overlain by deep-water laminated dolostone in the northwestern part of the MIG (Nanisivik Formation; Turner, 2009, 2011). During at least the initial phase of Nanisivik and Angmaat formation deposition, the MIG was tectonically active (Turner, 2009). Local, subaqueous debris flows were shed from fault scarps in the basin (Turner, 2004b; 2009), and wedges of terrigenous clastic material were deposited along graben-bounding faults (continued deposition of Fabricius Fiord

Formation; Jackson and Iannelli, 1981; Scott and deKemp, 1998).

Following deposition of the Nanisivik and Angmaat formations, the MIG was uplifted and tilted to the northeast, and underwent significant erosion, (Turner, 2011). The MIG was later re-submerged, and regional shale and limestone of the Victor Bay Formation were deposited as a northwest-deepening ramp during an interval of tectonic quiescence (Iannelli et al., 1992; Sherman et al., 2000, 2001, 2002; Turner, 2011). Uplift and tilting then occurred, and strata in the northwestern part of the basin were karsted even as strata in the southeastern part of the basin were drowned (conformably overlain by Athole Point Formation; Sherman et al., 2002). The tectonic history of the Nunatsiaq Group (upper part of the Bylot Supergroup) remains enigmatic, but probably reflects yet another type of basin regime that included an impressive influx of terrigenous material (Knight and Jackson, 1994; Sherman et al., 2002).

3.4 **Methods**

This study is based on rock descriptions at macroscopic to microscopic scales.

Stratigraphic section measuring and detailed lithofacies mapping were undertaken in the field along with detailed sampling. Field work encompassed nine mounds and mound remnants (Table 1 and 2), some available only in core. Over 700 samples were cut into slabs for analysis under low-power binocular microscope on fresh and weathered surfaces.

Over 200 thin sections were prepared from representative lithofacies samples from all mounds. Thin sections were half-stained with alizarin red and potassium ferricyanide following the methods of Dickson (1966) and examined under transmitted light with a

low-power binocular microscope, and under transmitted polarised light and cross-polarised light under a petrographic microscope. Fifty polished thin sections of the best-preserved material were prepared, and of these, several were examined under cathodoluminescence (CL) using a microscope-mounted Technosyn cold-cathode luminescence system (model 8200 Mk11) operated at a voltage between 10 and 15 kV with a beam current of 250-400 μ A. Results of CL work are qualitative because of beam current variability during operation.

Samples for stable C and O isotope analysis were microdrilled using a 500 μ m tungsten carbide drill-bit on thin-section offcuts. Samples were prepared under a low-power binocular microscope with care taken to avoid late diagenetic phases. Approximately 0.5 mg of sample powder was weighed into glass vials followed by the addition of 0.1 ml of pure phosphoric acid to the side of the container. The containers were then capped and helium-flushed while horizontal to ensure no premature reaction of sample and acid. Samples were reacted at 50°C for 24 h, followed by extraction from sample vials in continuous flow. Measurements were performed at the G.G. Hatch Stable Isotope Lab (University of Ottawa) using a Delta XP mass spectrometer and Gas Bench II, both from Thermo Finnigan.

3.5 Results

3.5.1 *Mound Geometry and Paleoenvironments*

Ikpjarjuk Formation mounds are present where northwest-trending (most mounds) or west-trending (possibly Nanisivik mound) faults have been mapped in the central and northwestern Milne Inlet graben (Scott and deKemp, 1998; Turner, 2004a). At least nine mounds were once present, although some are preserved only as thin feather-edges of

their debris haloes (Shale Valley, Magda, Tremblay mounds; Table 1). The fault system with which mounds are affiliated is known to have been reactivated until the Cretaceous (Jackson et al., 1985); these faults are zones of enduring structural weakness. The fault zones were preferentially eroded during Pleistocene glaciation, and are now marked by northwest-trending valleys and fiords. Glacial removal of the parts of mounds centred over fault zones means that their most central parts are not generally preserved and cannot be characterised. It is possible that the centremost parts of mounds are locally preserved in the subsurface, such as in the Nanisivik area. Some mounds contain in situ benthic and pelagic facies, which are here referred to as ‘in situ’ facies because they are the most proximal of the preserved mound-related lithofacies.

Field relationships indicate that all known mounds began to accumulate during deposition of the upper Arctic Bay Formation black shale (Figs. 4 and 5). Mound bases expand markedly over shale of the surrounding level bottom (Fig. 6a and b); where thick mound facies overlie Arctic Bay shale, the basal ~10 m of the mound typically consists of carbonate intraclast / shale chip debrites with carbonate matrix, locally interlayered with shale (Fig. 6c). Mounds’ plan extent reaches lengths of ~12 km along fault zones (Fig. 6d); their distribution away from the valley exposures of northwest-trending fault zones is difficult to assess owing to the dearth of northeast-trending exposures.

In situ mound facies are present at five mounds (Table 1), all of which preserve mound-tops, and consist of clotted and featureless to faintly banded pale dolostone; there is no consistent pattern to the spatial distribution of these two facies. The thickness of in situ

mound lithofacies is 125 (K-Mesa) to >500 m (Nanisivik; Table 1). In situ mound lithofacies are described in detail below.

Unsorted debris accumulations <1 to ~30 m thick form the distal fringes of mounds where they reach their maximum plan extent, exactly at the contact of Arctic Bay Formation shale and completely terrigenous-free carbonate of the Nanisivik Formation (Fig. 6e and f). These distal upper-flank debrites are dominated by mound-derived clasts (up to cobble-sized), but also locally include centimetric Nanisivik Formation laminite clasts, chips of shale- and dololaminite-derived carbonate concretions, and shale chips (commonly bent). In the central MIG, the Bellevue and K-Mesa mounds accumulated in the transition zone between Iqqittuq and laterally equivalent Arctic Bay formations (lower mound) and between Angmaat and laterally equivalent Nanisivik formations (upper part of mound). The lower part of the Bellevue mound resembles that of the northwestern mounds, with the exception that its eastern end tapers out in the uppermost, outermost ramp facies of the Iqqittuq Formation (Fig. 7a).

Northwestern and central mounds' histories are distinct from one another in the nature of the upper mound flanks and overlying material. Five mounds preserve upper flank and mound-top facies.

At Uluksan, Red Rock, and Nanisivik mounds, the proximal, lower part of upper mound flanks, stratigraphically above the contact of Arctic Bay and Nanisivik formations, and forming the feather edges where mound facies reached their greatest plan extent, consist of accumulations of mound-derived debris; these accumulations locally exhibit crudely

clinoform-like surfaces (Fig. 7b). Such surfaces are also present at the eastern end of Bellevue mound (Fig. 7c).

The upper flanks of mounds and their overlying strata vary by location (western vs. central MIG). Upper flanks of the northwestern mounds exhibit tapering tongues or wedges of mound-derived debris that consists of millimetre- to decimetre-scale, angular clasts of white, mound-facies material (intraclast dolowackestone to (less commonly) dolorudstone) that are unsorted to sorted with pale brown dolomudstone matrix and local, larger, isolated clasts (Fig. 7d-f). These accumulations form chaotic to graded decimetre- to metre-scale interbeds interlayered with Nanisivik Formation dololaminite. Many of the millimetric white clasts are angular; some of the larger clasts contain discernible clotted mound fabric. Locally, some of the white clasts have thin cortices of finely crystalline dolostone. In some examples, several generations of cortical laminae are present and are strongly asymmetrical around the intraclasts. Some grains in the white-clast debrites are round and completely replaced with clear medium-crystalline dolomite with only a finely crystalline dolomite envelope preserved. White clasts are absent in the central MIG mounds. The western upper flank of the Bellevue mound, starting just above the basal debris halo, exhibits ooid dolopackstone interlayered with Nanisivik Formation dololaminite (Fig. 4).

All mounds with preserved tops have conspicuously flat upper surfaces, and contain subtle, centimetric to decimetric paleofractures filled with angular to rounded, centimetric to millimetric clasts of mound-facies rubble, which penetrate mounds up to 50 m from their flat upper surfaces (Fig. 8a and b). At Red Rock Mound, these fractures cross-cut

proximal mound flanks and contain clasts of white-clast debrite and Nanisivik Formation laminite. Similar paleofractures cross-cut moundlets at K-Mesa, Bellevue, and Red Rock mounds.

The strata overlying in situ mound facies differ by location. Uluksan mound is overlain by a thin interval of Nanisivik Formation, followed by a local, basal member of the Strathcona Sound Formation. At Uluksan mound there is at least one interval of synsedimentary-cement-rich beds that are extensively brecciated. At Nanisivik mound, several layers of synsedimentary cement are present in the Nanisivik Formation just above the debrites. Red Rock in situ mound facies are overlain by basal shale of the Victor Bay Formation, as is the Nanisivik mound, as indicated by the close stratigraphic relationship of mound-flank facies and Victor Bay Formation shale (Fig. 4). At K-Mesa, ooid dolograins abruptly overlies the flat mound-top. The lowermost exposures of ooid dolograins at K-Mesa are cross-cut by solution-enhanced breccia. Although the uppermost part of the Bellevue in situ mound facies are now erosionally exposed, and no overlying lithofacies are preserved, the presence of ooids in mound-top fractures and on the upper mound flank indicate that the mound was once overlain by ooid dolograins.

3.5.2 *In situ lithofacies*

3.5.2.1 *Clotted lithofacies*

Very large volumes of most of the mounds are dominated by a clotted texture, herein referred to as thrombolitic. Dolomitisation has produced significant variation in the level of detail preserved in the thrombolite lithofacies (Fig. 9). Three types of thrombolite lithofacies were documented: porous thrombolite, layered thrombolite, and densely packed thrombolite. Due to the extensive recent erosion of in situ mound facies, and

limited access to outcrop through the mounds, it is impossible to discern whether the level of detail documented, or type of thrombolite present in the thrombolite lithofacies is related to proximity to vents or other geographic controls.

3.5.2.2 *Porous thrombolite*

The porous thrombolite lithofacies is common at K-Mesa Mound and at Red Rock Mound, and rare at Bellevue Mound. In outcrop it is defined by clots, generally 1 to 2 cm wide and up to 4 cm high, of finely crystalline dolomite (Fig. 10a), which form a thrombolite framework, and rims of resistant-weathering, isopachous cement. Voids among the clots are filled either with dolomudstone, or coarsely crystalline dolomite cement (Fig. 10b). Clusters of clots form a range of morphologies, including irregular bush-like heads, branching or digitate structures, and massive but porous structures. In some examples, the clots are preferentially vertically oriented. In polished slabs the clot interiors are heterogeneous (Fig. 10b): they consist of finely crystalline pale grey to medium grey dolomite that contains millimetre-scale, coalesced clots that form the framework structure. Isopachous cement that rims the voids among clots is composed of clear, inclusion-rich dolomite. Geopetal structures are uncommon, but where present are defined by dolomudstone overlain by blocky, coarsely crystalline dolomite cement (Fig. 10b). In stained thin sections, the dolomudstone that fills voids is commonly more ferroan than the framework dolomite. In some void-filling dolomudstone, there are fine-sand-sized Fe-rich micritic clasts, and in rare examples, laminated intraclast packstone fills the voids (Fig. 10c). Replacement of clot centres with medium-crystalline clear dolospar is common.

Pervasive dolomitisation has affected all of the textures in the mounds, but crystal size variation and relict textural heterogeneity allow for distinct components to be discerned in thin section. The bulk of the clotted fabric is composed of heterogeneous, fine- to medium-crystalline (crystal size 25 to 100 μm), anhedral dolomite (Fig. 10c) with irregular patches of dolomicrite (clusters of $<4 \mu\text{m}$ crystals). The dolomicrite is present in wispy patches, generally appears white on polished slabs, and is most common defining millimetre-thick clot borders, but is locally patchily distributed through clot interiors. The dolomicrite is commonly more iron-rich (stained more intense blue) than the surrounding medium-crystalline dolomite. In some samples, equant and vaguely elongate micritic structures ($\sim 10 \mu\text{m}$), herein referred to as grumeaux (Cayeux, 1935; Bathurst, 1975), are present in clots (Fig. 10d).

The clots are rimmed by several types of isopachous dolomite cement (described further below; Fig. 9, Fig. 10d, 10f) that nucleated on clot margins. The base of the cement crystal layer is commonly indistinct and in partial optical continuity with finely crystalline dolomite that forms the outer surfaces of clots.

3.5.2.3 *Layered thrombolite*

The layered thrombolite lithofacies is most common at Red Rock mound (Fig. 11). The lithofacies is defined by cm-scale layers of massive, medium-crystalline dolostone, separated by mm-scale clotted layers. The parallel-bedded layers extend laterally for up to 10 m in outcrop, but overall are discontinuous, and are preferentially oriented parallel to the presumed paleo-horizontal (Fig. 11). In polished slab, the clots are defined by white, opaque, wispy, irregular patches of dolomudstone (Fig. 11).

In thin section the layers are defined by cm-scale layers of massive, fine- to medium-crystalline, anhedral dolomite crystals with patches of micritic dolomite. Micritic dolomite is present as continuous rims that define the margins of clots of medium-crystalline dolomite. The massive dolomite consists, therefore, of coalesced clots, with no void space between them, and with their long axes in a paleo-horizontal orientation. The micritic clot-rimming laminae are composed of iron-rich grumeaux. The same iron-rich micritic material is present in continuous (at the hand-sample scale) millimetre-thick laminae between the layers of massive dolomite. The layered thrombolite lithofacies is present throughout Red Rock Mound but is especially common at the top where it forms irregular mound-shaped buildups. The orientation of the layered thrombolites is not consistently parallel to paleohorizontal, and at the top of Red Rock Mound, they appear to form individual small mound-like buildups up to 10 m wide. Discontinuous outcrop exposure did not allow for further classification of these.

3.5.2.4 *Densely packed thrombolite*

The densely packed thrombolite facies consists of coalesced, recrystallised clots composed of medium-crystalline dolomite (Fig. 12). Primary voids and benthic cement are uncommon, and poorly defined where present. Individual clots in thrombolites are defined by heterogeneity in crystal size (25 to 100 μm). Clots are bush-shaped and are generally 1 cm by 1 cm. In outcrop, the lithofacies appears massive, or subtly mottled, but crystal size variations are apparent on polished slabs and in thin section (Fig. 12). Where this lithofacies is present at the base of a mound, solution seams are common, as are clasts of shale incorporated into the framework clots. At Bellevue Mound, this

lithofacies is commonly up to 10% silicified. Finely crystalline quartz preferentially replaced the margins of the clots.

In thin section, the densely packed thrombolite facies is composed of fine- to medium-crystalline, anhedral dolomite crystals. Clots and voids are poorly defined, but the overall texture appears to be digitate- to bush-shaped clots. In rare examples, wispy clusters of iron-rich grumeaux are concentrated along the presumed outer margin of clots.

3.5.2.5 *Synsedimentary Cement*

Synsedimentary cement is a significant component in many of the exposures of thrombolite lithofacies at Red Rock and K-Mesa mounds, and a minor component at Bellevue mound. Most cement types are isopachous and nucleated directly on clots (Fig. 9). Four types of synsedimentary cement are present: blunt-ended recrystallised crystals, fibrous length-fast dolomite, length-slow dolomite, and fibrous hematite-rich dolomite. In general, several generations of the same type of cement overgrow clots. Clots rarely overgrow cement. The cements are highly variable and are discussed in detail below.

3.5.2.6 *Blunt-ended recrystallised prisms*

At Red Rock Mound (and rarely at K-Mesa Mound) blunt-ended, recrystallised crystals are locally present (Fig. 13). The crystals are large (close to 1 mm long and $<50\ \mu\text{m}$ wide), completely replaced, and have square tips. The crystals are present only as overgrowths directly on replaced clots, and are generally overlain by fibrous, length-fast dolomite. All other textural features of the crystals were obliterated by the clear dolomite that now fills them.

3.5.2.7 *Fascicular, length-fast dolomite*

Fascicular, length-fast dolomite generally directly overgrows clots and rarely overgrows blunt-ended crystals (Fig. 13). The cement is isopachous, void-filling, pale brown in plane-polarised light, and inclusion-rich. This cement commonly forms crystal fans with sweeping extinction. Individual crystals are approximately 10 μm wide and up to 2 mm long. Well-preserved growth zones are defined by laminae of inclusions ($<1 \mu\text{m}$). This cement displays dull luminescence in CL, with rare brightly luminescent growth zones. This cement is overgrown by later generations of the same type of cement (but new crystal bundles), fills void space, or terminates in voids that are now occluded with later diagenetic cement.

3.5.2.8 *Fibrous length-slow dolomite*

Fibrous length-slow dolomite forms isopachous crusts 100 to 500 μm thick (Fig. 14). This cement most commonly directly overlies clots (rarely overlies blunt-ended crystals) and consists of bundles of crystals whose commonly curved long axes are perpendicular to clot surfaces (Fig. 14). Individual crystals are approximately 10 μm wide and around 100 μm long, whereas bundles of crystals are approximately 50 μm wide and around 100 μm long. Extinction sweeps along the long axis of the crystals and diverges outward through crystal bundles (Fig. 14). Well-defined growth zones are parallel to void margins, are continuous through neighbouring crystal bundles, and can be correlated between voids. Under cathodoluminescence, this cement has both non-luminescent and dully luminescent growth zones (Fig. 14c). Compositional growth zones are apparent, but the growth zonation under CL is diffuse and it is clear that recrystallisation has occurred. This cement is rarely overlain by internal sediment, and most commonly syntaxially overgrown by later burial-related dolomite cement. In rare examples, partial dissolution

of length-slow dolomite occurred prior to precipitation of later generations of syndimentary cement, as shown by cathodoluminescence growth zones that are truncated and overlain by later length-slow cement.

3.5.2.9 *Hematitic fascicular dolomite*

Hematitic fascicular dolomite was documented only at K-Mesa mound, where it is widespread (Fig. 15). In general, the cement encrusts replaced clots and fills voids. The cement is fibrous with abundant fluid inclusions ($<1 \mu\text{m}$), with growth zones defined by laminae of more abundant inclusions. Hematite inclusions ($<1 \mu\text{m}$) are post-depositional and confined to individual growth zones that have been recrystallized to blocky dolomite. Crystals are approximately $10 \mu\text{m}$ wide and up to $500 \mu\text{m}$ long. Individual growth zones are 20 to $100 \mu\text{m}$ thick. Individual crystals are continuous through growth zones. Some growth zones are recrystallised to clear, anhedral, finely crystalline dolomite. In CL, growth zones that preserve fibrous crystals are brightly luminescent, with hematite-rich zones displaying dull luminescence. Crystal termini are pointed.

3.5.2.10 *Euhedral dolomite*

Euhedral dolomite is isopachous and lines primary voids and early fracture systems (Fig. 16). In CL, euhedral dolomite is dully luminescent with growth zones that luminesce faintly yellow or red. Individual crystals are approximately $100 \mu\text{m}$ wide, and in general the maximum thickness of isopachous euhedral dolomite is $100 \mu\text{m}$. Euhedral dolomite is distinguished from later burial-related euhedral dolomite (not included in this study) because it contains abundant fluid inclusions (necked; less than $5 \mu\text{m}$ long) that are lacking in the later dolomite phase. In fracture systems, euhedral dolomite overgrows geopetal dolomitic crystal silt and, rarely, replaces primary dolomitised rock (Fig. 16).

Fractures that are lined with euhedral dolomite contain clasts, also isopachously lined with euhedral dolomite, of both clotted mound and clasts of dolowackestone to packstone of the white clast debrite lithofacies.

3.5.3 Dolomudstone

The dolomudstone lithofacies is characterised by finely crystalline anhedral dolomite with little crystal size variation. The dolomudstone is present in layers <0.5 cm thick, defined by very subtle crystal size variation between layers, or as thicker massive units with indistinct layer contacts (> 1 m). In some intervals, bedding is defined by laminae that are partly silicified. Locally, dolomite layers are recrystallised to medium-crystalline euhedral dolomite. Dolomudstone also fills primary void space in thrombolites.

3.5.4 Stable isotope results

The $\delta^{13}\text{C}$ isotope values of the Ikpiarjuk Formation are between 0 and + 4‰, which is typical for carbonate rocks of this age (e.g., Bartley and Kah, 2004). There is no correlation between $\delta^{13}\text{C}$ or $\delta^{18}\text{O}$ and the phase analysed (clot, carbonate mudstone, isopachous cement). Overall, $\delta^{13}\text{C}$ and $\delta^{18}\text{O}$ are slightly lower (up to 2‰) at Uluksan Mound (Fig. 17), but no other relationships among mounds were documented. There are no correlations between $\delta^{13}\text{C}$ and $\delta^{18}\text{O}$ and any of the trace elements or REE+Y.

3.6 Interpretation of basin depth

The present-day Milne Inlet graben is approximately 250 km long by 80 km wide. A range of carbonate and siliciclastic lithofacies indicates that the basin was shallowest in the SE and deepest in the NW part of the graben during deposition of the Ikpiarjuk Formation. A carbonate ramp accumulated in the SE part of the basin while black shale accumulated in the NW during precipitation of the carbonate mounds. There are few

constraints available to suggest the exact water depth of the basin during formation of the mounds, and the main control on paleo-water depth are the lateral facies relationships between shallow-water strata and related deep-water strata.

The style of sedimentation changed drastically between deposition of Arctic Bay Formation shale and deposition of the Nanisivik Formation. Turner (2009) interpreted the Arctic Bay-Nanisivik transition as tectonically triggered basin shallowing. This change corresponds to the change from a storm-dominated carbonate ramp (Iqqituq Formation) to a rimmed carbonate platform (Angmaat Formation) that built to sea level. In the Angmaat Formation, seafloor precipitates (e.g., crystal fans) are abundant, and it has been hypothesized that carbonate saturation was very high during this time interval (Kah and Knoll, 1996; Kah, 2000; Kah et al., 2001; Turner, 2009). The deep-water equivalent Nanisivik Formation is a medium crystalline laminated dolostone with no sedimentary structures except for very thin laminae of siliciclastic material (interpreted to be wind-blown dust). Turner (2009) suggested that the Nanisivik Formation represented sub-photic deposition because of the lack of any microbial sedimentary features; microbial lamination is abundant in the shallow-water equivalent (Angmaat Formation). Turner (2009) estimated that the Nanisivik Formation may have formed in water depths of approximately 90 m, based on the present-day relief between platform-margin carbonate strata (Angmaat Formation) and basinal carbonate strata (Nanisivik Formation). The change from Arctic Bay to Nanisivik Formation sedimentation is interpreted to be related to abrupt shallowing in the basin. The Ikpiarjuk Formation mounds probably accumulated in deeper-water conditions than those during deposition of the Nanisivik Formation.

The mounds in the shallower SE end of the basin accumulated at the bottom of a storm-dominated carbonate ramp (Iqqituq Formation). This relationship is best exposed at Bellevue Mound, where clinoform-like surfaces are exposed on the southeastern mound margin where ramp strata of the Iqqituq Formation onlap mound lithofacies. Clinoform relief is on the order of approximately 50 m (Fig. 7c), which provides a minimum constraint on water depth for the mound that is interpreted to have formed in the shallowest part of the basin. At this location, the Iqqituq Formation is interpreted have been deposited below wave-base. Therefore, a conservative estimate of paleo-water-depth at this location is >50 m. Bellevue Mound is near the shallow (SE) part of the MIG, and so mounds present in the NW part of the MIG are interpreted to have formed in even deeper-water conditions than did Bellevue mound. Clinoform-like surfaces on the order of ~50 m are present elsewhere in the basin and record minimum original paleotopography of the mounds (Fig. 7b).

There are no stromatolites in the vicinity of mounds (although stromatolites are present in contemporaneous shallow-water carbonates), mound distribution was controlled by faults, and water depth is constrained to > 50 m. It is impossible to estimate the depth of the photic zone in the MIG, but the absence of any evidence of phototactic behaviour in mound framework elements suggests that mounds formed below the photic zone or at most under low-light conditions.

3.7 Interpretation of in situ lithofacies

3.7.1 *Benthic precipitates*

3.7.1.1 *Thrombolites*

Thrombolitic fabric contains two benthic precipitate types: 1) microbial clotted fabric, and 2) syndimentary cement. Thrombolites (Aitken, 1967) are millimetric to centimetric benthic microbial carbonate clots, and are common in lower Paleozoic bioherms. The branching, framework-forming, mesoclotted fabric present in the Ikpiarjuk Formation (Fig. 10) is similar to the mesoclotted framework described by Aitken (1967), and Kennard and James (1986). It is generally accepted that thrombolites form by calcification of benthic microbial communities. The macroscopic and mesoscopic texture of the Ikpiarjuk Formation is identical to thrombolites: branching and digitate irregular structures with detrital material in voids among the framework components. Different from typical thrombolites is the abundant evidence of syndimentary cementation: isopachous, cloudy, bladed cement lines many of the voids among clots. The presence of geopetal structures in voids requires that the microbial clotted framework formed a positionally rigid structure.

The thrombolitic clots in the Ikpiarjuk mounds are recrystallised, whereas most of the syndimentary cements retain at least some primary textural and crystallographic features. This preservational contrast suggests that there was a difference in primary mineralogy or crystal size between microbial clots and abiogenic cement (Table 3; Fig. 9). Given that microbial clots and syndimentary cement precipitated almost coevally, it is most probable that the chemical microenvironment in microbial clots favoured precipitation of an unstable calcium carbonate mineral, probably aragonite, which

destructively recrystallised, over a stable calcium carbonate mineral that did not destructively recrystallise during diagenesis. The local preservation of grumeaux indicates that clot composition was not necessarily monomineralic. The clots are now recrystallised to dolomite. Both calcite and dolomite are trigonal, which means that during diagenesis calcite can recrystallise to dolomite syntaxially and retain primary texture features. Aragonite is orthorhombic, and during recrystallisation to calcite or dolomite primary textures are lost. The microbial clots were probably predominantly composed of aragonite, with grumeaux composed of calcite. Precipitation of calcium carbonate minerals in microbial mats is a complicated process that is controlled by a range of physiochemical conditions, such as the type of microbiota present, the composition of microbial extracellular polymeric substances (EPS), or the water content in the EPS (e.g., Hardiker and Majijevic, 2001; Dupraz et al., 2009). Furthermore, more than one type of calcium carbonate mineral can be produced in the same microbial mat; deep-water cyanobacterial microbialites in alkaline Lake Van are predominantly composed of aragonite, but electron microscopy showed that the aragonite crystals (30 to 100 nm) are covered in a 10 nm-thick film of amorphous calcium carbonate (Benzerara et al., 2006). The reason for aragonitic clots with calcite grumeaux is unknown, but possibilities include a difference in timing of precipitation or difference in composition of microbial community. Chemical conditions were probably different along the margins of clots (i.e., more interaction with pore water) which may explain why grumeaux are more commonly preserved along clot margins. The exact controls on the type of calcium carbonate minerals that precipitate, and the crystal shapes produced, are not currently

understood even in modern microbial mats (e.g., Benzerara et al., 2006; Dupraz et al., 2009).

No microfossils or vestiges of former microbial cells are preserved in the microbial clots, which suggests that *in vivo* calcification of microbial sheaths did not occur. There is no evidence of trapping and binding in the clots. The rare preservation of grumeaux in clots resembles structures described by Turner et al. (2000), in which there is a gradational relationship between grumelous texture and well-preserved tubular filamentous microbial microfossils; the grumelous texture was interpreted as post-mortem calcification of microbial sheaths that took place during decay of the organic matter. In the Neoproterozoic Beck Spring Dolomite, thrombolites contain distinct microbial textures that grade laterally into diffuse microstructures (Harwood and Sumner, 2011; 2012). Harwood and Sumner (2012) interpret such variability in microtexture to be due to the timing of lithification during decay of microbes. The grumelous texture locally present in microbial clots in the Ikpiarjuk Formation is similar in appearance to the textures described by Turner et al. (2000) and Harwood and Sumner (2012), and is conservatively interpreted to have formed during decay of the original organic matter.

The presence of abundant syndimentary cement suggests that abiogenic cement contributed stability to the framework constructed by the thrombolites (Fig. 10). A similar mechanism was proposed by Kah and Grotzinger (1992) to describe the formation of Paleoproterozoic thrombolites that contain a significant volume of syndimentary marine cement. Kah and Grotzinger (1992) suggested that the main source of stability in

thrombolites was inorganic encrustation of microbial communities by marine cement, rather than microbial activity.

The thrombolites in the Ikpiarjuk Formation mounds are not directly related to normal thrombolites, which in general are attributed to cyanobacteria (Aitken, 1967; Kennard and James; 1986; Turner et al., 2000). If a microbial community formed the thrombolitic texture present in the Ikpiarjuk mounds, it was probably not a photosynthetic community, but a consortium of chemosynthetic microbes that derived nutrients or energy from the vent fluids.

3.7.1.2 *Origin of early cements*

All of the cements described in this paper are interpreted as primary precipitates (Table 3; Fig. 9). The inclusion-rich nature and distribution as pore-filling cement along primary growth fabrics and overlain by internal sediment is strong evidence that these cements are symsedimentary. In addition to textural relationships, Hahn et al. (2015) demonstrated that the geochemistry of cements preserved characteristics of the original basin water. The lack of growth zones and the presence of diffuse crystal boundaries under CL indicate that all early cements were subject to diagenetic change, such that their present mineralogy is not necessarily representative of the primary mineralogy.

The blunt-ended recrystallised prisms retain no primary textures other than their external morphology. Based on crystal morphology, the bladed crystals were probably aragonite. Aragonite forms prismatic crystals and is orthorhombic, whereas dolomite is trigonal and does not recrystallise from aragonite syntaxially. Blunt-ended recrystallised prisms are present only directly overgrowing recrystallised clots, also interpreted as originally

aragonitic in composition. The mineralogical controls are discussed further under “synsedimentary diagenesis”.

Fibrous, length-fast dolomite closely resembles fascicular calcite first described by Kendall (1977). Fascicular calcite cement is common as pore-filling cement through the Phanerozoic. Both length-slow (Neoproterozoic cement; Hood et al., 2011; Hood and Wallace, 2012) and length-fast (concretions in Carboniferous coal; Richter et al., 2014) fascicular primary dolomite cements have been documented in the geologic record. Although the textural preservation of the dolomite cement documented in this study is excellent, the lack of preserved primary growth zones in CL suggest that it has recrystallised from its original state, and so the length-fast dolomite described in this study is interpreted to be a syntaxial replacement of fascicular calcite. The fibrous, hematite-rich dolomite cement documented at K-Mesa was also probably a primary fibrous calcite. The pointed crystal tips in this cement suggests a high-Mg calcite precursor. Hematite inclusions are most conspicuous along the boundaries of recrystallised zones and are related to later diagenesis.

Length-slow dolomite probably started as either primary dolomite or herringbone calcite. Two recent studies (Hood and Wallace, 2012; Hood et al., 2015) suggest that the presence of length-slow dolomite is a strong indicator of primary synsedimentary dolomite cement, because most seafloor calcite cement is length-fast, and dolomite replacing length-fast calcite will retain that optical length-fast quality. The length-slow dolomite in this study shows evidence of recrystallisation in CL, and therefore could not have been a stable form of dolomite originally. It is possible that the precursor cement

was a disordered proto-dolomite that recrystallised to a more stable dolomite during burial diagenesis, but still retained the length-slow optical character. Hood and Wallace (2012) described seafloor dolomitisation of Neoproterozoic reef components by a disordered proto-dolomite that later recrystallised to dolomite during burial diagenesis. This interpretation is supported by experimental work of Kaczmarek and Sibley (2011). The interpretation of Hood and Wallace (2012) is supported by the fact that synsedimentary marine dolomite precipitated along with proto-dolomite. In the Ikpiarjuk Formation mounds, the other synsedimentary cements that coprecipitated with the length-slow dolomite are high-Mg calcite and aragonite. The other possible precursor mineral of length-slow dolomite is herringbone calcite. Herringbone calcite is also length-slow, and is known to precipitate under similar deep-water, low-oxygen conditions (Sumner and Grotzinger, 1996). Herringbone calcite consists of alternating bands of pale and dark cement that consists of elongate crystals that are optically unoriented at their bases, with rotation of the c-axis along the crystal's length to be oriented perpendicular to crystal elongation, and are length-slow (Sumner and Grotzinger, 1996). In cross-polarised light, herringbone calcite displays extinction that sweeps up along the growth axis of the crystal (Sumner and Grotzinger, 1996). Almost all examples of herringbone calcite in the rock record have been dolomitised and so descriptions are slightly variable. The length-slow dolomite in the Ikpiarjuk Formation mounds is petrographically similar to other documented examples, especially herringbone calcite in the Mesoproterozoic Dismal Lakes reefs (Bartley et al., 2015), which precipitated in deep-water, possibly sub-photic conditions and overgrows deep-water microbialites. Whether the length-slow dolomite of this study represents precipitation of disordered proto-dolomite or herringbone calcite

does not change the interpretation that this cement precipitated in a depositional environment with high Mg/Ca.

All of the primary precipitates indicate high Mg/Ca in the basin water. Although fascicular optic calcite is generally interpreted to have precipitated in an environment with high Mg/Ca, Richter et al. (2011) demonstrated that radiaxial and fascicular optic calcite cements are not limited to high Mg/Ca environments and can precipitate anywhere from the marine environment to lacustrine environments in variable geochemical environments. The presence of former aragonite precipitates, however, does suggest that the depositional environment had elevated Mg/Ca.

Euhedral dolomite is interpreted to have precipitated as inclusion-rich dolomite after the Nanisivik Formation was exposed and eroded. The well-preserved growth zones in CL indicate that this cement is not recrystallised. The petrographic relationship of this cement with dolomitic crystal silt and mound-top fracture systems indicates that this cement is not a basin-floor precipitate like the other cements described in this study. Early diagenesis is discussed further below.

3.7.2 *Pelagic carbonate mud*

Carbonate mud was abundantly present in the water column around mounds, but not elsewhere in the basin during mound formation. The abundance of mud-filled voids among framework clots, together with large volumes of massive or laminated dolomudstone, indicate that suspended mud-grade particles were produced and deposited in the vicinity of the vent system (Fig. 18). The particulate carbonate is not a distal expression of resedimented shallow-water carbonate (Iqqittuq Formation; Turner, 2009) that was produced at the same time as the Ikpiarjuk Formation, nor is it geochemically

similar to minute amounts of pelagic carbonate that precipitated during deposition of the contemporaneous Arctic Bay Formation (Turner and Kamber, 2011; Hahn et al., 2015). The presence of dolomudstone as void-fill in the clot framework indicates that two types of carbonate precipitation were taking place contemporaneously: benthic (clots and cements) and water-column precipitates (carbonate mudstone). Vast accumulations of faintly banded carbonate mud in some mound locations indicate that, at some times or in some places, water-column precipitation was a much more significant contributor to sea-floor carbonate accumulations than was benthic precipitation. This localised, massive, and spontaneous water-column precipitation of carbonate particles probably reflects episodes of pronounced supersaturation, and may be somewhat analogous to whittings in modern carbonate environments, except that these precipitation events were localised to the direct vicinity of mounds and probably did not occur in the photic zone.

3.8 Discussion

3.8.1 *Mound and basin evolution*

All mounds nucleated during deposition of the upper Arctic Bay Formation black shale, at a time of syndepositional faulting along major fault zones in the MIG's interior (Turner and Kamber, 2012; Figs. 3,5). The presence of small 'moundlets' stratigraphically below the exposed bases of some mounds (Bellevue; Red Rock) suggests that mound nucleation was not entirely temporally or spatially uniform. The production of mound carbonate was much faster than the accumulation rate of terrigenous mud on the surrounding basin-floor, and mounds expanded markedly in their earliest growth phase. In situ mound accumulations (i.e., not resedimented debris facies) consist of benthic (microbially clotted) and pelagic (dolomudstone) components (described in detail below).

Mounds ceased to accumulate at a time corresponding to the abrupt transition between Arctic Bay and Nanisivik formations, contemporaneous with an abrupt change in basin-water chemistry from alkaline lake to marine (Turner, 2009; Turner, 2011). Mounds' maximum topography above the basin floor at the time when mound growth ceased was equivalent to or greater than the difference in stratigraphic elevation between the Arctic Bay Formation- Nanisivik Formation contact and the flat upper surfaces of mounds – a topographic differential of 100 m or more (possibly as much as 400 m at Nanisivik mound, implying greater fluid flow, higher supersaturation, and/or more subsidence during mound growth).

Mound accumulation ceased at all mounds when the entire basin underwent an abrupt change from terrigenous/carbonate-dominated (upper Arctic Bay Fm. in northwest; Iqqittuq Fm. in southeast) to terrigenous-free (Nanisivik Fm. in northwest; Angmaat Fm. in southeast). This event not only terminated delivery of clay-sized terrigenous material to the basin, but also produced shallowing everywhere, best shown by superposition of shallow-water Angmaat Formation lithofacies over outer-ramp facies of the Iqqittuq Formation at the newly established platform margin. Although the Nanisivik Formation contains no shallow-water features, its basin floor was probably shallower than that of the underlying Arctic Bay Formation.

The distal, lower upper mound debris facies at the Arctic Bay-Nanisivik formational contact was deposited during the abrupt transition and basin-wide shallowing event that produced the change from Arctic Bay Formation to Nanisivik Formation in the west and from Iqqittuq Formation to Angmaat Formation in the east. This chaotic material, present

in all mounds where distal flanks are exposed, may record a seismic resedimentation event(s). The coeval, lower part of the Nanisivik Formation is known to contain abundant evidence of resedimentation owing to basin-floor irregularity and syndepositional faulting (Turner, 2009).

Abrupt shallowing in the central and western MIG is supported by evidence of subaerial exposure of Ikpiarjuk Formation mounds, without any discernible, intervening, transitional (shallowing) mound facies. Shallowing and tectonic reorganisation were previously inferred to be the cause of the abrupt but conformable transition from Iqqittuq to Angmaat formations in the southeastern MIG, and of the development of a pronounced platform-margin zone (Angmaat Formation) at Tremblay Sound, where previously only a distal ramp had been present (Iqqittuq Formation; Turner, 2009). Abrupt subaerial exposure of mound-tops (and in the case of Bellevue mound, of an accumulation of Iqqittuq Formation microbial laminite at the mound margin; Figs. 4, 7) led to erosional bevelling of the mounds, producing their flat present-day upper surfaces. These flat subaerial exposure surfaces between mound-tops and overlying strata represent local islands of defunct, cemented mound carbonate that emerged during the abrupt shallowing event and existed briefly in the central MIG, but more persistently during accumulation of the Nanisivik Formation in the western MIG, particularly at Nanisivik. The presence of these localised exposure surfaces only on Ikpiarjuk Formation mound-tops strongly suggests that there was a third episode of uplift and tilting in the basin (the other two being after Nanisivik Formation deposition and after Victor Bay Formation deposition). The climate during deposition of the Ikpiarjuk Formation was arid, as demonstrated by coastal evaporites in the Iqqittuq Formation, which means that significant karsting would

not have occurred on Ikpiarjuk Formation mound-tops (Jackson and Cumming, 1981; Kah et al., 2001). The mound-tops were extensively eroded, as evidenced by the laterally extensive and very thick debrite accumulations, but the erosion of mound-tops was probably due to physical processes (i.e., wave-action) rather than chemical erosion (karsting).

Upper mound-flank lithofacies in the northwestern MIG, consisting of voluminous debrites and turbidites of white, mound-derived clasts, interlayered with Nanisivik Formation, are interpreted as material eroded from mound-tops during the protracted but local (limited to mounds) subaerial exposure interval. White-clast debrites span hundreds of metres of drill-core thickness in the Nanisivik mound (Table 1; Fig. 4), indicating that that mound was unusually highstanding and thick relative to the other northwestern mounds at the end of the growth interval, and that its uplift exposed an especially large volume of material to subaerial or very shallow-marine erosion, permitting accumulation of vast volumes of debris as mound-flanking wedges. The presence of cortices on some resedimented millimetric clasts suggests that mound-tops may have had an episode (and/or location) of shallow-water reworking during which clasts were reworked and carbonate precipitated on them to form crude cortoids, prior to their export down the lower part of the mound's upper flank. Angular coated grains with pronounced cortical asymmetry are present in white-clast debrites at Red Rock Mound (Fig. 7). It is possible that these record the development of pisoids (caliche) in the subaerially exposed parts of Red Rock Mound. Other than the large volume of debrites and the flat mound tops, no other conspicuous exposure surfaces or meteoric features are present.

The presence of solution-enhanced fractures in upper parts of mounds is probably due to post-Nanisivik Formation karsting before deposition of the Victor Bay Formation. These solution-enhanced fractures are filled with mound-derived clasts, including cortoid grainstone clasts, and in rare examples, clasts of Nanisivik Formation laminite. The solution-enhanced fractures are lined with isopachous inclusion-rich euhedral dolomite cement. In rare examples, this cement is predated by geopetal dolomitic crystal silt in primary voids.

Upper mound-flank lithofacies at Bellevue Mound consist of ooid dolograins interlayered with lower Nanisivik Formation dololaminite, indicating that the defunct mound-top was shallowly submerged and became the site of ooid shoal nucleation in the central MIG during deposition of the lower Nanisivik Formation. The absence of significant accumulations of white-clast debrite-turbidite in flanking Nanisivik Formation at Bellevue mound probably reflects a less significant volume of subaerially exposed and reworked mound rock than that experienced by the northwestern mounds. As has been demonstrated for two subsequent episodes of differential uplift in the MIG [post-Nanisivik/Angmaat Formation (Turner, 2009, 2011) and post-Victor Bay Formation (Sherman et al., 2002)], each episode of uplift was accompanied by tilting to the northeast, such that the northwestern end of the MIG experienced greater uplift than the central and eastern regions.

Strata immediately overlying mound-tops reflect the continuing evolution of the MIG's post-mound depositional history. The synsedimentary-cement-lined breccias in Nanisivik Formation above both Uluksan and Nanisivik mounds suggests that a second brief

interval of fluid expulsion may have occurred in the most northwestern part of the MIG. In the northwestern MIG, a local exposure surface separates in situ Uluksan mound facies from <100 m of overlying Nanisivik Formation, which is then truncated by another exposure surface representing the local coalescence of the post-Nanisivik unconformity (Turner 2011) and the post-Victor Bay unconformity (Sherman et al., 2002), such that no Victor Bay Formation is preserved. At Red Rock mound (and also probably Nanisivik mound), the mound-top unconformity was overprinted by the post-Nanisivik-Formation unconformity, such that the mound is directly overlain by lower Victor Bay Formation shale (Fig. 4). At Red Rock Mound, the Nanisivik Formation probably never accumulated directly on top of the mound. In contrast, the central-MIG mounds are directly overlain by ooid shoal facies of the Angmaat Formation, indicating that the post-mound episode of uplift and exposure was comparatively brief, and the absence of mound-flanking debrites reflects minimal resedimentation of mound-top material. The mound-growth interval in the central MIG was followed by brief, local exposure followed by accumulation of comparatively deep-water Nanisivik Formation; mounds in central MIG were not as severely affected by post-depositional differential uplift and erosion as were the northwestern-most mounds (Uluksan, Nanisivik, and Red Rock).

In summary, the nature of the local exposure surfaces and overlying strata highlights the effects of two previously identified intervals of differential uplift, tilting, and exposure [post-Nanisivik (Turner, 2009, 2011); post-Victor-Bay (Sherman et al., 2002)], and identifies a third such interval of uplift and tilting, limited to northwestern mounds, at the end of deposition of the Iqqittuq, Arctic Bay, and Ikpiarjuk formations. The effects of this newly identified episode were less pronounced than those of the later two events:

subaerial exposure developed only on the highstanding mound-tops of the Ikpiarjuk Formation. The uplift caused shallowing of the deep basin-floor into a new bathymetric zone (Nanisivik Formation conformably overlies Arctic Bay Formation). The absence of a conspicuous exposure surface separating the Iqqittuq and Angmaat formations in the shallow, southeastern part of the MIG suggests that the uplift was accompanied by tilting to the northeast, as in the later two uplift episodes, such that the southeastern basin floor was not exposed.

3.8.2 *Depositional environment*

The MIG was occupied by an alkaline lake during deposition of the Ikpiarjuk Formation mounds (Hahn et al., 2015), upper Arctic Bay Formation black shale, and Iqqittuq Formation carbonate ramp. Alkaline lakes typically have pH between 9 and 12, and are characterised by variable concentrations of cations Na, K, Mg, Ca and anions Cl^- , SO_4^{2-} , HCO_3^- , CO_3^{2-} (Garrels and Mackenzie, 1967; Cerling, 1994). The MIG depositional environment was anoxic (Turner and Kamber, 2012), below wave-base and probably below the photic zone (Turner, 2009; Hahn and Turner, 2013; Hahn et al., 2015). Such a depositional environment is not generally conducive to voluminous carbonate precipitation, which generally requires well-oxygenated and well-circulated water. In the Ikpiarjuk Formation, benthic and pelagic carbonate precipitation was driven by the interaction of vent fluid (rich in cations) with alkaline lake water (Hahn et al., 2015). The vent fluid must have been warm (though not hydrothermal) in comparison to the lake water, given that it was able to flow upwards, allowing for pelagic precipitates to form in the water column. The porous framework of the mounds does not display any obvious chimney features, a common feature of fluid seeps, or conspicuous conduits for focussed

flow. The vast deposits of mound-derived debrites indicate that the mounds had significant relief above the basin floor, in some cases upwards of 400 m.

The mounds were built in part by microbes (discussed further below) that probably were not cyanobacteria, given the interpreted water depth. At the beginning of mound growth, benthic precipitation may have been driven entirely by abiogenic processes producing a hard substrate on the basin floor, similar to modern microbial buildups at vents in Lake Van (Kempe et al., 1991). It is possible that as the porous, hard substrate developed, the passage of mildly heated vent fluid drew cold lakewater towards the mound structure by convection, in a manner similar to endo-upwelling of modern reefs, in which cold, nutrient-rich bottom-water is drawn into a reef structure through geothermal heating and rises through the reef providing nutrients to organisms at its surface (Rougerie et al., 1993).

Thrombolite formation generally preceded early cement precipitation and was a constant phenomenon throughout mound growth (Fig. 9). Locally, however, clots clearly post-dated (overgrew) benthic cements. Benthic cement nucleated on clots and continuously precipitated in framework void space, at times completely filling voids.

Three different types of high-magnesium carbonate cements are present in the mounds (aragonite, fibrous calcite, herringbone calcite). Aragonite is rare, only nucleated on microbial clots, and overgrown by high-Mg calcite. Fascicular calcite and herringbone calcite (or proto-dolomite; Kaczmarek and Sibley, 2011) never co-occur in the same void. Herringbone calcite is a poorly understood, unusual growth form of calcite that is limited to deep-water, low-oxygen conditions (Fig. 19). Herringbone calcite is thought to be

related to neomorphic recrystallisation of spherulites that form in water conditions with high dissolved inorganic carbon, low oxygen, and possibly elevated Fe^{2+} (Sumner and Grotzinger, 1996; Bartley et al., 2015). The Ikpiarjuk Formation mounds formed through the interaction of vent fluid and basin water in the presence of microbes. Fluid flux probably varied through time, and perhaps the presence of herringbone calcite versus fascicular calcite is a function of evolving pore fluid composition during different stages of fluid venting, as well as the state of decomposing organic matter in clots.

The syndimentary cement breccia was documented only near mound-tops and may reflect very late fluid venting. It is possible that either water conditions or vent fluid composition changed slightly and that an unstable carbonate phase precipitated, similar to cement breccias described by Hood et al. (2015). The cement breccia could have formed through the collapse of a dehydrating unstable carbonate phase such as ikaite. Ikaite, a common precipitate in alkaline lakes, is a hydrated form of carbonate that is stable only in cold water and dehydrates readily, causing shrinkage. The unusual cement-breccia facies was documented only very close to mound-tops, and may have been promoted by energetic hydrodynamic conditions in the upper water column. Alternatively, these cements were not caused by fluid seepage, and were entirely a function of the different physicochemical conditions present near mound-tops. Rapid cement precipitation is promoted by energetic water conditions with ample water circulation, which would have been present as mound-tops passed upwards through wave-base.

Euhedral dolomite cross-cuts dolomitised white-clast debrite lithofacies, which constrains the timing of dolomitisation to before euhedral dolomite precipitation. Euhedral dolomite

probably precipitated during shallow burial, discussed further below, after deposition of the Victor Bay Formation. The timing of precipitation of euhedral dolomite constrains the diagenetic environment of dolomitisation to synsedimentary to shallow burial. Hood and Wallace (2012) documented synsedimentary dolomitisation in a Neoproterozoic reef that began a few metres below the sediment-water interface. The sedimentary environment of the Ikpiarjuk Formation mounds was a low-oxygen, alkaline lake, with elevated Mg/Ca. All of these conditions are associated with removal of the kinetic inhibitors of dolomite precipitation. In some modern alkaline lakes, aragonite precipitates at the sediment-water interface, and dolomitisation occurs below the sediment-water interface (Müller et al., 1972). The mechanism of dolomitisation is discussed more thoroughly in Chapter 5.

Euhedral dolomite is present along the margins of voids associated with mound-top fractures, and also lines compaction-related fractures. The cement rarely overlies geopetal dolomitic crystal silt in fracture systems. In rare fractures systems that are lined with euhedral dolomite, clasts of Nansivik Formation are present, and the dolomitic silt is interpreted to post-date deposition of the Nansivik Formation. Euhedral dolomite is interpreted to have formed during shallow burial of the mounds.

3.8.3 Comparison with modern carbonate seep mounds

Hahn et al. (2015) concluded that vent fluid was non-hydrothermal groundwater rich in solutes. The measured $\delta^{13}\text{C}$ values of the Ikpiarjuk Formation mounds are in a range similar to contemporaneous carbonate strata in the basin, and do not contain any significant negative values. The lack of negative $\delta^{13}\text{C}$ values means that there is no conclusive evidence that methane was a significant component of the vent fluid. There are, however, very high levels of organic carbon in the contemporaneous Arctic Bay

Formation shale (Turner and Kamber, 2012), which suggests that hydrocarbons may have been produced in large quantities during formation of the mounds by (process).

Methane seeps that produce carbonate precipitates are common in the modern marine environment and are present through the Phanerozoic rock record. Carbonate is produced through anaerobic oxidation of methane (AOM) in the presence of sulphate-reducing bacteria (e.g., Alperin and Hoehler, 2009). Such seeps produce small mounds on the seafloor, or lenses of carbonate below the sediment-water interface. In general, the resulting carbonate rocks are highly porous and have a clotted texture. In many examples, macroscopic eukaryotes lived on the hard carbonate substrate produced through AOM. In general, these structures are only a few metres high, although there is one example in the modern environment, Hydrate Ridge in the Pacific Ocean, where chemohierms reach up to 90 m above the seafloor (Teichert et al., 2005). The chemohierms are characterised by clotted aragonite with abundant cement in voids among clots.

The Lost City Hydrothermal Field (LCHF) is located near the Mid-Atlantic Ridge, and is an off-axis, moderate temperature (~40-90°C), high-pH (~9-10.8), serpentinite-based vent system (e.g., Kelley et al., 2001; Fruh-Green et al., 2003; Ludwig et al., 2006). In this environment, carbonate chimneys up to 60 m tall and 15 m wide are accumulating around vents of fluid that contains a high concentration of methane. The carbonate material associated with active vents is characterised by a porous structure made up of aragonite, calcite, and brucite ($\text{Mg}(\text{OH})_2$). Aragonite and brucite are the dominant minerals in actively venting chimneys, and calcite fills pore space in inactive chimneys. In addition to a main central conduit, the chimneys contain variably well developed,

millimetre-wide, sinuous channels through the entire chimney structure, which were additional fluid conduits. The system contains many inactive vents where porosity is much lower, brucite is not present, and the dominant mineralogy is calcite with minor aragonite.

In an Ordovician example of Lost City-like AOM related to serpentinisation reactions, the associated carbonate minerals do not display negative $\delta^{13}\text{C}$ values (-1.5‰ to 0‰; Lavoie and Chi, 2010), and the carbon isotope composition was buffered by seawater during precipitation in an open system. The carbonate minerals directly overgrew seafloor pillow basalt, allowing for the interpretation of methane related to serpentinisation.

Ikpiarkjuk Formation mounds formed in an open system where methane-derived C isotope values may have been buffered by contemporaneous basin water. There are no volcanic rocks known to be associated with the Ikpiarkjuk Formation, so AOM related to serpentinisation reactions can not be demonstrated conclusively as it is in Lavoie and Chi (2010). The lack of negative $\delta^{13}\text{C}$ values does not rule out the possibility that AOM played a role in the production of carbonate, but it cannot be conclusively demonstrated that it did. The extreme enrichment in organic matter in the contemporaneous shale indicates that hydrocarbons produced during gradual burial were probably abundant, which allows allow for the possibility that methane may have been a component of the vent fluid.

The modern world contains several examples of carbonate mounds accumulating in alkaline lakes due to the mixing of subaqueous spring water and lake water. In Mono

Lake, California, large tufa mounds with variable carbonate mineralogy accumulate subaqueously at sites of calcium-rich groundwater discharge. Metastable carbonates such as ikaite ($\text{CaCO}_3 \cdot 6\text{H}_2\text{O}$) and gaylussite ($\text{Na}_2\text{Ca}(\text{CO}_3)_2$), as well as aragonite and calcite, all form depending on microenvironmental conditions such as lakewater temperature and proximity to vents (e.g., Council and Bennet, 1993; Thomas and Farmer, 2008). At Mono Lake, the carbonate precipitation is both biologically induced by cyanobacteria and completely non-biogenic. Benthic carbonate forms near the vents and pelagic carbonate (“whittings”) also forms (Thomas and Farmer, 2008).

Lake Abhé, in the east African rift, is a large, saline, alkaline lake where carbonate chimneys, up to 60 m high, accumulated subaqueously when the lake was deeper (Dekov et al., 2014). The carbonate chimneys form fault-parallel linear clusters, are composed of calcite, low-Mg calcite, and silica, and have been interpreted to have precipitated very rapidly due to mixing of groundwater (either warm or cool) with lakewater (Dekov et al., 2014). The precipitates are geochemically very similar to the Ikpiarjuk Formation mounds (Hahn et al., 2015), and are closer in scale to the Ikpiarjuk Formation mounds than other examples of modern seep-mounds, but lack the clotted fabric of the Ikpiarjuk Formation. There has been no detailed sedimentologic study of the Lake Abhé chimneys and the influence of microbes on the precipitation of the chimneys is currently unknown. Results reported by Dekov et al. (2014) indicate that the parts of the carbonate chimneys that were analysed are composed of skeletal, hollow calcite crystals, arranged in rows, that formed due to rapid precipitation. The chimneys contain alternating zones of calcite and low-Mg calcite, which was attributed to precipitation under dynamic geochemical conditions (Dekov et al., 2014)

Lake Van (Turkey) is an alkaline lake (Möller and Bau, 1993) where carbonate mounds and chimneys are accumulating in water depths of up to 100 m (Kempe et al., 1991; Cukur et al., 2015) at sites where calcium-rich groundwater enters the lake. Most of the carbonate mounds in Lake Van are small (0.5 - 2.0 m high; 10 - 300 m wide), but they are detectable seismically as linear groups along faults (Cukur et al., 2015), and chimneys up to 40 m high have been documented (Kempe et al., 1991). A hard calcite substrate formed inorganically at the initiation of fluid venting. The substrate was then colonised by benthic coccoidal cyanobacteria, which induced further precipitation of aragonite and calcite in carbonate chimneys (Kempe et al., 1991). The texture of microbialites in Lake Van is a clotted microcrystalline aragonite.

The Ikpiarjuk Formation mounds share many sedimentological similarities (i.e., clotted fabric, isolated carbonate build-ups, topographic elevation above the basin floor) with the seep types described above. In most examples of carbonate accumulating in alkaline lakes relating to fluid seepage, a cyanobacterial community is at least in part responsible for the precipitation of aragonite and calcite, which in some cases results in a clotted fabric. Along with the scale of the Ikpiarjuk Formation mounds, the main difference with seep types in modern alkaline lakes is that in the Ikpiarjuk Formation mounds there is no need to invoke a cyanobacterial (i.e., photosynthetic) community due to the deep-water depositional setting. It is not a problem that no exact analogue for Ikpiarkjuk Formation mounds has been described. The lithofacies in modern mounds are highly variable due to the variable nature of lacustrine environments. Small differences in chemistry (i.e., cations present, anions present, pH) and variability in microbiota present can have significant effects on what carbonate mineral precipitates and its growth form. For

example, aragonite, a mineral that precipitates under high Mg/Ca, is precipitated in microbial buildups in alkaline Lake Van, whereas alternating calcite and low magnesium calcite precipitate abiogenically in alkaline Lake Abhé. The scale of Ikpiarjuk Formation mounds is much greater than any mounds described in the literature; this may be a function of very voluminous fluid venting in the Ikpiarjuk Formation, or it may be in part a function of different Earth-surface systems. In Mesoproterozoic lakes and oceans, microbialites would have been able to build extensive microbial buildups because of the lack of benthic and pelagic metazoan grazers and competitors.

3.8.4 Paleobiology of the mounds

The vent-related deep-water depositional setting of the thrombolites in the Ikpiarjuk Formation mounds indicates that they are not directly related to normal, cyanobacterial thrombolites (e.g. Aitken, 1967; Pratt and James, 1982; Kennard and James; 1986). Numerous metabolically diverse bacteria types (*sensu lato*) are associated with carbonate precipitation (Castanier et al., 1999). In the case of the Ikpiarjuk mounds, however, numerous lines of geological evidence help to narrow down the type of microbes responsible for the clots.

The basin floor where mounds accumulated was probably below the photic zone (or in very low light conditions) and below wave-base. Coeval coastal strata contain sulphate evaporites (Iqqittuq Fm.; Jackson and Cumming, 1981; Kah et al., 2001), indicating that sulphate was present in the evaporating, oxidised upper part of the water column. The bottom-water was anoxic and had elevated total organic carbon associated with unrespired pelagic organic matter (Turner and Kamber, 2012). Rare-earth element geochemistry of the mounds indicates that the lower water column was alkaline, yet

calcium-carbonate-undersaturated (Hahn et al., 2015). The vent fluid, which originated as evaporatively concentrated and modified basin water, had an elevated Mg/Ca ratio (Hahn et al., 2015). The two well-preserved synsedimentary cements were calcite (probably high-Mg calcite), but the poorly preserved clots are preserved as interlocking dolomite crystals, suggesting an originally aragonitic composition; heterogeneous primary mineralogy of mound components indicates that microbial metabolism may have exerted some influence on thromboid mineralogy because the preferred mineralogy of 'abiogenic' precipitates that formed when vent and basin fluids mixed was high-Mg calcite.

Precipitation of carbonate was automatic upon mixing of the vent and basin fluid ('abiogenic' benthic cements and possibly 'abiogenic' pelagic carbonate muds), and yet the benthic microbial community could live, or at least be preserved, only in the vicinity of the vent fluid. Vent fluid, originally derived as sinking, oxidised brine that formed in adjacent shallow-water settings and sank through underlying rock, and from which Ca^{2+} had preferentially been removed by sulphate precipitation (Hahn et al., 2015), was not compositionally unusual except for its elevated cation content and high Mg/Ca ratio. Of the breadth of microbial metabolisms, the ones most compatible with carbonate precipitation under the established basin conditions are evaluated below.

The Ikpiarjuk Formation mounds accumulated in water depth >50 m, where light would have either been limited or absent. Several types of phototrophic microbes are adapted to low-light conditions, including different types of cyanobacteria, sulphur bacteria, and iron bacteria (Andersen et al., 2011; Crowe et al., 2014). The largest known modern

lacustrine microbial buildups are in alkaline Lake Van (Turkey) where Ca-rich springs discharge on the lake bottom, and microbialites grow at depths of up to 100 m (Kemp et al., 1991). Living cyanobacteria are present in Lake Van microbialites at 50 m water depth, which is shallower than the interpreted paleo-water depth of the Ikpiarjuk Formation mounds. Living cyanobacteria have been documented at depths of 100 m in an extremely clear lake in Antarctica (Andersen et al., 2011), and Lake Matano (Indonesia) is a chemically stratified, ferruginous lake where green photosynthetic sulphur bacteria live in water depths of up to 150 m, just below the oxic/anoxic boundary layer. In Lake Matano, however, the bacteria do not contribute much to primary productivity or nutrient cycling (Crowe et al., 2014). Bartley et al. (2015) described cusped deep-water microbialites in the Mesoproterozoic Dismal Lake Group that may have formed in low-light or sub-photoc conditions. Although the macro-scale texture of the microbialites described by Bartley et al. (2015) is different from the Ikpiarjuk Formation thrombolites, the internal clotted structure and abundance of carbonate cement share some similarities to the Ikpiarjuk Formation. The Dismal Lakes microbialites were constrained to have formed in water depth to between 12 m and 80 m, and were attributed to either low-light photosynthetic cyanobacteria, or, given the presence of pyrite in microbial microfacies, a sulphide-metabolising bacterial community that lived near a chemocline (Bartley et al., 2015). The Ikpiarjuk Formation mounds formed in water depths that may have been as shallow as the Dismal Lakes microbialites. Given that the mounds are limited to fluid-venting fault zones it is clear that the chemical (and temperature) gradient that would have been present in the vicinity of vents allowed for a unique microbial community to thrive, and the availability of light was only of secondary importance.

Aneorobic oxidation of methane (AOM) is a common metabolic process at submarine low-temperature vents in which methane forms a component of the vent fluid. During AOM, methane is oxidised by archaea in the presence of sulphate-reducing bacteria (e.g., Alperin and Hoehler, 2009), and very rarely Fe (III)-reducing bacteria (Crowe et al., 2011). The process results in passively precipitated carbonate with very negative $\delta^{13}\text{C}$ values. The Ikpiarjuk Formation carbonates are not depleted in ^{13}C relative to contemporaneous shallow-water carbonate strata in the basin, and lack pyrite, which would be expected from the activity of sulphate-reducing bacteria. However, it has been suggested that Precambrian cold-seep carbonates lacked negative $\delta^{13}\text{C}$ in carbonate associated with AOM, because of the much higher proportion of DIC present in Precambrian oceans: methane-seeps may not be distinguishable in Precambrian sedimentary rocks based only on their $\delta^{13}\text{C}$ signature (Bartley and Kah, 2004; Bristow and Grotzinger, 2013). One example of phosphatised putative methanotrophic archaea and sulphur-oxidising bacteria has been documented in Paleoproterozoic rocks (Lepland et al., 2013). These rocks are associated with depleted ^{13}C values in organic matter, and the phosphatised microfossils are attributed to AOM (Lepland et al., 2013), but there are no carbonate buildups associated with the microfossils.

Microbial chemoheterotrophs are capable of producing vast quantities of carbonate solids when exposed to unrespired organic matter (Castanier et al., 1999). Unrespired organic matter would have been continuously supplied in the lower, anoxic water column of the black-shale-accumulating Borden basin. Carbonate precipitation by bacterial heterotrophs in the absence of oxygen takes place as a by-product of either the nitrogen cycle or the sulphur cycle.

Passive carbonate precipitation occurs during bacterial sulphate reduction if sufficient Ca^{2+} is present (Castanier et al., 1999). Microbial metabolism of sulphur is traced back to the early Archean (e.g., Westall et al., 2015), and given that alkaline lakes are known to be highly productive ecosystems, bacterial sulfate reduction and either aerobic or anaerobic oxidation of sulphur were probably occurring in some parts of the alkaline lake. Bacterial sulphate reduction, however, is unlikely to have been the dominant process operating during formation of the mounds. During bacterial sulphate reduction, H_2S is produced, and in the presence of dissolved iron, pyrite then precipitates. Although Ikpiarjuk Formation microbial clots contain rare pyrite, it is not a significant component, and the pyrite does not display any preferential distribution that is limited to microbial clots. Sulphate was present in the basin, but vent fluids were derived as evaporitic brines in the shallow part of the basin, and sulphate would have been removed from the circulating groundwater by the precipitation of gypsum. Sulphate in the deep-water part of the basin was probably limited, because there is evidence that the bottom-water was ferruginous (Planavsky et al., 2011; Hodgkiss et al., 2015).

Ammonium was probably present in the lake's bottom-water (Hodgkiss et al., 2015). Anaerobic oxidation of ammonium (anammox) is a microbial process that requires ammonium (NH_4^+) and nitrite (NO_2^-) to be present, but the process occurs in the presence of Fe (III), rather than NO_2^- (e.g., Clement et al., 2005). During anammox, carbonate may be passively precipitated if Ca^{2+} and organic matter are present (Castanier et al., 1999). Nitrate reduction or anammox in the presence of Fe (III) results in the precipitation of iron oxide. Disseminated hematite is present in the Ikpiarjuk Formation, but has been attributed to burial diagenesis, and does not show preferential distribution in well-

preserved clotted fabrics, and therefore cannot be attributed to benthic microbial processes.

Regardless of the type of microbial metabolism, carbonate was produced because of the delivery of Ca^{2+} and Mg^{2+} by vent fluid. The alkalinity of the water already favoured abiogenic production of carbonate in the form of high-magnesium calcite. A similar mechanism is present in modern microbialites in Lake Van: a hard, abiogenic calcite substrate formed on the lake bottom where Ca^{2+} -rich spring water mixed with alkaline lake water. Coccoid cyanobacteria settled on the abiogenic calcite crust and built aragonitic microbialites. The microbialites constructed a semi-rigid, porous framework, which was then further encrusted by abiogenic calcite cement. Combined biogenic and abiogenic calcium carbonate precipitation is envisioned for the Ikpiarjuk Formation mounds (Fig. 3). There is no evidence for bottom currents in the black shale that was deposited during mound formation, and there is no clear means of delivering nutrients to the basin floor other than by settling of planktonic organic matter, so benthic chemotrophs away from mounds would probably have been nutrient-limited. Localised water circulation was almost certainly generated by thermal contrast in the vicinity of vents, which could have delivered nutrients (ammonium?) present in basin-water more consistently to bacteria in the vicinity of vents (Fig. 18). A fresh supply of nutrients, as well as Ca^{2+} and Mg^{2+} from vent fluids, could have been enough to drive mound formation.

In a study of calcium carbonate precipitation in modern microbial mats, Dupraz et al. (2009) describe up to seven types of microbes operating together in one mat, including:

1) photolithoautotrophs (cyanobacteria); 2) aerobic heterotrophs; 3) fermenters; 4) anaerobic heterotrophs; 5) sulphide oxidisers; 6) anoxyphototrophs; and 7) methanogens. Of these different metabolisms, only three have been demonstrated to be capable of producing calcium carbonate (photolithoautotrophs, anoxyphototrophs, anaerobic heterotrophs), whereas the others promote carbonate dissolution (Dupraz et al., 2009); the relative contribution of each microbe type dictates net carbonate production. Given the complexity of modern microbial carbonate buildups, the lack of organic matter preserved in the Ikpiarjuk Formation mounds, the lack of characteristic isotopic signals, and the possibility of low-light conditions, it is not possible to classify the microbes in the Ikpiarjuk Formation thrombolites beyond suggesting that they were probably anaerobic chemosynthetic autotrophs or some sort of bacterial (nitrate-reducing?) heterotroph.

3.9 Summary

This paper presents two important observations about Mesoproterozoic sedimentary systems: (a) carbonate depositional environments in the Mesoproterozoic are not limited to the shallow marine realm, and (b) microbial chemotrophs were present in deep-water environments and were capable of producing vast deposits of carbonate rocks.

This study presents a detailed sedimentologic and stratigraphic description of a series of very large carbonate mounds that formed due to groundwater venting into the bottom water of an alkaline lake. Six mounds and one erosional remnant are present in outcrop, and one is known from drill-core. The mounds formed via two mechanisms: (a) benthic precipitation (microbial carbonate and abiogenic cement), and (b) pelagic precipitation (carbonate mud in the water column in direct vicinity of vents). The mounds had

significant topographic relief above the basin floor as evidenced by thick buildups of mound-derived debrites. Each mound had a slightly different terminal growth history based on location in the basin.

This paper presents the first known macroscopically visible evidence of deep-water vent-related Mesoproterozoic chemotrophic microbes. Ikpiarjuk Formation thrombolites are important because they provide evidence that thrombolites are not necessarily exclusively shallow-marine buildups. The mounds do not fit any normal classification of Mesoproterozoic carbonate depositional environments. Mesoproterozoic carbonate rocks are generally interpreted as ramp-forming successions in sedimentary system that was gradually changing from cement-dominated to mud-dominated through the Proterozoic. The description of the Ikpiarjuk Formation mounds highlights that at least some Mesoproterozoic basins were more complicated than current models suggest.

3.10 **Acknowledgements**

Field work was financially supported by Canada-Nunavut Geoscience Office, an NSERC Discovery Grant to E. Turner, an NSTP Grant awarded to K. Hahn, and the Polar Continental Shelf Project (Natural Resources Canada). Field work was assisted by T. Chevrier and J. Mathieu. Dr. Mazen Saleh is gratefully acknowledged for reading through our draft and providing thoughtful feedback from the point of view of a microbiologist. Brian Pratt, Linda Kah, Julie Bartley, Alessandro Ielpi, Denis Lavoie, and Mairi Best are all acknowledged for providing helpful feedback on an early version of the manuscript.

3.11 References

- Aitken, J.D. 1967: Classification and environmental significance of cryptalgal limestones and dolomites, with illustrations from the Cambrian and Ordovician southwestern Alberta; *Journal of Sedimentary Petrology*, v.37, n. 4, p. 1163-1178
- Alperin, M.J. and Hoehler, T.M. 2009: Anaerobic methane oxidation by archaea/sulfate-reducing bacteria aggregates: 1. Thermodynamic and physical constraints; *American Journal of Science*, v. 309, p. 869-957
- Andersen, D.T., Sumner, D.Y., Hawes, I., Webster-Brown, J., and McKay, C.P. 2011. Discovery of large conical stromatolites in Lake Untersee, Antarctica; *Geobiology*, v. 9, p. 280-293
- Anbar, A.D., and Knoll, A.H., 2002, Proterozoic Ocean Chemistry and Evolution: A Bioinorganic Bridge?; *Science*, v. 297, p. 1137-1142
- Bartley, J.K., Kah, L.C., Frank, T.D., Lyons, T.W. 2015. Deep-water microbialites of the Mesoproterozoic Dismal Lakes Group: microbial growth, lithification, and implications for coniform stromatolites. *Geobiology*, v.13, p. 15-32
- Bathurst, R.G.C. 1975: Carbonate Sediments and their Diagenesis; *Developments in Sedimentology*, no. 12, Elsevier, Amsterdam, 658 p.
- Battison, L. and Brasier, M.D. 2012. Remarkably preserved prokaryote and eukaryote microfossils within 1 Ga-old lake phosphates of the Torridon Group, NW Scotland. *Precambrian Research*. v. 196-197. p. 204-217

- Benzerara, K., Menguy, N., Lopez-Garcia, P., Yoon, T., Kazmierczak, J., Tyliszczak, T., Guyot, F., Brown, G.E. 2006. Nanoscale detection of organic signatures in carbonate microbialites. *PNAS*, v. 103, n. 25, p. 9440-9445
- Britstow, T.F., and Grotzinger, J.P. 2013: Sulfate availability and the geological record of cold-seep deposits; *Geology*, v. 41, n. 7, p. 811-814
- Bradley, D.C. 2008. Passive margins through earth history. *Earth-Science Reviews* 91, 1-26.
- Butterfield, N.J., 2000, *Bangiomorpha pubescens* n. gen., n. sp.: implications for the evolution of sex, multicellularity, and the Mesoproterozoic/Neoproterozoic radiation of eukaryotes: *Paleobiology*, v. 26, no. 3, p. 386-404
- Canfield, D.E. 1998. A new model for Proterozoic ocean chemistry. *Nature*, v. 396, p. 450-452
- Castanier, S., Métayer-Levrel, G., Perthuisot, J., 1999, Ca-carbonates precipitation and limestone genesis – the microbiologist point of view: *Sedimentary Geology*, v. 126, p. 9-23
- Cayeux, L. 1935: *Les Roches Sedimentaires de France: Roches carbonates*; Masson, Paris, 463 p. Lake Turkana and its precursors in the Turkana Basin, East Africa (Kenya and Ethiopia) Gierlowski-Kordesch, E., Kelts, K., Cerling, T.E. (Eds.), 1994. *Global Geological Record of Lake Basins, Vol. 1.*
- Clement, J., Shrestha, J., Ehrenfeld, J.G., Jaffé, P.R., 2005, Ammonium oxidation couple to dissimilatory reduction of iron under anaerobic conditions in wetland soils: *Soil Biology and Biochemistry*, v. 37, p. 2323-2328

- Council, T.D. and Bennet, P.C. 1993. Geochemistry of ikaite formation at Mono Lake, California: Implications for the origin of tufa mounds. *Geology*. v 21, p. 971-974
- Crowe, S.A., Katsev, S., Leslie, K., Sturm, A., Magen, C., Nomosatryo, S., Pack, M.A., Kessler, J.D., Reeburgh, W.S., Roberts, J.A., González, L., Haffner, G.D., Mucci, A., Sundby, B., Fowle, D.A., 2011, The methane cycle in ferruginous Lake Matano: *Geobiology*, v. 9, p. 61-78
- Crowe, S.A., Maresca, J.A., Jones, C., Sturm, A., Henny, C., Fowle, D.A., Cox, R.P., Delong, E.F., Canfield, D.E., 2014, Deep-water anoxygenic photosynthesis in a ferruginous chemocline: *Geobiology*, v. 12, p. 322-339
- Cukur, D., Krastel, S., Çağatay, M.N., Damci, E., Meydan, A.F., Kim, S. 2015. Evidence of extensive carbonate mounds and sublacustrine channels in shallow waters of Lake Van, eastern Turkey, based on high-resolution chip subbottom profiler and multibeam echosounder data. *Geo-Mar Lett*, v. 35, p. 329-340
- Dekov, V.M., Egueh, N.M., Kamenov, G.D., Bayon, G., Lalonde, S.V., Schmidt, M., Liebetrau, V., Munnik, F., Fouquet, Y., Tanimizu, M., Awaleh, M.O., Guirreh, I., Le Gall, B., 2014. Hydrothermal carbonate chimneys from a continental rift (Afar Rift): Mineralogy, geochemistry, and mode of formation. *Chemical Geology* 387, 87-100.
- Denyszyn, S.W., Halls, H.C., Davis, D.W. and Evans, A.D. 2009: Paleomagnetism and U-Pb geochronology of Franklin Dykes in High Arctic Canada and Greenland: a revised age and paleomagnetic pole constraining block rotations in the Nares Strait region; *Canadian Journal of Earth Sciences*, v. 46, no. 9, p. 689–705.

- Dickson, J.A.D. 1966: Carbonate identification and genesis as revealed by staining; *Journal of Sedimentary Petrology*, v. 36, no. 2, p. 491-505
- Dostal, J., Jackson, G.D. and Galley, A. 1989: Geochemistry of Neohelikian Nauyat plateau basalts, Borden rift basin, northwestern Baffin Island, Canada; *Canadian Journal of Earth Sciences*, v. 26, no. 11, p. 2214–2223
- Dupraz, C., Reid, R.P., Braissant, O., Decho, A.W., Norman, R.S., Visscher, P.T., 2009, Processes of carbonate precipitation in modern microbial mats: *Earth-Science Reviews*, v. 96, p. 141-162
- Fruh-Green, G.L., Kelley, D.S., Bernasconi, S.M., Karson, J.A., Ludwig, K.A., Butterfield, D.A., Boschi, C., Proskurowski, G. 2003: 30,000 Years of Hydrothermal Activity at the Lost City Vent Field; *Science*, v. 301, p. 495-498
- Evans, D.A.D., Mitchell, R.N. 2011. Assembly and breakup of the core of Paleoproterozoic-Mesoproterozoic supercontinent Nuna. *Geology*, v. 39, n. 5, p. 443-446
- Garrels, R.M., Mackenzie, F.T., 1967. Origin of the chemical composition of some springs and lakes. In: Stumm, W. (Ed.), *Equilibrium Concepts in Natural Water Systems*. American Chemical Society, Washington, DC, pp. 222–242.
- Grotzinger, J.P., and James, N.P. 2000. Precambrian carbonates: evolution of understanding *in* *Carbonate Sedimentation and Diagenesis in the Evolving Precambrian World*. SEPM Special Publication 67, p.4-20
- Grotzinger, J.P., Watter, W.A., Knoll, A.H. 2000: Calcified metazoans in thrombolite-stromatolite reefs of the terminal Proterozoic Nama Group, Namibia; *Paleobiology*, v. 26, n. 3, p. 334-359

- Guo, X., and Chafetz, H.S. 2012: Large tufa mounds, Searles Lake, California; *Sedimentology*, v. 59, p. 1509-1535
- Hahn, K.E. and Turner, E.C. 2013: Deep-water carbonate mound lithofacies, Borden Basin, Nunavut; Geological Survey of Canada, Current Research 2013-11, 14 p
- Hahn, K.E., Turner, E.C., Babechuk, M.G., and Kamber, B.S. 2015. Deep-water seep-related carbonate mounds in a Mesoproterozoic alkaline lake, Borden Basin (Nunavut, Canada). *Precambrian Research* (2015).
- Harwood, C.L. and Sumner, D.Y., 2012, Origins of microbial microstructures in the Neoproterozoic Beck Spring Dolomite: variations in microbial community and timing of lithification: *Journal of Sedimentary Research*, v. 82, p. 709-722
- Harwood, C.L. and Sumner, D.Y., 2011, Microbialites of the Neoproterozoic Beck Spring Dolomite, Southern California: *Sedimentology*, v. 58, p. 1648-1673
- Heaman, L.M., LeCheminant, A.N. and Rainbird, R.H. 1992: Nature and timing of Franklin igneous events, Canada: implications for a late Proterozoic mantle plume and the break-up of Laurentia; *Earth and Planetary Science Letters*, v. 109, no 1-2, p. 117-131.
- Hodgkiss, M., Sans-Jofre, P., Kunzmann, M., Cole, D., Gibson, T., Crockford, P.W., Halverson, G.P., 2015, Nitrogen isotopes across a late Mesoproterozoic basin transect, Arctic Bay Formation, Nunavut: Poster session at AGU-GAC-MAC-CGU Joint Assembly, Montreal

Hood, A. v.S., Wallace, M.W., Drysdale, R.N. 2011. Neoproterozoic aragonite-dolomite seas? Widespread marine dolomite precipitation in Cryogenian reef complexes. *Geology*, v. 39, n. 9, p. 871-874

Hood, A.vS. and Wallace, M.W. 2012. Synsedimentary diagenesis in a Cryogenian reef complex: Ubiquitous marine dolomite precipitation. *Sedimentary Geology*. v.255-256, p. 56-71

Hood, A.vS., Wallace, M.W., Reed, C.P., Hoffman, K.-H., Freyer, E.E. 2015. Enigmatic carbonates of the Ombombo Subgroup, Otavi Fold Belt, Namibia: A prelude to extreme Cryogenian anoxia? *Sedimentary Geology*. v. 324, p. 12-31

Iannelli, T. R., 1992. Revised stratigraphy of the late Proterozoic Bylot Supergroup, northern Baffin Island, Arctic Canada; implications for the evolution of Borden Basin: Unpublished Ph.D. thesis, London, Canada, University of Western Ontario, 781 pp.

Jackson, G.D., and Cumming, L.M., 1981, Evaporites and folding in the Neohelikian Society Cliffs Formation, northeastern Bylot Island, Arctic Canada: Geological Survey of Canada 35-44, Paper 81-1C

Jackson, G.D. and Iannelli, T.R. 1981: Rift-related cyclic sedimentation in the Neohelikian Borden Basin, northern Baffin Island; *in* Proterozoic Basins of Canada, Geological Survey of Canada, Paper 81-10, p. 269–302.

Jackson, G.D., Iannelli, T.R., Knight, R.D., and Lebel, D. 1985. Neohelikian Bylot Supergroup of Borden Rift Basin, northwestern Baffin Island, District of Franklin. *in* Current Research, Part A, Geological Survey of Canada, Paper 85-1A, p. 639-649, 1985

- Kaczmarek, S.E., and Sibley, D.F. 2011. On the evolution of dolomite stoichiometry and cation order during high-temperature synthesis experiments: An alternative model for the geochemical evolution of natural dolomites. *Sedimentary Geology*, v. 240, p. 30-40
- Kah, L.C., 2000, Depositional $\delta^{18}\text{O}$ signatures in Proterozoic dolostones: Constraints on seawater chemistry and early diagenesis: *SEPM (Society for Sedimentary Geology) Special Publication*, n. 67, p. 345–360
- Kah, L.C. and Grotzinger, J.P. 1992: Early Proterozoic (1.9 Ga) Thrombolites of the Rocknest Formation, Northwest Territories, Canada; *Palaios*, v. 7, p. 305-315
- Kah, L.C., and Knoll, A.H., 1996, Microbenthic distribution of Proterozoic tidal flats: Environmental and taphonomic considerations: *Geology*, v. 24, p. 79–82
- Kah, L.C., Lyons, T.W., Chesley, J.T., 2001, Geochemistry of 1.2 Ga carbonate-evaporite succession, northern Baffin and Bylot Islands: implications for Mesoproterozoic marine evolution: *Precambrian Research*, v. 111, p. 203-234
- Kempe, S., Kazmierczak, J., Landmann, G., Konuk, T., Reimer, A., Lipp, A. 1991. Largest Known Microbialites Discovered in Lake Van, Turkey. *Nature*. v. 349, p. 605
- Kendall, A.C. 1977. Fascicular-optic calcite: a replacement of bundled acicular carbonate cements. *Journal of Sedimentary Petrology*. v. 47. p. 1056-106
- Kelley, D.S., Karson, J.A., Blackman, D.K., Frueh-Green, G.L., Butterfield, D.A., Lilley, M.D., Olson, E.J., Schrenk, M.O., Roe, K.K., Lebon, G.T. and Rivizzignot, P. 2001: An

off-axis hydrothermal vent field near the mid-Atlantic ridge at 30°N; *Nature*, v. 412, p. 145–149

Kennard, J.M., and James, N.P. 1986: Thrombolites and Stromatolites: Two Distinct Types of Microbial Structures; *Palaios*; v. 1, p. 492-503

Knight, R.D. and Jackson, G.D. 1994: Sedimentology and stratigraphy of the Mesoproterozoic Elwin Subgroup (Aqigilik and Sinasiuvik formations), uppermost Bylot Supergroup, Borden rift basin, northern Baffin Island; Geological Survey of Canada, Bulletin 455, p. 48.

Lavoie, D. and Chi, G. 2010: An Ordovician “Lost City” – venting serpentinite and life oases on Iapetus seafloor; *Canadian Journal of Earth Science*, v. 47, p. 199-207

LeCheminant, A.N. and Heaman L.M. 1989: Mackenzie igneous events, Canada: Middle Proterozoic hotspot magmatism associated with ocean opening; *Earth and Planetary Science Letters*, v. 96, no. 1–2, p. 38–48.

Lepland, A., Joosu, L., Kirsimäe, K., Prave, A.R., Romashkin, A.E., Crne, A.E., Martin, A.P., Fallick, A.E., Somelar, P., Upraus, K., Mänd, K., Roberts, N.M.W., Van Zuillen, M.A., Wirth, R., Schreiber, A., 2014, Potential influence of sulphur bacteria on Palaeoproterozoic phosphogenesis; *Nature Geoscience*, v. 7, p. 20-24

Li, Z.X., et al. 2008. Assembly, configuration, and break-up history of Rodinia: A synthesis. *Precambrian Research* 160, 179-210

Long, D.G.F. and Turner, E.C. 2012: Tectonic, sedimentary and metallogenic re-evaluation of basal strata in the Mesoproterozoic Bylot basins, Nunavut, Canada: are

unconformity-type uranium concentrations a realistic expectation?; *Precambrian Research*, v. 214–215, p. 192–209.

Ludwig, K.A., Kelley, D.S., Butterfield, D.A., Nelson, B.K., Fruch-Green, G. 2006: Formation and evolution of carbonate chimneys at the Lost City Hydrothermal Field; *Geochimica et Cosmochimica Acta*, v. 70, p. 3625-3645

Möller, P. and Bau, M. 1993. Rare-earth patterns with positive cerium anomaly in alkaline waters from Lake Van, Turkey. *Earth and Planetary Science Letters*. v. 117, p. 671-676

Pehrsson, S.J. and Buchan, K.L. 1999: Borden dykes of Baffin Island, Northwest Territories: a Franklin U-Pb baddeleyite age and a paleomagnetic reinterpretation; *Canadian Journal of Earth Sciences*, v. 36, no. 1, p. 65–73.

Poulton, S.W., and Canfield, D. 2011. Ferruginous Conditions: A Dominant Feature of the Ocean through Earth's History. *Elements*, v. 7, p. 107-112

Richter, D.K., Neuser, R.D., Schreuer, J., Gies, H., Immenhauser, A. 2011. Radial-fibrous calcites: A new look at an old problem. *Sedimentary Geology*. v. 239, p. 23-36

Richter, D.K., Heinrich, F., Gesle, A., Neuser, R.D., Gies, H., Immenhauser, A. 2014. First description of Phanerozoic radial-fibrous dolomite. *Sedimentary Geology*. v. 304, p. 1-10

Rougerie, F., and Wauthy, B. 1993. The endo-upwelling concept: from geothermal convection to reef construction. *Coral Reefs*, v. 12, p. 19-30

- Scott, D.J. and de Kemp, E.A. 1998: Bedrock geology compilation, northern Baffin Island and northern Melville Peninsula, Northwest Territories; Geological Survey of Canada, Open File 3633.
- Sherman, A.G., James, N.P. and Narbonne, G.M. 2000: Sedimentology of a late Mesoproterozoic muddy carbonate ramp, northern Baffin Island, Arctic Canada; *in* Carbonate Sedimentation and Diagenesis in the Evolving Precambrian World, J.P. Grotzinger and N.P. James (ed.); Society for Sedimentary Geology (SEPM), Special Publication 67, p. 275–294.
- Sherman, A.G., James, N.P. and Narbonne, G.M. 2001: Anatomy of a cyclically packaged Mesoproterozoic ramp in northern Canada; *Sedimentary Geology*, v. 139, p. 171–203.
- Sherman, A.G., James, N.P. and Narbonne, G.M. 2002: Evidence for reversal of basin polarity during carbonate ramp development in the Mesoproterozoic Borden Basin, Baffin Island; *Canadian Journal of Earth Sciences*, v. 39, p. 519–538.
- Stevens, T.O., and McKinley, J.P., 2000, Abiotic controls on H₂ production from basalt-water reactions and implications for aquifer biogeochemistry: *Environ. Sci. Technol.*, v. 34, p. 826-831
- Strother, P.K., Battison, L., Brasier, M.D., Wellman, C.H. 2011. Earth's earliest non-marine eukaryotes. *Nature*. v. 473. p. 505.
- Sumner, D.Y. and Grotzinger, J.P. 1996. Herringbone calcite: petrography and environmental significance. *Journal of Sedimentary Geology*. v. 66, p. 419-429

- Teichert, B.M.A., Bohrmann, G., Suess, E. 2005: Chemoherms on Hydrate Ridge — Unique microbially-mediated carbonate build-ups growing into the water column; *Paleogeography, Palaeoclimatology, Palaeocology*, v. 227, p. 67–85
- Thomas, M., and Farmer, J. 2008. (24-52-P) Genesis of Mono Lake Tufas by Microbially Mediated Carbonate Precipitation, *Astrobiology*, v. 8, n. 2, p. 416
- Turner, E.C., James, N.P., Narbonne, G.M. 2000: Taphonomic Control on Microstructure in Early Neoproterozoic Reefal Stromatolites and Thrombolites; *Palaios*, v. 15(2), p. 87-111
- Turner, E.C. 2004a: Kilometre-scale carbonate mounds in basinal strata: implications for base-metal mineralization in the Mesoproterozoic Arctic Bay and Society Cliffs formations, Borden Basin, Nunavut, Geological Survey of Canada, Current Research 2004-B4, 12 p.,
- Turner, E.C. 2004b: Origin of basinal carbonate laminites of the Mesoproterozoic Society Cliffs Formation (Borden Basin, Nunavut), and implications for base-metal mineralization; Geological Survey of Canada, Current Research 2004-B2, 1 CD-ROM,
- Turner, E.C. 2009: Mesoproterozoic carbonate systems in the Borden Basin, Nunavut; *Canadian Journal of Earth Sciences*, v. 46, no. 12, p. 915–938.
- Turner, E.C. 2011: Structural and stratigraphic controls on carbonate-hosted base metal mineralization in the Mesoproterozoic Borden Basin (Nanisivik District), Nunavut; *Economic Geology*, v. 106, no. 7, p. 1197–1223.

Turner, E.C. and Kamber, B.S. 2012: Arctic Bay Formation, Borden Basin, Nunavut (Canada): basin evolution, black shale, and dissolved metal systematics in the Mesoproterozoic ocean; *Precambrian Research*, v. 208–211, p. 1–18.

Westall, F., Campbell, K.A., Bréhéret, J.G., Foucher, F., Gautret, P., Hubert, A., Sorieul, S., Grassineau, N., Guido, D.M., 2015, Archean (3.33 Ga) microbe-sediment systems were diverse and flourished in a hydrothermal context: *Geology*, v. 43, no. 7, p. 615-618

Formation	Tectonic History	Sedimentary Environment	Reference
Sinasiuvik Fm.	Distal foreland basin?	Shallowing-upward Complex paleotopography	Knight and Jackson, 1994 Sherman et al., 2002
Aqigilik Fm.			
Strathcona Sound Fm. & Athole Point Fm.			
Victor Bay Fm.	Uplift/Tilting	Uplift and karsting in W end; Drowning and deepening in E (Athole Point Fm.)	Sherman et al., 2001 Sherman et al., 2002
	Quiescence	Re-submersion, NW-deepening ramp	
Nanisivik Fm.	Uplift/Tilting	Dramatic uplift and tilting to the NE	Turner, 2009 Turner, 2011 Turner and Kamber, 2012
Angmaat Fm.	Uplift in NW	NW MIG Active faults, local debris flows, soft sed. deformation Deep-water laminated dolostone	
Arctic Bay Fm.	Extension	Black shale deposition Alluvial fans at graben margins Fault-related carbonate mounds throughout basin	
Iqqittuq Fm.		SE MIG Rimmed carbonate platform	
Adams Sound Fm.	Gentle Subsidence	Shallow-marine sandstone	Long and Turner 2012
Nauyat Fm.		Basalt	
Rae Province Basement			

Figure 3-2 - Stratigraphy of the Bylot Supergroup

Figure 2: Stratigraphy of the Bylot Supergroup, with associated tectonic and depositional environments after Turner (2009, 2011), Turner and Long (2012), and Turner and Kamber (2012).

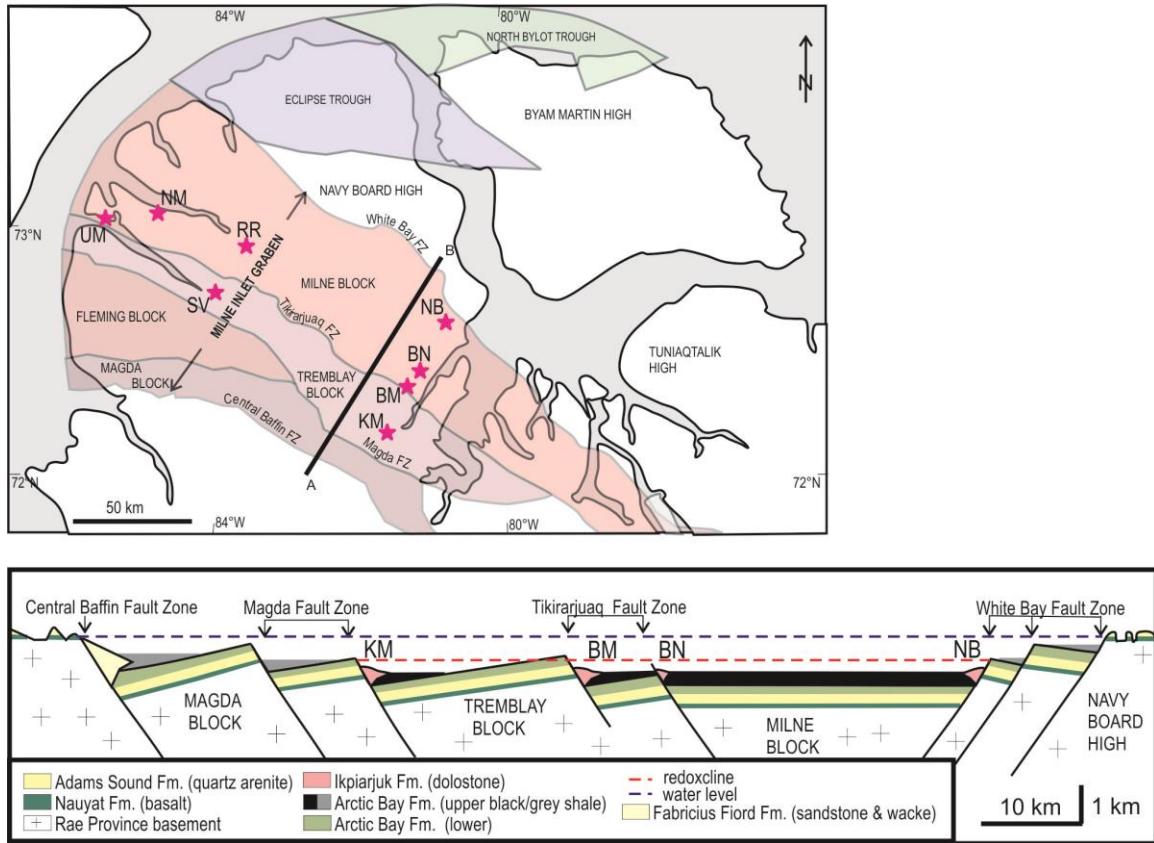


Figure 3-3 - Map of known mound exposures

Figure 3: Map of the Borden basin with all known mound exposures, illustrating basement blocks, sub-basins, and major fault zones at which the Ikpiarjuk Formation mound nucleated. (B) Schematic cross-section (A-B) through the Milne Inlet Graben (after Ianelli, 1992; Turner, 2011).

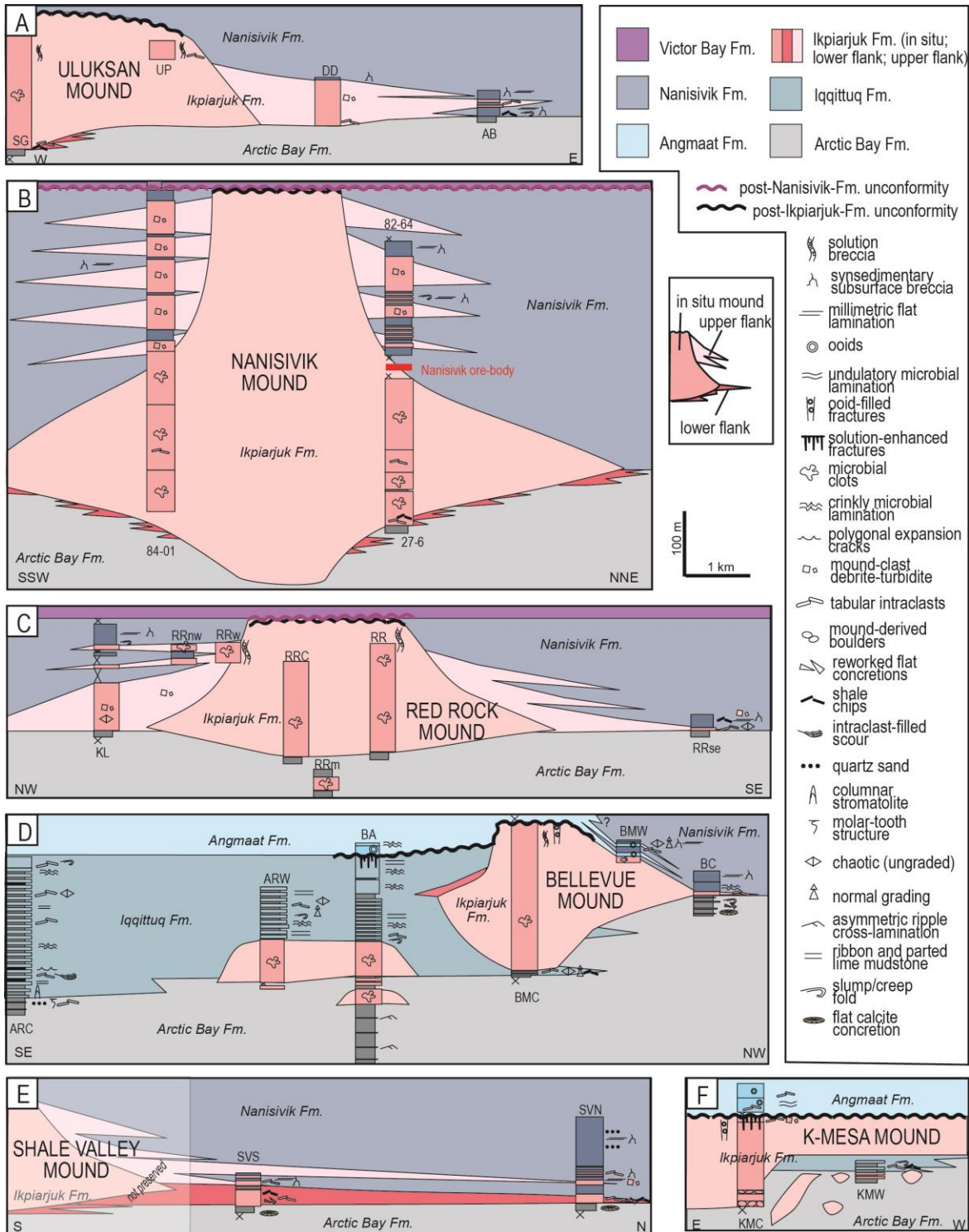


Figure 3-4 - Schematic diagrams of six mounds

Figure 4: Schematic diagrams of six mound exposures and their lithofacies distribution.

(A) Uluksan Mound. (B) Nanisivik Mound. (C) Red Rock Mound. (D) Bellevue Mound.

(E) Shale Valley Mound. (F) K-Mesa Mound.

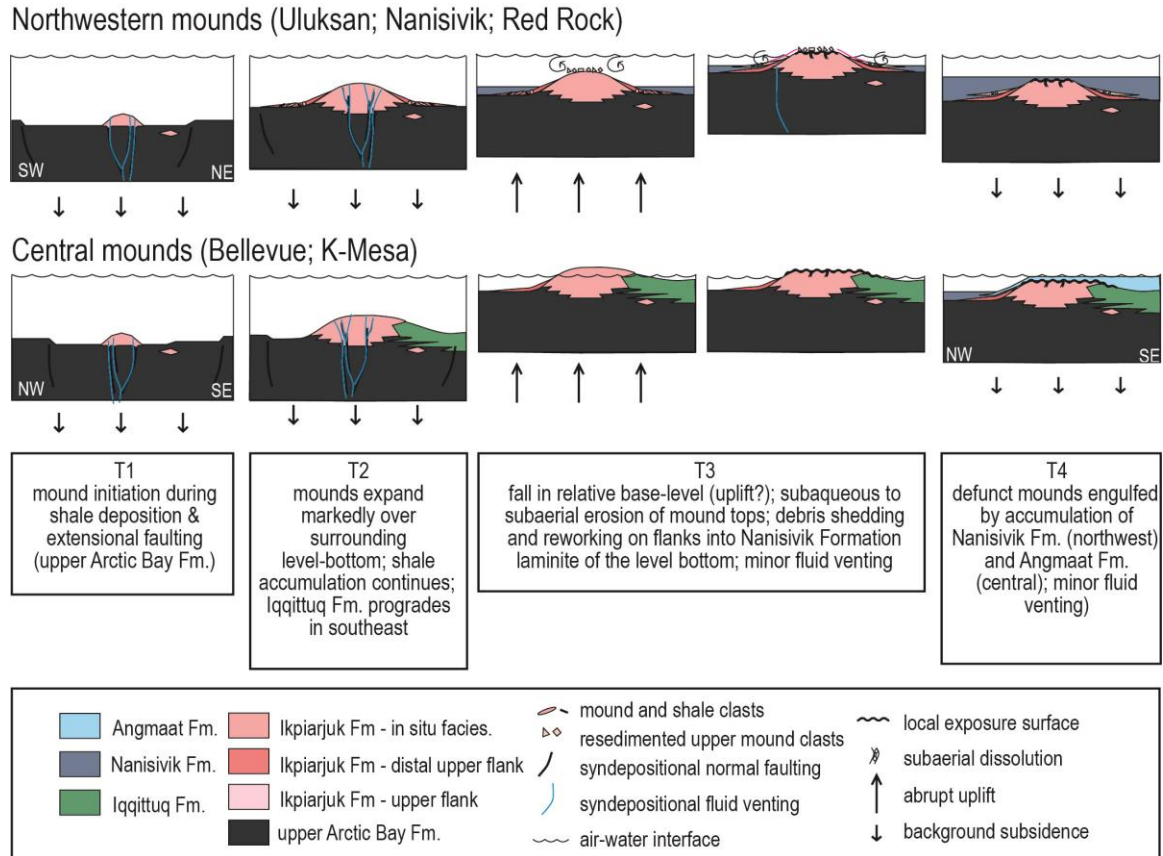


Figure 3-5 Mound histories

Figure 5: Mound histories for (A) northwestern MIG, and (B) central MIG, where Arctic Bay Fm. and all four carbonate formations converge at Bellevue Mtn. Mounds began growing during deposition of upper Arctic Bay Formation black shale and expanded rapidly coeval with continued shale deposition and progradation of a carbonate ramp (Iqqittuq Fm.) in the southeastern MIG. During T3, mounds in the northwestern MIG reached wave-base, where mound-tops were subaqueously eroded. Mounds were eventually subjected to subaerial erosion. In northwestern mounds, copious mound-derived debris was deposited on mound flanks as white-clast debrites. Many of the eroded particles were reworked and developed cortical laminae. In the northwestern MIG, a second brief episode of fluid venting may have occurred at Uluksan and

Nanisivik mounds. During T4, mounds were engulfed by Nanisivik Formation (northwestern MIG) or the Angmaat Fm. (central MIG).

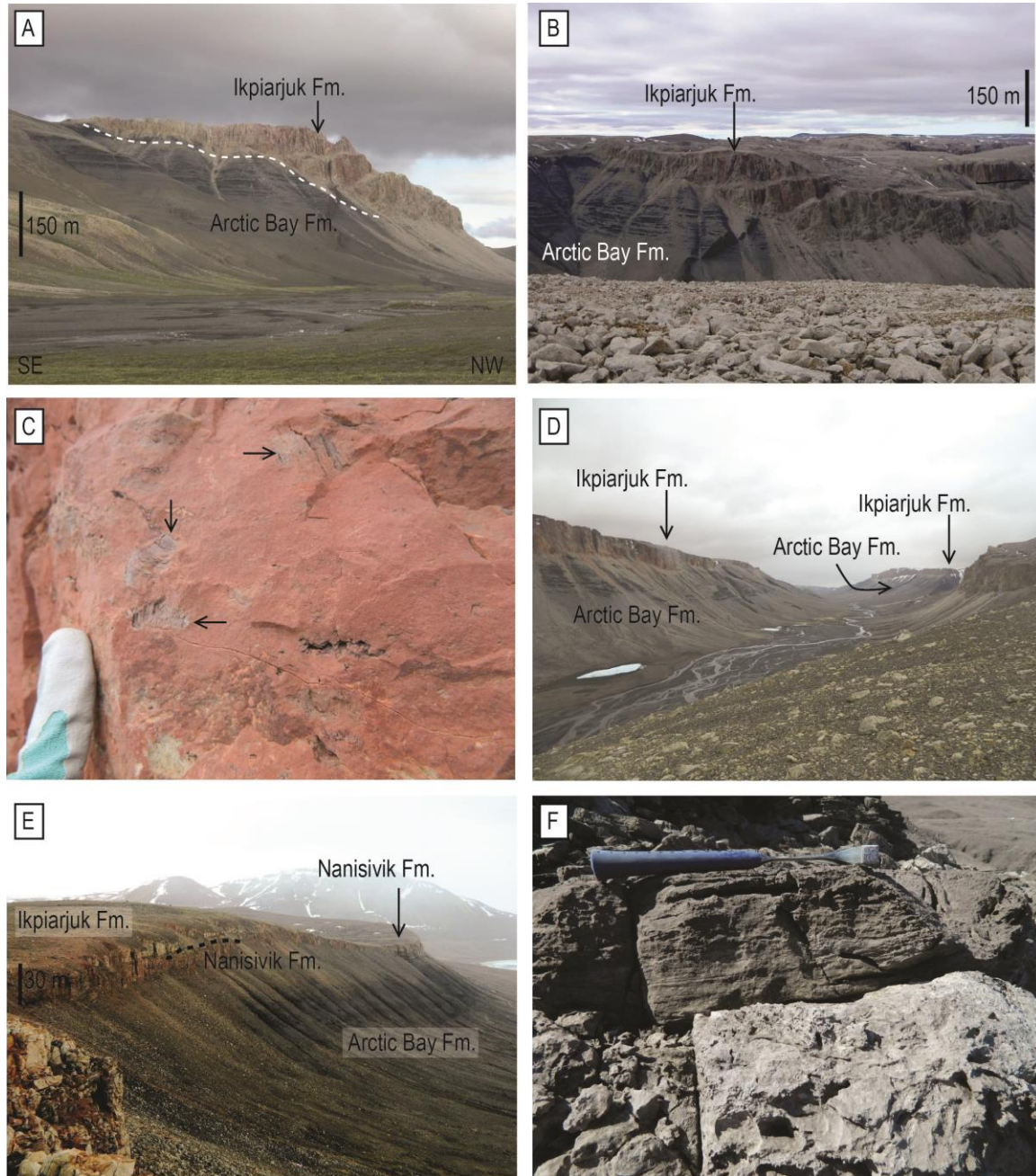


Figure 3-6 Mound exposure field photos

Figure 6: Mound exposures. (A) Outcrop of in situ mound lithofacies directly overlying Arctic Bay Formation shale (Red Rock Mound) with mound-base climbing away from inferred centre of mound. (B) Outcrop of climbing and expanding mound-base at Red Rock Mound. (C) Mound bases typically contain carbonate intraclasts and shale chips

(black arrows) in carbonate matrix (Uluksan Mound). (D) Red Rock Mound extends approximately 12 km SE along a fault zone in valley centre; view to SE. (E) Distal fringe of mound-derived debrite deposits at Uluksan Mound pinching out laterally at the contact between Arctic Bay Formation shale and overlying Nanisivik Formation. (F) Distal mound fringe (pale grey) is directly overlain by Nanisivik Formation dolostone (brown); Bellevue Mound.

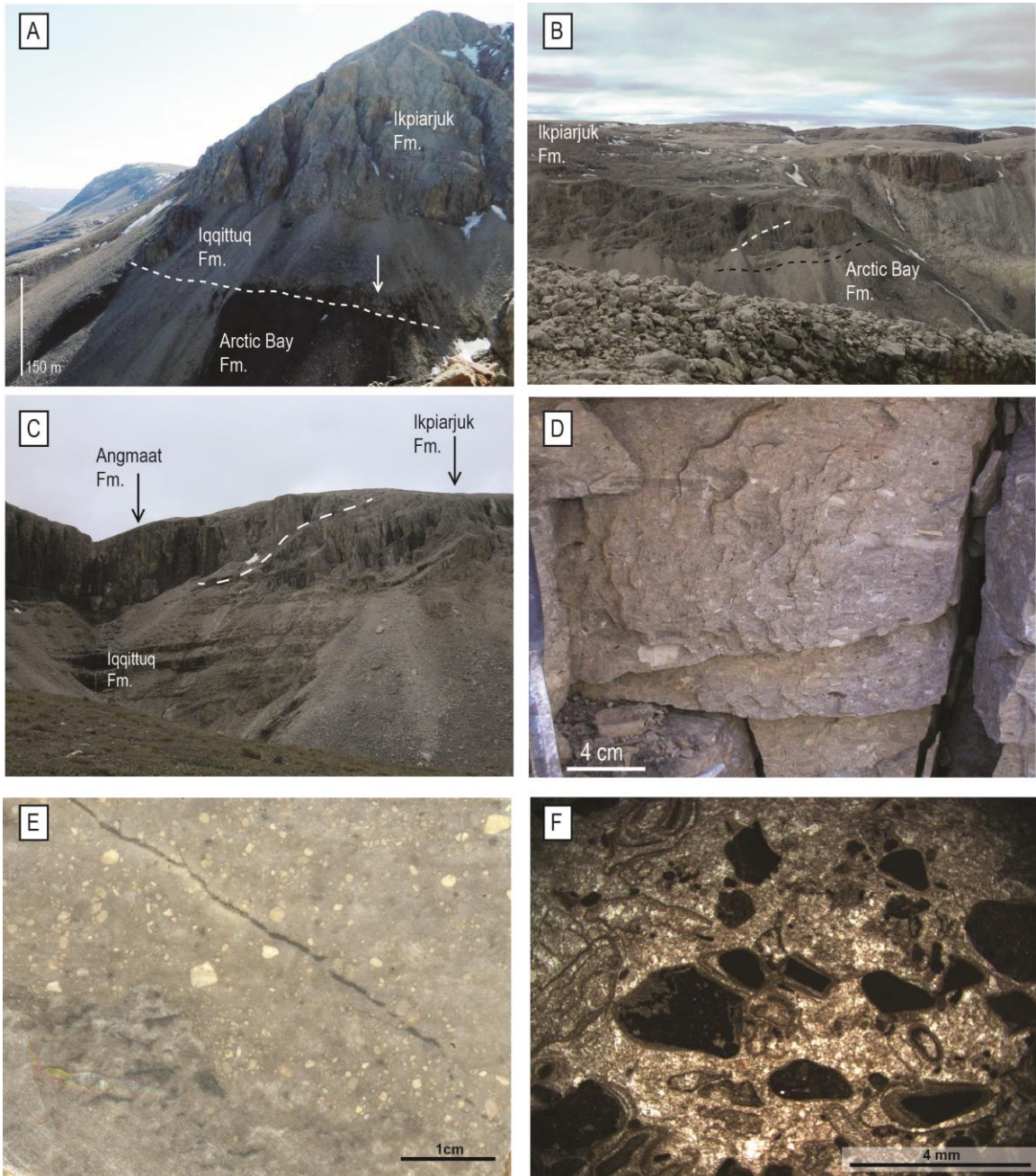


Figure 3-7 Mound exposure field photos

Figure 7: (A) Outcrop exposure of Bellevue mound where mound base interfingers with both Iqjittuq and Arctic Bay formations. (B) Clinoform-like surfaces (dashed white line on one) near the base of Red Rock mound. The contact with the Arctic Bay Formation shale is covered by talus, but it is inferred to be near the base of the mound outcrop. (C)

Outcrop exposure of clinoform-like surfaces at the southeastern distal fringe of Bellevue Mound. The mound overlies the Iqqittuq Formation and is overlain by and intertongued with the Angmaat Formation (dashed line is one example surface). (D) Outcrop of lower upper flank debris lithofacies with mound-derived clasts and Nanisivik Formation clasts (Shale Valley mound). (E) Cut slab example of white-clast debrite directly overlying the clotted lithofacies at Red Rock Mound. (F) Photomicrograph (plane-polarised light) depicting white clasts (dark in transmitted light) with thin cortical layers.

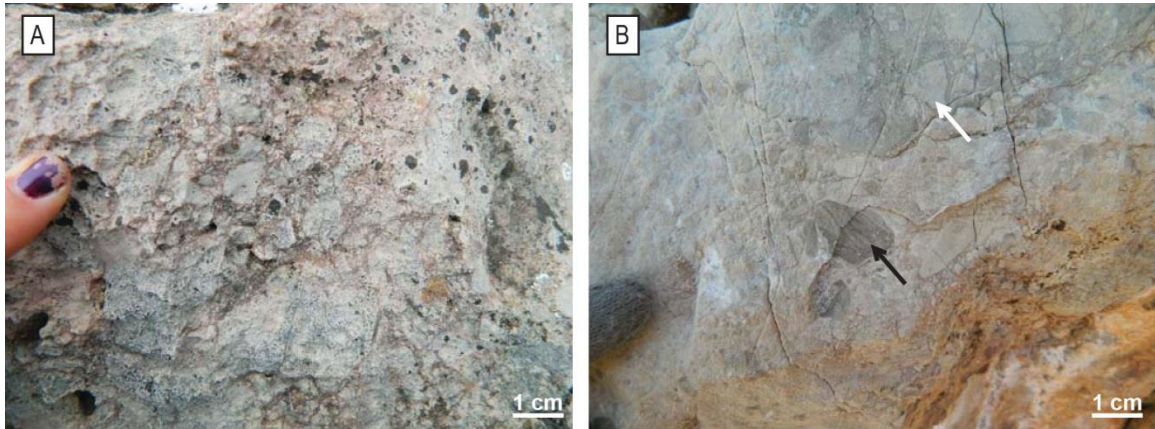


Figure 3-8 Outcrop photos of solution breccia

Figure 8: Outcrop of solution breccia at Red Rock mound, a complicated lithofacies that can contain different clast types. (A) Clasts are entirely mound-derived and surrounded by hematitic dolomite cement. (B) Hematite is not conspicuous and clasts of both Nanisivik Formation (black arrow) and mound-derived clasts (white arrow) are present.

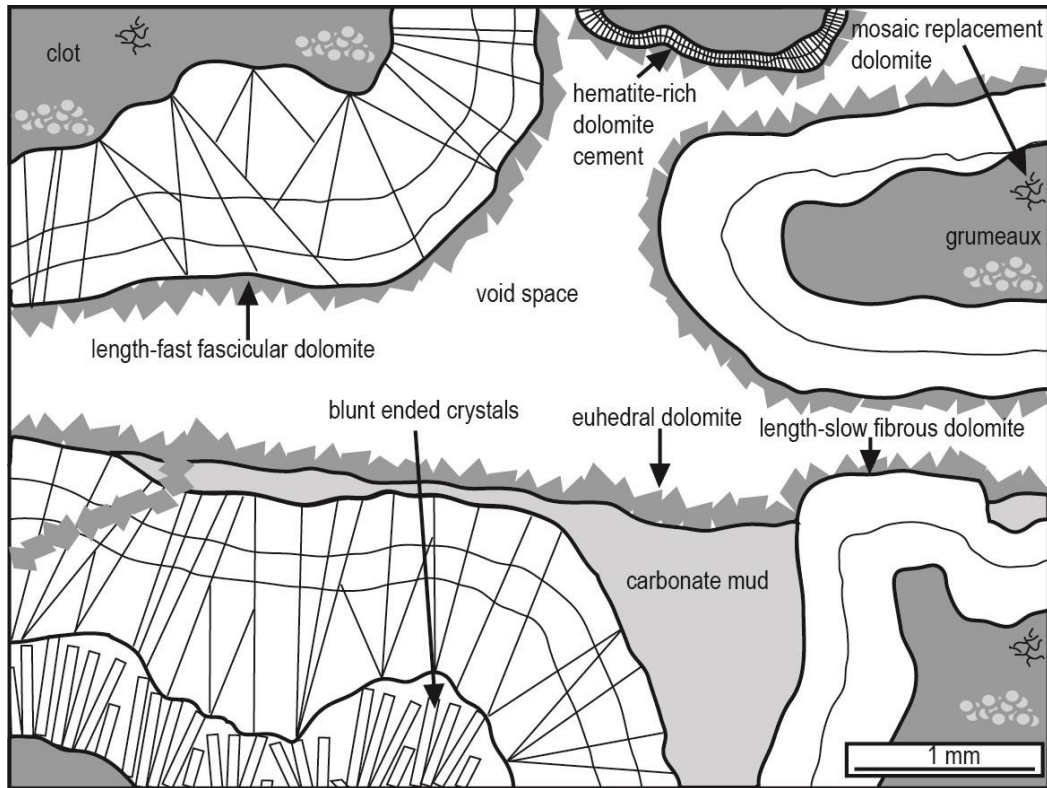


Figure 3-9 Schematic diagram of in situ mound

Figure 9: Schematic diagram of the in situ mound depositional components illustrating the distribution of clots, syndimentary cement, and dolomudstone (does not include massive accumulations of pelagic dolomudstone). Recrystallisation of clots may have occurred very early during the paragenetic history of the mounds.

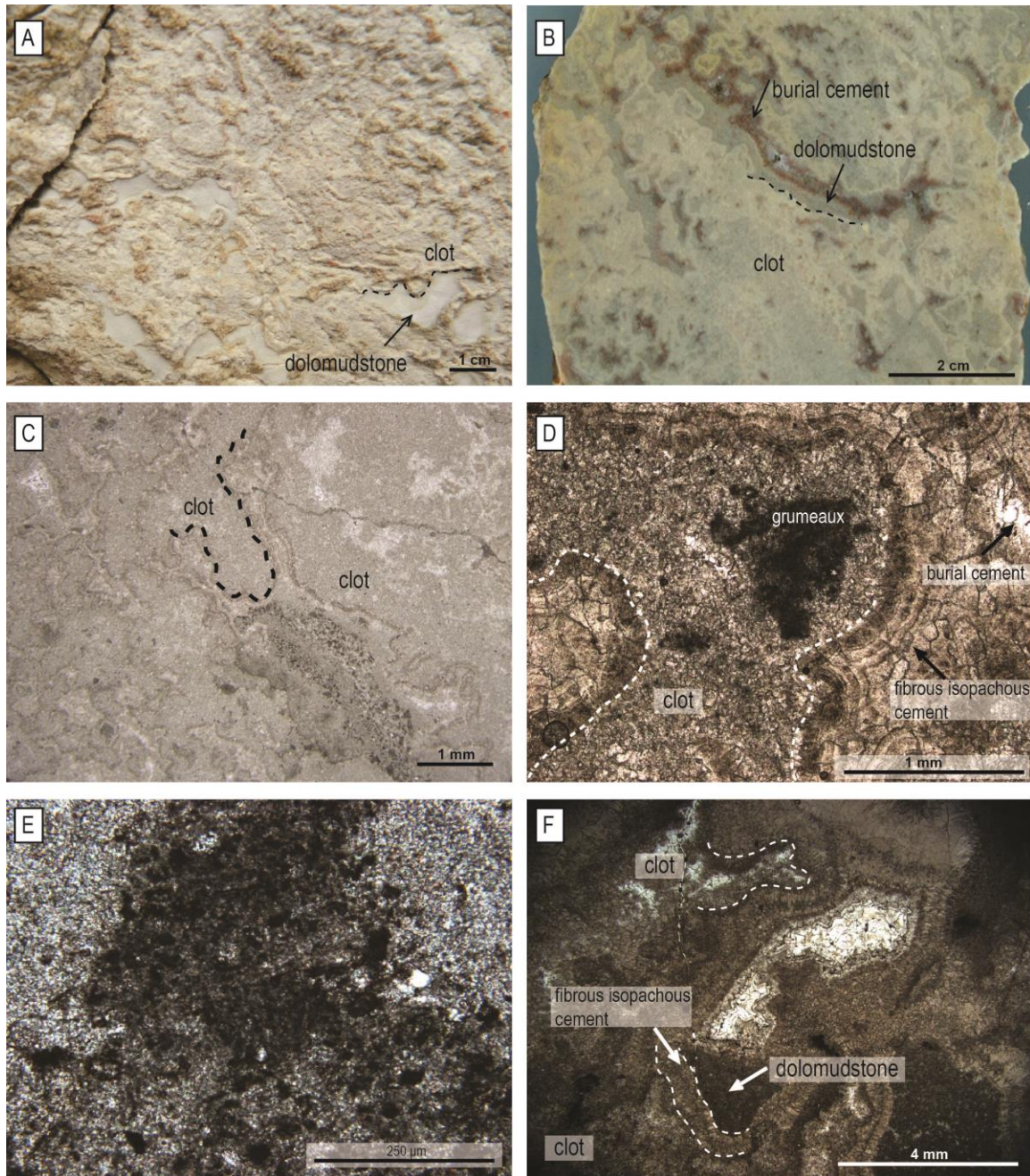


Figure 3-10 Porous thrombolite lithofacies

Figure 10: Porous thrombolite lithofacies. (A) Porous thrombolite lithofacies consists of clots of medium-crystalline dolomite that are rimmed by resistant-weathering isopachous cement. Voids among thrombolites are filled with dolomudstone. (B) Cut slab of porous thrombolite lithofacies highlights subtle features that are not always obvious in outcrops,

including variably preserved clots, isopachous cement, and voids filled with geopetal dolomustone and late diagenetic spar. Photomicrographs (C to D) in plane-polarised light of the porous thrombolite lithofacies. Most clots are recrystallised to finely-crystalline dolomite with rare preservation of microbial grumeaux (D and E). (F) Dolomudstone in a primary framework void. All images are oriented; D-E are in plane-polarised light.

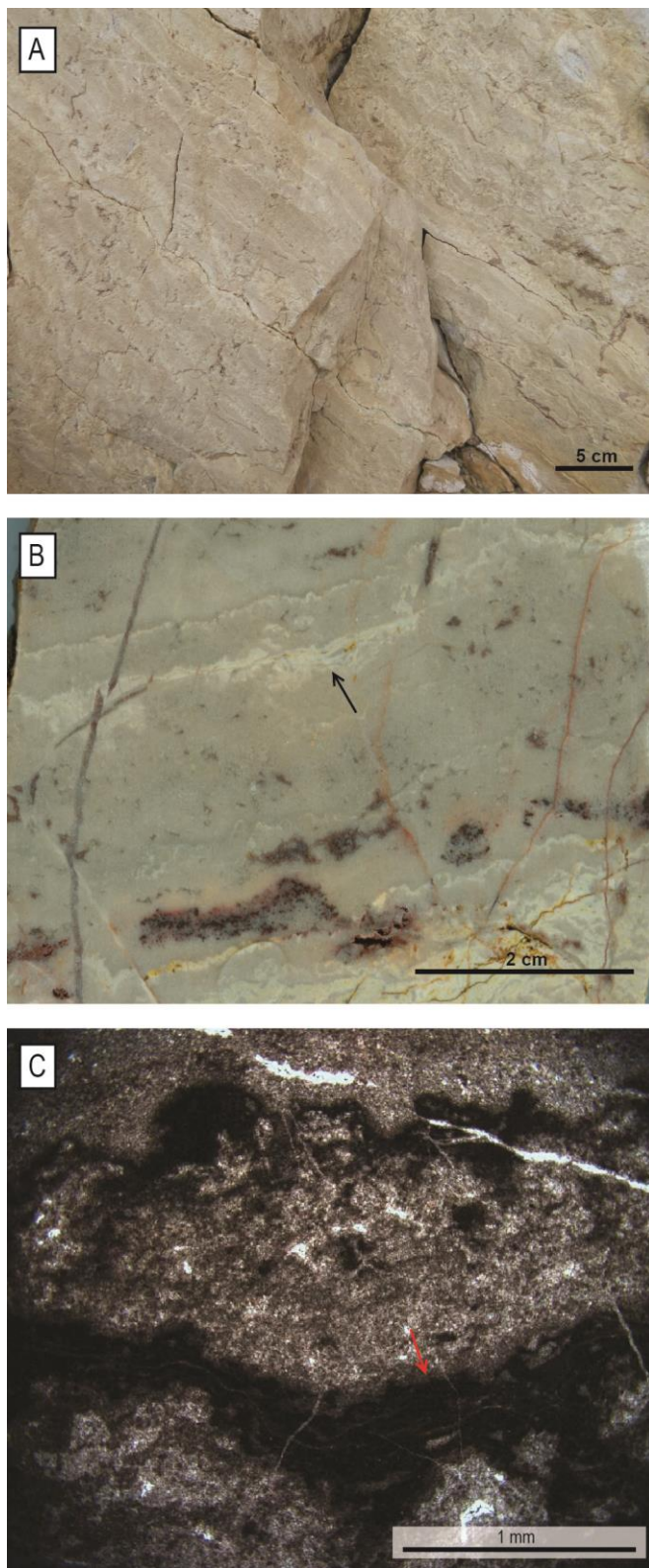


Figure 3-11 Layered thrombolite lithofacies

Figure 11: Layered thrombolite lithofacies at Red Rock mound in outcrop (A) and cut slab (B). This lithofacies is characterised by millimetric layers of clotted micrite (white lines in B) that separate centimetric layers of medium-crystalline dolomite with diffuse microbial clots throughout (not visible at this scale). (C) Thin section photomicrograph in plane-polarised light illustrating millimetric layers of clotted micrite (red arrow). Images are oriented.

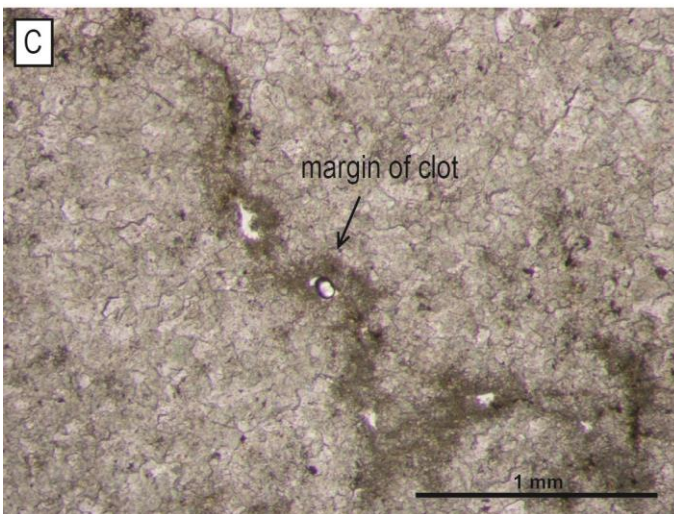
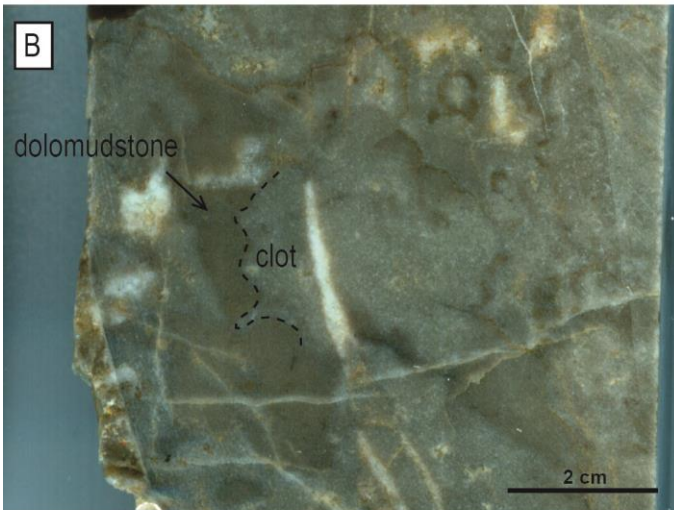
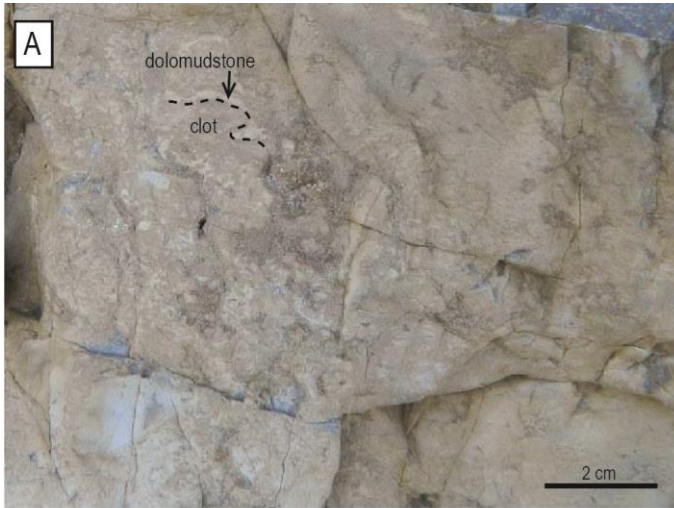


Figure 3-12 Densely packed thrombolite

Figure 12: Densely packed thrombolite lithofacies from Bellevue mound. In outcrop (A) and cut slab (B) massive thrombolite is a mottled fabric defined by variation in crystal size from medium-crystalline dolomite to very finely crystalline dolomite. (C) Clot margins (arrow) are defined by diffuse microbial clots that locally contain rare grumeaux. All images are oriented.

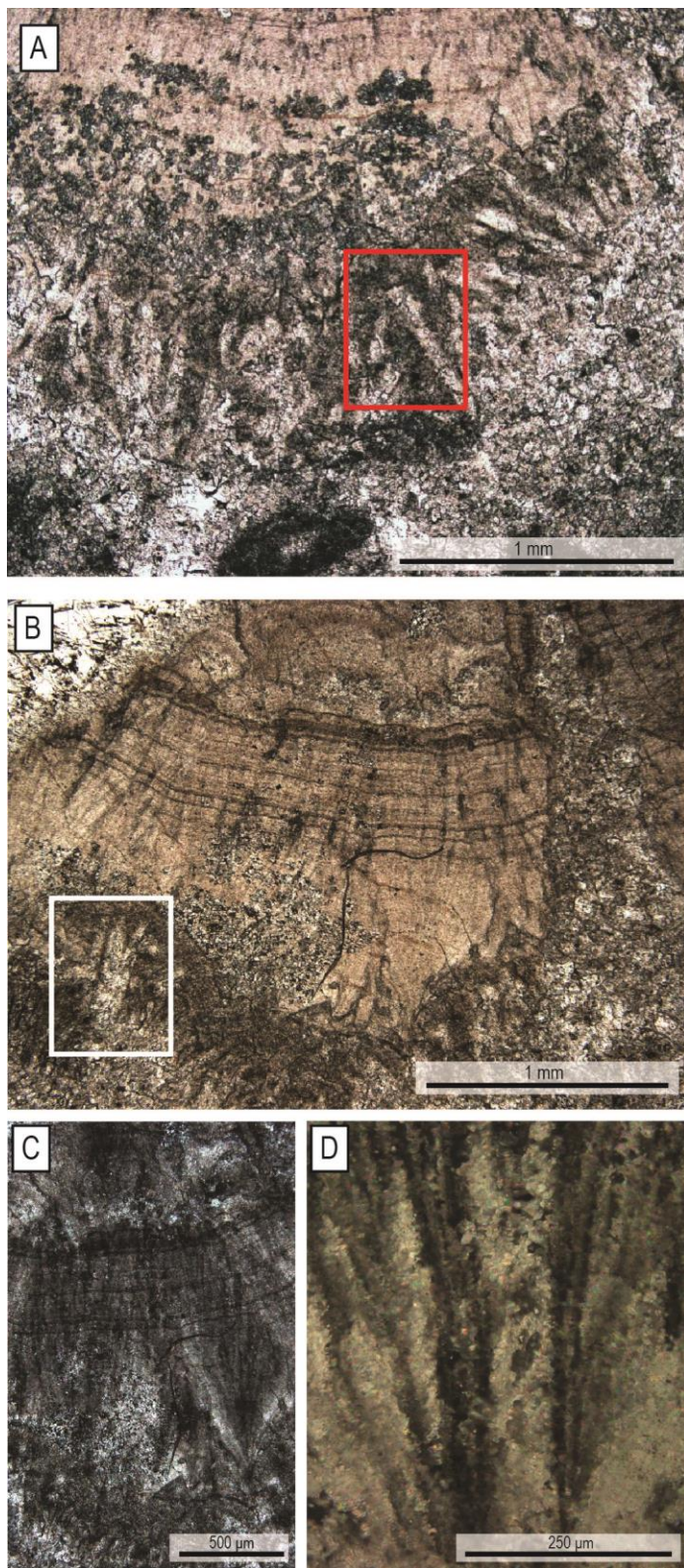


Figure 3-13 Photomicrographs of blunt-tipped crystals and length-fast dolomite

Figure 13: Photomicrographs in (A and B) plane-polarised light and (C and D) cross-polarised light of blunt-tipped recrystallised crystals (A and B in box), overgrown by fibrous bundles of length-fast dolomite. Well-preserved growth zones with sweeping extinction through crystal bundles and presented in (C) and (D). All images are oriented and samples are from Red Rock mound.

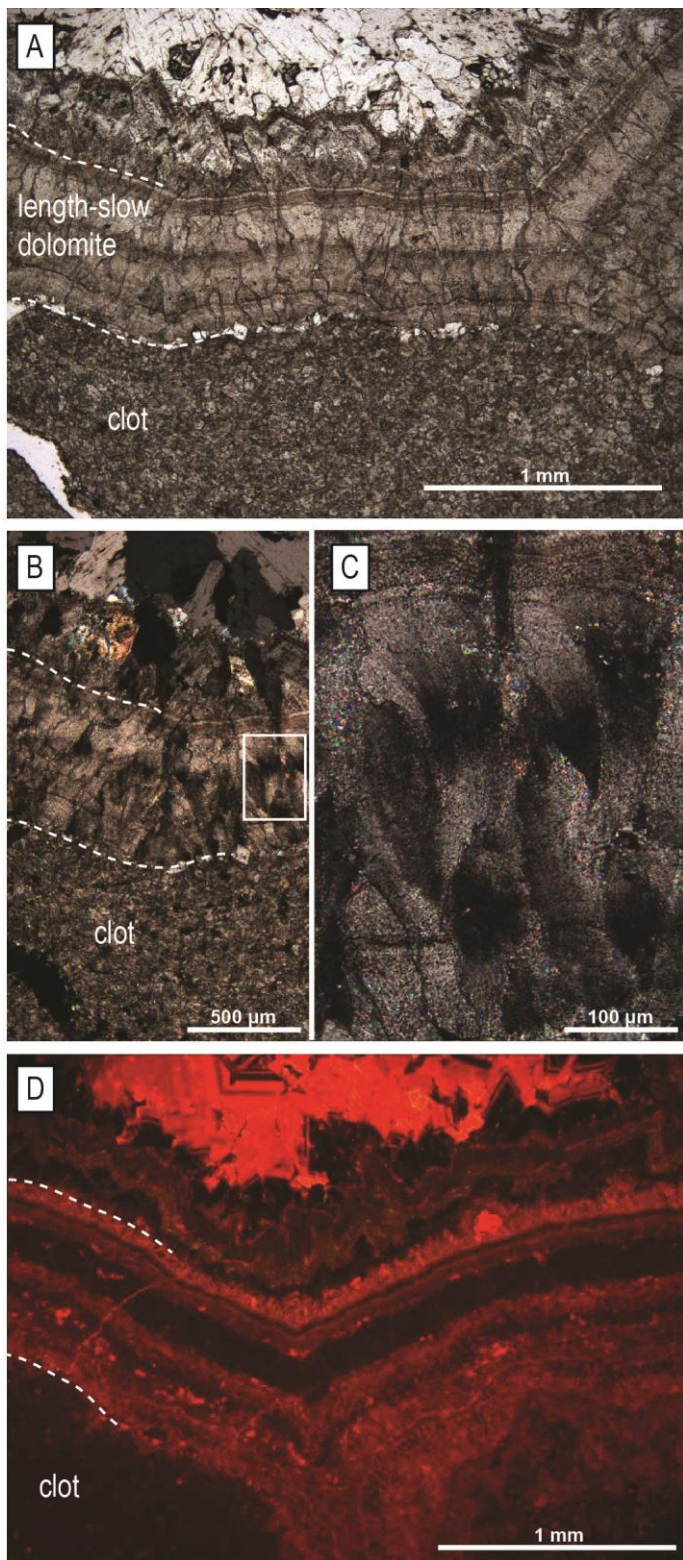


Figure 3-14 Photomicrographs of length-slow dolomite

Figure 14: Length-slow dolomite cement (A) in plane-polarised light, (B and C) cross-polarised light, and (D) cathodoluminescence. Length-slow dolomite is characterised by small bundles of crystals with extinction that sweeps along the length of the crystals (B and C). All images are oriented and samples are from Red Rock mound.

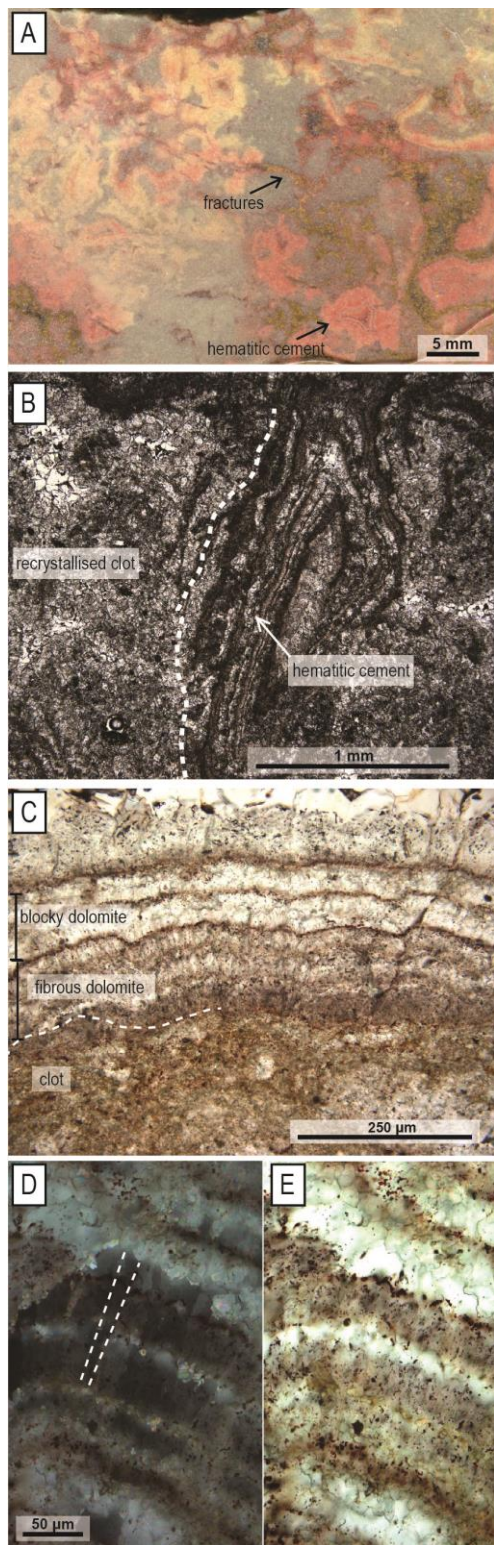


Figure 3-15 Photomicrographs of hematitic cement

Figure 15: Oriented images of hematite-bearing fibrous cement from K-Mesa. (A) Hematitic cement is confined to fractured zones at K-Mesa Mound. (B) Photomicrograph in plane-polarised light illustrating hematitic fibrous cement overgrowing a recrystallised clot. (C) Both very small fibrous crystals and inclusion-rich growth zoning are preserved despite replacement by clear dolomite. Photomicrograph in plane-polarised light. Photomicrographs of individual relict grain boundaries between recrystallised fibrous crystals in cross-polarised light (D) and plane-polarised light (E).

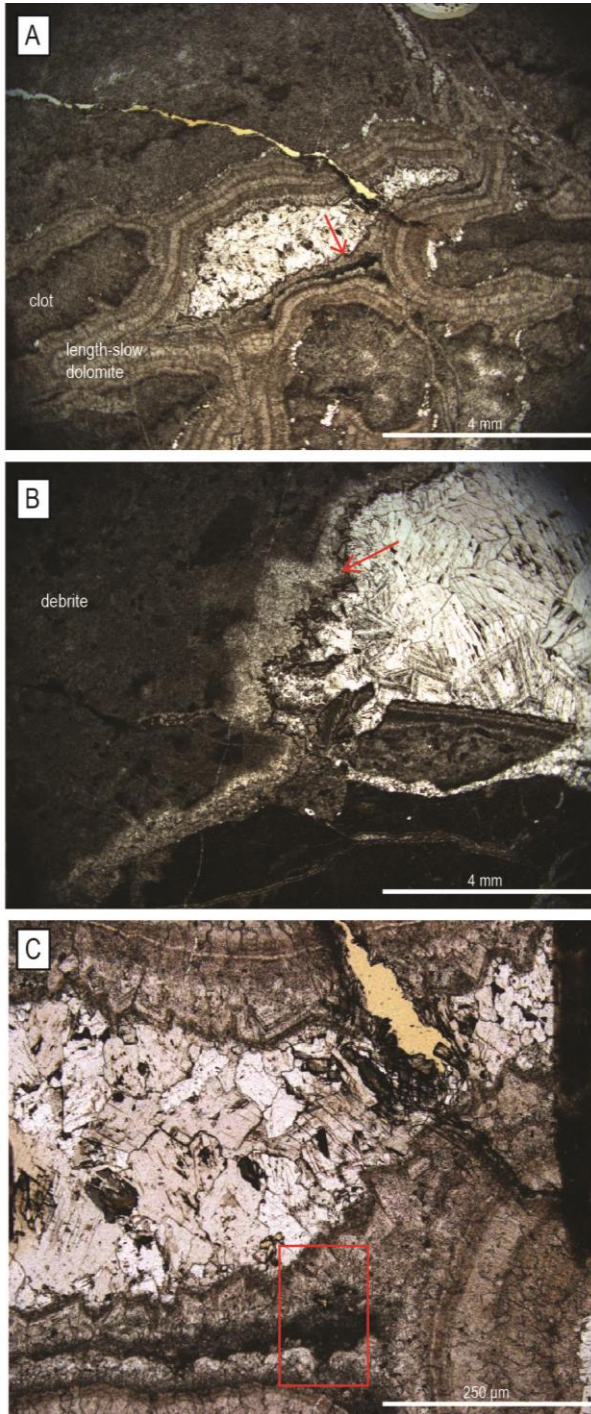


Figure 3-16 Photomicrographs of euhedral dolomite cement

Figure 16: Oriented photomicrographs of euhedral dolomite cement at Red Rock mound in plane-polarised light. Euhedral dolomite (red arrows) lines primary growth voids and

rarely overgrows geopetal dolomitic crystal silt (A and C), as well as fracture systems that cross-cut the white-clast debrite lithofacies (B). Late sparry dolomite occluding the pores is not addressed by this paper.

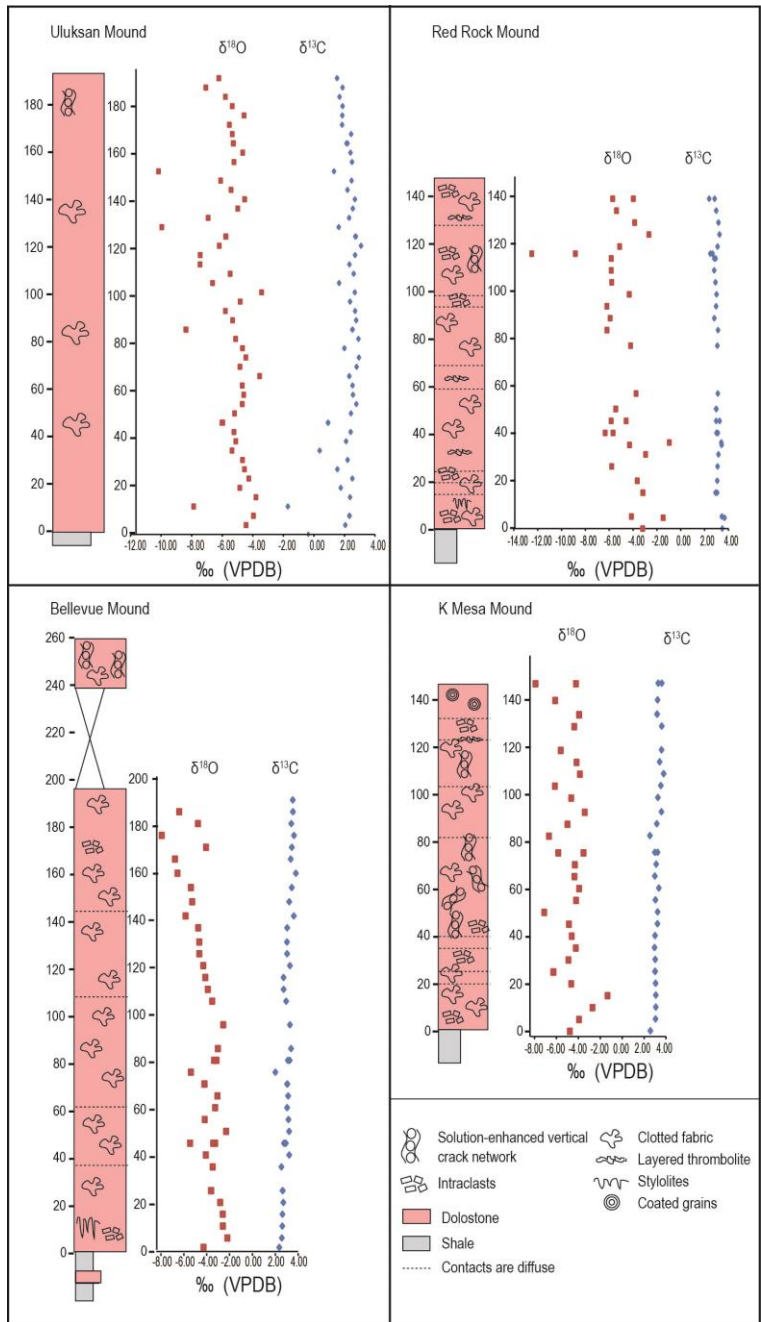


Figure 3-17 Chemostratigraphic sections

Figure 17: Chemostratigraphic ($\delta^{18}\text{O}$ and $\delta^{13}\text{C}$) sections through Uluksan, Red Rock, Bellevue, and K-Mesa mounds. No significant basin-wide trends are apparent in the stable isotope profiles.

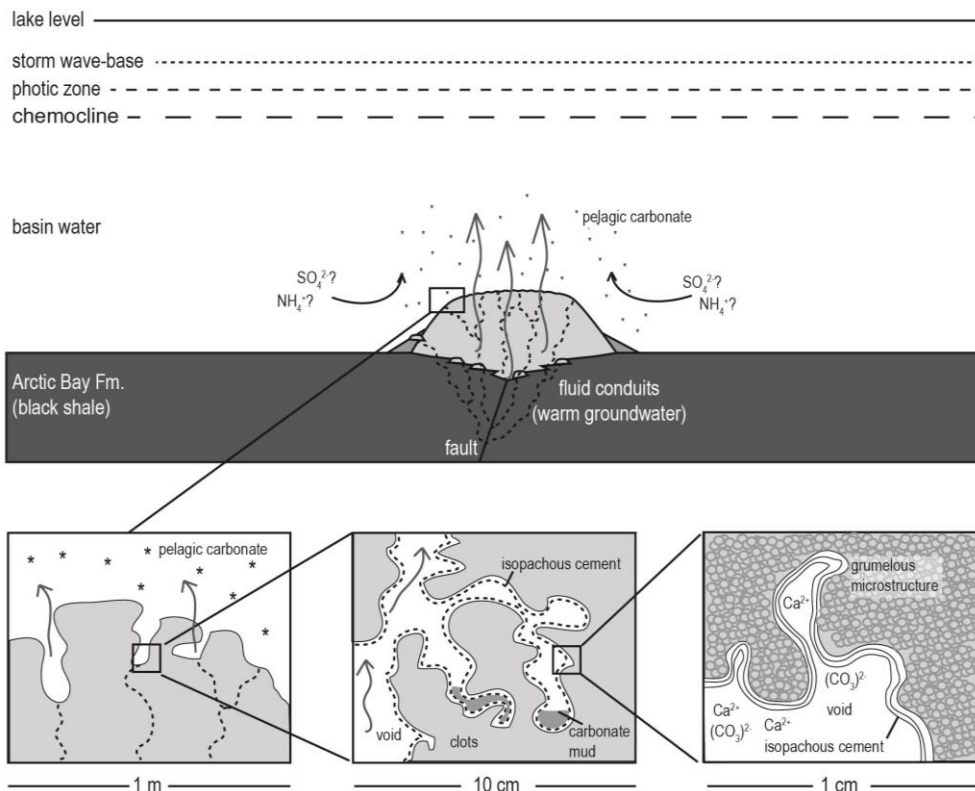


Figure 3-18 Interpretative diagram

Figure 18: Interpretative diagram of mound formation through benthic precipitation of clots and isopachous cement, and deposition of carbonate that precipitated pelagically. Mound growth occurred entirely beneath wave-base, the photic zone, and a chemocline. Mound growth was rapid, and outpaced background sedimentation of clay-sized hemipelagic particles. Slightly warm vent fluid (arrows) travelled through the mounds' porous framework. Upward movement of warm water generated local water circulation around mounds and delivered a fresh supply of nutrients required for microbial metabolism.

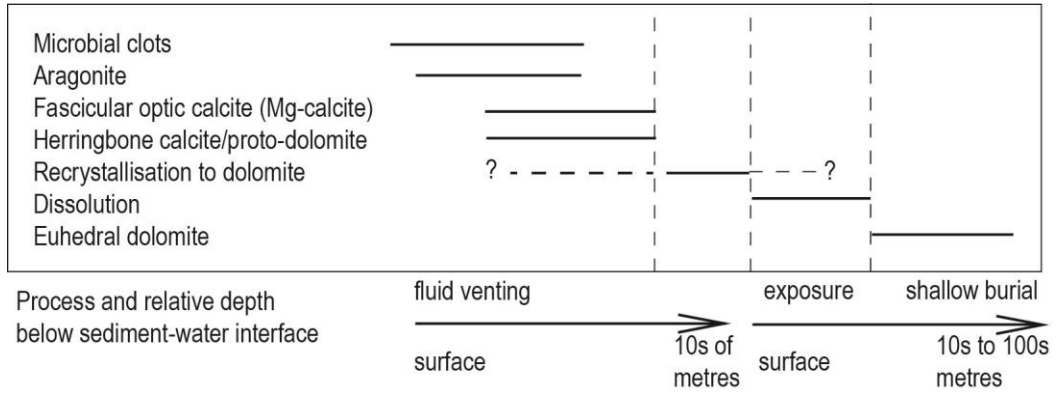


Figure 3-19 Paragenetic chart

Figure 19: Paragenetic chart of the various benthic components in Ikpiarjuk Formation mounds.

Table 3-1 - Summary of mound exposures

Mound	Type of exposure	Thickness of in situ facies	Paleoenvironments present	Fault zone
Uluksan Mound	sea-cliff	200 m	basal flank; core periphery; upper proximal and distal flank; mound top	unmapped splay of NW-trending Tikirarjuaq fault zone under Adams Sound
Nanisivik Mound	drill-core	>500 m	basal core(?); upper flank	suite of un-named faults, possibly extension of Tikirarjuaq fault zone
Red Rock Mound	valley cliffs	200 m	basal flank; core periphery; upper proximal and distal flank; mound top	NW-trending Tikirarjuaq fault zone
Shale Valley Mound	valley cliffs		upper distal flank (at contact of Arctic Bay and Nanisivik formations)	unmapped splay of Tikirarjuaq or Magda fault zone
Magda Mound	valley cliffs		upper distal flank (at contact of Arctic Bay and Nanisivik formations)	NW-trending Magda fault zone
Bellevue Mound	valley cliffs	225 m	basal flank; core periphery; upper distal flank; mound top	NW-trending Tikirarjuaq fault zone
K-Mesa Mound	valley cliffs	125 m	basal flank; core periphery; mound top	NW-trending Magda fault zone
Navy Board Mound	valley cliffs		basal core periphery(?)	NW-trending White Bay fault zone
Tremblay Mound	sea-cliff		upper distal flank (at contact of Iqqittuq and Angmaat formations)	un-named NW-trending fault group

Table 3-2 - Mound section locations

Basement block	Mound	abbrev.	Section	Coordinates (E/N) (NAD83)	UTM zone
Milne	Uluksan	SG	St George's	557972/8103124	16
		UP	Ulukione Point	559497/8182936	16
		DD	Dead Dog Lake	5590671/8104458	16
		AB	Arctic Bay	560799/8105760	16
Milne	Nanisivik	84-01	core at Deb claims mine hill above ore	577401/8105095	16
		82-64	body mine hill below ore	580900/8106800	16
		27-6	body	580900/8106800	16
Milne	Red Rock	KL	Kuhulu Lake	587656/8104378	16
		RRC	Red Rock central	591350/8098707	16
		RRM	Red Rock moundlet	591223/8099314	16
		RRSE	Red Rock southeast	597865/8096545	16
		RRw	Red Rock west	592879/8101109	16
		RRnw	Red Rock northwest	592938/8099097	16
Milne	Bellevue	ARC	Alpha River central	490991/8031274	17
		ARW	Alpha River west	488785/8033141	17
		BA	Bellevue-Alpha	487789/8033607	17
		BMC	Bellevue Mtn. central	485779/8034680	17
		BMW	Bellevue Mtn west	484650/8036145	17
		BC	Bellevue Canyon	483345/9031852	17
Milne	Bellevue North	BN	n/a	488879/8037438	17
Milne	Navy Board	NB	n/a	503565/8072100	17
Tremblay	Shale Valley	SVS	Shale Valley south	408627/8075263	17
		SVN	Shale Valley north	407981/8080783	17
Tremblay	K-Mesa	KMW	K-Mesa west	479351/8016572	17
		KMC	K-Mesa central	480323/8016536	17
Tremblay	Magda	MW	n/a	453183/8038058	17

Table 3-3 - Original mineralogy of primary phases

Primary phase	Original mineralogy
thromboids	aragonite
blunt-ended early cement	aragonite
length-fast fibrous dolomite	high Mg-calcite
length-slow fibrous dolomite	high Mg-calcite? dolomite?
hematitic isopachous cement	high Mg-calcite
pelagic mud in framework voids	high Mg-calcite or aragonite
pelagic carbonate mud as massive layers	high Mg-calcite or aragonite
white clasts	aragonite

Table 2-4 - Stable Isotope Results

Sample	Lithology	13C	18O	Sample	Lithology	13C	18O
12KM001	benthic ppt	2.62	-4.78	11BM011	benthic ppt	2.87	-5.45
12KM002	benthic ppt	3.09	-3.94	11BM012	benthic ppt	2.92	-3.43
12KM003	pelagic ppt	3.12	-2.71	11BM013	pelagic ppt	3.21	-2.30
12KM004	benthic ppt	3.12	-1.34	11BM014	benthic ppt	3.15	-4.17
12KM005	benthic ppt	3.10	-4.65	11BM015	benthic ppt	3.03	-3.26
12KM006	pelagic ppt	3.04	-6.27	11BM016	pelagic ppt	3.12	-3.06
12KM006-Dup	pelagic ppt	3.06	-6.29	11BM017	pelagic ppt	3.06	-4.20
12KM007	pelagic ppt	3.06	-4.90	11BM017-D	pelagic ppt	3.03	-4.18
12KM009	benthic ppt	3.00	-4.23	11BM018	pelagic ppt	2.01	-5.37
12KM010	pelagic ppt	3.05	-4.61	11BM019	benthic ppt	3.26	-3.14
12KM011	benthic ppt	3.27	-4.86	11BM020	benthic ppt	3.10	-3.35
12KM012	benthic ppt	3.28	-7.11	11BM021	benthic ppt	3.38	-3.02
12KM013	benthic ppt	3.08	-4.21	11BM023	benthic ppt	3.28	-2.55
12KM014	benthic ppt	3.39	-3.93	11BM024	benthic ppt	2.95	-3.51
12KM015	benthic ppt	3.03	-4.35	11BM025	pelagic ppt	2.73	-3.90
12KM016	pelagic ppt	3.15	-4.32	11BM026	pelagic ppt	2.72	-4.12
12KM017	benthic ppt	3.28	-3.53	11BM027	pelagic ppt	3.28	-4.30
12KM017-Dup	benthic ppt	3.03	-5.83	11BM028	pelagic ppt	3.03	-4.64
12KM018	benthic ppt	2.58	-6.68	11BM028-D	pelagic ppt	3.02	-4.64
12KM019	pelagic ppt	3.21	-4.99	11BM030	pelagic ppt	3.04	-4.74
12KM020	benthic ppt	3.63	-3.42	11BM031	pelagic ppt	3.62	-5.84
12KM021	benthic ppt	3.31	-4.65	11BM032	pelagic ppt	3.22	-5.27
12KM022	benthic ppt	3.58	-6.14	11BM033	pelagic ppt	3.44	-5.37
12KM023	benthic ppt	3.83	-3.86	11BM034	pelagic ppt	3.80	-6.55
12KM024	benthic ppt	3.47	-4.16	11BM035	pelagic ppt	3.35	-6.77
12KM025	benthic ppt	3.64	-5.61	11BM036	pelagic ppt	3.45	-4.06
12KM026	pelagic ppt	3.66	-4.37	11BM037	pelagic ppt	3.64	-7.93
12KM027	benthic ppt	3.24	-3.94	11BM038	pelagic ppt	3.40	-4.76
12KM027-Dup	benthic ppt	3.23	-3.92	11BM039	pelagic ppt	3.54	-6.40
12KM028	pelagic ppt	3.28	-6.12	11BM039-D	pelagic ppt	3.53	-6.42
12KM029	pelagic ppt	3.66	-4.22	11BM052	benthic ppt	3.52	-3.56
12KM030	pelagic ppt	3.34	-7.91	11BM053	benthic ppt	3.37	-5.65
12KM031	pelagic ppt	3.27	-7.31	11BM054	benthic ppt	3.43	-4.05
11BM002	benthic ppt	2.35	-4.27	11BM126	pelagic ppt	3.29	-8.50
11BM003	pelagic ppt	2.57	-2.19	11BM127	pelagic ppt	3.44	-6.48
11BM004	pelagic ppt	2.61	-2.58	11BM125	pelagic ppt	3.35	-7.24
11BM005	pelagic ppt	2.63	-2.59	11RR016	pelagic ppt	3.48	-3.20
11BM006	pelagic ppt	2.70	-2.82	11RR017	pelagic ppt	3.67	-1.48
11BM007	pelagic ppt	2.65	-3.62	11RR018	pelagic ppt	3.45	-4.14
11BM007-D	pelagic ppt	2.64	-3.61	11RR019	benthic ppt	3.05	-3.17
11BM008	pelagic ppt	2.54	-3.47	11RR019-D	benthic ppt	2.92	-3.18
11BM009	benthic ppt	3.22	-4.08	11RR020	benthic ppt	3.06	-3.65

11BM010	benthic ppt	2.76	-3.26	11RR021	benthic ppt	3.09	-5.79
Sample	Lithology	13C	18O	Sample	Lithology	13C	18O
11RR022	pelagic ppt	3.16	-2.95	03SG33	pelagic ppt	2.56	-4.59
11RR023	benthic ppt	3.40	-0.96	03SG33	pelagic ppt	2.53	-4.69
11RR024	benthic ppt	3.43	-4.30	03SG34	pelagic ppt	2.32	-3.55
11RR025	pelagic ppt	3.00	-5.68	03SG35	pelagic ppt	2.80	-4.84
11RR026	benthic ppt	3.11	-6.34	03SG36	pelagic ppt	2.95	-4.45
11RR027	benthic ppt	2.97	-5.84	03SG37	pelagic ppt	2.00	-4.67
11RR028	benthic ppt	3.26	-4.58	03SG38	pelagic ppt	2.92	-5.12
11RR029	benthic ppt	2.98	-5.46	03SG39	pelagic ppt	2.52	-8.38
11RR029-D	benthic ppt	2.96	-5.45	03SG39-D	pelagic ppt	2.53	-8.36
11RR030	benthic ppt	3.11	-3.75	03SG40	pelagic ppt	2.77	-5.32
11RR034	benthic ppt	3.07	-4.21	03SG41	pelagic ppt	2.70	-5.79
11RR035	benthic ppt	3.12	-6.19	03SG42	pelagic ppt	2.37	-4.82
11RR036	benthic ppt	2.81	-5.92	03SG43	pelagic ppt	2.68	-3.42
11RR037	benthic ppt	2.96	-6.20	03SG44	pelagic ppt	1.65	-6.63
11RR038	benthic ppt	3.00	-4.32	03SG45	pelagic ppt	2.61	-5.48
11RR039	benthic ppt	2.91	-5.79	03SG46	pelagic ppt	2.33	-7.45
11RR040	pelagic ppt	2.80	-5.83	03SG47	pelagic ppt	2.70	-7.44
11RR041	pelagic ppt	2.81	-5.83	03SG48	pelagic ppt	3.09	-6.19
11RR041-D	pelagic ppt	2.92	-5.83	03SG49	pelagic ppt	2.75	-5.77
11RR042	burial dol	2.48	-12.50	03SG49-D	pelagic ppt	2.71	-5.75
11RR042	pelagic ppt	2.66	-8.84	03SG49	pelagic ppt	1.63	-9.95
11RR043	benthic ppt	3.09	-5.13	03SG50	pelagic ppt	2.31	-6.92
11RR044	benthic ppt	3.25	-2.67	03SG51	pelagic ppt	2.55	-4.98
11RR045	benthic ppt	3.16	-3.87	03SG52	pelagic ppt	2.69	-4.53
11RR046	benthic ppt	2.97	-5.39	03SG53	pelagic ppt	2.20	-5.42
11RR048	benthic ppt	2.38	-5.71	03SG54	pelagic ppt	2.47	-6.10
11RR047	benthic ppt	2.84	-3.98	03SG55	burial dol	1.32	-10.17
03SG21	pelagic ppt	2.06	-4.44	03SG56	pelagic ppt	2.50	-5.23
03SG22	pelagic ppt	2.32	-3.96	03SG57	pelagic ppt	2.40	-4.66
03SG22-D	pelagic ppt	2.34	-3.96	03SG58	pelagic ppt	2.14	-5.26
03SG23	pelagic ppt	-1.70	-7.87	03SG58-D	pelagic ppt	2.20	-5.28
03SG24	pelagic ppt	2.37	-3.79	03SG59	pelagic ppt	2.44	-5.34
03SG25	pelagic ppt	1.76	-4.85	03SG60	pelagic ppt	1.85	-5.53
03SG26	pelagic ppt	2.52	-4.26	03SG61	pelagic ppt	1.86	-4.57
03SG27	pelagic ppt	1.54	-4.54	03SG62	pelagic ppt	1.88	-5.34
03SG28	pelagic ppt	2.21	-4.67	03SG63	pelagic ppt	1.68	-5.79
03SG29a	pelagic ppt	0.38	-5.36	03SG64	pelagic ppt	1.88	-7.07
03SG29b	pelagic ppt	2.11	-5.11	03SG65	pelagic ppt	1.52	-6.22
03SG29c	pelagic ppt	2.41	-5.23	12KM031	pelagic ppt	3.20	-6.86
03SG30	pelagic ppt	0.94	-5.96	12KM038	pelagic ppt	3.16	-7.49
03SG30-D	pelagic ppt	0.92	-6.02	12KM043	benthic ppt	3.40	-6.69
03SG31	pelagic ppt	2.43	-5.19	12KM043-D	benthic ppt	3.42	-6.69

03SG32	pelagic ppt	2.78	-4.69	12KM057	benthic ppt	1.47	-4.74
Sample	Lithology	13C	18O				
11BM080	mdst (lqq)	2.66	-3.11				
11BM085	grnst (Ang. Fm.)	3.18	-3.96				
11BM100	benthic ppt	3.07	-3.13				
11BM111	mdst (lqq)	3.48	-1.50				

Chapter 4

4. Diagenetic history of deep-water carbonate mounds in the Mesoproterozoic Nanisivik zinc district, Nunavut

K.E. Hahn, E.C. Turner, D.J. Kontak

Department of Earth Sciences, Laurentian University, Sudbury ON

4.1 Abstract

The Mesoproterozoic (1.1 Ga) Borden Basin (Nunavut) contains strata of the Bylot Supergroup, including extremely large, deep-water dolostone mounds (Ikpiarjuk Formation) whose distribution is controlled by syndepositional faults. Numerous Zn-Pb sulphide showings in the basin, including the past-producing world-class Nanisivik deposit, are controlled by stratigraphy and faults, and some of the showings are associated with the same faults as the Ikpiarjuk Formation mounds. Abundant primary void space in the Ikpiarjuk Formation's microbial mound framework contains several generations of early and late dolomite and other cement. The late (post-seafloor) cements in the Ikpiarjuk Formation were studied to (a) decipher the mounds' diagenetic history and (b) establish whether metal-bearing fluids associated with the regional showings used the fault systems associated with the Ikpiarjuk Formation as fluid conduits. This study used in situ analytical approaches, including detailed petrography, SEM analysis, fluid inclusion microthermometry and evaporate mound analysis, in situ LA-ICP-MS analysis, and SIMS analysis of O isotopes.

The Ikpiarjuk Formation contains at least six void-filling late cements: inclusion-rich euhedral dolomite (ED), finely crystalline clear dolomite (FCD), hematite-bearing

dolomite (HD), coarsely crystalline clear dolomite (CCD), quartz, replacive calcite (RC) and late calcite (LC). The average homogenisation temperatures of fluid inclusions in FCD, HD, CCD, and quartz are 110°C, 84°C, 117°C, and 154°C, respectively. Combined eutectic and ice melting ($T_m(\text{ice})$) temperatures of FCD, HD, and CCD inclusions indicate the fluids are both Ca-rich and saline (i.e., 20 to 37 equiv. wt.% NaCl). In contrast, the $T_m(\text{ice})$ for quartz-hosted inclusions indicates a lower-salinity NaCl fluid (i.e., 14 wt.% NaCl) than preceding phases. Average $\delta^{18}\text{O}$ values of dolostone, ED, FCD, CCD, quartz, RC and LC are +26.3‰, +34.3‰, +35.4‰, +24.5‰, +26.6‰, +15.2‰ and +9.5‰, respectively. Dolostone, ED, and FCD all have PAAS-normalised REEY patterns with LREE<HREE, no La or Gd anomalies, and positive Y anomalies. Hematite-bearing dolomite has abundant hematite inclusions and rare inclusions of pyrite, sphalerite, and galena. Coarsely crystalline clear dolomite has a PAAS-normalised REEY pattern with significant LREE depletion, and MREE>HREE. Calcite displays LREE<HREE, with a strong negative Ce anomaly.

The results suggest that five different fluids passed through the mounds. Fluid 1, responsible for precipitation of ED and a component of FCD, was saline, Na-rich and had oxygen isotope values that were probably sourced from seawater or slightly modified seawater ($\delta^{18}\text{O}_{\text{H}_2\text{O}} \sim 0 \pm 6\text{‰}$). Fluid 2, which was responsible for precipitating HD, and which contributed to the precipitation of FCD, was probably reduced, hydrothermal, saline and Ca(-Mg)-bearing, contained elevated Fe and Mn, was metal-bearing (hematite?, pyrite, sphalerite, galena), and had very heavy $\delta^{18}\text{O}_{\text{H}_2\text{O}}$ values ($\sim 13\text{‰}$). Fluid 3, responsible for precipitating CCD through mixing with fluid 2, was reduced, hydrothermal, saline and K-bearing, and had oxygen isotope values that were probably

sourced from modified seawater (~6‰). Fluid 4 was hydrothermal and contained elevated Na and little Ca+Mg, oxygen isotopes that were derived from modified seawater (~6‰), and was responsible for precipitating quartz. Fluid 5 was oxygenated meteoric water that was undersaturated with respect to dolomite, and was responsible for precipitating RC and LC. The fluid-flow history through the Ikpiarjuk Formation mounds shares some compositional similarities with fluids that generated the Nansivik Zn-Pb deposit, and the timing of precipitation of HD may be related to the ore-forming event at Nanisivik. Precipitation of ED, and partly FCD, occurred during shallow burial through autocementation. Fluids associated with FCD, HD, and CCD were probably mobilised during faulting contemporaneous with deposition of the upper Bylot Supergroup, because this interval was the most tectonically active time in the region's Mesoproterozoic to Recent history. Quartz was derived from seawater that had been modified through water-rock interaction, the timing of which is poorly constrained. Replacive calcite and calcite precipitated from high-latitude oxidised meteoric water at some point post-Mesozoic.

4.2 Introduction

The Mesoproterozoic Milne Inlet Graben (MIG; Fig. 1; Arctic Canada), filled with up to 6 km of sedimentary rocks of the Bylot Supergroup, contains very large carbonate mounds that formed during an episode of voluminous groundwater venting along faults into an alkaline lake (Jackson and Ianelli, 1981; Turner, 2009; Hahn et al., 2015). The mounds formed through interaction of discharging groundwater with anoxic, alkaline lake-water. Mounds contain abundant framework clotted carbonate that was precipitated by benthic microbes living in the vicinity of discharging vent water. Overlying the Ikpiarjuk Formation are strata of the Nanisivik Formation, consisting of laminated

dolostone interpreted to have formed in deep water in a marine basin (Turner, 2009; Turner, 2011). Numerous showings of Zn and Pb sulphides are present in the Nanisivik Formation, including the world-class carbonate-hosted Nanisivik Zn-Pb deposit (Clayton and Thorpe, 1982; Arne et al., 1991; Sangster, 1998). All of the showings in the MIG are at least in part structurally controlled (e.g., Sangster, 1998; Turner, 2011). Formation of the Nanisivik deposit was roughly contemporaneous with deposition of the upper Bylot Supergroup (Turner, 2011). The carbonate mounds of the Ikpiarjuk Formation formed along basin-floor faults that were reactivated repeatedly through the basin's depositional and post-depositional history (Jackson et al., 1985; Turner, 2009; Turner and Kamber, 2012). The mounds contain abundant primary void space that is filled with multiple generations of late cement (Hahn and Turner, 2013).

New developments in micro-analytical techniques provide the opportunity to undertake detailed diagenetic studies on carbonate rock using a combination of in situ analyses on very small sample sets (Mathieu et al., 2015). Fluid inclusion microthermometry provides information about the trapping temperature of a fluid, as well as the salinity and major cation composition of the fluid. The rare earth elements and yttrium (REE+Y) in carbonate cement have been shown to record characteristics of the primary fluid from which they precipitated, along with features inherited through fluid-rock interaction along the fluid pathway (e.g., Johanesson et al., 2000; Debruyne et al., 2016). Oxygen stable isotopes provide information about the source fluid (i.e., meteoric, seawater, magmatic). The use of combined in situ techniques was highlighted by a recent study (Mathieu et al., 2015), in which data obtained through fluid inclusion microthermometry, evaporate mound analysis, in situ rare earth element (REE) and major element analysis, and in situ

oxygen isotope analysis on a very small sample set provided the basis to decipher the diagenetic history of late Neoproterozoic and early Paleozoic sedimentary rocks on Victoria Island (Arctic Canada).

The purpose of this study is to characterise the diagenetic fluid-flow history in the Ikpiarjuk Formation mounds on a small set of well-constrained samples. Base metal mineralisation in the MIG is generally confined to the Nanisivik Formation, but the faults that the Ikpiarjuk Formation nucleated on seem to represent zones of repeated permeability generation during mild to significant tectonism. A further goal of this study is to evaluate whether mineralising events associated with the Nanisivik deposit (and regional showings) and are recorded in dolomite cements of the Ikpiarjuk Formation.

4.3 Geologic Setting

The Borden Basin is a late Mesoproterozoic intracratonic basin in the Canadian Arctic islands (Fig. 1). The basin contains three grabens, the largest of which is the Milne Inlet Graben (MIG; Jackson and Iannelli, 1981). The MIG contains several unusual carbonate units, including deep-water carbonate mounds of the Ikpiarjuk Formation, as well as an unusual deep-water dolostone of the Nanisivik Formation, which contains numerous Zn-Pb showings (e.g, Turner, 2009; Turner, 2011).

The basin formed during assembly of Rodinia, and most of the basin-filling strata are younger than 1.1 Ga (Fig. 2; Jackson and Iannelli, 1981; Turner and Kamber, 2012). The base of the stratigraphic succession consists of tholeiitic basalt of the Nauyat Formation, which erupted subaqueously during mild extension (Jackson and Iannelli, 1981; Dostal et al., 1989; Long and Turner, 2012). The basalt is overlain by sandstone of the Adams

Sound Formation, which was deposited regionally during sag-phase sedimentation (Long and Turner, 2012). The basin then experienced an interval of pronounced extension, during which black shale was deposited (Arctic Bay Fm.; Turner and Kamber, 2012). Displacement along graben-margin and intra-graben normal faults at this time is associated with deposition of graben-margin detrital wedges of the Fabricius Fiord Formation (Jackson and Iannelli, 1981) and development of basin-floor paleotopography (Turner and Kamber, 2012). During the latest stage of black shale deposition, voluminous fluid venting of ground water occurred along faults, resulting in accumulation of the Ikpiarjuk Formation carbonate mounds (Fig. 3; Turner, 2009; Hahn et al., 2015).

The Ikpiarjuk Formation mounds are up to 250 m thick, up to 12 km long, and are centred over regionally mapped faults. During accumulation of the Ikpiarjuk Formation, carbonate ramp strata accumulated in the southeastern part of the basin (Iqqittuq Fm.; Turner, 2009). During this depositional interval, the basin was filled with an alkaline lake (Hahn et al., 2015). The mounds contain vast accumulations of benthic microbial carbonate, which formed a rigid, porous structure (Hahn and Turner, 2013).

Dolomudstone, derived from pelagic precipitation of carbonate in the vicinity of vents, also forms significant deposits in the Ikpiarjuk Formation mounds (Hahn and Turner, 2013). A minor interval of differential uplift occurred after cessation of fluid venting, and the tops of several of the mounds were truncated during subaerial erosion (Hahn and Turner, Chapter 3).

The basin then experienced an abrupt tectonic associated with shallowing and connection to the global ocean. In the southeastern part of the basin, a cyclic, rimmed carbonate

platform (Angmaat Formation) developed while deep-water dolostone laminite of the Nanisivik Formation accumulated in the northwestern part of the basin (Turner, 2009). Mound-derived debrite tongues are present in the Nanisivik Formation near some mounds, indicating that the mounds had topographic relief above the seafloor during deposition of the Nanisivik Formation (Turner 2009, 2001; Hahn and Turner, 2013). The northwestern part of the basin was then uplifted, tilted, and eroded (Hahn and Turner, Chapter 3). Some mound-tops, and parts of the Nanisivik Formation, were removed. Mild normal faulting was then followed by marine flooding, and deposition of limestone and shale of the Victor Bay Formation's northwestward-deepening ramp (Sherman et al., 2001, 2002). A second episode of differential uplift occurred after deposition of the Victor Bay Formation, which was karsted in the west, even as the basin deepened in the east and accumulated strata of the Athole Point and Strathcona Sound formations (Sherman et al., 2002). The tectonic and stratigraphic history of the upper Bylot Supergroup is less well constrained during deposition of shallowing-upward siliciclastic rocks of the Aqigilik and Sinasiuvik formations. The entire basin is cross-cut by northwest trending dykes of the Franklin swarm (723 \pm 4 Ma; Heamen et al., 1992; Pehrsson and Buchan, 1999; Denyszyn et al., 2009).

Much of northern Baffin Island was later covered by up to 3 km of Paleozoic siliciclastic and carbonate rocks of the Arctic platform. Paleozoic strata were locally displaced along northwest-trending normal faults that were reactivated during the Ellesmerian orogeny (Dewing et al., 2007). The northwest-trending faults that cross-cut the Borden basin are probably part of the same group of extremely long-lived structures, which experienced many episodes of reactivation (Jackson et al., 1985).

Northern Baffin Island was then covered by up to 1.2 km of Cretaceous to Tertiary siltstone and sandstone (Dewing et al., 2007). These strata were locally affected by normal faulting during the Eocene Eurekan orogeny, which also reactivated faults in the Borden basin (Dewing et al., 2007).

4.4 Methods

4.4.1 Samples

Samples were collected from four outcrops of Ikpiarjuk Formation mounds during a detailed sedimentological study of the mounds (Fig. 1; Hahn and Turner, 2013). All samples ($n > 400$) were slabbed and examined under binocular microscope. Fifty polished thin sections were prepared based on the best preservation of the phases of interest. Thin sections were documented under plane-polarised, cross-polarised, and reflected light, and using qualitative cathodoluminescence (CL), in order to document the paragenetic history of the mounds. All mounds have a similar paragenetic history, and a small subset of well-characterised samples was selected for detailed micro-analytical work following the protocol of Mathieu et al. (2015).

4.4.2 Scanning electron microscopy (SEM) and energy dispersive spectroscopy (EDS)

The paragenesis of samples, initially established using standard petrographic techniques in plane- and cross-polarised light, was confirmed using SEM to identify dolomite and calcite on polished, carbon-coated thin sections. Samples were analysed using a JEOL 6400 SEM with INCA energy dispersive detector (EDS) detector and software at Laurentian University. A combination of point analysis and element mapping was used to identify compositional differences in dolomite. The instrument was operated at an

acceleration voltage of 20 kV, with beam current 1.005 nA and a 5-second counting time for point analysis.

4.4.3 *Laser ablation inductively coupled plasma mass spectrometry (LA ICP-MS)*

In situ LA-ICP-MS analyses were performed on unpolished and polished, uncovered thin sections using a RESolution M-50 laser attached to an X-Series II quadrupole mass spectrometer at Laurentian University (Sudbury, Canada). Samples were analysed with a spot size between 60 and 103 μm at 5 Hz with a fluence of $\sim 6 \text{ J/cm}^2$. The aerosol was carried to the ICP-MS in ultra-pure He, and ionisation was enhanced with a 5 mL/min addition of ultra-pure N_2 to the auxiliary Ar stream. The external standard NIST 612 was used, and Ca was used as an internal standard, its abundance depending on which phase was analysed (calcite or dolomite). A combination of line scans and spot analyses were performed on discrete components of the dolostone in order to explore the chemical characteristics of the petrographically defined carbonate components. Larger spot sizes were used where possible to enhance the REE signal in carbonate. Both burial-related, coarsely crystalline dolomite and dolomitised primary fabrics were analysed. The REE concentration in the samples analysed, especially the HREEs, was close to the detection limit of the instrument, and therefore anomalies in the HREEs were interpreted with caution. In situ LA-ICP-MS analysis was also performed on quartz, but the samples did not ablate and no data were obtained.

4.4.4 *Fluid inclusion microthermometry*

Fluid inclusions were first classified petrographically using the fluid inclusion assemblage (FIA) approach and classification recommended by Goldstein and Reynolds (1994). Observations were made using a combination of transmitted and reflected light

microscopy. Fluid inclusion microthermometry was undertaken on 100- μm -thick, doubly polished sections using a Linkham THMSG600 heating-freezing stage coupled to an automated controller unit mounted on an Olympus BX-51 microscope and QImaging video capture system that enabled magnification of small inclusions (i.e., $<5\ \mu\text{m}$) to facilitate observations of phase changes.

Thermometric measurements were carried out on FIAs, and for each assemblage several measurements of both homogenisation temperature (T_h) and ice melting temperature ($T_m(\text{ice})$) were made. Fluid inclusion salinity was calculated for these inclusions using the final $T_m(\text{ice})$ and the equation of Bodnar (1993). In several cases, samples were repeatedly frozen and reheated to ensure accurate measurement of $T_m(\text{ice})$ and thus salinity. Where inclusions permitted, observations were also recorded for first melting or eutectic melting (T_e) and melting of hydrohalite in addition to ice, which enable modelling of fluid chemistry in the $\text{H}_2\text{O}-\text{CaCl}_2-\text{NaCl}$ ternary system (Steele-MacInnis et al., 2011).

4.4.5 *Evaporate mound analysis*

Artificially decrepitated fluid inclusions produce evaporate mounds of solutes which are representative of the composition of a fluid inclusion and can be qualitatively used to document fluid composition (e.g., Kontak, 2004; Kontak, 2013; Mathieu et al., 2013). Evaporate mounds were artificially produced from selected chips previously used for thermometry. The chips were heated to 350°C at $60^\circ\text{C}/\text{min}$, and were held for 2 minutes at 350°C before rapid cooling, as recommended by previous workers (Haynes and Kesler, 1987; Haynes et al., 1988). Subsequently the chips were adhered to double-sided carbon

tape and carbon-coated for SEM-EDS analysis following the methods described above. The cements were next imaged on the SEM and mound fields identified, within which several mounds were then analysed to ensure that the mound chemistry was uniform. Where mounds were $<5 \mu\text{m}$, spot analyses were used, but where large mounds were encountered a raster mode was used instead.

In the above type of analysis, the mounds lay on the carbonate substrate from which they had been produced, hence this material contributed to the mound analyses. This problem was corrected by comparing the measured Ca:Mg ratio of the underlying carbonate material with the measured Ca:Mg ratio of the evaporate mound, and estimating the proportion of excess Ca or Mg in the mound compared to the underlying material, as discussed further in detail below.

4.4.6 Secondary ion mass spectrometry (SIMS)

Samples of all dolomite, quartz, and calcite phases were analysed for oxygen isotope composition using in-situ secondary ion mass spectrometry (SIMS). Samples were gold-coated and analysed at the University of Manitoba (Winnipeg, Manitoba) using a 2nA cesium (Cs^+) primary beam, accelerated (+10 kV) onto the sample. The instrument operated with a 250 V sample offset and 9eV secondary accelerating voltage. Detection of the ions used a Balzers SEV 1217 electron multiplier, coupled with an ion counting system. Standards of dolomite, quartz, and calcite, of known isotopic composition, were run during analyses in order to assess the precision of the results, which are estimated at $\pm 0.7\text{‰}$ (dolomite), $\pm 0.5\text{‰}$ (calcite), and $\pm 0.4\text{‰}$ (quartz). A more detailed account of the procedures is given in Mathieu et al. (2015).

4.5 Results

4.5.1 Petrography/Paragenesis

The Ikpiarjuk Formation consists entirely of dolostone. Dolostone textures are diverse, and reflect the depositional texture of the rocks. The Ikpiarjuk Formation contains large volumes of framework-forming microbial carbonate clots that are surrounded by multiple generations of isopachous and non-isopachous synsedimentary cement. Clots were originally aragonite, and are now composed of fine- to mediumly crystalline xenotopic dolomite crystals. The dolomite crystals are turbid owing to the presence of abundant, very small ($<1 \mu\text{m}$) fluid inclusions. Many clots also contain micron-scale spherical and elongate micritic structures (grumeaux; Cayeux, 1935; Bathurst, 1975). Synsedimentary isopachous cement that overgrows clots is also dolomite, but retains its distinct crystal fibres or blades. Although the original texture of the cement is preserved, no primary growth zones are evident in CL, which indicates that recrystallisation to dolomite occurred despite the well-preserved primary crystal structure. Vast zones of the Ikpiarjuk Formation contain beds of dolomudstone. Dolomudstone consists of very finely crystalline, xenotopic dolomite crystals that are rich in tiny inclusions ($<1 \mu\text{m}$). The framework voids among clots, although lined with isopachous, comparatively early cements (described in an earlier paper; Hahn and Turner, submitted), retained a significant volume of primary void space, now filled by several generations of later cement (described below). Vertically oriented, solution-enhanced fracture systems, probably related to subaerial exposure, cross-cut the Ikpiarjuk Formation near the mound-tops. Importantly, these vertically oriented fractures contain the same late void-filling cements as are in the clotted framework. The post-dolomitisation cements, listed in

paragenetic order, are: 1) inclusion-rich euhedral dolomite (ED), 2) finely crystalline clear dolomite (FCD), 3) hematite-bearing dolomite (HD), 4) coarsely crystalline clear dolomite (CCD), 5) quartz; 6) replacive calcite (RC), and 7) late calcite (LC) (Fig. 4). Not all cements are present in every zone of replacement or void-fill, but the relative order of cements is consistent in all mounds, and the paragenetic history of all mounds is similar (Fig. 4).

Inclusion-rich euhedral dolomite (ED) isopachously lines framework voids and solution-enhanced early fractures, and locally truncates primary fabrics where it recrystallised dolomitised mound rock. Individual crystals are up to 100 μm wide and display unit extinction that is optically continuous with the synsedimentary isopachous cement that it most commonly overgrows. At Red Rock mound, ED overlies dolomitic geopetal crystal silt in voids. Inclusion-rich euhedral dolomite luminesces dull yellow and exhibits local, subtle compositional growth zones under CL (Fig. 5), and contains abundant necked fluid inclusions arranged along growth zones. Individual crystals of ED appear pale grey and cloudy owing to their abundance of fluid inclusions. Inclusion-rich euhedral dolomite is most common at Red Rock mound, present at Bellevue mound, and rare at K-Mesa mound.

Finely crystalline clear dolomite is a very thin rim ($< 50 \mu\text{m}$) that overgrows ED in optical continuity. Finely crystalline clear dolomite follows the crystal shape of ED, with sharp boundaries between the two phases. Under CL, FCD is brightly luminescent, with non-luminescent growth zones. Finely crystalline clear dolomite contains very rare aqueous fluid inclusions and passes gradationally into overlying HD (Fig. 5). Finely

crystalline clear dolomite is present at Red Rock mound, Bellevue mound, and K-Mesa mound, but its thickness and abundance are variable.

Hematite-bearing dolomite is a continuous overgrowth of FCD and contains abundant micron-scale inclusions of pyrite, sphalerite, and galena. Hematite forms spherical particles that may have originally been pyrite. Rare sphalerite and galena form very tiny particles (~1 μm) that are only detectable on the SEM. Tiny (microns) needles of goethite inclusions locally co-occur with hematite inclusions. Hematite-bearing dolomite represents the hematite-bearing outer margin of FCD crystals, and it is overgrown by CCD. Very small empty pits (decrepitated fluid inclusions? solution-derived?) are present along growth zones. On the SEM, it is apparent that some of the hematite and sulphide inclusions line these pits, but elsewhere the hematite inclusions are true mineral inclusions in the crystals of HD. In stained thin section, HD is blue (ferroan). In samples that lack hematite-bearing dolomite, a layer of blue-stained dolomite, also classified as HD, overlies FCD. Fluid inclusions are locally abundant in HD. In CL, compositional growth zones are apparent in HD, with non-luminescent and brightly luminescent zones present. Hematite-bearing dolomite is most common at Red Rock mound and K-Mesa mound, but is also present at Bellevue mound.

Coarsely crystalline clear dolomite (Fig. 5) is medium- to coarsely crystalline, anhedral, and inclusion-poor, and in sharp contact with whatever cement is present in voids that it fills. Coarsely crystalline clear dolomite crystals are not optically continuous with earlier cement. In CL, compositional growth zones are well defined and continuous through neighbouring crystals.

Quartz is present as replacement of host dolostone, ED, and CCD, and also fills void space. Locally, quartz cement overlies massive specular hematite. At Bellevue mound, hematite is disseminated through mound dolostone, and is especially concentrated along the outer margins of coarsely crystalline, euhedral, dolomite cement (HD). Quartz replaces the outer margin of dolomite cement, in contact with hematite. Quartz is medium- to coarsely crystalline, anhedral, and nearly free of inclusions (Fig. 6). Where associated with specular hematite, quartz contains a zone of acicular goethite inclusions along the crystal contact with hematite. Where quartz replaced dolomite in the absence of massive hematite, it contains rare, micron-sized hematite inclusions.

Rare replacive calcite is present in Red Rock, Bellevue, and K-Mesa mounds. Replacive calcite is most common in hematite-bearing growth zones of HD, but is rarely present in CCD (Fig. 6). The replacive calcite contains extremely abundant hematite and goethite inclusions. The inclusions in replacive calcite are much more abundant than those in the zoned dolomite that it replaces. Late calcite is present only at Bellevue Mound, where it fills void space that remained after quartz precipitation.

4.5.2 *Fluid inclusion petrography*

All cement phases contain aqueous (A) fluid inclusions with both liquid (L) and vapour (V), which define fluid inclusion assemblages (FIA) of primary and secondary origin, as defined by Goldstein and Reynolds (1994). Primary AFIAs are distributed along growth zones, whereas secondary AFIAs are distributed along healed fractures.

Only FIAs deemed of primary origin, and conforming to 'Roedder's Rules' (Bodnar, 2003) were used for microthermometric analysis. The FIAs that conform to 'Rodder's

Rules' require (i) the trapping of a homogeneous fluid; (ii) that the inclusions remain a constant-volume system (isochoric); and (iii) that no chemical exchange occurred since their entrapment.

Inclusions in ED are very small (<5 μm wide) with highly irregular shapes, and display L:V ratios that range from 20:80 to 90:10 (Fig. 7a). No FIAs in ED displayed consistent L:V. Inclusions in FCD are extremely rare, and where present are very small (<5 μm). Very rare AFIA's have consistent L:V of 90:10. In HD, fluid inclusions are slightly larger than in FCD, and FIAs with consistent L:V of 90:10 are more common (Fig. 7b). Larger (10-20 μm), necked inclusions are also present in HD, and these FIAs follow primary growth zones. In CCD, primary FIAs are rare and comprise very small inclusions (~5 μm or less; Fig. 7c) with L:V of 85:15, as well as larger, necked inclusions. Replacive calcite contains very rare, very small (1-3 μm) primary FIAs with L:V of 85:15, as well as large (20 μm) necked inclusions. Primary inclusions in quartz are exceedingly rare, and the FIAs comprise very small (<5 μm) inclusions with consistent L:V of 85:15; they are present only near the contact with hematite (Fig. 7e). Several large (10 μm), necked inclusions are associated with tiny primary FIAs. No primary FIAs were documented in replacive calcite or late calcite.

4.5.3 Microthermometry and salinity

Where fluid inclusions were large enough and conformed to 'Roedder's Rules', fluid inclusion microthermometry was completed. No microthermometry was performed on the ED cement because none of the inclusions conformed to 'Roedder's Rules', and microthermometry was performed only on samples that had consistent L:V (Table 1). In

FCD, Th values of 107°C and 111°C were obtained on one FIA with (n=2; average 110°C). The small inclusion size precluded obtaining accurate Tm(ice) values. In HD, two FIAs were homogenised with Th values between 85°C and 93°C, with averages of 88°C (n=4) and 89°C (n=7), respectively. The very small size of inclusions made obtaining Te and Tm(ice) difficult. With repeated runs (multiple freeze-thaw cycles), the Te values were estimated at -60°C, as bracketed by observations between -63°C and -59°C. Furthermore, when the inclusions were held at -50°C, the contained solids coarsened, and it was apparent that hydrohalite had melted. In some inclusions, the final melting temperature of +4°C is attributed to metastable hydrohalite (Goldstein and Reynolds, 1994). The salinity in HD ranged from 22 to 37 wt. % eq. NaCl, with calculated CaCl₂ between 18 and 36 wt.% (Oakes et al., 1990; Steel-MacInnis et al., 2011; Fig. 8). In CCD, the inclusions have Th values between 103°C and 140°C for four FIAs, with average Th values of 125°C (n=3), 105°C (n=3), 120°C (n=5), and 118°C (n=2). The Te values could not be documented with confidence in any of the FIAs in this dolomite, but when inclusions were held at -50°C the contained solids coarsened and it was apparent that all hydrohalite was gone. The Tm(ice) was between -30°C and -20°C. The salinity in CCD ranged from 20-35 wt. % eq. NaCl, with calculated CaCl₂ of 19-24 wt. % (Oakes et al., 1990; Steel-MacInnis et al., 2011). A single primary FIA in quartz yielded a Th value between 149° and 158°C, with an average of 154°C (n=3), a Te of -30°C, and Tm(ice) of -10°C. Values for Tm(ice) were difficult to obtain for inclusions in quartz, and in fact what was recorded was a sudden change in shape of the vapour bubble back to its original rounded shape before freezing. This later observation is considered to reflect Tm(ice). No microthermometric values were obtained from the late calcite cement

4.5.4 *Evaporate mounds*

Evaporate mounds were analysed directly on the dolomite host crystals from which they were generated. This caused problems in interpreting the data, because the produced mounds were very small, and the host dolomite was included with mounds during the SEM-EDS point analysis. In order to correct for the inevitable contribution of host dolomite to the measured cation composition of the evaporate mound, the Ca:Mg of the dolomite cement was measured and compared to the Ca:Mg of the analysed mound. In order to estimate the Ca and Mg composition of the mound, a correction was applied (Mathieu et al., 2013). Applying the correction assumes that the evaporate mound contains only Ca, or only Mg, rather than some combination of the two. Although this correction results in an incorrect value of the relative proportions of Ca and Mg in the mound, it allows the estimation of whether a mound contains significant Ca or Mg, in addition to the other cations, compared to the host dolomite. The microthermometric freezing data presented above independently confirm that many of the fluid inclusions are, in fact, rich in Ca.

For all cements, there is a large range in mound size, from $<5 \mu\text{m}$ to $20 \mu\text{m}$. Mound shape is a function of mound composition: NaCl- and KCl-dominated mounds are generally isolated cubes or clusters of cubes, whereas mounds with significant Ca are irregular masses (Fig. 7f and g). The dominant anion present is Cl, generally in stoichiometric proportions to the cations (i.e., NaCl), and in rare cases S is present. The results of evaporate mound analysis were plotted on ternary diagrams in order to compare the relative proportions of cations (Figs. 9,10). Inclusion-rich euhedral dolomite and FCD were plotted on the same ternary diagram because the very small crystal size of FCD

precluded accurately differentiating its mounds from mounds produced from the adjacent ED. In general, mounds from ED and FCD are Na-rich. The Ca:Mg of mounds is similar to the Ca:Mg of underlying host dolomite, and thus reflects the composition of the underlying host and not the mound, as mentioned above. Mounds produced from HD contained variable Na and K values, ranging from subequal proportions of Na and K to more K-rich. The Ca:Mg ratio of the mounds was higher than the Ca:Mg of host dolomite in several mounds, which implies that the inclusions truly contained Ca. Sulphur is always present in mounds produced from HD. The exact anion concentrations are not estimated because errors in the estimated Ca+Mg component of the mounds would propagate through the calculations. Coarsely crystalline clear dolomite contains highly variable Na:K, and the Ca:Mg of the mounds ranges from greater than to less than the Ca:Mg of the host dolomite (Appendix 1).

4.5.5 Major, Trace, and REEs

The ratios of Ca and Mg are approximately 65:35 in dolostone and in the dolomite cements. Both replacive calcite and late calcite contain no Mg. There is some variability in the Ca-Mg ratio of HD and CCD, and compositional zoning due to the presence of either Mn or Fe, or both, up to 3 wt. %, is present. The trace and REE concentrations for each diagenetic phase are summarised in Table 2 and Figure 11. Dolostone samples have variable Fe (103-1288 ppm) and Mn contents (264-614 ppm), with average concentrations of 671 ppm and 501 ppm, respectively. Aluminium and Sr concentrations display a lower range of values of 22-128 ppm (average 56 ppm) and 35-41 ppm (average 37 ppm), respectively. Inclusion-rich euhedral dolomite has a similar range of values as dolostone: Fe is 269-1390 ppm (average 602 ppm), Mn 99-443 ppm (average 283 ppm),

Al 33-125 ppm (average 80 ppm), and Sr 29-50 ppm (average 37 ppm). Finely crystalline clear dolomite contains higher Mn and Fe than host dolostone and ED. The Fe concentration in FCD ranges from 810-3380 ppm (average 2020 ppm), and the Mn concentration ranges from 664-950 ppm (average 770 ppm). Aluminium and Sr in FCD display similar concentrations to dolostone and ED of 70-114 ppm (average 89 ppm) and 40-80 ppm (average of 24 ppm). Coarsely crystalline clear dolomite contains the highest average Fe and Mn of all cements, with Fe 93-7000 ppm (average 2415 ppm) and Mn 281-4400 ppm (average 2067 ppm). The Al content of CCD is slightly higher than that of the other cements, with a range of 60-159 ppm and average of 103 ppm. The Sr of CCD is slightly lower than that of other cements, with a range of 14-23 ppm and average of 19 ppm. Replacive calcite has highly variable Fe and Mn, with ranges from 31-12600 ppm (average 5537 ppm) and 0-1730 ppm (average 556 ppm), respectively. Aluminium content of RC is also highly variable, with ranges from 0-1150 ppm (average 370 ppm). There is very little Sr in RC, with a range from 0.8-4.1 ppm (average 2.2 ppm). Late calcite contains very little Fe, Al, and Sr, with ranges from 0.95-1.45 ppm, 10.5 ppm, and 0.3-0.5 ppm, respectively.

Trace and REE+Y data are presented in Table 2 and post-Archean Australian shale-normalised (PAAS; Pourmand et al., 2012) REE+Y patterns are presented in Figure 11. The Σ REE for all phases are approximately similar, except for CCD, which contains a slightly higher average concentration of the REEs. There are no REE+Y data for HD because the abundance of hematite inclusions in HD made it impossible to analyse only the dolomite component without incorporating iron oxides. Iron oxides can have a much higher concentration of REEs than dolomite (e.g., Prakash et al., 2012), so any results

from HD that incorporated hematite or goethite would not be an accurate representation of HD. No REE data are available for quartz because of problems with in situ laser ablation of quartz related to the coupling of the laser energy and quartz. An attempt was made to analyse quartz, but the results showed only the REE content of the glass slide beneath the sample chip.

The average Σ REEs for dolostone, ED, FCD, CCD, RC, and late calcite are 2.45 ppm, 1.96 ppm, 4.32 ppm, 8.67 ppm, 1.90 ppm, and 1.56 ppm, respectively. Dolostone, ED, and FCD all yielded similar PAAS-normalised REEY patterns. These patterns have a slight positive slope, a slight positive Ce anomaly (Table 2; Fig. 12), and a slight positive Eu anomaly (Table 2). There are no La or Gd anomalies in the cements, and Y/Ho is >35 . The normalised REE+Y pattern of CCD is completely different from the same normalised REE+Y patterns of the other phases. The CCD normalised REE pattern is characterised by a significant depletion in the LREEs, a bulge in REEs from Nd to Tb, a positive Y anomaly, and a systematic decrease in the HREEs. Overall, its Σ REE is higher than in all other cements due to its MREE enrichment, and in addition a very slight positive Ce anomaly is present. Replacive calcite displays an enrichment of HREEs, with a positive Y anomaly, slight positive Eu anomaly, and significant negative Ce anomaly (Fig. 13). Late calcite displays a REE+Y pattern similar to that of replacive calcite, but the negative Ce anomaly is much more pronounced and there is no positive Y anomaly. The differing Ce anomalies are illustrated in Figure 13.

4.5.6 *Stable O isotopes*

The dolostone of the Ikpiarjuk Formation has a range of $\delta^{18}\text{O}_{\text{SMOW}}$ values from +26.1 to +27.2‰, with a mean of +26.3‰. Inclusion-rich euhedral dolomite ranges from +33.4 to +35.0‰, with a mean of +34.3‰. Finely crystalline clear dolomite ranges from +34.2 to +35.8‰, with average of +35.4‰. It was not possible to analyse HD without incorporating hematite inclusions, which alter the oxygen isotope value; there are no data for HD. Coarsely crystalline clear dolomite ranges from +21.6 to +28.2‰, with an average of +24.5‰. Replacive calcite ranges from +11.4 to +18.6‰, with an average of +15.2‰. Quartz ranges from +25.1 to +26.8‰, with an average of +26.55‰. Calcite ranges from +8.0 to +10.5‰, with an average of +9.5‰.

In order to estimate the $\delta^{18}\text{O}_{\text{H}_2\text{O}}$ of the fluid that precipitated each phase, a temperature of formation must be known. The temperature of homogenisation (measured on fluid inclusions) provides a trapping temperature that would be valid if the cements had formed at surface. The cements did not form at surface, however, so a pressure correction calculation must be applied to the Th data using estimated burial depths. The exact burial depth is unknown for all phases but can be reasonably estimated to be less than 6 km (the total thickness of the Bylot Supergroup above the Ikpiarjuk Formation; Scott and de Kemp, 1998). For dolomite, the fluid composition (i.e., $\delta^{18}\text{O}_{\text{H}_2\text{O}}$) was calculated using the fractionation equation of Horita et al. (2014), for calcite the equation of O'Neill et al. (1969) was used, and for quartz the equation of Sharp and Kirschner (1994) was used. The calculated $\delta^{18}\text{O}_{\text{H}_2\text{O}}$ values of the fluids are discussed below.

4.6 Discussion

4.6.1 Sources and interaction of fluids

Understanding the diagenetic history of the Ikpiarjuk Formation requires determining where cement-precipitating fluids came from. Several fluid sources are present in the crust: (1) seawater, (2) meteoric water, (3) magmatic water, and (4) metamorphic water. A further fluid sub-type is seawater that has been significantly modified in its solute composition either by evaporation or by extensive interaction with rock in the subsurface, which are herein referred to as modified seawater. The Borden basin is cross-cut by Franklin dykes (723 Ma), which correspond to the only known magmatic event that could have contributed magmatic water to the buried basin, and the basin is essentially unmetamorphosed. The fluids that could have affected the buried basin are therefore meteoric water, seawater, and seawater modified by evaporation or fluid-rock interaction. Below the cements are discussed first based on each analytical technique applied, and then the cement-precipitating-fluid sources are interpreted by combining all available information.

4.6.2 Temperature of fluid entrapment and pressure correction of fluid inclusions

Fluid inclusion Th measurements are made under the pressure conditions at Earth's surface (i.e., lab conditions), and represent only a minimum possible value for the true temperature of formation; a pressure correction must be applied to all fluid inclusion Th values in order to estimate the true trapping temperature for any FIA that formed below Earth's surface. The Ikpiarjuk Formation contained abundant void space, which, during burial, would have been occupied by fluid. The pressure in buried rock pores would have been the result of hydrostatic \pm some unknown amount of hydrostatic pressure. The burial

depth of the Ikpiarjuk Formation at the times of the various cementation events is not well constrained because the timing of most cement precipitation events is unknown, and even if the age of each cement were known, the total thickness of overlying strata at most times is not clear owing to the stratigraphic complexity of the area's sedimentary history. The mounds are on average 200 m thick, and at maximum burial would have been covered by up to 9 km of sedimentary rocks, because the Bylot Supergroup is up to 6 km thick, and Phanerozoic strata on Baffin Island are up to 3 km thick (Scott and de Kemp, 1998; Dewing et al., 2007). There is a major unconformity between the Bylot Supergroup and overlying Paleozoic strata such that, in places, Paleozoic strata directly overlie the Ikpiarjuk Formation. It is therefore assumed that a maximum burial depth of 6 km is more reasonable for the Ikpiarjuk Formation because much of the upper Bylot Supergroup was eroded prior to deposition of the Paleozoic (and younger) strata. The fault zones over which mounds nucleated could have developed permeability with each episode of reactivation, and the mounds themselves were permeable fluid, but it is unknown whether strata directly overlying mounds contained fluid conduits as well. In order to apply a pressure-correction to the measured T_h , it is assumed that all pressure is lithostatic, in order to estimate the maximum true trapping temperature. The pressure-correction was applied using measured wt.% equivalent NaCl. There are no experimental models that use a KCl or CaCl₂ system, but in general it is assumed that the systems would behave in a similar manner (Kontak and Sangster, 1995). Salinity was measured on all but the calcite cements, and the pressure-correction was calculated using Bodnar and Vityk (1994) for wt. % eq. NaCl saline fluids (Table 1). For a cement that precipitated at or near the surface (0 km depth), the difference between T_h and the

pressure-corrected temperature is 0°C, but for a cement that precipitated at a depth of 9 km from a saline fluid (20 wt.% eq. NaCl), there is a difference of ~110°C between T_h and the pressure-corrected temperature. Although in these equations all pressure is assumed to be lithostatic, in reality pressure was a combination of hydrostatic and lithostatic pressure. The calculated corrections are, therefore, probably an overestimate of true trapping temperature.

The pressure-corrected temperature for each cement was plotted against two estimates of a normal geothermal gradient in a sedimentary basin (Fig. 14; Allen and Allen, 2005). In order to be considered hydrothermal, a fluid must exceed the ambient temperature of the host rock by at least 5°C (Machel and Lonnee, 2002). Finely crystalline clear dolomite is considered hydrothermal if it precipitated at a depth <8 km for a geothermal gradient of 25°C/km, or <6 km for a geothermal gradient of 30°C/km. Hematite-bearing dolomite is considered hydrothermal if it precipitated at a burial depth of less than approximately 4 km. Coarsely crystalline clear dolomite is considered hydrothermal if it precipitated at a burial depth of less than 6 km. Quartz is considered hydrothermal for all burial depths. There are no microthermometric data for replacive calcite or late calcite. For reasons outlined below, at least half of the late cement phases documented are interpreted to have precipitated during deposition of the upper Bylot Supergroup, which constrains the maximum burial depth to less than 6 km. Significant erosion of the Bylot Supergroup occurred prior to deposition of sandstone in the Cambrian (Gallery Formation). In some parts of the Borden basin, Gallery Formation sandstone directly overlies Ikpiarjuk Formation mounds or Nanisivik Formation, which indicates that even if cement

precipitation post-dated deposition of the upper Bylot Supergroup, maximum burial depth of mounds could not have exceeded 6 km.

4.6.3 Evolution of fluid salinity

The measured salinity range for FCD, HD, and CCD are 20 wt. % eq. NaCl, between 22 and 37 wt. % eq. NaCl, and between 20 and 25 wt. % eq. NaCl, respectively. The application of the H₂O-NaCl-CaCl₂ ternary (Fig. 8; Oakes et al., 1990; Steele and MacInnis, 2014), indicates that some inclusions are CaCl₂-dominated, whereas others contain no Ca (not plotted). The variation in fluid composition and the range in measured salinity are consistent with mixing of various fluids. The salinity of quartz is much lower than that of the earlier phases and is NaCl-dominated, which indicates a completely different fluid from the other fluids. The mixing and fluid sources fluids are discussed below in the context of evaporate mound composition.

4.6.4 Evaporate mound geochemistry

The evaporate mound data for each cement differ from one another, which requires chemical evolution of the diagenetic environment. The fluids evolved from Na-dominated (ED and possibly FCD), to Ca-dominated (possibly FCD and HD), to K and Na-dominated (CCD and quartz). The changes in fluid inclusion composition represent distinct fluids that migrated through the Ikpiarjuk Formation.

Evaporate mounds produced from ED and FCD were dominated by Na with some K, and only one field of mounds contained significantly elevated Ca+Mg. The field of mounds that contained elevated Ca:Mg, and a significant K component probably formed from a different fluid than the Na-dominated mounds. The Na mounds were most easily

recognised as originating from ED, and mounds with elevated Ca+Mg and K are interpreted to be from FCD. These results are consistent with the differing calculated $\delta^{18}\text{O}_{\text{H}_2\text{O}}$ between ED and FCD, and reflect the mixing of fluids of different composition.

4.6.5 REE+Y composition of cements

The shape of REEY patterns of carbonate minerals closely reflects the fluid from which they precipitate and provides useful information about the fluid source (e.g., Webb and Kamber, 2000; Nothdurft et al., 2004). Interpreting REE+Y patterns in marine carbonate rocks is relatively simple, because of the predictability and limited range of marine processes. Interpreting the REE patterns of diagenetic carbonate phases is more complicated: the REE+Y of diagenetic carbonate minerals originate in a complex fluid pathway, starting with the original REE composition of a fluid, which then reacts with different rock types along the total fluid pathway. Significant changes in the REE+Y pattern of groundwater can develop in less than 10 km of fluid transport through an aquifer, if the bedrock composition varies along the fluid path (Johannesson et al., 2000). The REE+Y in a fluid (and resulting precipitated mineral phases) are controlled by redox, pH, elemental composition, and fluid temperature. Furthermore, the REE pattern measured in carbonate can be drastically influenced by trace amounts of siliciclastic particles or Fe or Mn oxyhydroxides. Because an in-situ approach for elemental analysis was used in this study, visible Fe oxides were avoided during analysis. There is no correlation between REE+Y abundance or slope and Al, Fe, or Mn, and so contamination is not considered to have influenced REE patterns in any but three samples of RC (discussed further below).

Dolostone, ED, and FCD all display nearly identical PAAS-normalised REE+Y patterns: the patterns display a positive slope, with a positive Y anomaly and a variably positive Eu anomaly. Hahn et al. (2015) presented a detailed geochemical study of mound dolostone depositional components. It was concluded that the REE+Y pattern of the host dolostone represents the primary REE+Y composition of the basin water from which it precipitated. Hahn et al. (2015) also demonstrated that the host carbonate precipitated due to the interaction of seep fluid (flat REE patterns normalised to local shale), with alkaline lake water (LREE<HREE; no La or Gd anomaly normalised to local shale). Similar REE patterns develop in seawater (LREE<HREE), but the distinguishing characteristic of the Ikpiarjuk Formation dolostone is its lack of positive La and Gd anomalies. If the REEs in ED and FCD were sourced from seawater (because LREE<HREE), then positive La and Gd anomalies should be present. There is no La or Gd anomaly in ED or FCD, which indicates that either the fluid originated as seawater, and La and Gd were preferentially removed during fluid-rock interaction, or, more probably, that the REEs were derived by dissolution of Ikpiarjuk Formation sedimentary phases (discussed further below).

Hematite inclusions in HD complicate interpretation of the source fluid. Finely crystalline clear dolomite contains significantly more Fe and Mn than ED, which indicates that it precipitated in a reducing environment, probably during deeper burial than ED, or with a fluid composition that changed; the same would be true for HD, which is petrographically related to FCD. The hematite inclusions in HD are spherical and may be former pyrite framboids: in rare examples pyrite framboids are present in HD and are identical in size and shape to hematite inclusions. Precipitation of pyrite is consistent with the interpretation that HD was a reduced fluid. High Mn and Fe are features of reduced fluids

that had interacted with shale (Budd, 1997), which is consistent with the heavier isotopic composition of $\delta^{18}\text{O}$ of FCD.

The REE+Y pattern of CCD displays an extremely low LREE/MREE (Fig. 12). The extreme depletion in LREE is much greater than what is measured in normal meteoric water or seawater, and it is probably the result of modification of a fluid along its flow-path, where it developed an extreme LREE-depletion. Fractionation of LREEs is generally the result of LREE-retention in stable complexes (Cl-, F-) at the site of mineral deposition, or by Rayleigh fractionation of LREE-selective minerals along the fluid pathway (Debruyne et al., 2016). Coarsely crystalline clear dolomite exhibits flat MREE and HREE to elevated MREE/HREE. When Rayleigh fractionation along a fluid pathway is the dominant process, the resulting REE pattern exhibits an elevated HREE/MREE, which is not the case in CCD. The extreme depletion of only the LREEs in CCD is probably the result of preferential removal of them from the fluid due to precipitation of a mineral along the flow path. Both monazite and apatite contain elevated LREE and are present in diagenetic environments. In general, both shale and granitoids have a flat REE pattern. The REE pattern of CCD is, therefore, probably the result of a fluid that had interacted with either shale or basement granitoids in which monazite or apatite precipitated along the flow path and removed the LREEs. There is a positive Eu anomaly in CCD, but the Eu anomaly should be interpreted with caution because this anomaly can be a function of the choice of normalisation (e.g., Hahn et al., 2015). This study's data are presented normalised to PAAS, but when the data are normalised to MuQ, which is not shown, there is no consistently positive Eu anomaly, and in fact in many samples the Eu anomaly is negative. Hahn et al. (2015) interpreted a negative Eu anomaly in vent-related

carbonate to reflect significant water-rock interaction along the flow path of the vent fluid. Fluid inclusion data for CCD constrain T_h to approximately 120°C, but depending on the burial depth for CCD precipitation, the trapping temperature may have been greater than 200°C at a burial depth >7 km. For temperatures below 200°C, Eu is trivalent during transport and cannot fractionate (i.e., become enriched) relative to neighbouring REEs (Bau, 1997; Bau et al., 2010). The Eu anomaly was, therefore, probably inherited from the source fluid. The REE data of CCD indicate that it formed in a high F:R setting, because the host does not control the chemistry of the new phase, in contrast to all earlier phases.

Replacive calcite is most commonly present in HD and rarely present in CCD. Five analyses of RC yielded two distinct REE patterns. All patterns display LREE<MREE and MREE>HREE, but two of the samples have a distinct negative Ce anomaly (<0.25; Fig. 13). All of the samples have a high Y/Ho (>40), and Eu anomalies are variable. The shapes of the patterns are similar to those of CCD, but the total REE abundance is lower than in CCD. The patterns containing a positive Ce anomaly have much higher Al, Fe, and Mn concentrations than the patterns with a negative Ce anomaly. Replacive calcite contains abundant hematite and goethite inclusions, and so it is possible that the material analysed was slightly contaminated by such inclusions (Fig. 16). The combination of LREE depletion and negative Ce anomaly, and low total REEs suggests that the original fluid was probably oxidised meteoric water, which had incorporated some REEs from the phase that it was replacing (Fig. 16). Replacive calcite probably precipitated under low fluid-rock ratios.

Late calcite displays a REE pattern with significant PAAS-normalised LREE/MREE depletion (0.09), MREE>HREE, a relatively low Y/Ho (18), and a significant negative PAAS-normalised Ce anomaly (0.04; Fig. 13). The LREE<MREE is probably a feature inherited from the source fluid, and the MREE>HREE is probably a feature acquired through interaction with rock along the fluid pathway. The Ce anomaly is a function of the fluid being oxidised. The negative Ce anomaly and low total REEs indicates that the source fluid was oxidised meteoric water. Late calcite probably precipitated from the same fluid as RC, but at a higher fluid-rock ratio.

The REE+Y of each cement phase indicates that at least three different fluid types migrated through the Ikpiarjuk Formation mounds. In summary, the features of these fluid types are (1) a fluid with REEs sourced from the host rock (ED, FCD), (2) a fluid that had interacted with either shale or granitoids and that was modified through precipitation of monazite along the flow path (CCD), and (3) a fluid that contained very little REEs (RC and LC).

4.6.6 O isotope composition of cements

Oxygen isotope values of the precipitating fluids were calculated using the estimated trapping temperature values, for cogenetic cement phases obtained from pressure-corrected Th values from fluid inclusion data when available, and using an upper (120°C) and lower (20°C) temperature limit when such temperature data were not available (Fig. 14). The exact depth of burial is unknown during each stage of diagenesis, but conservative estimates for each stage are applied to the data based on geological constraints. Dolomitisation and the precipitation of ED are interpreted to have occurred

between the surface environment and a burial depth of less than 2 km. Finely crystalline clear dolomite is interpreted to have formed at a burial depth of 3 km, and coarsely crystalline clear dolomite is interpreted to have formed between 3 and 6 km burial depth. The burial depth of quartz is unknown, and the burial depth of RC and LC is interpreted to be less than 1 km. The calculated fluid $\delta^{18}\text{O}_{\text{H}_2\text{O}}$ values are reported below for estimated burial depths. Results are summarised in Table 3 and Figure 14.

No Th data were available for dolomitisation, so the $\delta^{18}\text{O}_{\text{H}_2\text{O}}$ fluid was calculated to be -13.4‰ at 20°C, or +2.8‰ at 120°C. Calculated $\delta^{18}\text{O}_{\text{H}_2\text{O}}$ values for the host dolostone dolomitizing fluids could indicate low-latitude meteoric water, if dolomitisation occurred at temperatures below 60°C, or from seawater if dolomitisation occurred above 60°C (Fig. 14). Because the MIG was occupied by an alkaline lake during mound deposition, the original $\delta^{18}\text{O}_{\text{H}_2\text{O}}$ values are unknown, but the light composition of calculated $\delta^{18}\text{O}_{\text{H}_2\text{O}}$ values may reflect the original composition of the lake water, which would have had lighter $\delta^{18}\text{O}_{\text{H}_2\text{O}}$ values than those of contemporaneous seawater (Kah, 2000; Kah et al., 2001).

No Th was available for ED, so the $\delta^{18}\text{O}_{\text{H}_2\text{O}}$ of the fluid was calculated to be -5.4‰ for 20°C, and at +10.84‰ for 120°C. Inclusion-rich euhedral dolomite and FCD exhibit heavier $\delta^{18}\text{O}_{\text{H}_2\text{O}}$ values than those of the host dolostone. The precipitation temperature of ED is unconstrained by calculated values of $\delta^{18}\text{O}_{\text{H}_2\text{O}}$, suggesting that if precipitation occurred at a temperature below 60°C, the fluid could have been seawater (or modified seawater); if the ED precipitated at a higher temperature, it would have required addition

of heavy oxygen (Fig.14). Heavy $\delta^{18}\text{O}$ can be acquired through interaction of fluid with sedimentary rocks.

The calculated fluid $\delta^{18}\text{O}_{\text{H}_2\text{O}}$ for FCD is +13‰ for a burial depth of 3 km. No oxygen isotope data are available for HD (Fig. 14). The similarities in REE+Ys and calculated $\delta^{18}\text{O}_{\text{H}_2\text{O}}$ values of precipitating fluids for ED and FCD indicate that they were probably derived from the same fluid

There are no $\delta^{18}\text{O}$ values for HD, as noted above, because the abundance of hematite inclusions precluded its accurate analysis. Hematite-bearing dolomite is a continuous overgrowth of FCD, with no distinct crystal boundary between the two. Hematite-bearing dolomite does, however, display lower Th values than FCD (and ensuing CCD), these being 110°C and 117°C for FCD and CCD versus 84°C for HD, respectively.

The CCD $\delta^{18}\text{O}_{\text{H}_2\text{O}}$ fluid value was calculated to be between +2 and +5‰ for a burial depth of 3 km, and between +6 and +10‰ for a burial depth of 6 km. The calculated fluid $\delta^{18}\text{O}_{\text{H}_2\text{O}}$ values for CCD display a very broad range from +2‰ to +10‰, which indicates a mixed fluid that contained seawater with an unmodified $\delta^{18}\text{O}_{\text{H}_2\text{O}}$ value.

Quartz was calculated to have a $\delta^{18}\text{O}_{\text{H}_2\text{O}}$ value of +3.6‰ for a Th value of 154°C, or up to +12‰ for a burial depth of up to 6 km. The calculated $\delta^{18}\text{O}_{\text{H}_2\text{O}}$ values of the precipitating fluid suggest precipitation of a fluid derived from mixing of seawater with some isotopic modification by contact with sedimentary rock (Fig. 14).

Replacive calcite was calculated to have a $\delta^{18}\text{O}_{\text{H}_2\text{O}}$ value of -20.5‰ at 20°C, and -5.7‰ at 120°C. Lastly, the fluid that precipitated late calcite has a calculated $\delta^{18}\text{O}_{\text{H}_2\text{O}}$ value of -

25.8‰ at 20°C, and -11.5‰ at 120°C. Because both calcites probably precipitated at less than 1 km burial depth, they probably precipitated at a temperature close to 20°C. The calculated fluid $\delta^{18}\text{O}_{\text{H}_2\text{O}}$ values are consistent with precipitation from a high-latitude meteoric fluid.

The distinct calculated $\delta^{18}\text{O}_{\text{H}_2\text{O}}$ for each cement indicates that multiple fluids flowed through the Ikpiarjuk Formation mounds: isotopically light fluid is responsible for dolomitising the Ikpiarjuk Formation, seawater-derived fluid was the dominant fluid present during precipitation of ED, FCD precipitated from very isotopically heavy fluid, CCD and quartz both precipitated from slightly modified seawater-derived fluid, and RC and LC precipitated from very isotopically light, meteoric fluid.

4.6.7 Fluids

The combined analysis of fluid inclusion microthermometry and evaporate mound analysis, in-situ LA-ICP-MS analysis, and in-situ SIMS oxygen isotope analysis suggests that at least five distinct fluids interacted with the Ikpiarjuk Formation mounds during diagenesis. In summary, and outlined in detail below, ED precipitated predominantly from fluid 1 under low fluid-rock conditions. Finely crystalline clear dolomite precipitated from a mixture of fluid 1 and fluid 2 under low fluid-rock ratios, which resulted in a slightly different REE pattern than ED, and heavier calculated $\delta^{18}\text{O}_{\text{H}_2\text{O}}$ than ED, as well as a mixed Na-Ca(-Mg) composition of evaporate mounds. Hematite-bearing dolomite precipitated from fluid 2, with some mixing of fluid 3. Coarsely crystalline clear dolomite precipitated from fluid 3, which probably mixed with fluid 2. Quartz

precipitated from fluid 4, which may have mixed with fluid 3. Replacive calcite and late calcite precipitated from fluid 5.

The fluids, outlined in detail below, are best defined by the dominant cation identified during evaporate mound analysis. No evaporate mounds were produced from RC or late calcite, and the fluid from which they precipitated is defined based on a combination of REE+Y and calculated $\delta^{18}\text{O}_{\text{H}_2\text{O}}$ values.

Fluid 1, responsible for precipitation of ED and a component of FCD, was saline, Na-rich and had oxygen isotope values that were probably sourced from seawater or slightly modified seawater ($\delta^{18}\text{O}_{\text{H}_2\text{O}} \sim 0 \pm 6\text{‰}$). The simplest explanation for the source of fluid 1 is unmodified seawater that filled primary pore space in Ikpiarjuk Formation mounds during early diagenesis. The timing of diagenesis is described further below.

Fluid 2, which was responsible for precipitating HD, and which contributed to the precipitation of FCD, was probably hydrothermal, saline and Ca(-Mg)-bearing, contained elevated Fe and Mn, and was metal-bearing (hematite?, pyrite, sphalerite, galena).

Sulphur was a significant measured anion in evaporate mounds in addition to Cl. Two options are considered for the source of fluid 2: (1) a brine generated through evaporation, or (2) a fluid that was modified through water-rock interaction. The Borden basin was filled with alkaline lake-water for only part of its depositional history, and with seawater for the rest of it. During the alkaline lake interval, the primary mineralogy of carbonate precipitates indicates high Mg/Ca in the basin water (Hahn et al., 2015; Chapter 3), and so it is expected that brine generated during evaporation would have elevated Mg/Ca. Gypsum precipitated during the alkaline lake interval and would have

removed Ca from any brine generated. Later in the deposition of the Bylot Supergroup, climatic conditions were humid (influx of terrigenous sediment in upper Bylot Supergroup), and it is unlikely that brine would have been generated through evaporation. The elevated Ca in fluid 2 was probably sourced from fluid-rock interaction, possibly during dissolution of limestone elsewhere in the basin or through interaction with Ca-rich rocks along the fluid flow path. The hydrothermal nature of fluid 2 implies that it must have migrated from somewhere deeper in the basin. The calculated fluid $\delta^{18}\text{O}_{\text{H}_2\text{O}}$ of FCD is very heavy ($> +13\text{‰}$), which is consistent with its being sourced from rock (such as dissolved carbonate). Dissolution of carbonates elsewhere in the basin could have contributed to the heavy calculated fluid $\delta^{18}\text{O}_{\text{H}_2\text{O}}$ values of FCD.

Fluid 3, responsible for precipitating CCD through mixing with fluid 2, was hydrothermal, saline and K-bearing. Fluid 3 had a distinct REE+Y pattern and elevated total REEs compared to other fluids, and had interacted extensively with potassium-bearing rocks. The crystalline basement beneath the Borden basin is Paleoproterozoic gneiss (Scott and de Kemp, 1998), which could have provided a source of K for fluids. Both the Nauyat Formation basalt at the base of the Bylot Supergroup, and the Arctic Bay Formation (shale and siltstone) have elevated potassium contents (Dostal et al., 1989; Turner and Kamber, 2012; Hahn et al., 2015). It is not possible to distinguish which rock type the fluid interacted with in order to become enriched in potassium. The REE+Y pattern of fluid 3 displays a strong depletion in the LREE, which suggests that monazite (or apatite) precipitated along the flow path. The calculated fluid $\delta^{18}\text{O}_{\text{H}_2\text{O}}$ values of CCD (average $\sim 6\text{‰}$) are much lower than those calculated for FCD ($\sim 13\text{‰}$), which is consistent with a completely different fluid source than FCD (and HD), and some

calculated fluid $\delta^{18}\text{O}_{\text{H}_2\text{O}}$ are consistent with a derivation from seawater ($\sim 2\text{‰}$). Fluid 3 probably originated as modified seawater that interacted extensively with rocks of the Bylot Supergroup along its flow path.

Fluid 4 was hydrothermal and contained elevated Na and little Ca+Mg. Fluid 4 is differentiated from fluid 1 by its much heavier calculated $\delta^{18}\text{O}_{\text{H}_2\text{O}}$ ($\sim 6\text{‰}$). The salinity of this fluid was greater than that of seawater, which indicates that the fluid was either evaporatively concentrated and originated as brine, or interacted with evaporite rocks in the subsurface, or hydrated basement rocks (e.g., clay alteration). Either evaporation of seawater (Ward and Halley, 1985) or interaction with sedimentary rocks in the subsurface (e.g., Kesler et al., 1997) can explain the Na-rich nature and heavy calculated $\delta^{18}\text{O}_{\text{H}_2\text{O}}$ of the fluid.

Fluid 5 was meteoric water that was undersaturated with respect to dolomite. No evaporate mounds were produced, but the salinity of fluid 5 is presumed to be low due to its meteoric origin. The fluid was responsible for replacive calcite, which preferentially dedolomitised HD, and in very rare examples CCD. Hematite-bearing dolomite contains abundant inclusions as well as abundant empty pits, and was probably much more chemically reactive than other dolomite phases.

4.6.8 Comparison with base metal showings in the Borden Basin

The Nanisivik carbonate-hosted zinc deposit formed ca. 1.1 Ga, and is presumed to be synchronous with the deposition of the upper Bylot Supergroup (Turner, 2011; Hnatyshin et al., submitted). Dolomite is an ore-stage gangue mineral at Nanisivik, and because there are inclusions of sphalerite and galena in this study's HD, as well as significant

hematite (possibly after pyrite) in Ikpiarjuk Formation mounds, a comparison with the Nanisivik ore body is necessary.

There is little published literature on the dolomite associated with the Nanisivik ore body. Oxygen isotopes of gangue dolomite are approximately +14 to +22‰ V-SMOW (Ghazban et al, 1990). Calculated $\delta^{18}\text{O}_{\text{H}_2\text{O}}$, using Th values of this cement stage (Morden, 2011), of the dolomite-precipitating fluid yields $\delta^{18}\text{O}_{\text{H}_2\text{O}}$ values of approximately -8‰ to 0‰. The wide range in $\delta^{18}\text{O}$ values is probably a reflection of multiple fluid sources, including a fluid with $\delta^{18}\text{O}_{\text{H}_2\text{O}}$ characteristic of mid- to possibly low-latitude (for the Proterozoic) meteoric water, and a fluid with $\delta^{18}\text{O}_{\text{H}_2\text{O}}$ characteristic of seawater or an isotopically heavier fluid. The $\delta^{18}\text{O}_{\text{H}_2\text{O}}$ of seawater during the late Mesoproterozoic may have been as low as -6‰, and fluid inclusions from dolomite gangue are saline (Kah et al., 2001; Hnatyshin et al., submitted). Evaporate mound analysis of fluid inclusions in sphalerite and dolomite indicate that the main ore fluid was Na-rich and had incorporated a significant amount of Ca+Mg by interaction with the dolostone host rock (Hnatyshin et al., submitted). The Na-rich fluid was probably mobilised by far-field tectonic stress associated with Rodinia orogenesis (Turner, 2011; Hnatyshin et al., submitted). A second, K-rich fluid, which post-dates ore-formation, was a volumetrically insignificant fluid at Nanisivik (Hnatyshin et al., submitted).

There are numerous other Zn-Pb showings through the Borden Basin (Sangster, 1998; Turner, 2011), and the study by Hnatyshin et al. (submitted) addresses whether the Hawker Creek showing (Sangster, 1998; showing #7) is temporally related to Nanisivik. Rhenium-osmium dating on the Hawker Creek showing defined two model ages for

pyrite, including 1082 ± 23 Ma (nearly identical to Nanisivik), and 413 ± 6 Ma (Hnatyshin et al., submitted). Hnatyshin et al. (submitted) speculated that the Nanisivik-aged pyrite at Hawker Creek is mineralisation associated with the Nanisivik ore-forming event, and the Ordovician age represents either recrystallisation or a new generation of pyrite. Potassic alteration of the mine dyke at Nanisivik and the younger Re-Os age at Hawker Creek indicate that there was fluid-flow through the Borden basin during the Ordovician (Sherlock et al., 2004).

A preliminary study on fluid inclusions in dolomite and calcite associated with the Surprise Creek showing (showing #20; Sangster, 1998; Zn-Pb-Cu), documented three mineral assemblages that formed at different times in the diagenetic history (Mathieu et al., 2015b). The earliest mineral assemblage at Surprise Creek contains two generations of dolomite followed by pyrite, sphalerite, galena, and barite. Dolomite has calculated $\delta^{18}\text{O}_{\text{H}_2\text{O}}$ between +8‰ and +18‰ SMOW, Th of 110°C to 140°C, and evaporate mounds that contain significant Ca+Mg as well as significant K. This assemblage was interpreted to reflect mixing of two fluids including a hot, saline, sulphide-bearing fluid, and a cooler, less saline fluid. The shale-normalised REE+Y patterns of dolomite indicate that fluids interacted with basement rocks at depth. The Surprise Creek showing has been tentatively related to the Nanisivik ore-forming event (Turner, 2011).

The calculated fluid $\delta^{18}\text{O}_{\text{H}_2\text{O}}$ isotopes of FCD and CCD in the Ikpiarjuk Formation, evaporate mound compositions, and REE+Y patterns share some similarities with the Surprise Creek dolomite. The proposed fluids types responsible for precipitating FCD and CCD are similar to the mechanism suggested for the Surprise Creek dolomite.

Although with the current data set it is not possible to constrain the relative timing of each of these phases, the processes that led to their formation are probably similar. If there were two main Zn-Pb mineralisation events in the Borden Basin (~1100 Ma, and ~413 Ma), then it can be proposed that HD (and the Surprise Creek showing) is related to one of these. The fluids that precipitated HD in the Ikpiarjuk Formation also share some characteristics with other carbonate-hosted base metal districts including evidence of fluid mixing (e.g., Savard and Chi, 1998; Gleeson and Turner, 2007) and fluids that are generally <150°C (e.g., Leach et al., 2005).

No $\delta^{18}\text{O}$ data are available for HD in the Ikpiarjuk Formation mounds, but calculated $\delta^{18}\text{O}_{\text{H}_2\text{O}}$ for FCD and CCD both suggest fluids that had interacted substantially with rock and inherited a signature that is heavier than seawater. Fluid inclusion microthermometry of HD indicates a very Ca-rich fluid. The fluid-flow history through the Ikpiarjuk Formation mounds shares broad similarities with the Nanisivik deposit: a Na-rich fluid evolved to a Ca(-Mg)+Na fluid, followed by a K-rich fluid. Based on the current data-set it is not possible to link the sphalerite and galena inclusions in HD directly to the Nanisivik ore-forming event. It is possible, however, to suggest a connection based on the geological constraints. The tectonic history of this part of Baffin Island has been relatively simple since deposition of the Bylot Supergroup in the late Mesoproterozoic. The Nanisivik ore body formed ca. 1.1 Ga, presumably in response to far-field effects of the Grenvillian orogeny (Hnatyshin et al., submitted), a fluid event that may have been synchronous with deposition of the upper Bylot Supergroup. Other than intrusion of the Franklin dykes in the Neoproterozoic, no tectonic or sedimentary episode is known from the remainder of the Proterozoic. Early to middle Paleozoic sedimentation on Baffin

Island took place under regionally stable epicratonic conditions, and the only unusual Paleozoic event was mysterious potassic alteration of a Franklin dyke cross-cutting the Nanisivik ore-body in the Ordovician (ca. 461 Ma; Sherlock et al., 2004). The Ellesmerian orogeny and ensuing opening of the Sverdrup basin in the late Paleozoic could have had far-field stress effects in the Borden basin, but no tectonic or sedimentary features associated with these events have been identified. Eocene extension reactivated normal faults during the Eurekan orogeny (Dewing et al., 2007). The most tectonically active part of the geologic history of this part of Baffin Island was probably the repeated tectonism that took place during sediment accumulation in the Mesoproterozoic.

4.6.9 *Timing of fluid-flow events*

Inclusion-rich euhedral dolomite cross-cuts dolomitised host-rock lithofacies.

Dolomitisation of the host rock probably occurred very early in the diagenetic history of the mounds. Hood and Wallace (2012) documented synsedimentary dolomitisation in a Neoproterozoic reef that began a few metres below the sediment-water interface.

Dolomitised Ikpiarjuk Formation contains Fe and Mn contents that are elevated in comparison with Phanerozoic limestone, but the Fe and Mn contents are lower than what is usually expected when rock has been dolomitised in a deep burial environment. The Fe and Mn contents of the Ikpiarjuk Formation are similar to those of primary dolomite cement documented by Hood and Wallace (2012), probably reflecting deposition in a reducing depositional setting environment. These conditions are associated with removal of the kinetic inhibitors of dolomite precipitation. In some modern alkaline lakes, aragonite precipitates at the sediment-water interface, and dolomitisation occurs below the sediment-water interface (Müller et al., 1972; Last, 1990). There are greater than fifty

occurrences of either syndimentary dolomite, or dolomite that precipitated in interstitial pore waters in near-surface environments in modern saline lakes (e.g., Deckker and Last, 1988; Last, 1990). In many examples of modern lacustrine dolomite, bacterial sulphate reduction has been documented to play a role in removing the kinetic factors that usually inhibit precipitation of dolomite (e.g., Wright, 1999; Deng et al., 2010). Although the exact mechanism of dolomitisation of the Ikiparjuk Formation is unknown, the depositional setting (saline, alkaline lake), low Fe and Mn contents, and calculated basin-water like $\delta^{18}\text{O}_{\text{H}_2\text{O}}$ of the dolomitizing fluids are consistent with dolomitisation in a near-surface setting by fluids that were derived from the basin and not significantly modified from the original composition.

Inclusion-rich euhedral dolomite is the earliest cement that precipitated after sedimentation and syndimentary cementation. Its relationship with near-contemporaneous geopetal dolomitic crystal silt constrains its timing to after subaerial erosion of either the Nanisivik Formation or the Victor Bay Formation (Fig. 17). Similar dolomitic geopetal crystal silt is present in exposure-related voids in the Nanisivik Formation, and so the dolomitic silt in the Ikiparjuk Formation is interpreted to have accumulated after subaerial erosion of the Nanisivik Formation. Inclusion-rich euhedral dolomite cement fills fractures that cross-cut and offset primary fabrics. It post-dates dolomitisation of the primary host dolostone: locally, ED replaces up to 500 μm of the dolomitic host rock along fractures. Inclusion-rich euhedral dolomite cement has a calculated $\delta^{18}\text{O}_{\text{H}_2\text{O}}$ value indicative of seawater, but its REE pattern is the same as that of the host dolostone. The calculated $\delta^{18}\text{O}_{\text{H}_2\text{O}}$ value of the host dolostone is significantly lighter than that of ED. The dolostone and ED could only have been derived from fluids

of the same composition if host rock dolomitisation occurred at temperatures between 60°C and 120 °C, and ED precipitated at a temperature between 20°C and 60°C. Given that dolomitisation must have occurred very early in the diagenetic history, at a depth probably less than 1 km, it probably occurred at a temperature below 60°C, and therefore was associated with a different source fluid than that of ED. The total REE, Fe, Mn, and Sr content of ED are all very similar to those of host dolostone. The REE are generally present in solution in very low concentrations, much lower than the concentration at which they are incorporated into carbonate rocks. There is petrographic evidence that dissolution was associated with ED precipitation: ED fills compression-related fractures that formed during shallow burial and contains an outer rim of insoluble material that was released during pressure-solution. Inclusion-rich euhedral dolomite therefore records precipitation under a low fluid-rock ratio, in which the original fluid was (modified?) seawater, but the major cations were incorporated from the host dolostone. The timing of this cement precipitation is uncertain, but the Ikpiarjuk Formation was resubmerged after subaerial exposure of the Nanisivik Formation, and any pore space would have been flooded with marine water. Because the cement post-dates some compaction, as shown by ED filling fractures that cross-cut the dolostone, it probably precipitated during shallow burial associated with deposition of the lower Victor Bay Formation. Inclusion-rich euhedral dolomite cement is not present in K-Mesa Mound, and is rare at Bellevue Mound. Each mound had a slightly different post-depositional history, because mounds accumulated on different basement blocks. Basement blocks experienced differential uplift repeatedly after deposition of the Ikpiarjuk Formation, which caused mounds to have slightly different early diagenetic histories.

As discussed above, some similarities exist between the process that led to precipitation of HD, and the process that led to the Nansivik ore-forming event and possibly other Zn-Pb showings in the Borden basin. Two mineralising events have been documented: the main one at ~1100 Ma, and a possible secondary one at ~416 Ma. Based on the current data-set it is not possible to constrain the timing of HD, but the most conservative interpretation is that it is related to the Nansivik ore-forming event because (1) the Nansivik ore-forming event may have been a regional event with numerous, broadly contemporaneous showings (Turner, 2011), (2) if the HD fluid were related to the later mineralising event, that would mean that almost no diagenetic cements are preserved in the abundant voids of the Ikpiarjuk Formation over a span of ~600 million years, which seems improbable, and (3) the early diagenetic history of the Ikpiarjuk Formation was during the most tectonically active time of the region and would have been the best opportunity for large-scale fluid migration.

The timing of the remaining fluid-flow events is less well constrained. Coarsely crystalline clear dolomite probably represents continuous precipitation from an evolving fluid that had also precipitated the preceding dolomites. The REE pattern of CCD is consistent with a seawater-derived brine that had interacted extensively with other rock units. The fluid inclusions indicate a mixed K-Na-Ca(+Mg) fluid. The hydrothermal temperature of CCD is compatible with a fluid derived from a depth >6 km. It is possible that the Franklin magmatic event provided a heat source, but there is no indication of magmatic-derived $\delta^{18}\text{O}$ in CCD. Coarsely crystalline clear dolomite is abundant in all mounds and records a very large-scale fluid-flow event with a high fluid-rock ratio.

The timing of quartz precipitation is unclear. The $\delta^{18}\text{O}$ values suggest a seawater-derived fluid, and fluid inclusions are saline and lack the Ca associated with earlier cement.

Homogenisation temperature indicates a hydrothermal fluid with a different composition from that of the preceding cements.

The REE pattern and $\delta^{18}\text{O}$ values of replacive calcite and late calcite indicate an oxidised meteoric water. The calculated $\delta^{18}\text{O}_{\text{H}_2\text{O}}$ is very negative ($< -16\text{‰}$) and indicates a high-latitude meteoric fluid. Laurentia was located at low- to mid-latitude through the Neoproterozoic and much of the Paleozoic (Li et al., 2008; Torsvik et al., 2012). It was not until the Mesozoic that Laurentia reached high latitude (Torsvik et al., 2012). The timing of replacive calcite and calcite precipitation cannot be further constrained beyond suggesting that they are Mesozoic or younger.

4.7 Summary

Void-filling cements in Ikpiarjuk Formation mounds record the fluid-flow history of the MIG. Voids contain multiple generations of dolomite cement, each characterised by specific REEY patterns, $\delta^{18}\text{O}$ values, and fluid inclusion thermal and compositional data; the voids also contain quartz and calcite cements. The cements record, in paragenetic order, the following cement-precipitating events: 1) precipitation of ED through autocementation in the shallow burial realm, sometime after deposition of the Victor Bay Formation (fluid 1); 2) progressive mixing of Ca-rich, hydrothermal fluid with seawater-derived pore water, which resulted in the precipitation of FCD followed by hematite- and sulphide-bearing HD (fluid 2); 3) continued hydrothermal dolomite precipitation (CCD) from a high-Ca fluid that mixed with a K-bearing fluid (fluid 3); 4) hydrothermal quartz

precipitation (fluid 4), and 5) replacive calcite and late calcite precipitation by meteoric water (fluid 5) at some time in or since the Mesozoic.

Sulphide inclusions in HD provide a possible link to the Nanisivik Pb-Zn mineralising event (and possibly other mineral showings) throughout the MIG. Further analytical work would be required to determine if the sulphides and HD in the Ikpiarjuk Formation are from the same fluid-flow event as the Nanisivik ore-generating event, but a similar temperature and high-Ca fluid composition support a link. The paragenetic sequence of events in the Ikpiarjuk Formation mounds constrains fluid-flow of metal-bearing fluids to the timing of deposition in the upper Bylot Supergroup.

4.8 **Acknowledgements**

Field work was supported by Canada-Nunavut Geoscience Office, Polar Continental Shelf Project (NRCan), a Natural Sciences and Engineering Research Council Discovery Grant to ECT, and a Northern Scientific Training Program Grant to KEH. Field work was assisted by T. Chevrier and J. Mathieu. J. Mathieu is gratefully acknowledged for help with fluid inclusion work and sample preparation. LA-ICP-MS analysis were completed with the help of J. Petrus. Sample prep and SIMS analysis for oxygen isotopes were completed by R. Sharpe at University of Manitoba facilities that are supported by funding to M. Fayek.

4.9 **References**

Allen PA, Allen JR .2005. Basin Analysis: Principles and applications (eds. Allen PA & Allen JR). Blackwell Publishing Ltd. Malden MA USA, p. 549.

- Arne, D.C., Curtis, L.W., and Kissin, S.A. 1991. Internal zonation in a carbonate-hosted Zn-Pb-Ag deposit, Nanisivk, Baffin Island, Canada: *Economic Geology*, v. 86, p. 699-717
- Bathurst, R.G.C. 1975: *Carbonate Sediments and their Diagenesis; Developments in Sedimentology*, no. 12, Elsevier, Amsterdam, 658 p.
- Banner, J.L., and Hanson, G.N.1990. Calculation of simultaneous isotopic and trace element variations during water-rock interaction with applications to carbonate diagenesis: *Geochimica et Cosmochimica Acta*, v. 54, p. 3123-3137
- Bau, M. 1991. Rare-earth element mobility during hydrothermal and metamorphic fluid-rock interaction and the significance of the oxidation state of europium: *Chemical Geology*, v. 93, p. 219-230
- Bau, M., Möller, P., and Dulski, P., 1997. Yttrium and lanthanides in eastern Mediterranean seawater and their fractionation during redox-cycling: *Marine Chemistry*, v. 56, p. 123-131
- Bau, M., Balan, S., Schmidt, K., and Koschinsky, A. 2010. Rare earth elements in mussel shells of the Mytilidae family as tracers for hidden and fossil high-temperature hydrothermal systems: *Earth and Planetary Science Letters*, v. 299, p. 310-316
- Bodnar, R.J.,1993. Revised equation and table for determining the freezing point depression of H₂O-NaCl solutions: *Geochimica et Cosmochimica Acta*, v. 57, p. 689-684.

Bodnar, R.J., 2003. Introduction to fluid inclusions. In: Fluid inclusions: Analysis and interpretation (eds Samson I et al.), Short course series vol. 32. Mineralogical Association of Canada, pp. 1-8.

Bodnar R.J., and Vityk M.O. 1994. Interpretation of microthermometric data for H₂O-NaCl fluid inclusions. In: Fluid inclusions in minerals, methods and applications (eds. De Vivo B & Frezzotti ML). Virginia Tech, Blacksburg, VA, p. 117-130.

Budd, D.A., 1997. Cenozoic dolomites of carbonate islands: their attributes and origin: Earth-Science Reviews, v. 42, p. 1-47.

Butler I.B., and Rickard D. 2000. Framboidal pyrite formation via the oxidation of iron (II) monosulphide by hydrogen sulphide: Geochimica Acta, v. 64, p. 2665-2672.

Clayton, R.H., and Thorpe, L. 1982. Geology of the Nanisivik zinc-lead deposit: Geological Association of Canada Special Paper 25, p. 739-758

Cayeux, L. 1935: Les Roches Sedimentaires de France: Roches carbonates; Masson, Paris, 463 p.

De Deckker, P., and Last, W.M. 1988. Modern dolomite precipitation in continental saline lakes, Australia, Geology, v. 16, p. 29-32

Debruyne, D., Hulsbosch, N., and Muechez, P. 2016. Unravelling rare earth element signatures in hydrothermal carbonate minerals using a source-sink system: Ore Geology Reviews, v. 72, p. 232-252

Deng, S., Dong, H., Lv, G., Jiang, H., Yu, B., and Bishop, M.E. 2010. Microbial dolomite precipitation using sulfate reducing bacteria and halophilic bacteria: Results from Qinghai Lake, Tibetan Plateau, NW China: *Chemical Geology*, v. 278, p. 151-159

Denyszyn, S.W., Halls, H.C., Davis, D.W. and Evans, A.D. 2009. Paleomagnetism and U-Pb geochronology of Franklin Dykes in High Arctic Canada and Greenland: a revised age and paleomagnetic pole constraining block rotations in the Nares Strait region: *Canadian Journal of Earth Sciences*, v. 46, no. 9, p. 689–705.

Dewing K., Turner E., and Harrison J.C. 2007. Geological history, mineral occurrences, and mineral potential of the sedimentary rocks of the Canadian Arctic archipelago. In: *Mineral Deposits of Canada: A synthesis of Major deposit-types, district metallogeny, the evolution of geological provinces, and exploration methods* (ed. Goodfellow WD) no. 5. Geological Association of Canada, Mineral Deposits division, Special publication, pp. 733-753.

Dostal, J., Jackson, G.D. and Galley, A. 1989. Geochemistry of Neohelikian Nauyat plateau basalts, Borden rift basin, northwestern Baffin Island, Canada: *Canadian Journal of Earth Sciences*, v. 26, p. 2214–2223

Elderfield, H. and Greaves, M.J. 1982. The rare elements in seawater: *Nature*, v. 296, p. 214-219.

Fedo C.M., Nesbitt, H.W., and Young, G.M. 1995. Unravelling the effects of potassium metasomatism in sedimentary rocks and paleosols, with implications for paleoweathering conditions and provenance: *Geology*, v. 23, p. 921-924.

- Frimmel, H.E. 2009. Trace element distribution in Neoproterozoic carbonates as paleoenvironmental indicator: *Chemical Geology*, v. 258, p. 338-353
- Ghazban, F., Schwarcz, H.P., and Ford, D.C.1990. Carbon and Sulfur Isotope Evidence for In Situ Reduction of Sulfate Nanisivik Lead-Zinc Deposits, NWT, Baffin Island, Canada: *Economic Geology*, v. 85, p. 360-375
- Gleeson S.A., and Turner W.A. 2007. Fluid inclusion constraints on the origin of the brines responsible for Pb-Zn mineralization at Pine Point and coarse non-saddle and saddle dolomite formation in southern Northwest Territories: *Geofluids*, v. 7, p. 51-68.
- Goldstein, R.H., and Reynolds, T.J.1994. Systematics of fluid inclusions in diagenetic minerals: *Society for Sedimentary Geology Short Course 31*, 199 p.
- Hahn, K.E. and Turner, E.C. 2013. Deep-water carbonate mound lithofacies, Borden Basin, Nunavut: *Geological Survey of Canada, Current Research 2013-11*, 14 p
- Hahn, K.E., Turner, E.C., Babechuk, M.G., and Kamber, B.S. 2015. Deep-water seep-related carbonate mounds in a Mesoproterozoic alkaline lake, Borden Basin (Nunavut, Canada): *Precambrian Research*, v. 271, p. 173-197.
- Haynes, F., and Kesler, S.E. 1987. Chemical evolution of brines during Mississippi Valley-Type mineralization: evidence from east Tennessee and Pine Point: *Economic Geology*, v.82, p. 53-71
- Haynes, F., and Kesler, S.E. 1988. Compositions and sources of mineralizing fluids for chimney and manto limestone-replacement ores in Mexico: *Economic Geology*, v. 83, p. 1985-1992

Heaman, L.M., LeCheminant, A.N. and Rainbird, R.H. 1992: Nature and timing of Franklin igneous events, Canada: implications for a late Proterozoic mantle plume and the break-up of Laurentia: *Earth and Planetary Science Letters*, v. 109, p. 117–131.

Hnatyshin, D., Kontak, D.J., Turner, E.C., Creaser, R.A., Morden, R., Stern, R.A. Geochronologic (Re-Os) and fluid-chemical constraints on the formation of the Mesoproterozoic-hosted Nanisivik Zn-Pb deposit, Nunavut, Canada: Evidence for early diagenetic, low-temperature conditions of formation. Submitted.

Hood, A.vS. and Wallace, M.W. 2012. Synsedimentary diagenesis in a Cryogenian reef complex: Ubiquitous marine dolomite precipitation: *Sedimentary Geology*, v. 255-256, p. 56-71

Horita, J., 2014. Oxygen and carbon isotope fractionation in the system dolomite–water–CO₂ to elevated temperatures: *Geochim. Cosmochim. Acta*, v. 129, p. 111–124.

Iannelli, T. R., 1992. Revised stratigraphy of the late Proterozoic Bylot Supergroup, northern Baffin Island, Arctic Canada; implications for the evolution of Borden Basin: Unpublished Ph.D. thesis, London, Canada, University of Western Ontario, 781 pp.

Jackson, G.D. and Iannelli, T.R. 1981. Rift-related cyclic sedimentation in the Neohelikian Borden Basin, northern Baffin Island; in *Proterozoic Basins of Canada*: Geological Survey of Canada, Paper 81-10, p. 269–302.

Jackson, G.D., Iannelli, T.R., Knight, R.D., and Lebel, D. 1985. Neohelikian Bylot Supergroup of Borden Rift Basin, northwestern Baffin Island, District of Franklin. in *Current Research, Part A*, Geological Survey of Canada, Paper 85-1A, p. 639-649, 1985

- Johannesson, K.H., Zhou, X.P., Guo, C.X., Stetzenbach, K.J., and Hodge, V.F., 2000. Origin of rare earth element signatures in groundwaters of circumneutral pH from southern Nevada and eastern California, USA: *Chemical Geology*, v. 164, p. 239-257.
- Kesler, S.E., Vennemann, T.W., Frederickson, C., Breithaupt, A., 1997. Hydrogen and oxygen isotope evidence for origin of MVT-forming brines, southern Appalachians: *Geochim. Cosmochim. Acta*, v. 61, p. 1513–1523.
- Knight, R.D. and Jackson, G.D. 1994. Sedimentology and stratigraphy of the Mesoproterozoic Elwin Subgroup (Aqigilik and Sinasiuvik formations), uppermost Bylot Supergroup, Borden rift basin, northern Baffin Island; Geological Survey of Canada, Bulletin 455, p. 48.
- Kontak, D.J. 1995. A study of fluid inclusions in sulfide and nonsulfide mineral phases from a carbonate-hosted Zn-Pb deposit, Gays River, Nova Scotia, Canada: *Economic Geology*, 93, 793-817.
- Kontak, D.J. 2004. Analysis of evaporate mounds as a complement to fluid-inclusion thermometric data: case studies from granitic environments in Nova Scotia and Peru: *The Canadian Mineralogist*, v. 42, p. 1315-1329.
- Kontak, D.J. 2013. Fluid inclusion evaporate mound analysis: A rapid, efficient and informative means of determining fluid chemistry in hydrothermal systems: *Atlantic Geology*, v. 49, p. 34

- Kontak, D.J., and Sangster, D.F. 1995. Aqueous and Liquid Petroleum Inclusions in Barite from the Walton Deposit, Nova Scotia, Canada: A Carboniferous, Carbonate-Hosted Ba-Pb-Zn-Cu-Ag Deposit: *Economic Geology*, v. 93, p. 845-868
- Last, W.M. 1990. Lacustrine dolomite – an overview of modern, Holocene, and Pleistocene occurrences: *Earth Science Reviews*, v. 27, p. 221-263
- Leach, D.L., Sangster, D.F., Kelley, K.D., Large, R.R., Garven, G., Allen, C.R., Gutzmer, J., and Walters, S. 2005. Sediment-hosted lead-zinc deposits; a global perspective. In: *Economic Geology; One Hundredth Anniversary Volume, 1905-2005* (eds Hedenquist JW et al.), pp. 561-607. Society of Economic Geologists, Littleton, Colorado.
- LeCheminant, A.N. and Heaman L.M. 1989. Mackenzie igneous events, Canada: Middle Proterozoic hotspot magmatism associated with ocean opening: *Earth and Planetary Science Letters*, v. 96, no. 1–2, p. 38–48.
- Li, Z.X., et al. 2008. Assembly, configuration, and break-up history of Rodinia: A synthesis: *Precambrian Research*, v. 160, p. 179-210
- Long, D.G.F. and Turner, E.C. 2012. Tectonic, sedimentary and metallogenic re-evaluation of basal strata in the Mesoproterozoic Bylot basins, Nunavut, Canada: are unconformity-type uranium concentrations a realistic expectation?; *Precambrian Research*, v. 214–215, p. 192–209.
- Machel, H.G., Lonnee, J. 2002. Hydrothermal dolomite – a product of poor definition and imagination: *Sedimentary Geology*, v. 152, p. 163-171.

- Mathieu J., Kontak, D.J., Turner, E.C., 2013. A fluid inclusion study of diagenetic fluids in Proterozoic and Paleozoic carbonate rocks, Victoria Island, NWT: *Geofluids*, v. 13, p. 559-578
- Mathieu, J., Kontak, D.J., Turner, E.C., Fayek, M., Layne, G. 2015. Geochemistry of Phanerozoic diagenesis on Victoria Island, NWT, Canada: *Chemical Geology*, v. 415, p. 47-69
- McCaffrey, M.A., Lazar, B., Holland, H.D. 1987. The evaporation path of sea water and the coprecipitation of Br⁻ and K⁺ with halite: *Journal of Sedimentary Petrology*, v. 57, p. 928-937.
- Morden, R. 2011. A fluid inclusion study of the Nanisivik Zn-Pb deposit, Nunavut, with implications for the origin of mineralization. Unpublished B.Sc. thesis, Laurentian University, Sudbury, Ontario, Canada, 40 p.
- Müller, G., Irion, G., and Förstner, U. 1972. Formation and diagenesis of inorganic Ca-Mg carbonates in the lacustrine environment: *Naturewissenschaften*, v. 59, p. 158-164
- Nothdurft, L.D., Webb, G.E., and Kamber, B.S., 2004. Rare earth element geochemistry of Late Devonian reefal carbonates, Canning Basin, Western Australia: Confirmation of a seawater REE proxy in ancient limestones: *Geochimica et Cosmochimica Acta*, v. 68, p. 263-283.
- Oakes, C.S., 1990. The system NaCl-CaCl₂-H₂O: I. The ice liquidus at 1 atm. total pressure: *Geochimica et Cosmochimica Acta*, v. 54, p. 603-610

O'Neil, J.R., Clayton, R.N., and Mayeda, T.K., 1969. Oxygen isotope fractionation in divalent metal carbonates: *J. Chem. Phys.*, v. 51, p. 5547–5558.

Pehrsson, S.J. and Buchan, K.L. 1999: Borden dykes of Baffin Island, Northwest Territories: a Franklin U-Pb baddeleyite age and a paleomagnetic reinterpretation: *Canadian Journal of Earth Sciences*, v. 36, p. 65–73.

Pourmand, A., Dauphas, N., Ireland, T.J., 2012. A novel extraction chromatography and MC-ICP-MS technique for rapid analysis of REE, Sc and Y: Revising Cl chondrite and Post-Archean Australian Shale (PAAS) abundances: *Chem. Geol.*, v. 291, p. 38–54.

Sangster, D: Mineral deposits compilation and metallogenic domains: northern Baffin Island and northern Melville Peninsula, Open File 3635.

Savard, M.M., and Chi, G. 1998. Cation study of fluid inclusion decrepitates in the Jubilee and Gays River (Canada) Zn-Pb deposits – Characterization of ore-forming brines: *Economic Geology*, v. 93, p. 920-931.

Scott, D.J. and de Kemp, E.A. 1998: Bedrock geology compilation, northern Baffin Island and northern Melville Peninsula, Northwest Territories; Geological Survey of Canada, Open File 3633.

Sharp, Z.D., Kirschner, D.L., 1994. Quartz–calcite oxygen isotope thermometry: a calibration based on natural isotopic variations: *Geochim. Cosmochim. Acta*, v. 58, p. 4491–4501.

Sherlock, R.L., Lee, J.K.W., and Cousens, B.L. 2004. Geologic and Geochronologic Constraints on the Timing of Mineralization at the Nanisivik Zinc-Lead Mississippi

Valley Type Deposit, Northern Baffin Island, Nunavut, Canada: *Economic Geology*, v. 99, p. 279-293

Sherman, A.G., James, N.P. and Narbonne, G.M. 2001: Anatomy of a cyclically packaged Mesoproterozoic ramp in northern Canada: *Sedimentary Geology*, v. 139, p. 171–203.

Sherman, A.G., James, N.P. and Narbonne, G.M. 2002: Evidence for reversal of basin polarity during carbonate ramp development in the Mesoproterozoic Borden Basin, Baffin Island; *Canadian Journal of Earth Sciences*, v. 39, p. 519–538.

Steele-MacInnis, M., Bodnar, R.J., and Naden, J. 2014. Numerical model to determine the composition of H₂O-NaCl-CaCl₂ fluid inclusions based on microthermometric and microanalytical data: *Geochimica et Cosmochimica Acta*, v. 75, p. 21-40

Sutherland, R.A., and Dumka, D. 1995. Geology of Nanisivk mine: *Society of Economic Geologists Guidebook Series 22*, p. 4-12

Torsvik, T.H., Van der Voo, R., Preeden, U., Mac Niocaill, C., Steinberger, B., Doubrovine, P.V., van Hinsbergen, D.J.J., Domeier, M., Gaina, C., Tohver, E., Meert, J.G., McCausland, P.J.A., Cocks, L.R.M., 2012. Phanerozoic polar wander, palaeogeography and dynamics: *Earth Sci. Rev.*, v. 114, p. 325–368.

Turner, E.C. 2009. Mesoproterozoic carbonate systems in the Borden Basin, Nunavut: *Canadian Journal of Earth Sciences*, v. 46, no. 12, p. 915–938.

- Turner, E.C. 2011. Structural and stratigraphic controls on carbonate-hosted base metal mineralization in the Mesoproterozoic Borden Basin (Nanisivik District), Nunavut: *Economic Geology*, v. 106, no. 7, p. 1197–1223.
- Turner, E.C. and Kamber, B.S. 2012. Arctic Bay Formation, Borden Basin, Nunavut (Canada): basin evolution, black shale, and dissolved metal systematics in the Mesoproterozoic ocean: *Precambrian Research*, v. 208–211, p. 1–18.
- Ward, W.C., Halley, R.B., 1985. Dolomitization in a mixing zone of near-seawater composition, Late Pleistocene, northeastern Yucatan Peninsula: *J. Sediment. Petrol.*, v. 55, p. 407–420.
- Webb, G. E., and Kamber, B.S., 2000. Rare earth elements in Holocene reefal microbialites; a new shallow seawater proxy: *Geochimica et Cosmochimica Acta*, v. 64, p. 1557-1565.
- Wright, D.T. 1999. The role of sulphate-reducing bacteria and cyanobacteria in dolomite formation in distal ephemeral lakes of the Coorong region, South Australia: *Sedimentary Geology*, v. 129, p. 147-157

4.10 Figures

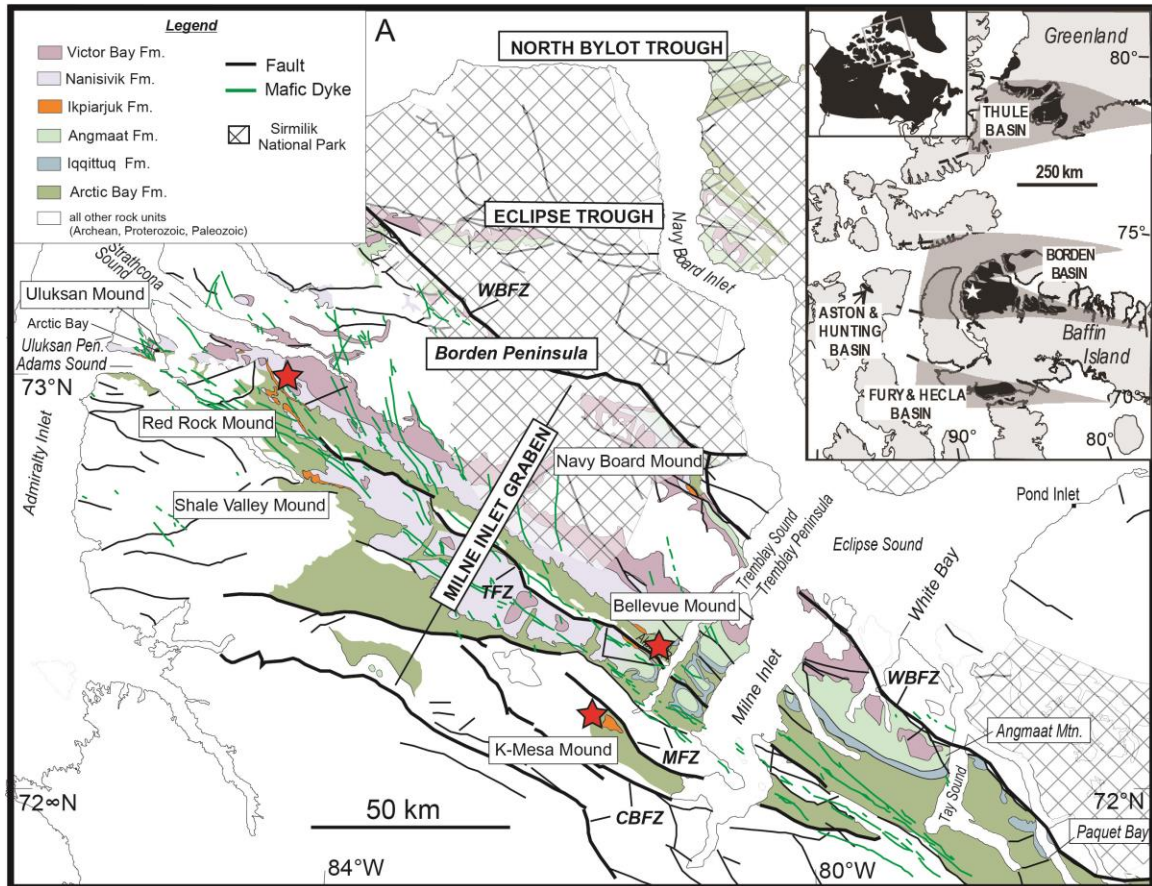


Figure 4-1 - Geological map

Figure 1: A) Geological map of the Milne Inlet Graben (MIG); only Mesoproterozoic units relevant to this paper are shown. Six areas of mound exposure are known from outcrop, and samples in this study are from three of them (red stars; map modified from Scott and deKemp, 1998, and Turner, 2009). Major syndepositional fault zones are labelled (CBFZ=Central Baffin fault zone, MFZ=Magda fault zone, TFZ=Tikrarjuaq fault zone, WBFZ=White Bay fault zone). B) The Bylot basins of the Canadian Arctic islands, with the Borden Basin highlighted. Black indicates present-day exposure; grey shows inferred former basin extents (from Jackson and Iannelli, 1981).

Formation		Tectonic History	Sedimentary Environment	Reference	
Bylot Supergroup	Sinasiuvik Fm.	Distal foreland basin?	Shallowing-upward Complex paleotopography	Knight and Jackson, 1994 Sherman et al., 2002	
	Aqigilik Fm.				
	Strathcona Sound Fm. & Athole Point Fm.				
	Victor Bay Fm.	Uplift/Tilting	Uplift and karsting in W end; Drowning and deepening in E (Athole Point Fm.)	Sherman et al., 2001 Sherman et al., 2002	
	Nanisivik Fm.	Uplift/Tilting	Dramatic uplift and tilting to the NE; erosion	Turner, 2009 Turner, 2011 Turner and Kamber, 2012	
	Angmaat Fm.				
	Arctic Bay Fm.	Extension	Black shale deposition Alluvial fans at graben margins Fault-related carbonate mounds throughout basin	Prograding carbonate ramp in SE	
	Iqqittuq Fm.				
	Adams Sound Fm.	Gentle Subsidence	Shallow-marine sandstone		Long and Turner 2012
	Nauyat Fm.		Basalt		
Rae Province Basement					

Figure 4-2 - Tectonic history

Figure 2: Stratigraphy of the Bylot Supergroup, with associated tectonic and depositional environments after Turner (2009, 2011), Turner and Long (2012), and Turner and Kamber (2012).

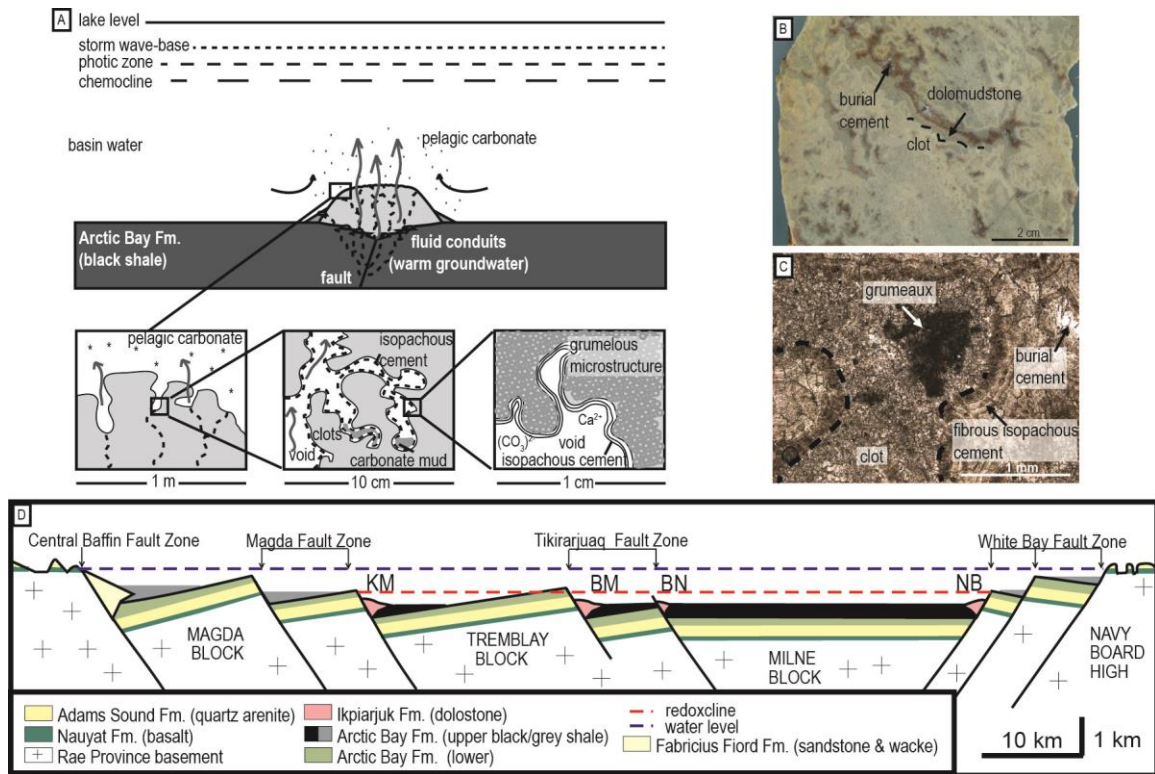


Figure 4-3 -Basin cross section

Figure 3: A) Interpretative diagram of mound formation through benthic precipitation of thrombolites (clots) and isopachous cement, and deposition of carbonate that precipitated pelagically. Mound growth occurred entirely beneath wave-base, the photic zone, and a chemocline. Slightly warm vent fluid (arrows) travelled through the mound in the porous network of microbial clots and voids. Upward movement of warm vent water generated local water circulation around mounds. B) Polished slab of Ikpiarjuk Formation thrombolite showing heterogeneous clot texture of clots, dolomudstone-filled geopetal structure, and burial-related cement. C) Plane-polarised photomicrograph showing grumelous texture in microbial clots surrounded by isopachous fibrous cement. C) Schematic cross-section through the Milne Inlet Graben (after Iannelli, 1992; Turner, 2011), illustrating basement blocks, sub-basins, and major fault zones at which the

Ikpiarjuk Formation mounds nucleated. Fault zones were major fluid conduits through the basin's depositional history.

	Red Rock Mound	Bellevue Mound	K-Mesa Mound
dolomitisation	100%	100%	100%
euhedral dolomite	common	present	rare
FCD	common	present	present
HD	common	present	common
CCD	common	common	common
quartz	rare	present	absent
replacive calcite	rare	rare	rare
late calcite	absent	rare	absent

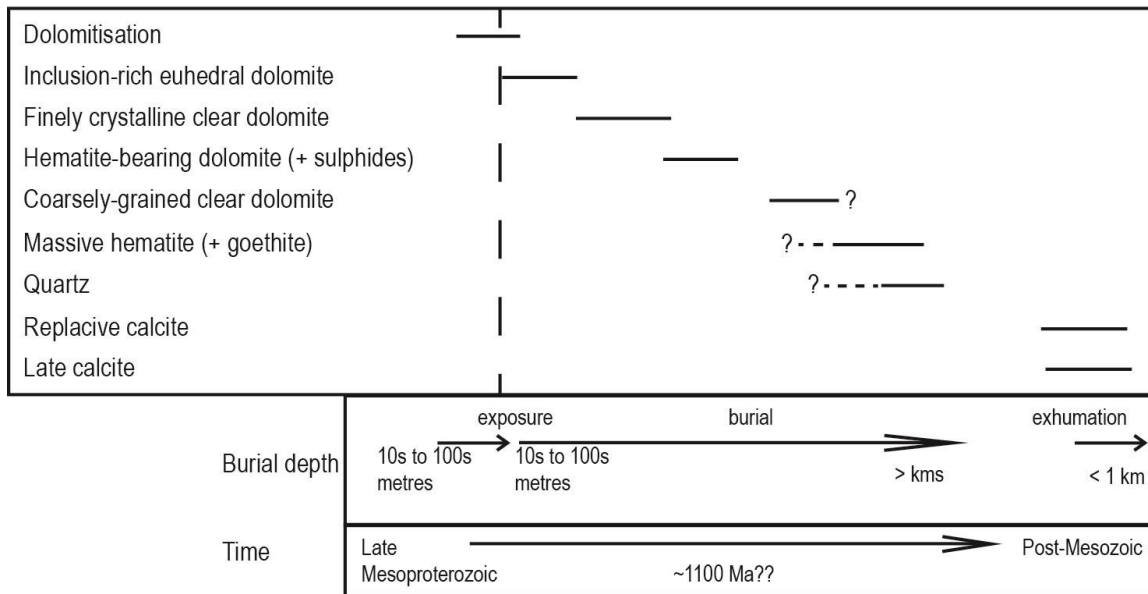


Figure 4-4 - Paragenetic chart

Figure 4: The paragenesis of the Ikpiarjuk Formation is based on data from three mounds. The relative timing of each phase is shown, with proposed absolute timing of each event.

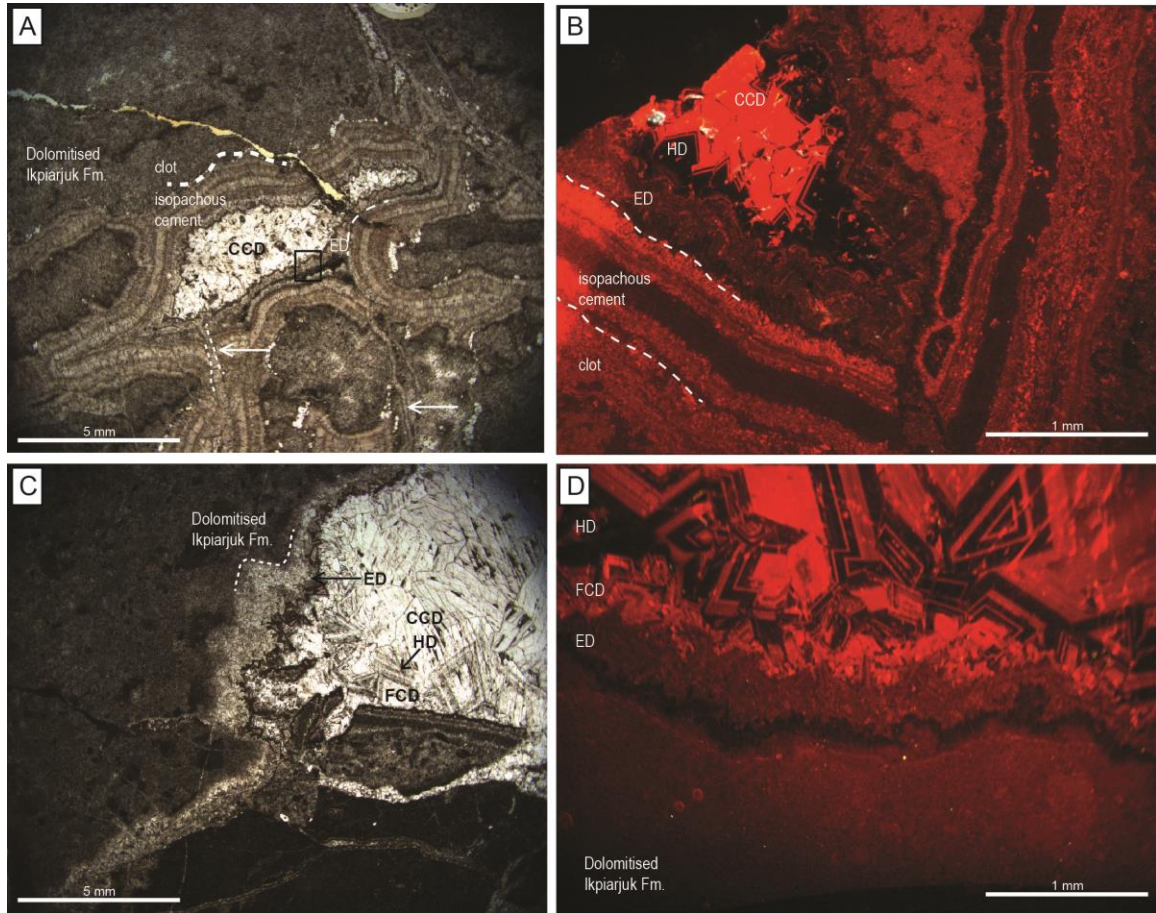


Figure 4-5 - Photomicrographs of paragenetic history

Figure 5: Photomicrographs illustrating the paragenetic history at Red Rock Mound. A) Primary voids lined with multiple generations of isopachous syndimentary cement are filled with coarsely crystalline late coarsely crystalline clear dolomite (CCD). Inclusion-rich euhedral dolomite (ED) overlies dolomitic silt that accumulated after deposition of the Nanisivik Formation (black box), isopachously lines primary voids, and cross-cuts primary fabric of the Ikpiarjuk Formation (white arrows). The dark rind along the outer margin of ED contains insoluble particulates generated during pressure solution, which were not incorporated into the crystal structure of dolomite. B) CL image of syndimentary and late void-filling cements. Inclusion-rich euhedral dolomite is

overlain directly by hematite-bearing dolomite (HD), followed by CCD. In this example, HD is not hematite-bearing, and is distinguished from CCD only by its non-luminescent character in CL. C) Inclusion-rich euhedral dolomite lines solution-enhanced fractures and recrystallises previously dolomitised Ikpiarjuk Formation dolostone. Finely crystalline clear dolomite (FCD) forms a thin rim of inclusion-free crystals. Hematite-bearing dolomite forms coarsely crystalline, zoned, inclusion-rich crystals. Coarsely crystalline clear dolomite is anhedral, free of inclusions, and fills remaining void space. D) In CL, ED is characterised by dull luminescence, FCD is brightly luminescent, and HD is non-luminescent, with brightly luminescent growth zones.

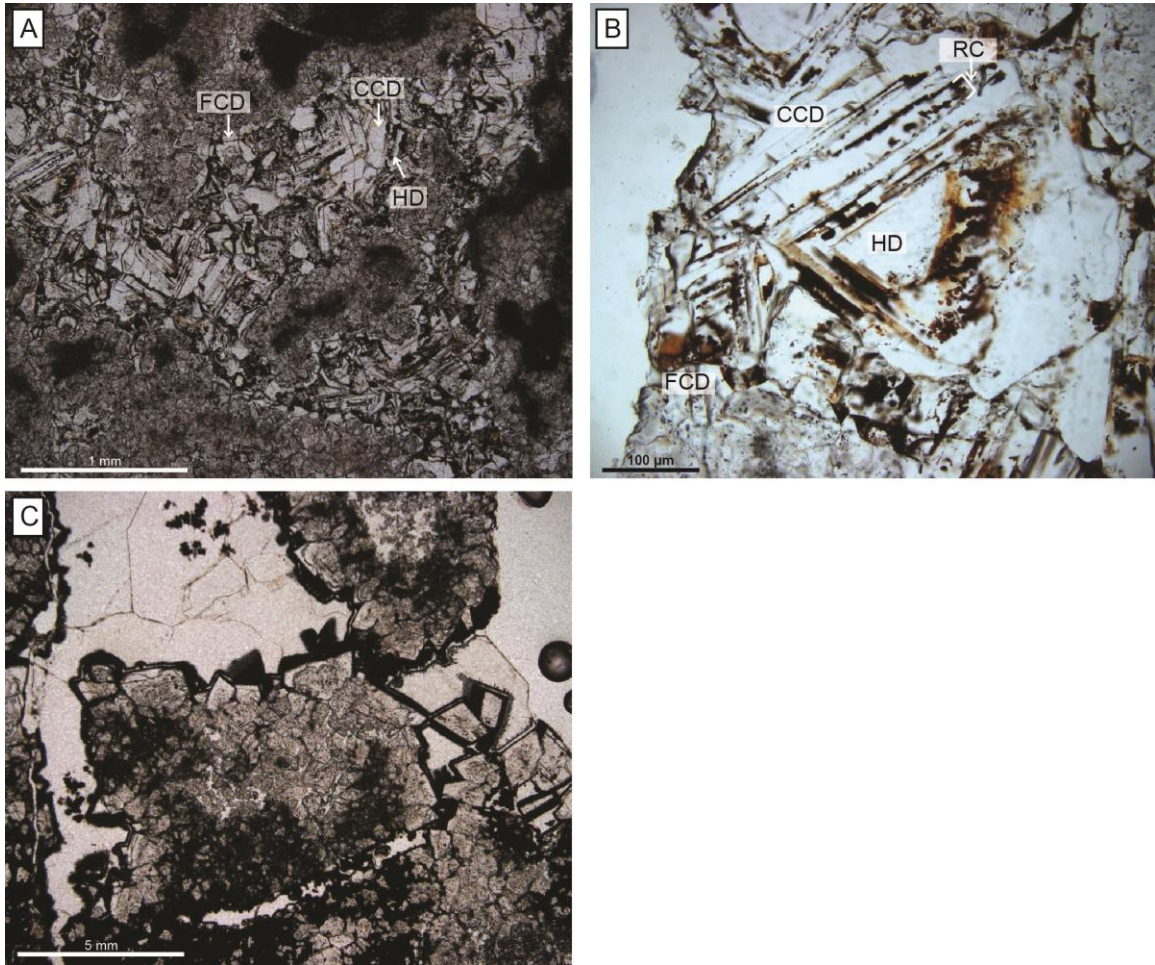


Figure 4-6 - Photomicrographs of paragenetic history (2)

Figure 6: Photomicrographs of cements at K-Mesa and Bellevue Mounds. A) and B) Well-developed crystals of hematite-bearing dolomite (HD), which overlie a very thin rim of finely crystalline clear dolomite (FCD). Coarsely crystalline clear dolomite (CCD) fills remaining void space. B) Replacive calcite (RC) is confined to inclusion-rich growth zones in HD, but it is indistinguishable from HD in plane-polarised light. C) Quartz (clear) fills void space after dolomitised host rock and hematite.

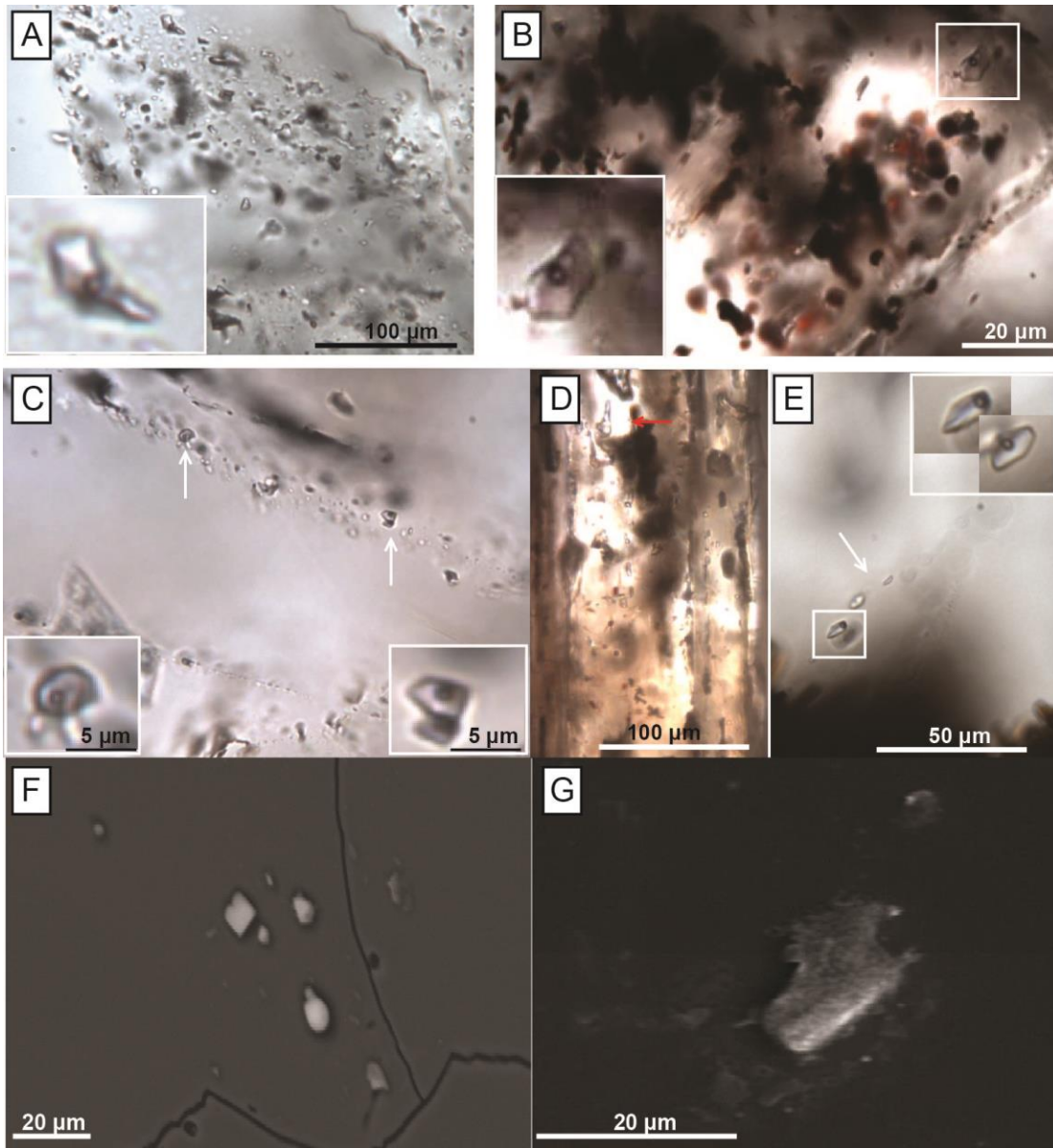


Figure 4-7 - Photomicrographs of fluid inclusions

Figure 7: Photomicrographs of doubly polished thick sections in plane-polarised transmitted light illustrating fluid inclusions in different cement phases. A) Abundant but necked inclusions in inclusion-rich euhedral dolomite (microthermometry was not done on these inclusions). B) A large inclusion (white box) in hematite-bearing dolomite (HD). Large inclusions are rare in HD, but several much smaller inclusions with similar liquid-

vapour ratios are present. C) A primary crystallographic growth plane of very small (1-3 μm) inclusions along with several much larger, but necked, inclusions (white box). D) Fluid inclusions in hematite- and galena-bearing HD at K-Mesa. Galena inclusions are discernible only under SEM, and are not visible in plane-polarised light. E) Rare primary FIA in quartz cement in close proximity to goethite inclusions (brown euhedral crystal). F) SEM image of NaCl cubic evaporate mounds produced from ED. G) SEM image of irregular Ca-bearing evaporate mound produced from HD.

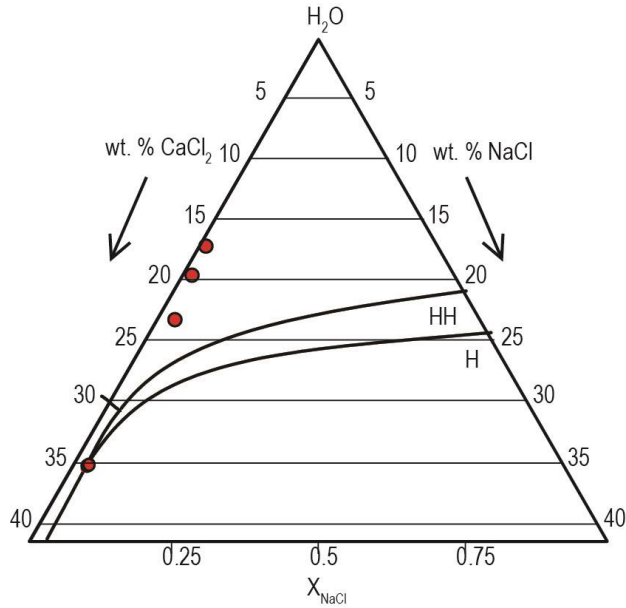


Figure 4-8 - H₂O-NaCl-CaCl₂ ternary diagram

Figure 8: Results of thermometric runs in which the final melting temperatures of both ice and hydrohalite (and rarely metastable antarticite) are plotted in the ternary system H₂O-NaCl-CaCl₂ (after Oakes et al., 1990). Data points were generated using an Excel VBA Macros (Steele-MacInnis et al., 2010) to numerically determine the H₂O-NaCl-CaCl₂ composition of fluid inclusions. Note that most inclusions measured are Ca-rich.

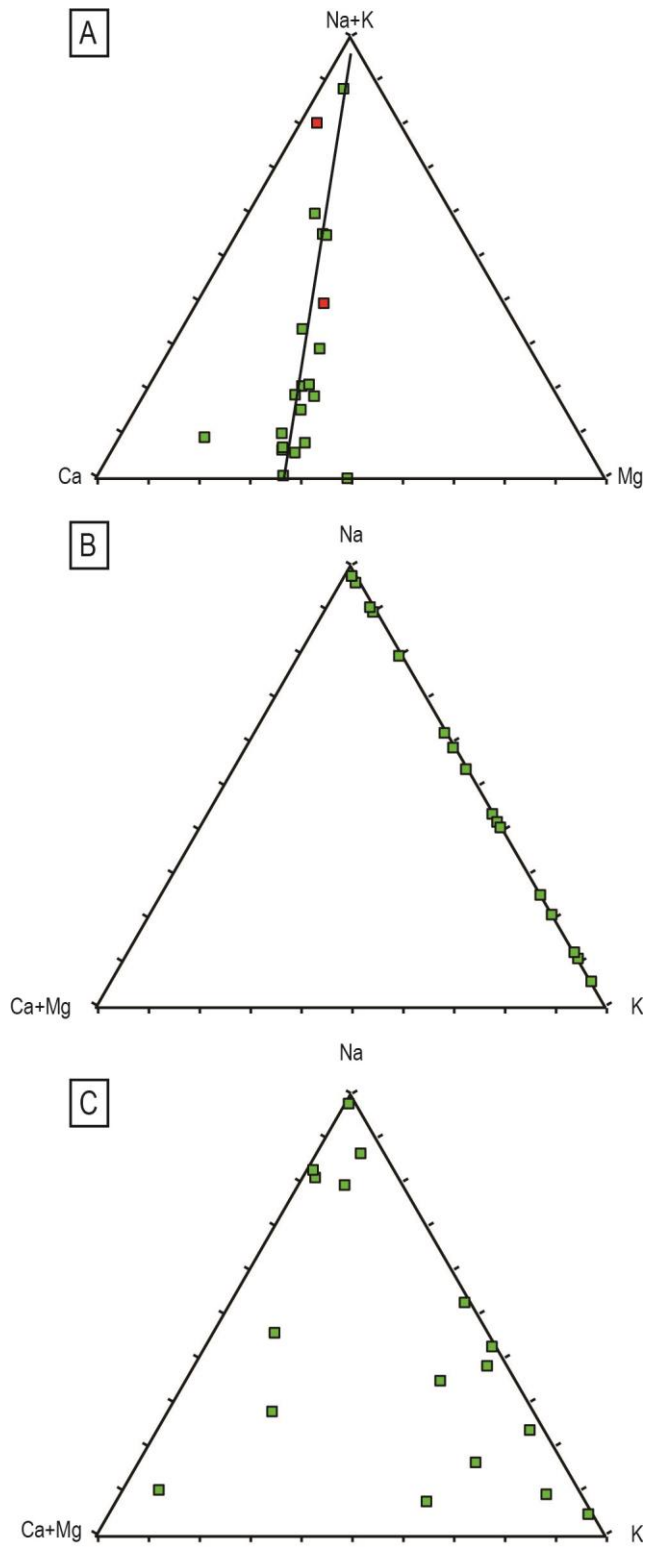


Figure 4-9 - Results of SEM-EDS analysis of evaporate mounds

Figure 9: Results of SEM-EDS analysis for all evaporate mounds plotted in ternary compositional space. A) All mound data plotted in Ca-Na+K-Mg space in order to illustrate the inherited Ca+Mg values inherited from the host dolomite. The average Ca:Mg of host dolomite (black line) illustrates that some evaporate mounds deviate strongly from the compositional trend of host dolomite. B) All mound data plotted in Ca+Mg-Na-K space with Ca+Mg component removed in order to illustrate the range in Na-K values. C) All mound data plotted in Ca+Mg-Na-K space after the Ca:Mg influence of the host dolomite was removed by applying a correction based its Ca:Mg.

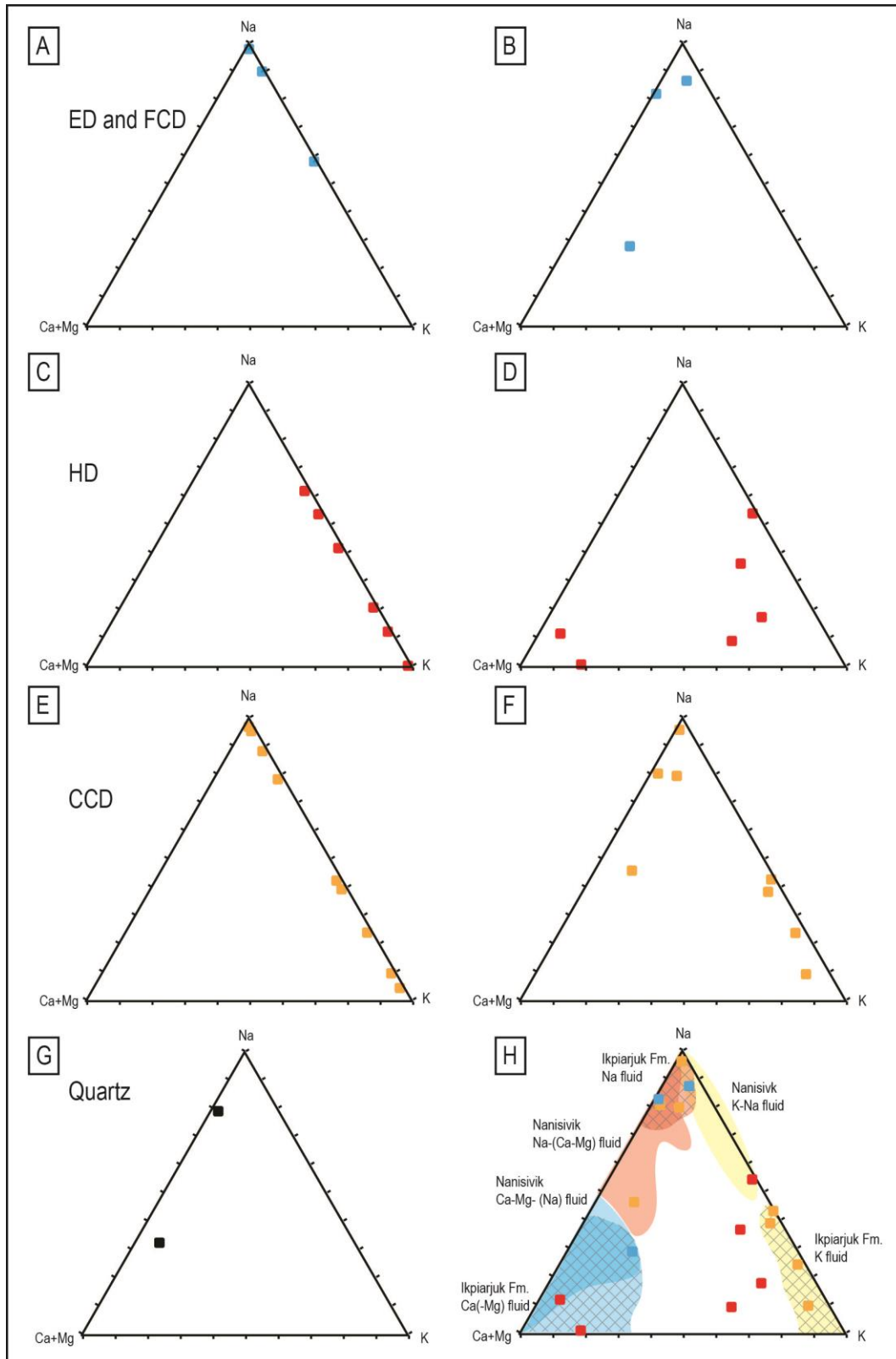


Figure 4-10 - Results of SEM-EDS analysis of evaporate mounds (2)

Figure 10: Results of SEM-EDS analysis for evaporate mounds for different cements plotted in Ca+Mg-Na-K ternary space. For each cement, the results are shown with the Ca+Mg component removed (A,C, and E), and with the corrected Ca+Mg included (B,D, and F). Note that applying a correction to the data produces a qualitative result because the correction assumes that only Ca or Mg (and not both) were present in an evaporate mound (see text for further discussion). Inclusions in HD and CCD are independently known to contain significant Ca based on the results of thermometric runs (see Fig. 8). The results of SEM-EDS analysis plotted for quartz in G do not require a correction. In (H), all Ca+Mg-corrected results are plotted and illustrate that at least three different fluids (diamond pattern fields) migrated through the Ikpiarjuk Formation. These fluids that migrated through the Ikpiarjuk Formation mounds share some compositional similarities with the recorded fluid flow history of the Nanisivik deposit (solid fields; Hnatyshin et al., submitted).

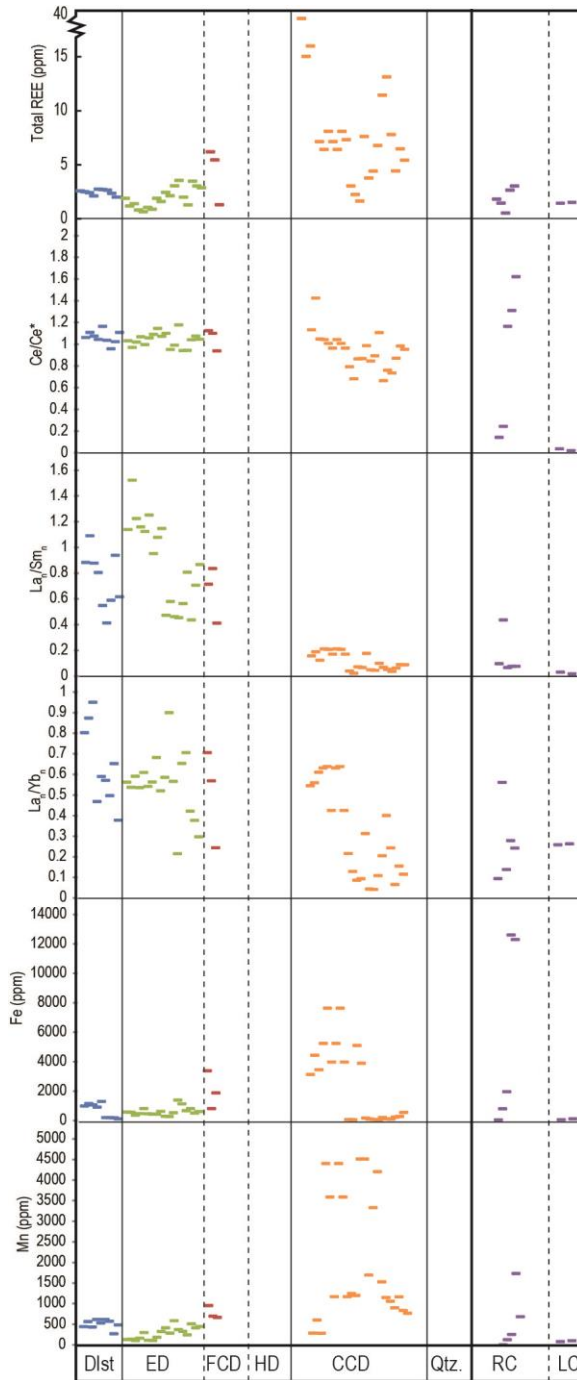


Figure 4-11- Summary of LA-ICP-MS results

Figure 11: Summary of chemical differences between the different cements, measured through LA-ICP-MS and arranged in relative paragenetic order from left to right. There are no laser data for hematite-bearing dolomite (HD) or quartz. A bold, solid line

indicates that a significant time gap may exist between cements. A fine, solid line indicates that a small time gap (millions of years) may exist between cements, and a dashed line indicates that cement precipitation may have been continuous. The width of the columns are a function of the number of analyses per cement type, and not a function of the duration of each precipitation event.

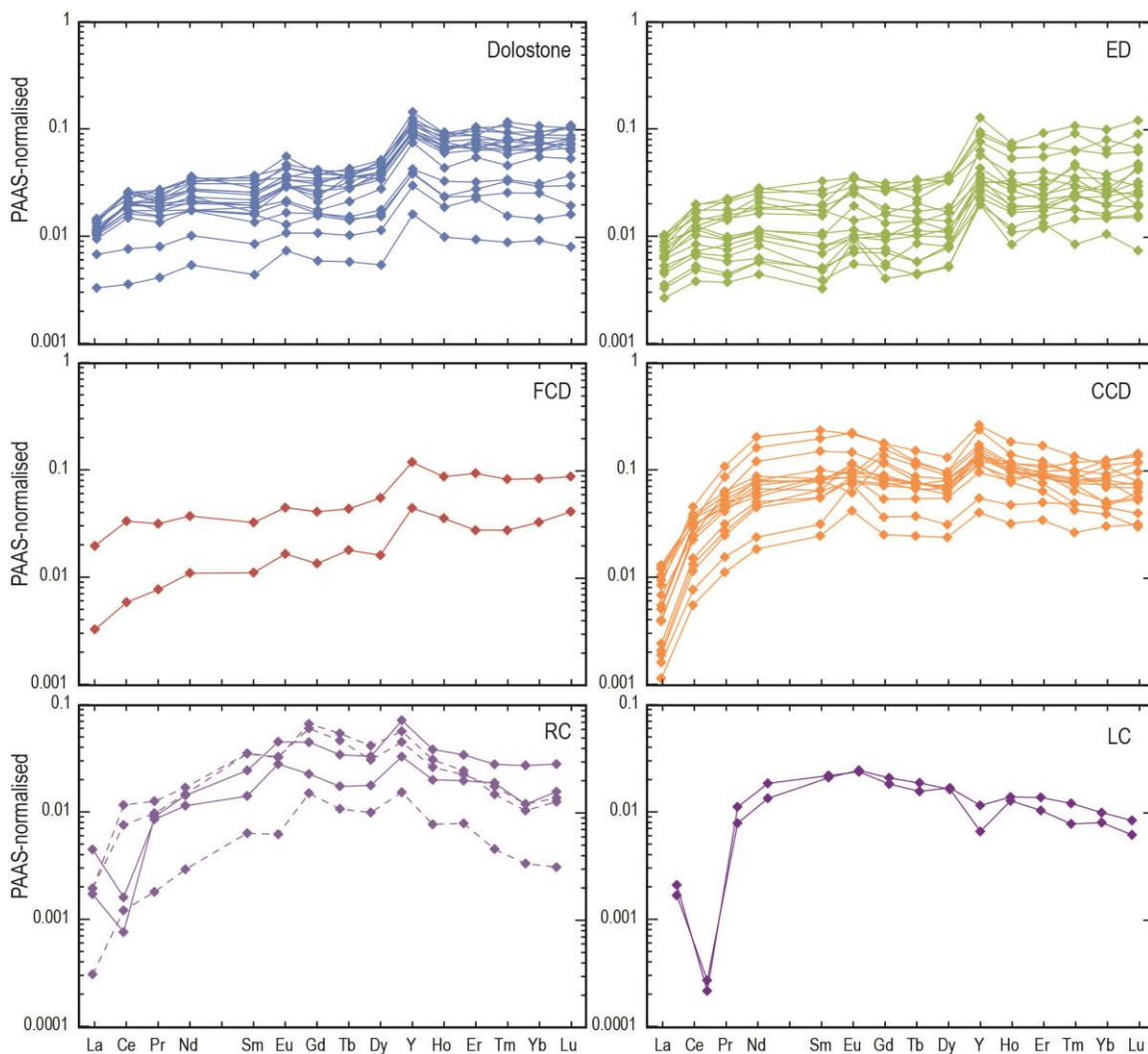


Figure 4-12 - PAAS-normalised REE plots

Figure 12: Post-Archean Australian Shale (PAAS) normalised REE+Y plots of some diagenetic phases of the Ikpiarjuk Formation (PAAS values of Pourmand et al., 2012); data was acquired with LA-ICP-MS analysis in all cases (see text for discussion). (A) Recrystallised dolostone of the Ikpiarjuk Formation. (B) Inclusion-rich euhedral dolomite (ED) cement. (C) Finely crystalline clear dolomite (FCD). Note that no REEY data for hematite-bearing dolomite were obtained because of the abundance of inclusions. Hematite-bearing dolomite is presumed to have a similar REEY to FCD. (D) Coarsely

crystalline clear dolomite (CCD). (E) Replacive calcite (RC). Note the presence of two distinct REEY patterns. The middle-REE bulge in dashed line patterns may indicate that iron oxides were included in spot analyses. (F) Late calcite (LC).

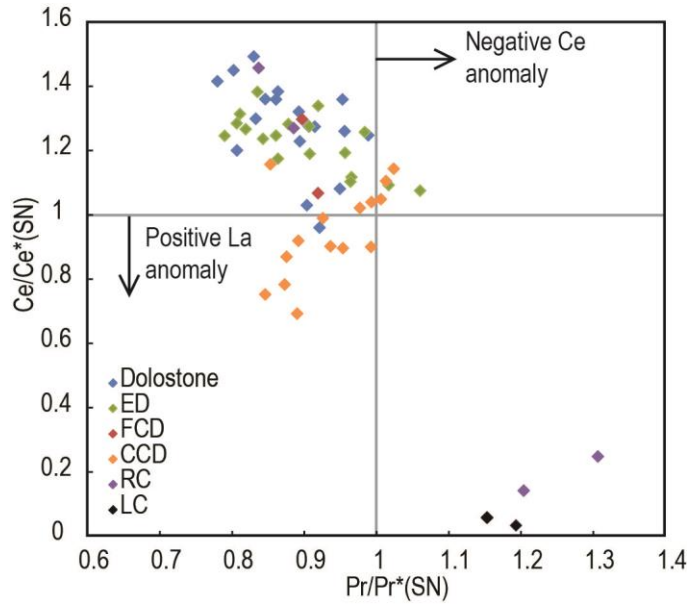


Figure 4-13 - La and Ce anomaly discrimination diagram

Figure 13: La and Ce anomalies were calculated using the method of Bau et al. (1997) and plotted on an anomaly discrimination diagram. Most phases display a positive Ce anomaly and a negative La anomaly when normalised to PAAS. Coarsely crystalline clear dolomite displays a positive La anomaly, but the extreme depletion in La compared to the other REEs may complicate the anomaly calculation. Calcite displays a strongly negative Ce anomaly.

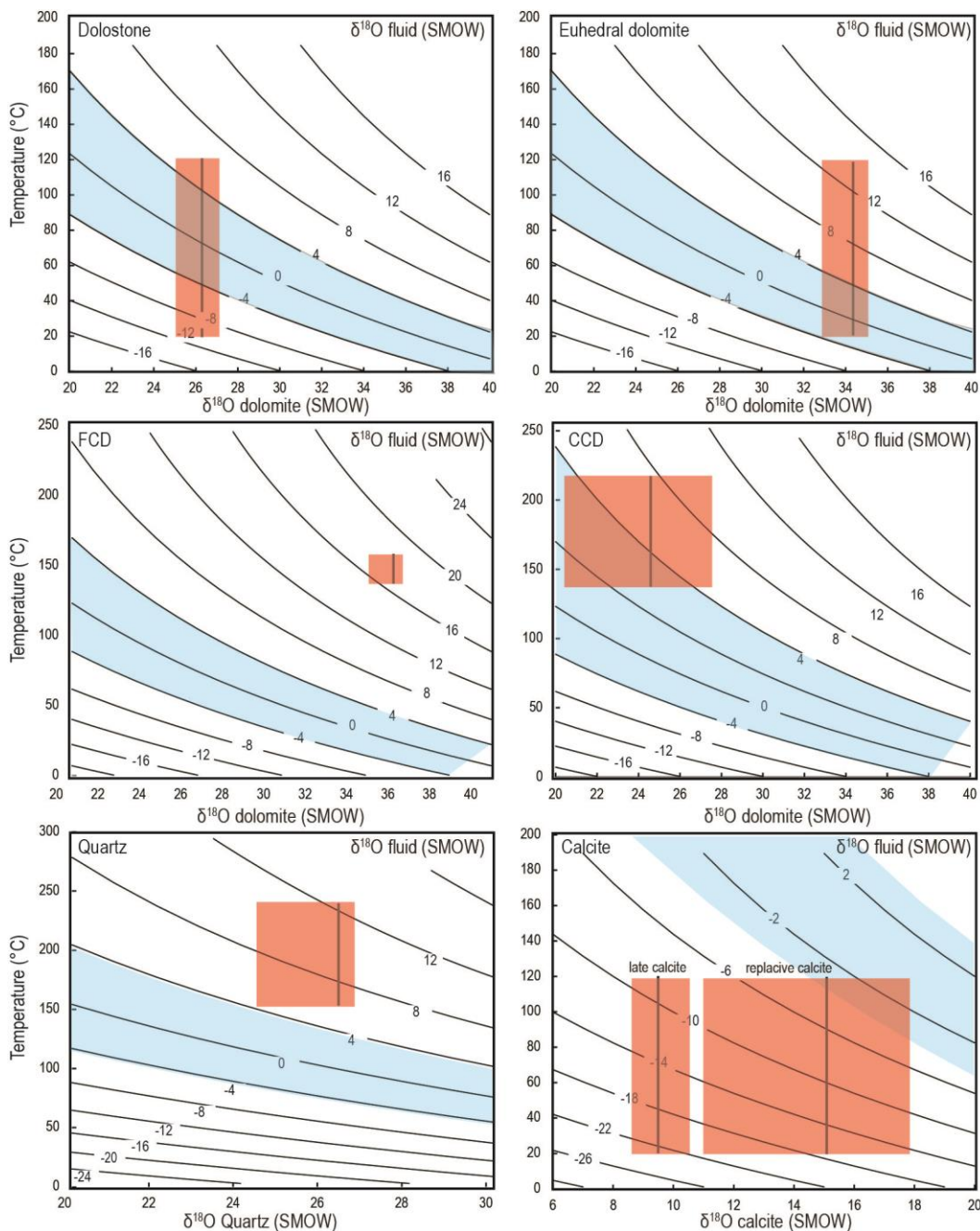


Figure 4-14 - Oxygen isotope data

Figure 14: Plots of oxygen isotope data for dolostone and cement phases versus temperature with isopleths for possible $\delta^{18}\text{O}_{\text{H}_2\text{O}}$ values (in ‰) for these phases. The curved isopleths for $\delta^{18}\text{O}_{\text{H}_2\text{O}}$ were calculated using mineral fraction equations for dolomite (Horita et al., 2014), calcite (O'Neill et al., 1969), and quartz (Sharp and

Kirschner, 1994). The blue fields represent the range in $\delta^{18}\text{O}_{\text{H}_2\text{O}}$ of seawater, and the red fields represent the calculated $\delta^{18}\text{O}_{\text{H}_2\text{O}}$ of the cement precipitating fluids. (A) Possible $\delta^{18}\text{O}_{\text{H}_2\text{O}}$ values calculated for the Ikpiarjuk Formation dolostone assuming a temperature range of 20°C to 120°C (red field). Sedimentary carbonate dolomitisation may have taken place in seawater-derived fluid at a range of temperatures. (B) A range of possible $\delta^{18}\text{O}_{\text{H}_2\text{O}}$ values was calculated for inclusion-rich euhedral dolomite (ED), given the lack of temperature constraints. Inclusion-rich euhedral dolomite could have precipitated from seawater only if it formed at a temperature below 60°C. (C) The trapping temperature of finely crystalline clear dolomite (FCD) is estimated to be ~150°C (Th of 110°C) for a burial depth of 3 km, which means the calculated $\delta^{18}\text{O}_{\text{H}_2\text{O}}$ is much heavier than that of fluid derived entirely from seawater. Hematite-bearing dolomite contains too many hematite inclusions to accurately measure $\delta^{18}\text{O}$. (D) The trapping temperature of coarsely crystalline clear dolomite (CCD) is estimated to be between 140°C and 220°C for a burial depth between 3 km and 6 km, and calculated $\delta^{18}\text{O}_{\text{H}_2\text{O}}$ for those temperatures indicates that seawater could have been a significant component of the fluid. (E) The trapping temperature of quartz is estimated to be between 150°C and 240°C for a burial depth between 0 km and 6 km. Calculated fluid $\delta^{18}\text{O}_{\text{H}_2\text{O}}$ values for quartz are slightly higher than those of seawater. (F) Calculated fluid $\delta^{18}\text{O}_{\text{H}_2\text{O}}$ for replacive calcite and late calcite for a range of temperatures between 20°C and 120°C. Replacive calcite and calcite precipitated in a near-surface environment, and most likely at less than 60°C. High-latitude meteoric water must have been the fluid source for calcite (and replacive calcite)

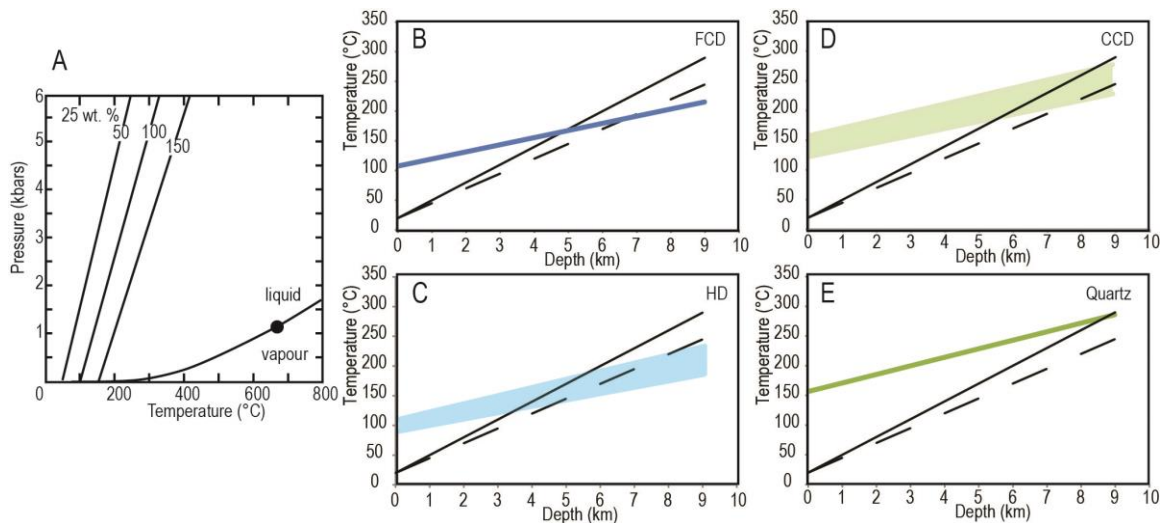


Figure 4-15 - Pressure-temperature diagrams

Figure 15: (A) Pressure-temperature diagram showing isochores, or iso- T_h lines, for a fluid of 25 wt. % NaCl having three different densities, as reflected by their variable T_h values (50, 100, and 150°C); diagram is modified after (Bodnar (2003)). The isochores illustrate that, depending on the temperature of formation and fluid entrapment, a pressure-dependent correction has to be applied to the measured T_h values for fluid inclusions in order to determine the true temperature of entrapment. For example, an inclusion with a T_h value of 150°C that was trapped at an inferred depth of about 6 km requires a 2 kbar pressure correction, which equates to an entrapment temperature of about 225°C. In the present study a pressure correction is applied to the measured T_h values in order to estimate the true trapping temperatures of inclusions in the different cements. (B through E) Plots of pressure-corrected fluid temperatures (i.e., T_h values in coloured lines) versus burial depth calculated using equations in Bodnar and Vityk (1994). Note that the width of the coloured lines reflects the range in measured T_h values. See text for further discussion of the pressure corrections. The areas above the geothermal gradients of 25°C/km (dashed line) and 30°C/km (solid line) (Allen and Allen, 2005) for given burial depths are considered hydrothermal. (B) Finely crystalline clear dolomite (FCD). (C) Hematite-bearing dolomite (HD) has a range in salinity and measured T_h , and the field of possible pressure-

corrected temperatures is plotted based on the minimum and maximum salinities and temperatures. (D) Coarsely crystalline clear dolomite (CCD) has a range in salinity and measured T_h , and the field of possible pressure-corrected temperatures is plotted based on the minimum and maximum salinities and temperatures. (E) Quartz.

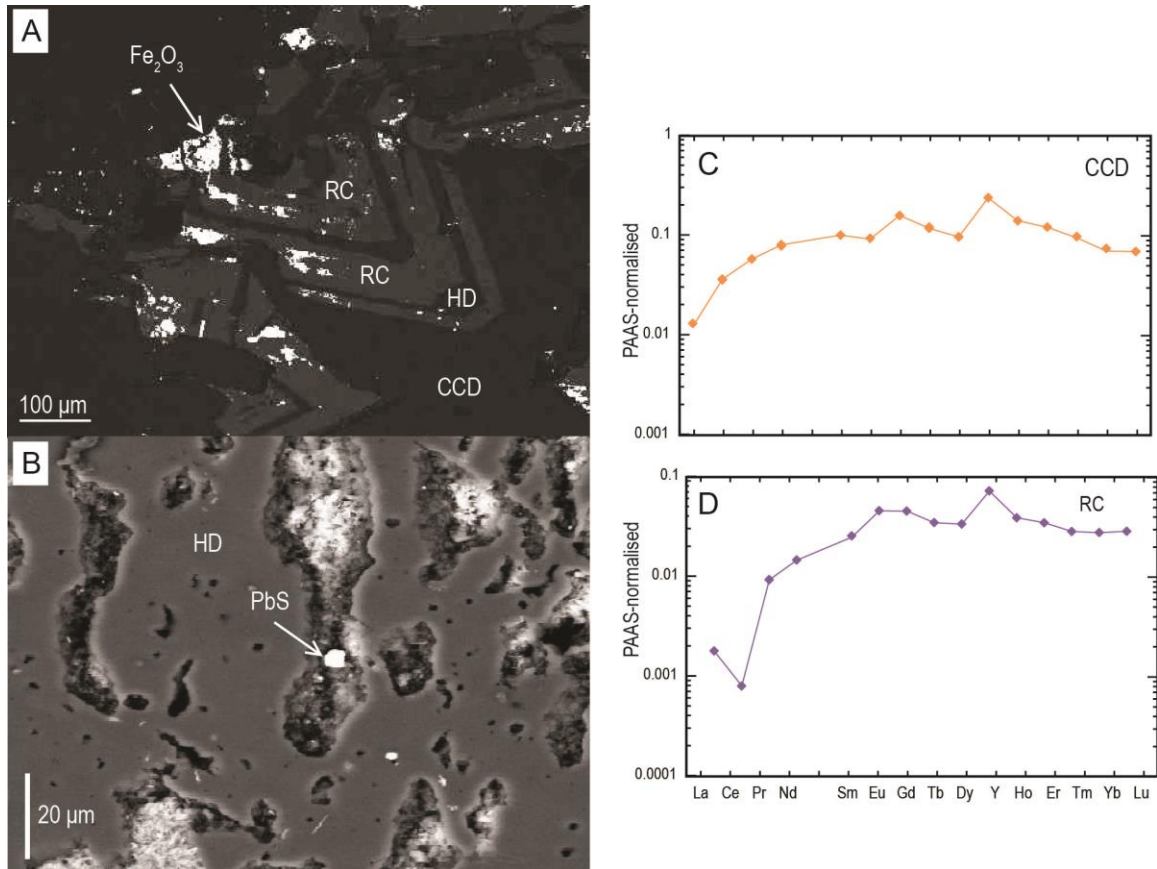
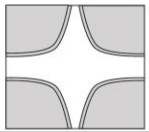
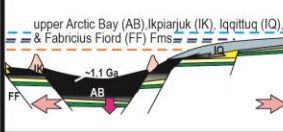
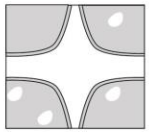
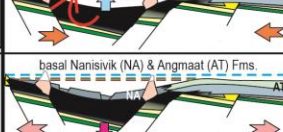
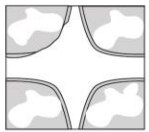
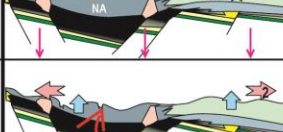
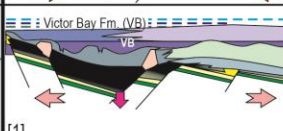
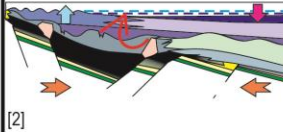
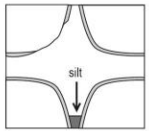
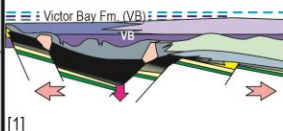
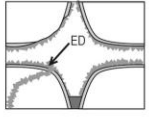
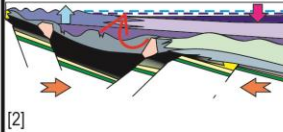
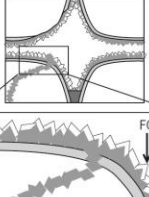
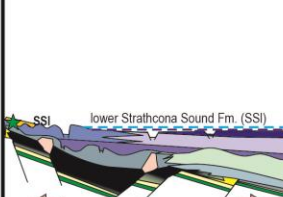


Figure 4-16 - Backscattered electron image

Figure 16: (A) Backscattered electron image from the SEM illustrating calcite replacing (RC) dolomite in hematite-bearing (HD) growth zones. Coarsely crystalline clear dolomite (CCD) overgrows HD. (B) In backscattered SEM, tiny galena inclusions appear in decrepitated fluid inclusion pits hosted by HD. (C) and (D) Corresponding PAAS-normalised REEY plots are shown for CCD (C) and RC (D). The strong negative Ce anomaly in calcite indicates that it precipitated from an oxidised fluid, probably at a burial depth of less than 1 km.

Figure 17: (diagram on following page) Summary diagram of the paragenetic stages recorded in Ikpiarjuk Formation voids and replacement cements. The temperature of homogenisation (T_h) as well as the pressure corrected temperature (T_p) for interpreted burial depths are reported. Tectono-sedimentary events are from Turner et al. (submitted). The Ikpiarjuk Formation mounds formed about ca. 1.1 Ga during fluid venting into an alkaline lake. Dolomitisation probably occurred just below the sediment-water interface while the basin was filled with an alkaline lake, and was complete prior to precipitation of inclusion-rich euhedral dolomite (ED). Prior to precipitation of ED, the mounds were uplifted and in places karsted. During subsequent drowning of the mounds the framework pore space was filled with marine water. ED precipitated during chemical compaction of the mounds, with by marine water that was modified through pressure solution generated from the compacting mounds (fluid 1). During continued burial cementation, reduced hydrothermal fluids (fluid 2) moved up along porous fault zones and mixed with the fluid 1, resulting in the precipitation of finely crystalline clear dolomite (FCD) under low fluid-rock (F-R) ratios. Fluid 2 hydrothermal fluids continued moving up fault zones and hematite-bearing dolomite (HD) was precipitated under a higher fluid-rock ratio than FCD. Coarsely crystalline clear dolomite (CCD) was precipitated under high F-R ratios and was generated by mixing of a new fluid (fluid 3) with fluid 2. Fluid 3 was potassium bearing with an extreme LREE depletion and was generated by fluids that were sourced either from shale or granitoids where precipitation of monazite occurred along the flow path. At some unknown time in quartz-precipitating, saline fluid was passed through the mounds (Fluid 4). Uplift and erosion took place and meteoric water infiltrated mounds at depths of <1 km, and dedolomitised hematite-bearing growth zones of HD. Replacive

calcite (RC) was precipitated under low F-R ratios during dedolomitisation of HD (and rarely CCD) and late calcite (LC) filled remaining pore space in mounds at high F-R ratios.

Late Diagenetic Events	Th and Tp(°C)	salinity (wt. %) and composition	calculated ¹⁸ O _{H2O}	REE+Y Fe, Mn (ppm)	F-R ratio	Interpretation	Legend	Tectono-sedimentary events
						deepening upward; pronounced faulting; fluid venting syndimentary cement	<ul style="list-style-type: none"> — water surface - - storm wave-base - - base photic zone - - O₂ chemocline → compression ← extension ↑ uplift ↓ pronounced subsidence ↓ gentle subsidence 	
						uplift and tilting	<ul style="list-style-type: none"> □ primary depositional components □ dolomitisation 	
						normal faulting		
	NA	NA	-13‰ (20°C) +2.8‰ (120°C)	Fe: 671 Mn: 501	NA	gentle subsidence		
						uplift, tilting, exposure; minor, local truncation of benthic isopachous cement		
						[1] abrupt flooding with marine water; extension; rare geopetal silt		
						[2] tilting; uplift and karsting (W) and drowning(E); compaction of mounds. Precipitation of euheudral dolomite during physical and chemical compaction of Ikpiarjuk Formation mounds. Fluid 1 is generated from in situ pore fluids derived from marine water and modified during fluid-rock interaction during compaction. REE released from Ikpiarjuk Formation during pressure solution are incorporated into fluid 1.		
	Th:110 Tp:145 (3 km)	20 (Ca+Mg)>Na	-5.4‰ (20°C) +10.8‰ (120°C)	Fe: 2020 Mn: 770	low	normal faulting; continued compaction Mixing of fluid 1 and fluid 2 . Fluid 2 is hydrothermal and Ca(-Mg)-rich and has fluid ¹⁸ O _{H2O} characteristic of dissolved carbonate rocks		

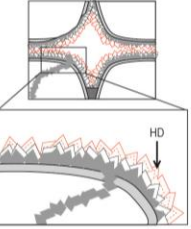
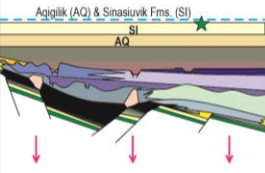
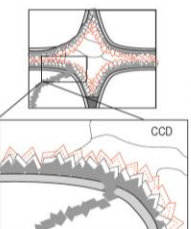
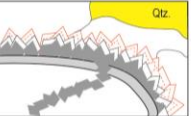
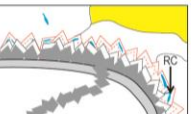
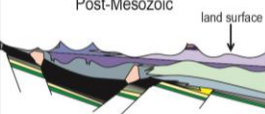
Late Diagenetic Events	Th and Tp(°C)	salinity (wt. %) and composition	calculated ¹⁸ O _{H2O}	REE+Y Fe, Mn (ppm)	F-R ratio	Interpretation	Tectono-sedimentary events
 <p>HD with hematite, +/- pyrite, sphalerite, galena</p>	Th: 84 Tp: 117 to 124 (3 km)	22 to 37 (Ca+Mg)>K>Na	NA	NA	med	pronounced deepening; SE-directed minor thrusts; continued compaction Fluid 2 is present at a higher water-rock ratio and precipitates dolomite 2 (+hematite, pyrite, sphalerite, galena). The timing of fluid 2 is probably contemporaneous with deposition of the upper Bylot Supergroup.	
 <p>? Timing unclear CCD</p>	Th: 117 Tp: 150 (3 km) Tp: 190 (6 km)	20 to 25 K>(Ca+Mg)>Na	-5.4‰ (20°C) +10.8‰ (120°C)	Fe: 2415 Mn: 2067	high	Mixing of fluid 2 and fluid 3 . Fluid 3 is saline, hydrothermal, and contains K>Na and Ca(-Mg). Fluid 3 is generated through extensive interaction with a K-bearing rock (possibly shale beneath the Ikpiarjuk Fm. (Arctic Bay Fm.) or basement blocks in the MIG). Timing is unclear.	
 <p>? Timing unclear Qtz quartz</p>	Th: 154 Tp: 240 (6 km)	14 Na>(Ca+Mg)	-5.4‰ (20°C) +10.8‰ (120°C)	NA		Fluid 4 is saline, hydrothermal, and contains Na>(Ca+Mg) Timing is unclear	
<p>non-deposition; erosion and exposure</p>							
 <p>(Post-Mesozoic) RC LC</p>		NA	-20.5‰ (20°C) -5.7‰ (120°C) -25.8‰ (20°C) -11.5‰ (120°C)	Fe: 1.0 Mn: 0.0	low?	Fluid 5 has a calculated oxygen isotope characteristic of high-latitude meteoric water. The timing of fluid 5 must be post-Mesozoic	

Figure 4-17 - Summary diagram of paragenetic stages

Table 4-4 – LA-ICP-MS elemental concentrations (ppm)

Type	12KM005 DLST	12KM005 DLST	12KM005 DLST	RR036d_3 DLST	RR036d_4 DLST	RR045a_1 DLST	RR045a_2 DLST	RR045a_3 DLST	RR045c_3 DLST	11RR036 ED	11RR036 ED
Al	22.3	25.8	22.1	113.5	128.7	45.4	38.7	28	79.6	81.4	82.6
V	0.635	0.677	0.583	2.568	1.912	3.24	3.78	3.42	6.95	3.12	0.843
Mn	440	562	432	614	530	614	573	265	482	128.6	134.2
Fe	978	1151	1056	905	1288	185	189.5	179	103.4	569	557
Sr	36.54	37.9	36.93	38.2	35.9	37.5	35.8	41.6	35	38.71	29.4
Y	0.733	0.674	0.665	0.852	1.004	0.855	0.861	0.764	0.886	1.11	0.517
Zr	0.212	0.156	0.142	0.152	0.186	0.33	0.082	0.104	0.23	0.503	0.263
Nb	0	0	0	0	0	0	0	0	0	0	0
Ba	10	10	3	2	2	6	3	4	2	1	1
La	0.438	0.448	0.423	0.323	0.360	0.320	0.323	0.346	0.259	0.382	0.230
Ce	1.072	1.070	1.002	0.783	1.074	0.972	0.894	0.907	0.711	0.736	0.446
Pr	0.127	0.113	0.112	0.095	0.126	0.140	0.138	0.121	0.085	0.071	0.050
Nd	0.461	0.453	0.457	0.428	0.567	0.626	0.679	0.540	0.444	0.304	0.221
Sm	0.105	0.087	0.102	0.085	0.139	0.164	0.116	0.078	0.089	0.071	0.032
Eu	0.024	0.019	0.015	0.025	0.035	0.039	0.031	0.021	0.025	0.013	0.009
Gd	0.092	0.092	0.088	0.101	0.118	0.119	0.143	0.100	0.105	0.058	0.045
Tb	0.013	0.012	0.012	0.012	0.018	0.024	0.017	0.013	0.013	0.012	0.005
Dy	0.088	0.076	0.081	0.092	0.114	0.106	0.117	0.078	0.090	0.085	0.042
Ho	0.022	0.016	0.015	0.022	0.023	0.023	0.025	0.017	0.022	0.020	0.013
Er	0.059	0.051	0.044	0.061	0.088	0.085	0.075	0.056	0.069	0.057	0.035
Tm	0.009	0.009	0.007	0.010	0.010	0.014	0.009	0.008	0.012	0.012	0.006
Yb	0.055	0.051	0.045	0.069	0.061	0.056	0.065	0.053	0.069	0.068	0.043
Lu	0.010	0.008	0.005	0.011	0.011	0.013	0.010	0.008	0.011	0.013	0.007
La/La*	0.79	1.09	1.09	1.21	0.99	0.79	0.97	0.98	1.41	1.73	1.59
Ce/Ce*	1.06	1.11	1.08	1.04	1.16	1.04	0.96	1.02	1.11	1.03	0.97
Eu/Eu*	1.00	0.92	0.65	1.21	1.09	1.01	1.12	1.07	1.15	0.76	1.14
Pr/Pr*	1.03	0.93	0.94	0.93	0.92	1.01	0.98	0.98	0.86	0.85	0.90
TotalREE	2.57	2.50	2.41	2.12	2.74	2.70	2.64	2.35	2.00	1.90	1.18
Y/Ho	34.1	43.5	43.5	39.3	43.3	36.7	34.6	43.9	40.3	54.7	39.5

Type	11RR036 ED	RR045e_1 ED	RR045e_2 ED	RR045e_3 ED	RR048b_1 ED							
Al	101.4	65.1	33.2	125	80.3	126	96.3	30.8	39.9	52.2	90	
V	0.862	2.11	4.56	1.137	1.006	1.349	1.079	0.689	0.676	0.811	5.11	
Mn	102.1	162.6	296.7	111.9	99.9	180.5	321	412	284	584	369	
Fe	360	459	808	454	431	431	612	286	269	526	1390	
Sr	31.49	29.55	32.45	37.5	33.67	33.52	34.2	47.7	45.6	41.4	50	
Y	0.564	0.383	0.353	0.407	0.352	0.559	0.616	0.767	0.666	1.001	2.241	
Zr	0.49	0.108	0.147	0.345	0.221	0.89	0.259	0.076	0.204	0.268	0.529	
Nb	0	0	0	0	0	0	0	0.0063	0.00000463	0.0043	0.0332	
Ba	1	1	4	1	1	3	1	3.55	4.31	3.99	5.3	
La	0.266	0.142	0.116	0.195	0.153	0.341	0.287	0.281	0.315	0.351	0.379	
Ce	0.539	0.312	0.245	0.422	0.339	0.787	0.652	0.897	0.795	1.055	1.263	
Pr	0.057	0.033	0.028	0.044	0.034	0.075	0.070	0.121	0.117	0.162	0.1567	
Nd	0.251	0.156	0.120	0.169	0.158	0.308	0.294	0.625	0.486	0.753	0.684	
Sm	0.046	0.026	0.022	0.033	0.034	0.067	0.053	0.126	0.115	0.161	0.177	
Eu	0.012	0.007	0.011	0.012	0.008	0.022	0.011	0.0289	0.0164	0.0335	0.0396	
Gd	0.054	0.031	0.024	0.033	0.041	0.077	0.059	0.107	0.093	0.166	0.18	
Tb	0.009	0.004	0.004	0.007	0.005	0.012	0.010	0.0146	0.0125	0.019	0.0281	
Dy	0.051	0.027	0.027	0.041	0.040	0.058	0.056	0.095	0.071	0.166	0.186	
Ho	0.015	0.007	0.006	0.011	0.008	0.022	0.013	0.019	0.0179	0.0259	0.0492	
Er	0.046	0.023	0.025	0.033	0.029	0.052	0.037	0.0649	0.0416	0.075	0.1711	
Tm	0.008	0.004	0.002	0.007	0.005	0.013	0.007	0.0084	0.0068	0.0099	0.0298	
Yb	0.045	0.027	0.019	0.036	0.027	0.050	0.055	0.048	0.035	0.062	0.176	
Lu	0.009	0.004	0.002	0.007	0.004	0.011	0.005	0.0064	0.005	0.0078	0.0315	
La/La*	1.60	1.74	1.25	1.12	1.64	1.32	1.24	1.07	0.80	0.80	0.79	
Ce/Ce*	1.02	1.07	1.00	1.06	1.09	1.14	1.07	1.10	0.95	0.99	1.18	
Eu/Eu*	0.95	1.03	1.94	1.25	1.01	1.30	0.81	1.04	0.66	0.94	0.92	
Pr/Pr*	0.88	0.84	0.95	0.94	0.84	0.87	0.91	0.90	1.07	1.02	0.96	
TotalREE	1.41	0.80	0.65	1.05	0.89	1.90	1.61	2.44	2.13	3.05	3.55	
Y/Ho	37.1	51.8	61.9	36.0	42.9	25.1	48.9	40.4	37.2	38.6	45.5	

Type	RR048c_1 ED	RR048c_2 ED	RR048c_3 ED	SG72c_1 ED	SG72c_2 ED	11RR024 FCD	RR036e_3 FCD	RR036e_4 FCD	11BM022 CCD	11BM022 CCD	11BM022 CCD
Al	49.5	41.5	125.2	128	107.6	114	83.8	70.6	77	207	58.5
V	1.17	2.052	4.38	2.71	3.06	0.995	1.156	1.29			
Mn	324	241.4	506	410	443	953	694	664	284	602	281
Fe	1121	664	809	495	605	3380	810	1870	3130	4430	3450
Sr	35.46	33.29	38.21	38.08	32.6	20.4	42.8	8.75	14.06	15.66	16.16
Y	0.583	0.463	1.344	1.543	1.661	2.001	2.08	0.787	2.72	2.76	6.99
Zr	0.47	0.112	0.244	0.58	0.235	0.062	0.098	0.223	0.135	0.298	0.058
Nb	0.04	0.0054	0.0074	0.048	0.006	0.0037	0.0005	0.0022	0.0048	0.0225	0.0032
Ba	5.4	0.94	1.47	3.7	0.755	0.027	0.68	7.4	0.7	4.3	0.304
La	0.277	0.2068	0.443	0.437	0.422	0.853	0.848	0.144	0.84	0.89	2
Ce	0.722	0.464	1.241	1.113	0.948	2.524	2.12	0.38	5.18	6.59	13
Pr	0.1103	0.0633	0.1685	0.1328	0.106	0.312	0.238	0.059	0.87	0.87	2
Nd	0.438	0.273	0.734	0.494	0.558	1.273	0.999	0.298	4.91	4.63	14
Sm	0.104	0.0542	0.215	0.131	0.103	0.253	0.215	0.074	1.13	1	3
Eu	0.0317	0.012	0.0407	0.042	0.0334	0.0625	0.052	0.0195	0.200	0.194	1
Gd	0.095	0.0624	0.165	0.16	0.151	0.254	0.237	0.079	0.8500	0.7390	2
Tb	0.0174	0.0087	0.023	0.0287	0.0251	0.0405	0.0372	0.0155	0.0870	0.0870	0
Dy	0.086	0.06	0.172	0.166	0.173	0.263	0.28	0.083	0.4920	0.4770	1
Ho	0.0207	0.0119	0.0358	0.0439	0.0455	0.055	0.0581	0.024	0.0790	0.0821	0
Er	0.0452	0.0353	0.103	0.128	0.127	0.147	0.174	0.0521	0.1990	0.2090	0
Tm	0.0096	0.005	0.0178	0.0253	0.0174	0.0209	0.023	0.0078	0.0226	0.0258	0
Yb	0.0424	0.0293	0.105	0.116	0.142	0.1208	0.149	0.059	0.1540	0.1590	0
Lu	0.0119	0.0053	0.0162	0.0237	0.0175	0.0203	0.0229	0.0109	0.0228	0.0255	0
La/La*	0.68	1.04	0.86	0.78	1.90	0.78	1.08	1.07	0.53	0.50	0.41
Ce/Ce*	0.94	0.94	1.04	1.07	1.05	1.13	1.10	0.94	1.13	1.42	1.05
Eu/Eu*	1.22	0.89	0.88	1.18	1.15	1.01	0.96	0.97	0.94	0.98	1.05
Pr/Pr*	1.11	1.01	1.00	1.02	0.83	0.99	0.93	0.97	0.93	0.88	0.97
TotalREE	2.01	1.29	3.48	3.04	2.87	6.20	5.45	1.31	15.04	15.98	39.56
Y/Ho	28.2	38.9	37.5	35.1	36.5	36.4	35.8	32.8	34.4	33.6	33.8

Type	KM005a_7 CCD	KM005a_8 CCD	KM005a_9 CCD	12KM005 CCD	12KM005 CCD	12KM005 CCD	11RR024 CCD	11RR04 CCD	RR036a_1 CCD	RR036a_2 CCD	RR036a_3 CCD
Al	60.7	165	101.9	60.7	165	101.9	104.2	124.9	68.9	67	85.6
V	2.08	4.15	1.278	2.08	4.15	1.278	0.056	0.071	1.115	0.835	0.421
Mn	4400	3589	1168	4400	3589	1168	1245	1198	4510	4510	1692
Fe	5230	7630	3970	5230	7630	3970	54.2	48.4	5090	3880	172
Sr	23.89	23.03	15.01	23.89	23.03	15.01	22.68	19.56	17.24	16.37	18.82
Y	2.819	2.412	4.14	2.819	2.412	4.14	1.642	0.678	0.969	0.715	1.957
Zr	0.234	0.249	1.59	0.234	0.249	1.59	0.035	0.0126	0.127	0.0005	0.0032
Nb	0.0101	0.0039	-1.933E-06	0	0	0	0.0022	0.002	0.0117	0	0
Ba	0.89	0.097	5.93	1	0	6	0.009	0.0041	1.05	0.071	0.056
La	0.562	0.517	0.527	0.562	0.517	0.527	0.148	0.038	0.0709	0.0505	0.453
Ce	2.254	1.973	2.295	2.254	1.973	2.295	1.569	0.552	0.493	0.356	2.447
Pr	0.368	0.332	0.43	0.368	0.332	0.430	0.433	0.183	0.1173	0.0846	0.473
Nd	1.615	1.507	2.123	1.615	1.507	2.123	2.89	1.214	0.636	0.495	2.324
Sm	0.563	0.527	0.654	0.563	0.527	0.654	0.809	0.373	0.207	0.161	0.546
Eu	0.0971	0.0713	0.1053	0.097	0.071	0.105	0.2135	0.1251	0.0852	0.0485	0.1154
Gd	0.783	0.684	0.898	0.783	0.684	0.898	0.613	0.252	0.211	0.145	0.442
Tb	0.093	0.0738	0.099	0.093	0.074	0.099	0.0663	0.0313	0.0317	0.0208	0.0567
Dy	0.452	0.418	0.485	0.452	0.418	0.485	0.316	0.145	0.159	0.121	0.34
Ho	0.0733	0.0656	0.0928	0.073	0.066	0.093	0.0514	0.0222	0.0319	0.0214	0.0568
Er	0.16	0.1411	0.224	0.160	0.141	0.224	0.1171	0.054	0.0934	0.0644	0.166
Tm	0.0205	0.0138	0.0262	0.021	0.014	0.026	0.0143	0.00567	0.0136	0.0074	0.0227
Yb	0.089	0.081	0.124	0.089	0.081	0.124	0.0686	0.0296	0.082	0.0541	0.145
Lu	0.0139	0.0105	0.0181	0.014	0.011	0.018	0.0103	0.00469	0.0165	0.0083	0.0191
La/La*	0.51	0.55	0.51	0.51	0.55	0.51	0.26	0.16	0.31	0.35	0.40
Ce/Ce*	1.04	1.01	0.96	1.04	1.01	0.96	0.79	0.68	0.86	0.87	0.99
Eu/Eu*	0.70	0.58	0.68	0.70	0.58	0.68	1.36	1.71	1.71	1.32	1.01
Pr/Pr*	1.08	1.07	1.05	1.08	1.07	1.05	0.93	0.97	1.06	1.00	1.06
TotalREE	7.14	6.42	8.10	7.14	6.42	8.10	7.32	3.03	2.25	1.64	7.61
Y/Ho	38.5	36.8	44.6	38.5	36.8	44.6	31.9	30.5	30.4	33.4	34.5

Type	RR045b_1 CCD	RR045b_2 CCD	RR045b_3 CCD	RR048a_1 CCD	RR048a_2 CCD	RR048a_3 CCD	SG72b_1 CCD	SG72b_2 CCD	SG72b_3 CCD	12KM005 RC	12KM005 RC
Al	188	131.3	159.6	89.3	71.2	84.9	69.1	66.9	63.9	0	30.2
V	1.063	0.263	1.439	2.842	0.348	0.296	5.86	4.32	4.25	0.008	0.029
Mn	3330	4200	1529	1146	1059	898	1165	835	765	0.24	123
Fe	93	56.8	35.5	208	105.8	92.3	225	278	547	31.6	796
Sr	21.1	21.01	21.52	28.91	19.09	14.83	22.65	13.21	11.66	0.782	4.51
Y	1.68	2.087	2.35	4.59	3.01	2.005	2.475	2.67	2.437	2.067	0.951
Zr	0.15	0.05	0.035	0.083	0	0.0024	0.44	0.03	0.0275	0.0216	0.0186
Nb	0.013	0	0.0027	0.025	0.00039	0.00117	0.0265	0.0038	0	0	0
Ba	2.5	0.44	0.49	0.61	0.073	0.045	2.8	0.58	0.41	0.023	0.032
La	0.083	0.091	0.239	0.408	0.367	0.17	0.106	0.221	0.175	0.0814	0.212
Ce	0.733	0.846	1.92	2.088	2.868	1.537	0.96	1.85	1.424	0.0716	0.151
Pr	0.185	0.2019	0.351	0.642	0.803	0.454	0.235	0.39	0.31	0.0976	0.092
Nd	1.2	1.26	2.128	4.27	5.36	3.185	1.355	2.07	1.79	0.566	0.454
Sm	0.362	0.428	0.509	1.276	1.52	0.975	0.363	0.526	0.423	0.178	0.103
Eu	0.1	0.133	0.13	0.255	0.248	0.1681	0.0931	0.1	0.089	0.0581	0.0361
Gd	0.309	0.469	0.474	1.017	1.014	0.661	0.428	0.486	0.412	0.287	0.145
Tb	0.046	0.0632	0.062	0.1277	0.1015	0.0669	0.0638	0.0647	0.0583	0.0323	0.0164
Dy	0.279	0.363	0.408	0.661	0.487	0.321	0.349	0.353	0.302	0.187	0.1
Ho	0.053	0.0769	0.0785	0.122	0.0767	0.0514	0.069	0.068	0.0651	0.0427	0.0223
Er	0.175	0.207	0.196	0.313	0.1718	0.1187	0.182	0.159	0.17	0.1112	0.0639
Tm	0.0235	0.027	0.0331	0.0373	0.0179	0.0119	0.0279	0.0217	0.0226	0.0133	0.00893
Yb	0.193	0.22	0.22	0.199	0.0917	0.0701	0.163	0.143	0.152	0.0866	0.0378
Lu	0.0204	0.0355	0.0374	0.0311	0.0146	0.0079	0.0306	0.0143	0.0253	0.013	0.0072
La/La*	0.32	0.30	0.43	0.48	0.35	0.32	0.26	0.27	0.32	0.48	0.96
Ce/Ce*	0.84	0.89	1.11	0.66	0.76	0.73	0.87	0.98	0.95	0.14	0.24
Eu/Eu*	1.22	1.31	1.15	0.97	0.91	0.95	1.02	0.86	0.91	1.28	1.42
Pr/Pr*	0.94	0.95	0.91	0.95	0.93	0.91	1.02	1.04	0.98	1.27	1.37
TotalREE	3.76	4.42	6.79	11.45	13.14	7.80	4.43	6.47	5.42	1.83	1.45
Y/Ho	31.7	27.1	29.9	37.6	39.2	39.0	35.9	39.3	37.4	48.4	42.6

Type	12KM005 RC	12KM005 RC	12KM005 RC	03BM028 LC	03BM028 LC
Al	70	600	1150	10.5	10.5
V	0.45	3.6	2.58	0.0062	0.0066
Mn	249	1730	680	0	0
Fe	1960	1.26E+04	1.23E+04	1.45	0.95
Sr	1.096	2.54	2.38	0.51	0.334
Y	0.443	1.64	1.3	0.22	0.383
Zr	0.0017	0.037	0.55	0.0021	0.0071
Nb	0	0.00E+00	0.00E+00	0.00031	0.00052
Ba	3.1	32	23.1	0.97	1.19
La	0.0146	0.092	0.092	0.0911	0.1135
Ce	0.114	0.71	1.09	0.0292	0.0233
Pr	0.0195	0.105	0.136	0.0974	0.1377
Nd	0.116	0.58	0.67	0.609	0.839
Sm	0.0465	0.255	0.257	0.175	0.183
Eu	0.0080	0.0415	0.0420	0.036	0.035
Gd	0.096	0.424	0.384	0.1530	0.1340
Tb	0.0101	0.051	0.0439	0.0203	0.0169
Dy	0.056	0.234	0.173	0.1053	0.1088
Ho	0.0086	0.0343	0.0292	0.0163	0.0177
Er	0.0256	0.079	0.073	0.0387	0.0511
Tm	0.00216	0.007	0.0083	0.0043	0.0066
Yb	0.0106	0.033	0.038	0.0293	0.0362
Lu	0.00143	0.0058	0.0063	0.0033	0.0045
La/La*	0.46	0.46	0.28	0.63	0.53
Ce/Ce*	1.16	1.31	1.62	0.06	0.03
Eu/Eu*	0.63	0.62	0.65	0.94	0.94
Pr/Pr*	0.90	0.90	0.90	1.22	1.26
TotalREE	0.53	2.65	3.04	1.41	1.71
Y/Ho	51.5	47.8	44.5	13.5	21.6

Table 4-5 - Summary of SIMS results

Summary table of average SIMS $\delta^{18}\text{O}$ isotope values for different phases and calculated $\delta^{18}\text{O}_{\text{H}_2\text{O}}$ of the fluid that precipitated the minerals. The isotopic composition of water relative to Vienna Standard Mean Ocean Water (V-SMOW) was calculated using mineral fraction equations for dolomite (Horita et al., 2014), calcite (O'Neill et al., 1969), and quartz (Sharp and Kirschner, 1994). Calculated $\delta^{18}\text{O}_{\text{H}_2\text{O}}$ isotope values are displayed for homogenisation temperatures (T_{h}) in parentheses, or were calculated based on end-member estimates of 20°C (low) and 120°C (high) when no T_{h} were available. See Figure 14 and text for discussion of calculate $\delta^{18}\text{O}_{\text{H}_2\text{O}}$ at pressure-corrected temperatures.

Mineral	$\delta^{18}\text{O}$ V-SMOW (‰)	$\delta^{18}\text{O}_{\text{H}_2\text{O}}$ @ 20 V-SMOW (‰)	$\delta^{18}\text{O}_{\text{H}_2\text{O}}$ @ 120 V-SMOW (‰) or (T_{h})
Dolostone	26.3	-13.44	2.8
ED	34.3	-5.4	10.84
FCD	35.4	-	10.81 (110)
HD	-	-	-
CCD	24.5	-	0.86 (120)
Quartz	26.55	-	3.63 (154)
RC	15.2	-20.5	-5.7
LC	9.5	-25.8	-11.5

Chapter 5

5. Concluding Statements

5.1 Conclusions

This thesis provides the first complete sedimentologic and diagenetic description of the Ikpiarjuk Formation dolostone mounds. Below, the initial research questions are answered based on the results presented in chapters 2 to 4.

- *Were there vents, and if so what was their composition?*

The vent-fluid composition was established in Chapter 2 and classified based on the shale-normalised REE+Y patterns of the vent-related dolostone. The mounds formed due to groundwater discharging into an alkaline lake. The groundwater emerged through basin-floor faults and was probably derived from basin water that had been modified through evaporation and subsequent water-rock interaction with basalt and basement rocks beneath the MIG. The vent-fluid had flat shale-normalised REE+Y patterns and a negative Eu anomaly.

- *What was the chemistry of the basin water?*

The basin water has REE+Y patterns that are similar to those of alkaline lake-water patterns. The lake was saline, alkaline, and probably chemically stratified. The interpretation of the basin water as alkaline lake water makes it impossible to determine whether the Ce anomaly in the REE+Y patterns was the result of a redox-stratified water column. The conclusion that the basin was filled with an alkaline lake brings into question the validity of chemostratigraphic reconstructions for other Mesoproterozoic basins that have not been conclusively demonstrated to be marine.

- *What type of microbes lived in the vicinity of vents?*

The microbial metabolisms that are most compatible with both the known geochemical conditions during formation of the Ikpiarjuk Formation and the precipitation of carbonate are chemoheterotrophs (sulphur- or nitrogen-related). Regardless of the exact microbial metabolism, the Ikpiarjuk Formation thrombolites provide direct evidence of benthic microbial communities in a deep-water lake; this is a new and important observation because Precambrian thrombolites are rare and generally assumed to be exclusively shallow-water microbial build-ups in marine environments. Many recent studies in Precambrian sedimentology are focussed on identifying controls on the diversification of eukaryotes and the cycling of nutrients in the global ocean. Mesoproterozoic lakes had significant microbial communities, which indicates that life was abundant in aqueous terrestrial settings, and that studies on the diversification of life and nutrient cycling should include lacustrine settings.

- *What are the economic implications of these repeatedly reactivated fault-zones?*

Chapter 2 demonstrated that there was probably significant dissolved metal in the vent-fluid flow, but Chapter 4 showed that several different fluids had passed through Ikpiarjuk Formation mounds during burial diagenesis. Sulphide inclusions in one generation of dolomite cement, as well as shared fluid characteristics with the Nanisivik ore-forming fluids, suggests a possible link in timing of major fluid-flow events in the MIG. Further analytical work would be required to test the possible relationship of these fluid-flow events. Chapter 4 showed that primary void space in the Ikpiarjuk Formation

was modified by the passage of at least five different fluids throughout their burial history.

5.2 Future work

Chapter 2 concluded that Ikpiarjuk Formation mounds accumulated in an alkaline lake, based on shale-normalised REE patterns and sedimentologic considerations. Future work could compare geochemical analyses of contemporaneous carbonates elsewhere in the basin (Iqqittuq Fm.) with carbonates that directly overlie the mounds and were presumably deposited in a marine setting (Angmaat Fm.). Geochemical analysis of the mechanism whereby REEs are incorporated into microbial and non-microbial carbonate minerals in modern vent settings in alkaline lakes is a promising area for future research.

In Chapter 3, it was interpreted that depositional fabrics in the mounds were formed by chemotrophic microbes exploiting vent fluid in a deep-water environment. In this study it was not possible to confirm what exact type of microbes were present. The field exposures of the mounds are vast, most mound exposures are inaccessible cliffs, and many areas were not thoroughly sampled due to logistical difficulties of working in the Arctic. It is possible that further sampling could identify better preserved microbial carbonate.

The relationship of dolomite-cement-precipitating fluids with the Nanisivik Zn-Pb deposit remains unclear. Linking the timing of fluid-flow events to Nanisivik gangue was beyond the scope of this dissertation, but future work could include testing the relationship through additional analytical techniques such as in situ sulphur isotope analysis. The widespread presence of hematite nodules in mounds also remains

unresolved and could be the focus of future work. The dolomitisation of mound depositional phases remains enigmatic. The “dolomite problem” in Precambrian carbonate rocks is currently an unresolved issue, and no explanation comfortably accounts for the vast amount of Precambrian dolostone. Several recent studies on Neoproterozoic dolomite have confirmed that dolomite was a primary depositional component in some rare systems, and that syndimentary dolomitisation was widespread (Hood and Wallace, 2012; Hood et al., 2015). This thesis documents that high-Mg calcite and aragonite were the primary minerals when the mounds first accumulated, but Chapters 3 and 4 show that dolomitisation occurred early in the diagenetic sequence of events. Further study of the mechanism for dolomitisation, for example, through modelling of water-rock ratios using stable oxygen isotopes (e.g. Mathieu et al., 2015), could help advance the understanding of Precambrian dolomite.

5.3 References

Hood, A.vS. and Wallace, M.W. 2012. Syndimentary diagenesis in a Cryogenian reef complex: Ubiquitous marine dolomite precipitation. *Sedimentary Geology*. v.255-256, p. 56-71

Hood, A.vS., Wallace, M.W., Reed, C.P., Hoffman, K.-H., Freyer, E.E. 2015. Enigmatic carbonates of the Ombombo Subgroup, Otavi Fold Belt, Namibia: A prelude to extreme Cryogenian anoxia? *Sedimentary Geology*. v. 324, p. 12-31

Mathieu, J., Kontak, D.J., Turner, E.C., Fayek, M., Layne, G. 2015. Geochemistry of Phanerozoic diagenesis on Victoria Island, NWT, Canada: *Chemical Geology*, v. 415, p. 47-69